IMMUNOCARCINOGENESIS:
EXTRACELLULAR VESICLES FROM MACROPHAGES MEDIATE INFLAMMATION AND TUMORIGENESIS IN COLITIS-ASSOCIATED CANCER

By

Evran Ural

A DISSERTATION

Submitted to
Michigan State University
in partial fulfillment of the requirements
for the degree of

Biomedical Engineering – Doctor of Philosophy

2025

ABSTRACT

Many conditions of chronic inflammation, such as ulcerative colitis, predispose an individual to developing cancer. The predisposition of chronically inflamed tissue to neoplasia and malignancy is referred to as immunocarcinogenesis. Colitis is characterized by relapsing episodes of inflammation and ulceration in the colonic mucosa. Macrophages play an important role in regulating the immune response in colitis, and secrete proinflammatory factors that may promote colitis-associated cancer. Extracellular vesicles (EVs) have been shown to mediate colitis and colon cancer progression, and there is accumulating evidence suggesting that the activation states of macrophages influence EV secretion and signaling effects in inflammation and cancer. Macrophages in the ulcerated colonic submucosa are exposed to increased levels of bacterial endotoxins, so we sought to model EVs from colitis in culture using EVs from lipopolysaccharide (LPS)-activated macrophages. To investigate the impact of EVs from macrophages on mediating colitis-associated cancer, we characterized EVs from LPS-activated macrophages, treated colon cells and tumors with isolated macrophage EVs, and analyzed the inflammatory and pro-tumorigenic effects in vitro and in vivo. Our results provide evidence that EVs released from LPS-activated macrophages increase inflammation in the colonic epithelium, can promote cell growth, lead to anchorage-independent growth, induce pro-tumorigenic protein expression in transformed cells, and significantly alter the local immune environment. These findings suggest that macrophage-derived EVs may serve as key mediators between colonic inflammation and cancer development, and identify specific EV proteins as potential therapeutic targets to interrupt the progression of colitis-associated malignancy.

Keywords: Inflammatory bowel disease, ulcerative colitis, colorectal carcinoma, field cancerization, immunocarcinogenesis, extracellular vesicles, soluble factors, transformation, lipopolysaccharide, tumor-associated macrophage, tumor-educated macrophage, tumor-residing macrophage, myeloid-derived suppressor cell

This research is dedicated to my crazy uncle,

Ferruh Beceriklisoy

He was a crystal clean soul with so much passion and wisdom from living life to the fullest. He passed away of colon cancer during my PhD research and left the world a more hilarious, hopeful and soulful place than how he found it.

ACKNOWLEDGEMENTS

I am honored to have been in the second graduate student cohort of the Biomedical Engineering program at Michigan State University, and do my PhD research in the Institute for Quantitative Health Sciences and Engineering (IQ). Built specifically to encourage a collaborative environment, the IQ provided me with the invaluable opportunity to work with brilliant, supportive scientists. The collaborative environment provided by supportive faculty at IQ and MSU has allowed me to feel comfortable to truly learn and explore my gaps in knowledge, which are aligning more with the gaps of knowledge of humankind.

First and foremost, I am appreciative to my PhD advisor, Dr. Christopher H Contag. Chris has been my #1 supporter since day one and he has always had my best interest at heart. Since the beginning Chris has always encouraged my raw passion and curiosity, enabling me to explore and collaborate; I respect him not only as a brilliant scientist and excellent mentor, but also as a human who treats everyone with respect and compassion regardless of their stage in life or status. In my graduate studies, Dr. Contag helped guide my study designs and we continuously discussed how to best conceptualize immunocarcinogenesis and the studies that supported it. Over the years, I have come to Chris with a lot of novice questions and concerns, and he has always responded with keen observations, openness, calmness, kindness and compassion. I always leave his office feeling more motivated and energized to continue pursuing my passion in this project. He has changed my perspective on approaching a problem, experimental design, and even mistakes; he has always encouraged us to use independent thinking to be solution-oriented without judgement, and he always created an environment in the lab where we felt safe to be transparent about our errors and concerns. Throughout my research years, he has guided me to learn how to think independently, and helped determine how to comprehend and express the complex data that our studies revealed. Dr. Contag's significant contributions to analyzing and comprehending the data in my dissertation and our manuscript in preparation have proved essential to improving our understanding of the emerging field of immmunocarcinogenesis.

I am also sincerely grateful to my mentor and role model Dr. Karen Liby, who tragically passed away from colon cancer while I was writing this thesis. Karen, I did not get the chance in your lifetime to formally thank you for the generous amount of time you have dedicated to strengthening my research proposal and training plan. I honestly could not have completed this journey without your invaluable support. Not only did your course teachings establish my foundational understanding of cancer biology and chronic inflammation, but the opportunity to attend your weekly lab meetings vastly improved my skills in critical reasoning, from literature analysis to experimental design and data interpretation. You

guided me to avoid ambiguity when communicating my science by consistently ensuring everyone in the room is aware of basic definitions to seemingly simple words that actually have complex meanings such as "transformation" and "drug", and you have helped me understand the intricacies of formulating a testable, specific hypothesis, and in selecting biomarkers and experimental models. Rest in peace, Karen; the world is a better place because of your contributions to cancer research and your kind approach to supporting and improving the world around you. I will always look up to you as an incredible, inspirational woman and strive to live my life with the same open-mindedness, unwavering grit, and empowering presence.

I would also like to thank my advisory committee members Dr. Aitor Aguirre, Dr. Michael Bachmann, Dr. Adam Moeser, and Dr. Xuefei Huang. You have all truly had my best interest at heart and have allowed this process to be seamless for me despite many obstacles and challenges. Aitor, I will never forget your excellent teaching and mentoring ability, your transparency, and how patiently you answered all the random questions I fired at you in the Stem Cell Engineering course. Michael, your guidance in cancer biology, genetics, chemical use, and mindfulness has transformed the way I view the world; you are the most altruistic person I know, and I highly value your perspective on cancer biology and on life. Adam, you have kindly and patiently helped guide me through my in vivo experimental designs and grant writing and the MSU GI group meetings were an excellent experience for me. Xuefei, your direction has been invaluable for me to learn immunology, develop relevant models, and work harder to obtain quality data to support my hypothesis; you are truly an inspirational scientist with an amazing knack for directing and empowering students to reach their potential.

I am also incredibly appreciative of Dr. Stephan Rogalla, a former member of the Contag Lab and current collaborator. Stephan, the amazing opportunity you provided for me to come to Stanford as a visiting scholar is one I will never forget. Your intellectual contributions to our in vivo model and experimental design have been essential. Learning such a niche type of injection technique from you was hands down the coolest thing I've done in my PhD. Shadowing you was enlightening and hilarious, and your transparency opened my eyes to the ups and downs of clinical practice and research in gastroenterology. Seeing you successfully balance clinical practice, collaborative research, mentoring, and family while approaching life with lightheartedness and spreading love made me aspire to establish a career and life like yours.

I am very grateful to the faculty who mentored me through rotations, especially Drs Anna Moore, Dana Spence, and Bryan Smith. Dr. Anna Moore especially has been a huge mentor for me throughout the years; she has helped my self-confidence, presentation skills, understanding scientific concepts, and has

been a key female mentor in my career. Dr. Moore has an inspiring work ethic, and a profound ability to dissect a complex problem into a logical organization that is so easy to comprehend—this is true genius. Anna, thank you for always being honest and real with me; your keen observations of my progress as a scientist and career woman have truly been vital to my success. Dr. Dana Spence has always had my back, and made science fun and safe for us, getting rid of unnecessary hoops for us students to have to go through. Dr. Bryan Smith taught me some amazing science concepts, especially cancer immunotherapy, and has been a brilliant professor for me.

I also want to thank Dr. Masamitsu Kanada for always making himself available to support me in whatever experimental pickle I found myself on a given day. Without your tip to prevent crystal violet wells from drying, I would still be trying to optimize that protocol to this day. In fact, many of my experiments would have gone astray without your expert advice. You have helped me with my skills in literature searching and comprehension through our review article during COVID, and you always motivate me to search the literature for amazing discoveries in the highest impact journals.

Next, I am so appreciative of all of the Contag Lab members, many of whom will be my friends forever. I am especially thankful to Dr. Ashley Makela for all her scientific and emotional support throughout the years. Your genius experimental design, patient direction, helping me to ask more appropriate questions and how to search literature has truly shaped my career as a scientist. To my dear friend and future collaborator Dr. Chima Maduka, I thank you for all your patience and love as we grew into full blown scientists side by side. You are truly brilliant, hardworking, and such a bright light in this world, and I look forward to hearing about your many successes moving forward. To Emily Neeb, this project progressed much farther as a result of your hard work and intellectual contributions. Not only are you a bright, positive energy in the lab, you have earned my utmost respect not only as a scientist but as a human and a close friend. Ahmed Zarea, we've been good friends since day one, and I'm so lucky that we will be friends forever; I will always be grateful for how you supported me when I needed you most. To my lab siblings Drs Victoria Toomajian, Emily Greeson, and Cody Madsen: you all are hilarious, woke, and I would never have had nearly as much fun and ~~in~~sanity throughout the years without you. Tony Tundo, you have always been a positive, motivating presence in the lab and have supported me through thick and thin. Thank you for your inspiring, thought-provoking conversations and vulnerability; I look forward to a lifelong friendship with you. Roxy, it has been amazing to get to know you and work with your positive and motivating spirit. To all the new and old members and collaborators, I have truly enjoyed working side by side with you even for a short time, and I look forward to continuing our relationships as colleagues and friends. I am also extremely grateful to the Liby Lab members for their

support, especially Dr. Ana Sofia Mendes-Leal for your excellent expert advice on my aims and experimental design, Jess Moerland for training me in macrophage characterization techniques and your thoroughly written protocols, and Dr. Lyndsey Reich for providing me with mice for bone marrow isolation.

Dr. Maryam Sayadi, thank you for your brilliant support in bioinformatics and analyzing my mass spectrometry and RNA sequencing data. I have truly enjoyed collaborating with you, and you really pulled through for me when I needed you. Dr. Matt Bernard, you are a powerhouse in your work ethic and a genius in your workflow. Thank you for teaching me flow cytometry from complete novice level to a 20-fluor panel with patience and grace. You took so much care to thoroughly help optimize my experimental design and staining protocols, and make sure I had the utmost quality of data and data analysis. I am also extremely grateful for Dr. Daniel Vocelle, who always goes above and beyond to help me succeed in my experiments. I could not have submitted single cell RNA sequencing samples without your support and for that I am so excited and thankful. Dr. Meena Sudhakaran, along with becoming my good friend over the years, your tips were essential for getting me through some serious ruts in macrophage differentiation and activation; I could not have developed my experimental model without you. Dr. Jamie Bernard and Nat Ato Yawson, you were amazing in helping me with soft agar assay to detect anchorage-independent growth capacity, a key component to my project story. Dr. Neil Robertson generously trained me to use the ZetaSizer instrument in the ISTB and helped optimize the protocol to determine EV concentration during COVID when the ZetaView was broken for months; this allowed me to run some crucial EV transfer experiments in a timely manner. A special thank you goes to Dr. Stephanie Watts and team for provision of the IncuCyte S3 for my cell growth kinetics studies.

Thank you to everyone who helps run the Biomedical Engineering program and the IQ. Particularly, to the Graduate Chairs while I was there – Drs Mark Worden, Erin Purcell and Dana Spence. Thank you for believing in me and for your leadership. Thank you to Tiffany who always had my best interest at heart; you supported me through my difficult times - I am forever grateful. I will never forget the patience and kindness you have shown me throughout the years. Thank you to each and every one of the administrative staff in IQ- this place would not run without you.

Thank you to my family for their support not only during this journey, but always. I appreciate everything you have done. I am so very lucky to have a mother, father, and sisters that believe in me like you all do. To my crazy uncle Ferruh, who passed away from colon cancer during my research, you have changed my perspective in life, and I am a better person existing in a better world because of you. Thank you to my amazing cohort, department friends, division friends, my best friend Justin Creeden who's

always had my back with no judgment and all love, and all my besties Chantal, Donovan, Lucy, Everett, Marco, and so many others whose connections fuel my passion for life. Rest in peace to Quentin Whitsitt, honorary PhD in BME; your kind heart and gentle spirit will be forever missed.
The biggest thank you goes to the sources of funding which helped make this journey easier. To the Cornelius Endowment, and the Biomedical Engineering department fellowships. I truly appreciate the effort and support that goes in to raising funds to support research such as mine.

TABLE OF CONTENTS

LIST OF ABBREVIATIONS

IBD	Inflammatory bowel disease
UC	Ulcerative colitis
CRC	Colorectal carcinoma
CAC	Colitis-associated cancer
EVs	Extracellular vesicles
SFs	Soluble factors
CM	Conditioned medium
GALT	Gut-associated lymphatic tissue
LPS	Lipopolysaccharide
PGE_2	Prostaglandin E_2
TAM	Tumor-associated macrophage
ROS	Reactive oxygen species
RNS	Reactive nitrogen species

CHAPTER 1:

INTRODUCTION

MOTIVATION

Chronic inflammation precedes more than 20 percent of cancers[1]. More than 3 million Americans are inflicted with inflammatory bowel disease (IBD)[2], and patients suffering from IBD have a 3-4-fold increased risk of colorectal carcinoma (CRC)[3]. Early detection of neoplastic lesions in IBD is difficult because colonoscopy is not sensitive enough to detect precancerous dysplasia that is typically indistinguishable from the surrounding inflamed mucosa[4]. The inflammation-dysplasia-cancer sequence in ulcerative colitis (UC), a form of IBD, is characterized by chronic inflammation via ulcers in the lining of the large intestine[5]. UC typically begins with increased expression of proinflammatory cytokines and transcription factors such as TNF-α, STAT3 and NF-κB, and subsequent dysplasia with p53 mutations, and carcinoma often progresses with the accumulation of mutations in several signaling pathways including K-ras and APC [6, 7]. Interestingly, these mutations are often found in the opposite sequence of that which occurs in sporadic colon cancer[8] . Chemopreventive agents investigated for use in IBD-associated CRC include treatments targeting immune cell-secreted soluble factors such as proteins/cytokines and lipids/prostaglandins[9, 10], as well as downstream signaling pathways including anti-inflammatory drugs such as aspirin[11, 12], 5-aminosalicylates[13] , inhibitors of cyclooxygenase[14] and lipoxygenase activity[15] or reactive oxygen species (ROS) scavengers[16] and other antioxidants[17]. However, the success of these clinical trials has been inconsistent for decades[18], and CRC still accounts for 15 percent of deaths in IBD patients[19]. These studies suggest there may be other immune cell-secreted mediators that play key roles in predisposing chronically inflamed tissues to transformation. In my project, I have aimed to elucidate novel potential therapeutic targets and biomarkers of IBD-associated CRC.

RATIONALE

In acute inflammation, tissue damage leads to cell loss and stem cell stimulation, while activated immune cells secrete signaling molecules intended for pathogen destruction and wound healing. These signals promote cell motility, proliferation, chemotaxis, and survival. However, in chronic inflammation these signals are continuously delivered to cells in the surrounding tissues [9, 10], with the potential to induce a contiguous field of preneoplastic cells.

Field cancerization, or field effect, refers to the presence of expanded populations of cells that have undergone initiation and/or acquired various molecular and phenotypic alterations that have not yet developed into microscopically detectable neoplasia[20, 21]. The theory of field cancerization suggests that regions, or 'fields', of tissues contain cells expressing preneoplastic biomarkers that represent an intermediate stage between normal tissue and microscopically detectable transformation[22]. Biomarkers

of field effect are clinically detectable[21, 23] and can predict local neoplasia[24]. These biomarkers of field cancerization are often not microscopically detectable and may include a single underlying oncogenic mutation [23], chromatin disorder[25, 26] and other epigenetic alterations[27, 28], cytoskeletal disorganization[29], dysregulated expression of proteins[30], metabolites[31], microRNAs[32], and decreased apoptosis[33]. Chronic inflammatory conditions are known to promote field cancerization; when this process is mediated by chronic inflammation, we call this field effect immunocarcinogenesis. In ulcerative colitis patients, for example, inflammation-induced field effect biomarkers include chromosomal instability[34] , founder mutations in p53 and K-ras genes [23], aneuploidy[35], and epigenetic changes such as DNA methylation[36]. Chronic inflammation-associated cancer thus parallels the established multi-step carcinogenesis model where cells with various nanoscopic alterations (genetic, epigenetic, metabolic, or molecular) expand under inflammatory conditions to form a cancerization field, which then progresses to microscopically detectable neoplasia with additional changes[22]. The goal of this project is to elucidate signaling mediators in chronic inflammation that promote field cancerization and precede neoplastic transformation and tumorigenesis.

I propose that extracellular vesicles (EVs) are a candidate signaling driver that effectively predispose gut epithelium to malignant transformation, i.e., mediate immunocarcinogenesis, and that these EVs may further promote tumor progression. EVs are membrane-bound vesicles involved in intercellular communication known to transfer bioactive cargo. EVs contain a high information content comprised of nucleic acids, proteins, and lipids[37] that can change the phenotypes of other cells at a distance, i.e., in the absence of direct cell-cell contact. Importantly, EV communication can be specific or non-specific[38], received by fusion with plasma membrane, endocytosis, phagocytosis, or cell surface protein interactions[39]; this communication potentiates EV-mediated transfer of aberrant signals from chronically activated immune cells to surrounding cells such as gut epithelial cells, mediating pathological tissue states. In fact, EVs have been reported to be involved in maintaining intestinal homeostasis, as well as the pathogenesis and progression of IBD[40, 41] and CRC[42]. EVs have been shown to mediate interactions between various cell types, including immune-immune, tumor-immune, stroma-immune, immune-tumor and immune-stromal cell EV in intercellular signaling[43]. For example, EVs from granulocytic myeloid-derived suppressor cells (g-MDSCs) can suppress CD4 T cell proliferation in vitro, and attenuate DSS-induced colitis in vivo in mice[44]. Dendritic cell (DC)-secreted EVs can activate $CD8^+$ cytotoxic T lymphocyte (CTL) cells to a certain degree via antigen presentation in the absence of direct cell-cell contact[45]. Cancer cell EVs can serve as a chemoattractant to direct cell migration and immune

cell recruitment, driving immunosuppressive pro-tumorigenic immune phenotypes[46]. Mast cell EVs have been shown to increase EMT of lung airway epithelial cells[47].

Furthermore, EVs are relatively stable in the bloodstream and can travel long distances in the body in animal models (high range of influence)[48] and likely in humans. EV stability, relative lack of specificity in delivery to cells, high information content and range of influence suggests that immune cell-secreted EVs may promote motility and survival in surrounding cells present within the colonic epithelium such as epithelial cells and fibroblasts. Under conditions of chronic inflammation, these recipient cells may lose growth regulation and become uncontrolled, characteristic of premalignancy[40, 49]. This EV transfer may occur over extended periods of time in chronic inflammation leading to a prolonged premalignant state susceptible to malignant transformation.

Macrophages play a key role in IBD[50] and CRC[51], and immune-epithelial cell EV crosstalk aids in regulating intestinal homeostasis and driving disease progression in IBD[40] and CRC[52, 53]. Colon tumor-residing macrophages, tumor-associated macrophages (TAMs) and TAM-derived EVs are known to enhance colon cancer progression[54, 55] . However, macrophages are differentially activated in the context of colitis, and different pathways for activating macrophages has been shown to affect EV profiles and functional signaling effects in recipient immune and cancer cells (See "EVs secreted by activated macrophages", Chapter 2 Introduction). It is known that macrophage EVs are involved in mediating the polar states of colonic homeostasis (normal) and inflammation[40]. However, EVs released by macrophages in colitis and their potential role in driving colitis-associated cancer has yet to be fully investigated. In chapters 2 and 3 of my dissertation, I attempt to elucidate the contents and signaling effects of EVs from macrophages in colitis, and their role in mediating colitis-associated cancer. I utilize a pre-established model of macrophages in colitis, i.e., lipopolysaccharide (LPS)-activated macrophages, isolate and characterize secreted macrophage EVs, and characterize these macrophage EV signaling effects in recipient colon cells, colonic epithelium, and in the tumor microenvironment.

FOUNDATIONAL THESIS OF THIS WORK

Hypothesis and Overview: Because immune cell-derived EVs may deliver aberrant signals to the intestinal epithelium, I hypothesized that in colitis, activated macrophages secrete EVs that promote colitis-associated cancer by creating a highly susceptible premalignant state. To test this hypothesis, I modeled macrophage behavior in colitis by activating macrophage cell lines with LPS, as has been previously preported[56]. I then isolated EVs from these LPS-activated macrophages and characterized their contents and downstream signaling effects on recipient colon cells and in the tumor microenvironment. I hypothesized that EVs from LPS-activated macrophages would contain pro-

tumorigenic contents that increase the capacity of recipient colon cells to grow, transform, and promote colitis-associated cancer. I have tested this hypothesis by completing the following specific aims.

1. Elucidating the signaling effects of EVs from LPS-activated macrophages on colonic epithelium, and identifying potential molecular EV mediators of the changes observed in colonic epithelium.
    i. Characterizing the effects of EVs from LPS- and non-activated macrophages on colonic epithelial inflammation and tumorigenesis in mice.
    ii. Comparing the protein content profiles in EVs from LPS- and non-activated macrophages.
2. Elucidating the effects of EVs from LPS-activated macrophages on colon epithelial cell growth capacity, protein expression, and tumor progression
    i. Characterizing effects of EVs from LPS-activated macrophages on colon cell growth in monolayer, anchorage-independent growth in soft agar, and inflammatory/tumorigenic protein and transcript expression.
    ii. Characterizing the effects of EVs from LPS-activated macrophages on mouse tissue before and after induction of colon cancer.

In parallel to my research on LPS effects on macrophages and secreted particles in the environment of colitis, I have also examined macrophage responses to biomaterials known to induce chronic inflammation in the absence of LPS through regulation of immunometabolism, i.e., how metabolic reprogramming of immune cells drives their inflammatory response. In these collaborative studies, we attempted to investigate the mechanism by which polylactic acid (PLA), an otherwise excellent candidate for biodegradable bone implants, induces excessive amounts of chronic inflammation in vivo. Previously, PLA implant-induced chronic inflammation was thought to occur from lactate increasing tissue acidity. Dr. Chima Maduka, a former graduate student in the Contag lab, hypothesized that PLA induces inflammation and fibrosis due to PLA breakdown products signaling to recipient cells such as macrophages and fibroblasts. We tested this hypothesis through the following aims:

1. Characterizing the effects of PLA breakdown products on fibroblasts and macrophage activation in vitro culture;
2. Characterize how PLA breakdown products influence the immune infiltrate surrounding in vivo subcutaneous implants.

We characterized the effects of breakdown products of PLA on recipient macrophages and fibroblasts, and identified lactate as a signaling driver of chronic inflammation via immunometabolism, i.e., how metabolic reprogramming of immune cells drives their inflammatory response. Inhibiting glycolysis in

recipient macrophages with various glycolytic inhibitors decreased the inflammatory response to implants in vitro and in vivo. This finding revealed a mechanism of how PLA drives chronic inflammation that has the potential to revolutionize the field of biodegradable implants by identifying new targets for therapy, and here serve as a sterile model of chronic inflammation.

By conducting both of these studies, I was able to compare and contrast immune cell populations in two very distinct forms of chronic inflammation that derive from two orthogonal molecular mediators of inflammatory responses.

CHAPTER SUMMARIES

Chapter 2: I discovered that EVs from LPS-activated macrophages modeling colitis contain elevated levels of a protein known to promote colitis-associated cancer, whereas EVs from non-activated macrophages modeling colonic homeostasis contained elevated levels of a protein known to suppress colitis-associated cancer. I also discovered that macrophage-secreted EVs increase inflammation in the colonic epithelium of mice harboring the $APC^{min/+}$ tumor suppressor mutation, but not in healthy wild-type mice.

Chapter 3: I discovered that EVs from LPS-activated macrophages modeling colitis increase colon cancer cell growth, anchorage-independent growth, and expression of pro-tumorigenic IL-17 signaling proteins. I also discovered that EVs from LPS-activated macrophages mediate the tumor immune microenvironment through preconditioning tumor sites before tumor induction as well as through directly signaling to the tumor immune microenvironment inducing differential expression of immature and immunosuppressive myeloid cell populations.

Chapter 4: I contributed to the discovery that PLA breakdown products, lactate monomers and/or oligomers, induce macrophage and fibroblast activation through increasing glycolysis, and consequently that macrophage activation can be mitigated through local delivery of glycolytic inhibitors. These findings were later further validated in rat studies, and have the potential to revolutionize the field of bioimplants.

Chapter 5: Our studies revealed that EVs from LPS-activated macrophages significantly increased inflammation in orthotopic models of $APC^{min/+}$ mice, and altered the tumor immune microenvironment in our subcutaneous model of colitis-associated cancer. We also observed that LPS and lactic acid activation of macrophages produced distinct metabolic signatures, with LPS favoring glycolysis while lactic acid enhanced both glycolysis and mitochondrial respiration. These findings highlight potential mechanisms by which inflammatory mediators could promote cancer in predisposed tissues. Further

studies with targeted manipulation of specific EV cargo proteins could validate these mediators as potential therapeutic targets to reduce cancer risk in patients with colitis.

CHAPTER 2:

EXTRACELLULAR VESICLES FROM LIPOPOLYSACCHARIDE-ACTIVATED MACROPHAGES INDUCE COLONIC INFLAMMATION IN $APC^{MIN/+}$ MICE AND UPREGULATE PROTEINS KNOWN TO PROMOTE COLITIS-ASSOCIATED CANCER

INTRODUCTION

The colon contains one of the largest populations of macrophages in the body, and these cells play a prevalent role in regulating tissue homeostasis[57] and mediating colitis-associated cancer[58]. Macrophage polarization is plastic, and generally exists within a spectrum between a proinflammatory state (M1) to a pro-regenerative state (M2). Macrophage activation occurs in response to many different signals, such as those from invading microbes and/or their secreted signaling molecules, or from surrounding epithelial or submucosal stromal cells[59]. The plasticity of macrophage polarization is especially apparent during disease states. For example, in colitis-associated cancer, macrophages secrete both proinflammatory and immunosuppressive cytokines such as TNF-α (M1), IL-6 (M2), and IL-1 that contribute to disease progression[60]. In the context of cancer, M1 macrophages typically exhibit cytotoxic and phagocytic properties, and activate T cell responses contributing to anti-cancer immune surveillance; in contrast, M2 macrophages generally function as immunosuppressive cells that promote tumor development and progression[22]. How macrophage plasticity can be modulated is a focus of immunotherapy in cancer treatment.

Table 2.1 Macrophage markers and associated polarization states.

Macrophage marker	Associated polarization state
CD14	M0/M1
CD86	M1
CXCL10	M1
IL-12	M1
IL-23	M1
MHC II	M1
TNF-α	M1
Arg	M2
CCL22	M2
CD163	M2
CD200R	M2
CD206	M2
FN1	M2
IL-6	M2
IL-10	M2

Interestingly, EVs have even been shown to affect macrophage polarization and inflammation. In the IBD model of DSS-treated mice, visceral adipose tissue secreted EVs containing miR-155 that increased CD86 (a M1 proinflammatory cell surface marker) and decreased CD206 (a M2 pro-

regenerative cell surface marker) expression on macrophages[61]. In the same model, stromal cell-derived EVs contain TNF-α-stimulated gene/protein 6 and increased CD206 and Arg1 (M2) expression in macrophages[62]. Bone marrow-derived mesenchymal stem cell-derived EVs decreased macrophage expression of CD86, IL-12 (M1) and TNF-α (M1), and increased expression of CD163 (M2), CD200R (M2) and IL-10 (M2) [56]. Endothelial cell-derived EVs can decrease macrophage responsiveness to lipopolysaccharide (LPS) by downregulating NF-κB activity, TNF-α and IL-1β production, and increasing IL-10 production[63]. DLD-1 CRC EVs contain miR-145 that decreased TNF-α and IL-12p40 (M1) and increased IL-10 and CD206 expression in macrophages[64]. SW620 CRC-derived EVs contain miR-21-5p and miR-200a that decrease MHC II (M1) and increase CD206 and PD-L1 expression in macrophages[65]. HCT116 CRC-derived EVs containing CD133 increased THP1 macrophage expression of CCL22 and FN1 (M2 markers) mRNA, and decreased CD86 expression[66]. Additionally, HCT116 CRC cells were found to secrete oncogenic p53 in EVs, and oncogenic p53-containing EVs effectively increased THP1 macrophage expression of tumor-supportive IL-1β, TNF-α, IL-6, and MMP9[67]. SW480 CRC EVs decreased MHC II and increased CD14 and CXCL10 (M1) expression in THP1s; SW620 CRC EVs increase THP1 CD14 expression and secretion of IL-6 (M2), CXCL10 (M1), IL-23 (M1) and IL-10[68]. Building on these published reports, we explored how differential activation of macrophages is known to affect secreted EV profiles.

EVs secreted by activated macrophages

EVs from tumor-associated or tumor-educated macrophages have been shown to enhance colon cancer progression[54, 55]. Tumor-associated macrophages (TAMs) have been observed to secrete relatively large numbers of EVs in MC38 CRC tumors, i.e., 60% of tumor EVs were derived from TAMs, suggesting that EVs from TAMs may influence the biology of the TME without requiring direct cell-cell contact[69]. Importantly, macrophage-secreted EVs do not always reflect the phenotype of the source cells; interestingly, TAMs from MC38 tumors resembled a M2-like phenotype, whereas the EVs secreted by these source TAMs resembled more of those from a M1-like phenotype[69]. Moreover, TAM-derived EVs with M1-like profile were associated with improved prognosis in patients with CRC[69].

Most studies utilize EVs from macrophages in culture due to the challenging nature of isolating derivative cell subtype-derived EVs in the highly complex environment of chronic inflammation. By comparing mass spectrometry proteomic analyses of EVs from whole MC38 tumors with EVs from macrophage-depleted MC38 tumors, Cianciaruso *et al*. was able to identify proteins present in EVs from macrophages in MC38 tumors[69]. Importantly, similarities were reported in protein contents of these EVs from macrophages in MC38 tumors relative to EVs secreted from cultured bone marrow-derived

macrophages (BMDMs) stimulated with IFNγ plus LPS, or IL-4, in culture[69]. This implies that EVs from macrophages stimulated in culture are representative of EVs from macrophages in vivo MC38 tumors.

Macrophage polarization state can differentially affect EV profiles as revealed by their RNA and protein contents. For example, RNA sequencing revealed that CD68 and CD163-expressing macrophages harvested from CRC patient tissues (considered TAMs) secreted EVs containing high levels of pro-tumorigenic miR-21-5p and miR-155-5p[55]. Relative to THP1 monocytes and primary human monocytes, IL-4-treated THP1 macrophages and primary human macrophages secreted EVs containing upregulated levels of immunosuppressive and pro-tumorigenic hsa-miR-21-5p, hsa-miR-24-3p, hsa-miR-29a-3p, hsa-miR-146b-5p, and hsa-miR-660-5p[70]. In another study, LPS and IFNγ induced expression of iNOS and CD68 in THP1 macrophages, whereas IL-4 induced expression of Arg1 and CD206 in THP1 macrophages[71]; IL-4-treated THP1 macrophages secreted EVs containing upregulated levels of pro-tumorigenic miR-501-3p[71] and miR-223[72]. IL-4-treated primary mouse peritoneal macrophage EVs expressed increased levels of anti-inflammatory lncRNA MEG3[73]. Tobacco smoke extract treatment of primary human monocyte-derived macrophages and THP1 macrophages increase cell and EV production of pro-tumorigenic MMP-14[74]. Guo *et al*. reported that IL-4 and IL-13 treatment of THP1 macrophages increased cell expression of M2 biomarkers CD163, CD206, Arg1 and IL-10, whereas it decreased expression of the M1 biomarkers iNOS, TNF-α, and IL-1β[75]. Pro-tumorigenic miR-186-5p, miR-135b-3p, and miR-1911-5p were upregulated in EVs from these M2-polarized THP1 macrophages as well as in EVs from the plasma of CRC patients in publicly available GEO datasets[75]. Mass spectrometry analyses were also performed on THP1 macrophage-derived EVs with and without interaction with the yeast *Candida albicans*, a common gastrointestinal microbe and opportunistic pathogen, revealing differential expression levels of proteins involved in signaling pathways related to immune response, signaling, and cytoskeletal reorganization[76]. PBMC-derived macrophages and dendritic cells secreted EVs that carried the enzymes LTA_4H and LTC_4S, both involved in proinflammatory leukotriene biosynthesis[77]; patients with IBD have elevated levels of leukotrienes, which increases the risk for developing cancer[78].

In murine Raw264.7 macrophages, IL-4 treatment increased Arg-1, CD163, and CD206 expression, while co-culture with CT26 CRC cells increased IL-10 expression[79]. In the same study, EVs from Raw264.7 macrophages treated with IFNγ and LPS induced an increased expression of CD68 and decreased expression of CD163 in recipient IL-4-treated Raw264.7 cells and recipient Raw264.7 cells co-cultured with CT26 CRC cells[79].

EVs from M2-like macrophages are typically considered to be pro-tumorigenic, whereas EVs from M1-like macrophages are generally deemed to have proinflammatory and antitumor properties.

For example, EVs from Raw264.7 macrophages treated with 100 ng/ml LPS expressed increased levels of proinflammatory iNOS, TNF-α, and IL-6 mRNA (measured by RT-qPCR) compared to EVs from non-treated Raw264.7 macrophages[80]. MonoMac-1 cells treated first with PMA and LPS, and then with GM-CSF expressed the M1 biomarkers IFNγ, IL-6 and TNF-α; MonoMac-1 cells treated with PMA and LPS, followed by M-CSF and dexamethasone expressed the M2 biomarker CD163 in both cells and EVs[81]. These EVs from LPS-treated MonoMac-1 macrophages interfered with neuronal signaling suggesting they may contribute to the pathogenesis of neuroinflammatory disease[81]. Treating J774A.1 monocyte/macrophages with 1 μg/ml LPS increased cell secretion of IL-6, whereas dexamethasone treatment increased secretion of IL-10; microarray analysis of these M1-like and M2-like J774A.1 EVs showed that J774A.1 cells treated with LPS secreted EVs that were functionally antiproliferative due to the miR-29a-3p they contained[82]. Ding *et al*. performed small RNA sequencing on EVs from IFNγ and LPS-treated THP1 macrophages; these M1-like EVs were found to express anti-migratory and anti-invasive miR-146a-5p and miR-146b-5p[83]. Small RNA sequencing by a different group showed that EVs from THP1 macrophages stimulated with IFNγ and LPS contained increased levels of proinflammatory miR-1246 compared to EVs from M0 THP1 macrophage[84]. In a model of myocardial infarction, Chen *et al*. Identified lncRNA MALAT1 in the LncDisease database[85] as an effective proinflammatory component within EVs from murine bone marrow-derived macrophages (BMDMs) treated with IFNγ and LPS[86]. MALAT1 is also commonly dysregulated in colorectal cancer[87], can mediate the Wnt/β-catenin signal pathway[88], and is associated with a poor prognosis of CRC patients[89].

However, the effects of EVs from M2-like and M1-like macrophages are very complex and are thus not always "completely" pro-tumorigenic or antitumorigenic, respectively. For instance, peripheral blood mononuclear cell (PBMC)-derived macrophages treated with GM-CSF followed by IL-4 expressed elevated M2 markers CCL13, MRC1, and CD209; PBMC-derived macrophages treated with M-CSF followed by LPS and IFNγ expressed elevated M1 markers CXCL11 and CCR7; small RNA sequencing showed EVs from LPS and IFNγ-treated PBMC-derived macrophages expressed increased levels of miRs involved in IL-6 proinflammatory signaling, proliferation, and activation of MYC and mTOR pathways involved in cancer initiation and progression[90]. EVs from these IL-4-treated PBMC-derived macrophages contained increased levels of miRNAs involved in pro-tumorigenic signaling pathways including MAP3K3, NF-κB, oxidative stress, and repression of MYC-responsive genes[90]. Contents of EVs from IFNγ and LPS-treated J774A.1 cell were compared to EVs from untreated and IL-4-treated J774A.1 cells via miRNA-Seq analysis, revealing differential expression of miRNAs involved in the tumor-related factors Wnt, HIPPO, and MAPK[91]. These EVs from IFNγ and LPS-treated J774A.1 cells, as well as EVs from GM-CSF and IFNγ-

activated peritoneal macrophages and bone marrow-derived macrophages, expressed high levels of proinflammatory miR-155[91, 92], which has been shown to be upregulated in CRC tissues and may be involved as an oncogene in colon carcinogenesis[93]. Both IFNγ and LPS-activated Raw264.7 and THP1 macrophages secrete EVs that express miR-222 [94], which promotes migration and invasion of CRC cell lines[95]. These observations support a significant role of EVs from activated macrophages in mediating colitis and colon cancer, potentiating their role in mediating colonic immunocarcinogenesis.

Experimental model

Gram negative bacterial lipopolysaccharide (LPS) stimulates monocytes and macrophages through the toll-like receptor 4 (TLR4)[96]. TLR4-deficient mice have been found to be protected against colitis-associated neoplasia in the AOM/DSS mouse model[96, 97], suggesting that LPS plays a significant role in this pathogenesis. Further evidence stems from the finding that bovine milk EVs reduce LPS-activated Raw264.7 expression of TLR4, MyD88, p65, iNOS, COX-2, and NLRP3 in vitro, and mitigate DSS-induced colitis in mice by inhibiting TLR4-NF-κB and NLRP3 signaling pathways, both of which are activated by LPS[98]. The increased permeability of the intestinal mucosa that is characteristic of ulcerative colitis allows for the influx of gram-negative bacterial components, including LPS, into the submucosal connective tissue; more so, in patients with IBD, LPS is absorbed into the blood where it can be detected in the plasma[99].

LPS activates TLR4 through a complex involving CD14 and MD-2, triggering MyD88-dependent and TRIF-dependent pathways that ultimately activate NF-kB, MAP kinases, and IRF3, leading to proinflammatory cytokine production[100]. These signaling cascades likely influence EV biogenesis, cargo selection, and EV secretion from macrophages[101]. In ulcerative colitis, gram-negative bacteria represent a significant proportion of microbes that infiltrate the ulcerated colonic submucosa where they encounter resident macrophages[102], making LPS stimulation a relevant model for macrophage activation in this disease. The LPS used in our studies was derived from E. coli (0111:B4), a well-characterized endotoxin widely used in research settings, shown to use TLR4 as its only receptor[103]. While this provides consistent experimental conditions, future studies could employ LPS from colonic E. coli strains, particularly those belonging to the B2 phylogenetic group that frequently colonize patients with ulcerative colitis[102], to better represent in vivo conditions of colitis-associated cancer.

Thus, macrophages activated with LPS were utilized as the source cells for EVs as a feasible model of macrophage EVs in the environment of colitis[56] that may lead to progression of dysplasia and immunocarcinogenesis. LPS-induced macrophage activation was verified, and subsequently secreted EVs were isolated and characterized. Because the activation status of source macrophages may not be fully

reflected in their secreted EVs[69], we characterized the contents of isolated EVs as well as their signaling effects. Mass spectrometry was utilized to profile protein contents of LPS-activated macrophage EVs as compared to non-activated macrophage EVs, to model resident macrophage EVs present in tissues as mediators of homeostasis. The effects of these inflammatory EVs upon injection into the rectal submucosa in mice with or without the tumor suppressor mutation $APC^{min/+}$ was also characterized.

Keywords: extracellular vesicles, tumor-associated macrophages, lipopolysaccharide

METHODS

Murine Cell Culture

Raw264.7 cells (ATCC) were cultured as directed by the manufacturer. Primary bone marrow-derived macrophages (BMDMs) were sourced from female C57Bl/6J mice (Jackson Laboratories) aged 6–10 weeks and cultured as previously described[104, 105]. Immortalized BMDMs (iBMDMs) were a gift from Dr. Andrew Olive's Laboratory at Michigan State University, J2-immortalized with c-myc and raf/mil oncogenes, as previously described[106], and were cultured in DMEM medium supplemented with 10% heat-inactivated fetal bovine serum (FBS) and 1% antibiotics (100 U/ml penicillin, 100 µg/ml streptomycin). Note that macrophages can become activated in overconfluent and acidic culture conditions.

Murine macrophage activation

Murine macrophage cell lines were seeded into a T150 cm^2 plate at a density of 4×10^6 Raw 264.7 cells/plate or 6×10^6 iBMDM cells/plate in DMEM medium supplemented with 1% extracellular vesicle (EV)-depleted FBS and antibiotics and incubated for 24 hours (h) before stimulation. Primary BMDMs from each mouse were seeded into four 10 cm dishes in DMEM with 10% EV-depleted FBS, antibiotics, and 10 ng/ml M-CSF (Prospec Bio, Cat. No. CYT-439), and incubated for 5 days (d); BMDMs were washed 1x with PBS before stimulation.

Macrophages were subsequently stimulated with final concentrations of 0-500 ng/ml lipopolysaccharide (LPS, Sigma Aldrich, Cat. No. L2630) in DMEM with 1% EV-depleted FBS and antibiotics. After 48 h treatment, conditioned medium was removed for EV isolation and cells were treated with TRIzol for RNA isolation.

Human macrophage cell culture, differentiation, and activation

The human acute promonocytic leukemia THP1 cell line (ATCC) was cultured as directed by the manufacturer in RPMI medium supplemented with 10% heat-inactivated FBS and 1% antibiotics (100 U/ml penicillin, 100 µg/ml streptomycin) at 37°C in a humidified atmosphere containing 5% CO_2. Note that macrophages can become activated in overconfluent and acidic culture conditions.

THP1 monocytes were seeded into T150 cm^2 plates at a density of 2×10^7 cells/plate in complete RPMI medium and allowed to incubate for 24 h. Cells were then treated with a final concentration of 50 ng/ml phorbol 12-myristate 13-acetate (PMA, Sigma-Aldrich, Germany) for 48 h to induce differentiation into adherent macrophage-like cells. After 48 h, THP1-derived macrophages were gently washed with PBS to remove dead and undifferentiated cells and stimulated with 0-500 ng/ml LPS in RPMI medium supplemented with 1% EV-depleted FBS and antibiotics. After treatment for 48 h, conditioned medium was removed for EV isolation and cells were treated with TRIzol for RNA isolation.

Reactive Oxygen Species detection assay

Activated and non-activated murine macrophages were incubated with 5 µM of CellROX Green reagent (Thermo, Cat. No. C10444)[107] according to manufacturer's instructions for 30 min, washed 3 times, and their fluorescence was measured in a Molecular Devices SpectraMax M3 spectrophotometer at excitation/mission (ex/em) maxima 485/520 nm to quantify oxidative stress via reactive oxygen species (ROS) production levels.

Griess assay to detect NO

Conditioned medium (CM) from macrophages that had undergone different treatments was harvested at various time points. Nitric oxide (NO) production was measured in the medium as nitrite using the Griess reaction, as previously described[108]. In short, 100 µl CM and a serial dilution of NO standards of known concentration in complete medium to generate a standard curve were seeded in a standard 96-well plate. Subsequently, 100 µl of a 1:1 mixture of Griess A reagent (0.1% N-1-naphthylethylenediamine dihydrochloride in DI H_2O) and Griess B reagent (1% sulfanilamide and 5% phosphoric acid in DI H_2O) was added to each well. Light absorption of plate wells at 550 nm was then measured in the Molecular Devices SpectraMax M3 spectrophotometer and experimental sample NO levels were determined relative to the standard curve.

Cytokine Measurement

After THP1-derived macrophage differentiation and stimulation, supernatants were collected and clarified by centrifugation and tested for cytokine production by the TNF-α DuoSet ELISA Development kit (R&D Systems, Cat. No. DY210) according to the manufacturer's instructions. Cytokine concentrations were determined using a standard curve prepared with recombinant human TNF-α provided in the kit. Absorbance was measured using the Molecular Devices SpectraMax M3 spectrophotometer. Experiments were performed with three independent macrophage preparations, each with appropriate vehicle controls. The statistical significance of the differences between untreated and LPS-treated

macrophages was determined via one-way ANOVA followed by Tukey's post-hoc analysis using GraphPad Prism.

EV Isolation via differential ultracentrifugation

Non-activated and LPS-activated macrophage cells were incubated at 37°C for 48 h to allow for EV production. Cell supernatants were centrifuged first at 600g for 10 min to remove any cells, and then at 2,000g for 20 min to remove apoptotic bodies and cell debris. Supernatants containing EVs and soluble factors (e.g., secreted proteins) were transferred into new tubes and centrifuged at 100,000g for 90 min to concentrate EVs[109]. The pelleted EVs were then resuspended with PBS and recentrifuged for greater purity before final resuspension in 200 µl PBS.

EV-depletion of FBS

Heat-inactivated fetal bovine serum (FBS) was ultracentrifuged in PET Thin-Walled ultracentrifuge tubes (Thermo Scientific, Cat. No. 75000471) with a Sorvall WX+ Ultracentrifuge equipped with an AH-629 rotor at 100,000g for 16 h at 4°C to pellet any EVs present in FBS. The supernatant was used as EV-depleted FBS.

Nanoparticle Tracking Analysis (NTA)

The size and concentration of extracellular vesicles were measured using a ZetaView® (Particle Metrix) Nanoparticle Tracking Analyzer, following the manufacturer's instruction. EVs were diluted in PBS between 400- and 10,000-fold to obtain a concentration within the recommended measurement range.

ZetaSizer (Dynamic Light Scattering) Analysis*

*Protocol written and optimized with Dr. Neil Robertson

Particle concentration of extracellular vesicles (EVs) was measured using the Malvern Pananalytical ZetaSizer Nano-ZS, as previously described[110]. In short, a serial dilution of EVs of known concentrations were recorded as standards, and a linear curve was generated of concentration (particles/ml) versus average count rate (kcps). Concentration of EVs in experimental samples was determined by measuring the Ave count rate as generated by the DLS instrument, divided by the attenuation factor to determine the actual particle concentration.

TEM imaging

Samples were prepared as previously described[111]. In short, EVs were fixed in 2% paraformaldehyde (PFA), immobilized on a carbon-coated EM grid, and negative stained with 1% uranyl acetate. Grids were imaged with a JEOL 100CXII transmission electron microscope operating at 100 kV, and images were captured on a Matataki Flash sCMOS digital camera.

Protein Gel Electrophoresis & Immunoblotting

EV protein concentrations were determined with the Pierce BCA Protein Assay Kit (Thermo Fisher, Cat. No. 23225) using albumin standards according to the manufacturer's protocol. EVs containing 5-20 µg protein were mixed with 4X sample buffer (Expedeon, NXB31010), 10X reducing buffer (Thermo, NP004) and deionized water to a volume of 10-20 µl, and samples were subsequently heated at 90°C for 5 min. Samples and Precision Plus Protein All Blue Standards (BioRad, 1610373) were loaded into Mini-PROTEAN TGX Stain-free Precast gels (BioRad, 4568093) and run with Tris/Glycine SDS Running Buffer (BioRad, 1610732) in the BioRad Mini-PROTEAN Tetra System at 100V for 60-80 min.

PVDF membranes were soaked in methanol for 2 min, washed in DI water, and soaked in 1X Trans-Blot Turbo Transfer Buffer (BioRad, 10026938) for 2 min. Filter paper was also soaked in Transfer buffer for 2 min. Blot and gel were then arranged in the following order: bottom (anode), filter paper, membrane, gel, filter paper, top (cathode), as the electric current moves from the cathode toward the anode and thus transfers the proteins from gel to membrane. Semi-dry membrane transfer was performed in the BioRad Trans-Blot Turbo Transfer System using the StandardSD protocol (25V, 1.0A, 30 min).

After transfer, membranes were blocked in 3-5% non-fat dry milk in TBST for 1 h at RT, or overnight at 4°C. All antibodies used for Western blot detection are listed in Table A.1. Membranes were stained with primary antibody in blocking buffer (BioRad, Cat. No. 12010020) overnight at 4°C. Membranes were then washed 3 times for 3 min with TBST and subsequently stained with secondary antibody in blocking buffer for 1-2 h at RT. Blots were again washed 3 times for 3 min with TBST. Blots were incubated with HRP substrate working solution for 1 minute using the Pierce ECL Western Blotting Substrate kit (Thermo, 32209) and imaged in the ChemiDoc MP Imaging System (BioRad). Bands on captured blot images were quantified using ImageJ software using the protein standards as reference.

EV proteomics sample preparation**

**Protocol was written with Dr. Douglas Whitten, adapted from Pierce TR0049.0 (www.piercenet.com)

Acetone precipitation of proteins for mass spectrometric analysis: Four volumes ice-cold 100% acetone were added to 1 volume protein solution, and samples were incubated overnight at -20°C. Samples were then pelleted at 14,000 g for 10 min and washed with 80% acetone/20% water and re-centrifuged. Supernatants were removed and sample tubes with pelleted protein were placed in a fume hood to allow the residual acetone to evaporate (5-10 min). Sample pellets were resuspended in 100 µl of 100 mM Tris in water (pH 8.5), and stored at -20°C until further use.

Proteolytic digestion: Protein samples, in 100 mM Tris, were mixed with 100 mM Tris-HCl (pH 8.5) supplemented to 6% (w/v) sodium deoxycholate (SDC) to a final volume of 270 µl[112]. Samples were then

reduced and alkylated by adding Tris(2-carboxyethyl)phosphine (TCEP) and chloroacetamide at 10 mM and 40 mM respectively, and incubated for 5 min at 45°C with shaking at 2000 rpm in an Eppendorf ThermoMixer C. Trypsin/LysC enzyme mixture, in 50 mM ammonium bicarbonate, was added at a 1:100 ratio (wt/wt) and the mixture was incubated at 37°C overnight with shaking at 1500 rpm in the Thermomixer. Final concentration of the digestion buffer was 100 mM Tris-HCl, 4% SDC and the volume of each digest was ~300 µl. After digestion, SDC was removed by phase extraction using ethyl acetate[113]. The samples were acidified to 1% TFA and subjected to C18 solid phase clean up using StageTips[114] to remove salts. Purified peptides were then dried by vacuum centrifugation and re-suspended to 20 µl in 2% acetonitrile/0.1% trifluoroacetic acid.

LC/MS/MS Analysis of EVs and soluble secreted factors**

EV samples were injected automatically using a Thermo EASY-nLC 1000 (Cat. No. LC120) onto a C18 trapping column (Thermo Acclaim PepMap RSLC 0.1mm x 20mm) and washed for ~5 min with buffer A (0.1% Formic Acid in water). Bound peptides were then eluted over 35 min onto a resolving column (Thermo Acclaim PepMap RSLC 0.075mm x 250mm) with a gradient of 5% Buffer B (B) to 10% Buffer B (B) in 2 min, ramping from 10%B to 25%B at 20min, 25%B to 40%B at 24 min, 40% B to 90%B at 25 min and held at 90%B for the duration of the run (Buffer B = 80% Acetonitrile/0.1% Formic Acid in water) at a constant flow rate of 300 nl/min. Column temperature was maintained at a constant temperature of 50°C using an integrated column oven (PRSO-V1, Sonation GmbH, Biberach, Germany).

Eluted peptides were sprayed into a ThermoScientific Q-Exactive mass spectrometer using a FlexSpray ion source. Survey scans were taken in the Orbi trap (35,000 resolution, determined at m/z 200) and the top 15 ions in each survey scan are then subjected to automatic higher energy collision induced dissociation (HCD) with fragment spectra acquired at 17,500 resolution.

Data analysis: The resulting MS/MS spectra were converted to peak peptide lists using MaxQuant software[115, 116] (v1.6.3.4, www.maxquant.org). The peptide list was compared against a protein database containing either all mouse or human sequences available from Uniprot (www.uniprot.org, downloaded 2023-01-31 or 2023-04-18, respectively), appended with common laboratory contaminants (downloaded from www.thegpm.org, cRAP project) using the Andromeda[117, 118] search algorithm, a part of the MaxQuant environment. The MaxQuant output was then analyzed using Scaffold, v5.2.2 (www.proteomesoftware.com) to probabilistically validate protein identifications. Assignments validated using the Scaffold 1% FDR (False Discovery Rate) confidence filter are considered true. Search parameters for all databases were as follows: allow up to 2 missed tryptic sites, fixed modification of

Carbamidomethyl Cysteine, variable modification of Oxidation of Methionine, peptide tolerance of +/- 4.5ppm, MS/MS tolerance of +/- 20ppm, FDR calculated using randomized database search.

In vivo inflammation studies

$APC^{min/+}$ mice and C57Bl/6 mice were purchased from Jackson Labs and kept in the Stanford animal facilities with approval from the Institutional Animal Care and Use Committee (protocol No. 27715). 100 µl of saline (PBS) or EVs from non-activated and LPS-activated iBMDM cells were injected into the rectal submucosa of 16-week-old male mice, guided by the Pentax EB-1170K pediatric bronchoscope, 3 times in 7 d. At the end of the week, mice were sacrificed via cervical dislocation under anesthesia with 2-3% isoflurane and underwent post-mortem dissection to remove colon tissues.

Hematoxylin and eosin (H&E) staining

Colonic tissues were rinsed with cold PBS, fixed in 4% paraformaldehyde, dehydrated, paraffin-embedded, and sliced into 10 µm sections. Next, the sections were stained with hematoxylin and eosin (Sigma-Aldrich, MHS1)[119]. The severity of inflammation was subsequently determined by experienced pathologists using a double-blind method. The scoring criteria for the degree of inflammatory cell infiltration was: score of 0, normal; score of 3 dense inflammatory infiltrate. The scoring criteria for crypt architecture: score of 0, normal; score of 0.5, rare clear regions with loss of crypt; score of 3, severe crypt distortion with loss of entire crypts. The scoring criteria for muscle thickening: score of 0, base of crypt sits on the muscularis mucosae; score of 3, marked muscle thickening present.

Statistical analysis

Statistical analyses were performed using Prism software (10.1.1, GraphPad Inc.). Statistical significance was determined via unpaired t-test for data with two groups, and via one-way ANOVA for data with multiple groups, followed by Tukey's post-hoc test. Two-way ANOVA was used to analyze data with more than one independent variable, followed by Tukey's post-hoc test. Data are expressed as mean +/- standard deviation (SD); comparisons with $p<0.05$ were considered significant findings.

RESULTS

Characterization of macrophage activation and secreted EVs

First, I cultured J774A.1 and Raw264.7 macrophage lines that originated from Balb/c mice known to have a Th2 dominant T cell repertoire. I found the laboratory stocks of J774A.1 cells did not secrete reactive nitrogen species (RNS) or reactive oxygen species (ROS) upon treatment with 1, 10, 100, 500 or 1000 ng/ml LPS at 12, 18, or 24 h (data not shown); this is most likely because previous lab member cultures of macrophages were desensitized to lipopolysaccharide (LPS) due to sustained stimulation[120] or because I was using DMEM medium as opposed to RPMI-1640[121].

Next, I stimulated Raw264.7 cells with combinations of different concentrations of LPS and interferon-γ (IFNγ), and quantified optimal activation levels over time with assays measuring cell secretion of ROS (Figure 2.1a,b) and RNS (Figure 2.1c,d), i.e., nitric oxide (NO). Morphological changes of LPS-activated Raw264.7 cells can be seen in Figure 2.1e.

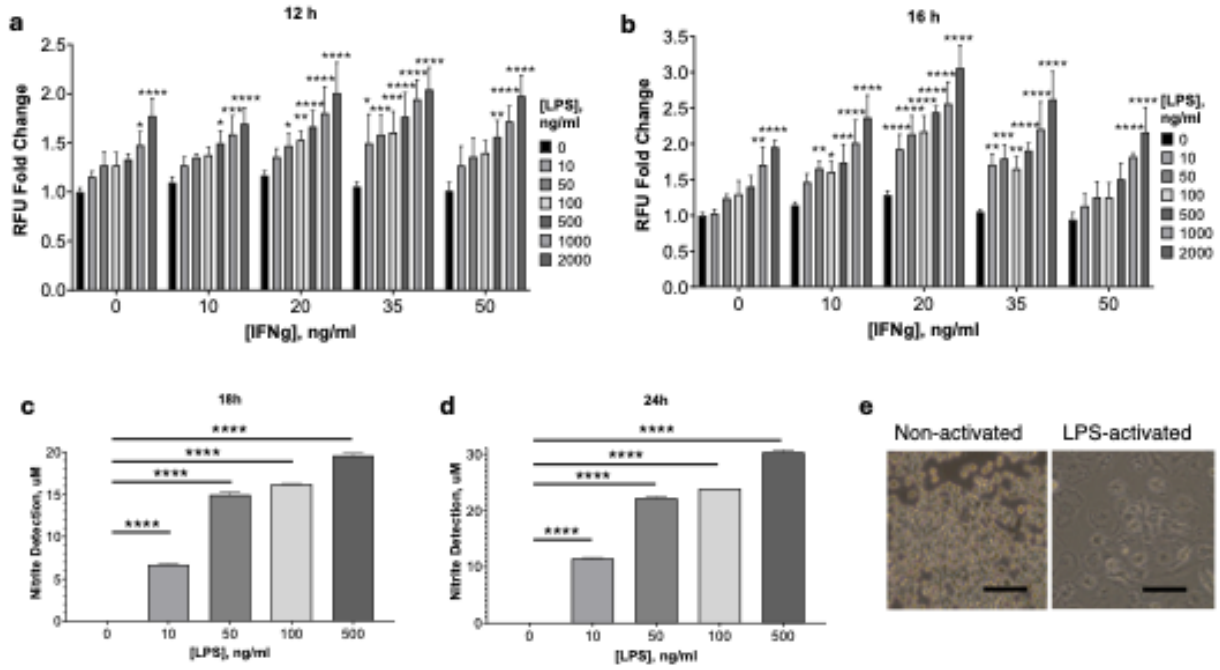

Figure 2.1 Raw264.7 (Raw) murine macrophages secrete reactive oxygen species (ROS) and reactive nitrogen species (RNS) when treated with different concentrations of lipopolysaccharide (LPS) and interferon-gamma (IFNg) at different timepoints. When activated with 10-2000 ng/ml LPS and/or 10-50 ng/ml IFNg, Raw cells secrete detectable levels of ROS at 12 h (a) and 16 h (b). When activated with 10-500 ng/ml LPS, Raw cells secrete detectable levels of RNS at 18 h (c) and 24 h (d). (e) Representative images showing morphology of non-activated and LPS-activated Raw cells in culture; scale bar, 50 um. *p<0.05, **p<0.01, ***p<0.001, ****p<0.0001, mean (SD); n=4, two-way ANOVA followed by Tukey's post-hoc test (a,b) and n=2, one-way ANOVA followed by Tukey's post-hoc test (c,d). RFU, relative fluorescence units.

Raw264.7 cells were thus utilized for my in vitro mouse cell experiments moving forward. I then isolated EVs from conditioned medium of non-activated and LPS-activated Raw264.7 cells growing in a flask for 48 h, i.e., sufficient time for EV secretion, and analyzed their particle count via the Nanoparticle Tracking Analyzer (Figure 2.2a,b). TEM images of individual particles of Raw264.7 EVs exhibited typical cup-shaped and rounded morphology and a size range of approximately 100-150 nm in diameter, representative of EVs (Figure 2.2c,d). Immunoblotting verified EVs from non-activated and LPS-activated Raw264.7 cells to express the EV biomarker Alix (Figure 2.2e)[122]. Thus, according to the MISEV 2018

standards[122], the particles we isolated from the conditioned medium of non-activated and LPS-activated Raw264.7 macrophages are verified as EVs.

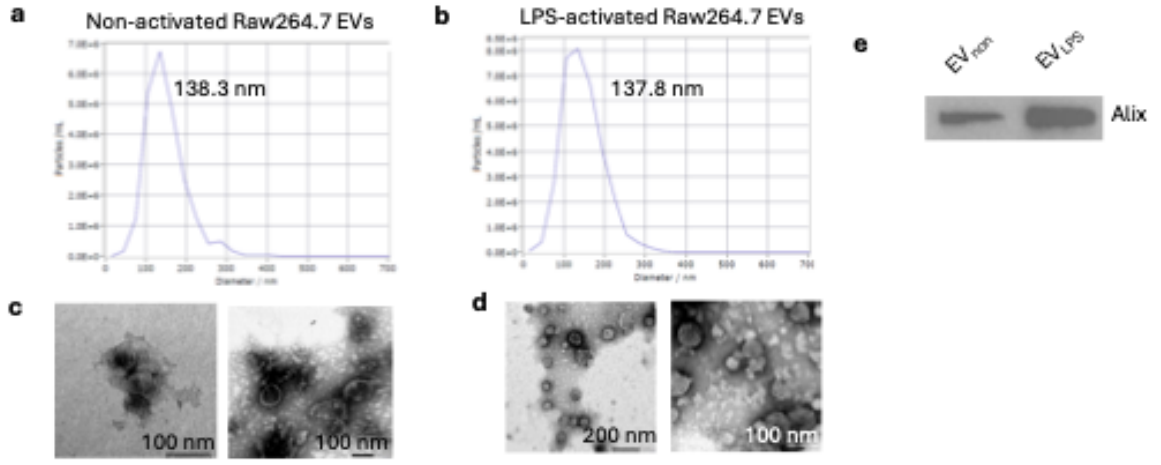

Figure 2.2 Characterization of extracellular vesicles (EVs) from Raw264.7 (Raw) murine macrophages that are non-activated or activated with 100 ng/ml lipopolysaccharide (LPS). (a) Size distribution curves of EVs from non-activated and LPS-activated Raw cells. (b) Transmission electron microscopy (TEM) images of EVs from non-activated (left) and LPS-activated (right) Raw cells; X60k scale bar, 100 nm. (c) Immunoblot analysis of EVs from non-activated and LPS-activated Raw cells.

During the first year of the COVID pandemic, the NTA ZetaView broke for several months. As necessity fosters innovation, I improvised to use the ZetaSizer, which uses dynamic light scattering (DLS) to determine particle size and zeta potential[123], as opposed to the ZetaView which employs nanoparticle tracking analysis (NTA) for size, concentration, and zeta potential measurements[124]. Dr. Neil Robertson in Dr. Anna Moore's lab had the idea of using EVs of known concentration (that I had previously counted on the NTA before it broke) as standards to determine the particle count of my newly isolated EVs. So, I created a linear standard curve of concentration (particles/ml) on the x-axis and ave count rate (kcps) on the y-axis ($r^2 > 0.99$). Using the average count rate of unknown samples, I could then calculate their concentration until the NTA was fixed.

Next, I investigated human cells as a more clinically relevant model. I confirmed LPS activation of THP1 monocytes by measuring cell culture secretion of the proinflammatory cytokine TNF-α with an ELISA. Interestingly, seeding 18 million cells in a T75 flask caused cells to secrete more TNF-α, indicating macrophage proinflammatory activation, as compared to cells in flasks seeded with a lower number of cells, i.e., 17 million cells (Figure 2.3a). This may be because cell interactions at different confluency affects macrophage activation levels[125], or because more cells secreted more detectable levels of TNF-α.

THP1 cells are promonocytes that grow in suspension culture and can be differentiated into macrophages that develop different characteristics such as granularity and differentiation-dependent cell surface markers [126]. M1-activated THP1 cells (via LPS and/or IFNγ stimulation) have been found to lack expression of ROS or nitric oxide like murine macrophages[127] but they do consistently secrete proinflammatory cytokines such as TNF-α. After many attempts, Dr. Meena Sudhakaran generously helped me optimize THP1 differentiation with phorbol 12-myristate 13-acetate (PMA) in the Contag Lab (see methods; note that treating THP1 cells on the day after seeding to acclimate in suspension will produce more reproducible results). To confirm PMA-induced differentiation of THP1 cells into macrophages, I used flow cytometry to detect the relative expression per cell of the activation marker CD11b at 48 h and 72 h in response to differing concentrations of PMA (Figure 2.3b). CD11b was not expressed on THP1 promonocytes but was expressed on approximately 60-75% of differentiated THP1-derived cells. To confirm activation of THP1-derived macrophages, I analyzed their TNF-α secretion using an ELISA. THP1 cells differentiated into macrophages upon exposure to 50 ng/ml PMA for 48 h or 72 h and when subsequently stimulated with 500 ng/ml LPS, secreted over 12000 ng/ml TNF-α on average, over 11-times more than untreated THP1 monocytes (Figure 2.3d).

To determine if there was a temporal component to this TNF-α secretion profile, I treated THP1 monocytes with 0, 100, or 200 ng/ml PMA for 48 h and then stimulated the cells with 500 ng/ml LPS for 4 or 24 h. I found that LPS-activated THP1 macrophages secrete more TNF-α at 24 h than at 4 h (Figure 2.3c). I then did a LPS concentration titration measuring TNF-α secretion from THP1 cells differentiated into macrophages through exposure to 50 ng/ml PMA for 72 h, and then stimulated with lower, more physiologically relevant concentrations of LPS. I found that 10, 50, and 100 ng/ml LPS also induced proinflammatory activation of THP1 macrophages (Figure 2.3e). I also found that at these LPS concentrations, adding 20 ng/ml IFNγ to THP1 macrophages did not significantly increase secretion of the proinflammatory cytokine TNF-α (Figure 2.3f). So, I ultimately decided to differentiate THP1s into macrophages with 50 ng/ml PMA for 48 h, and stimulate with 100-500 ng/ml LPS for 48 h for THP1-secreted EV isolation and administration onto colon cells.

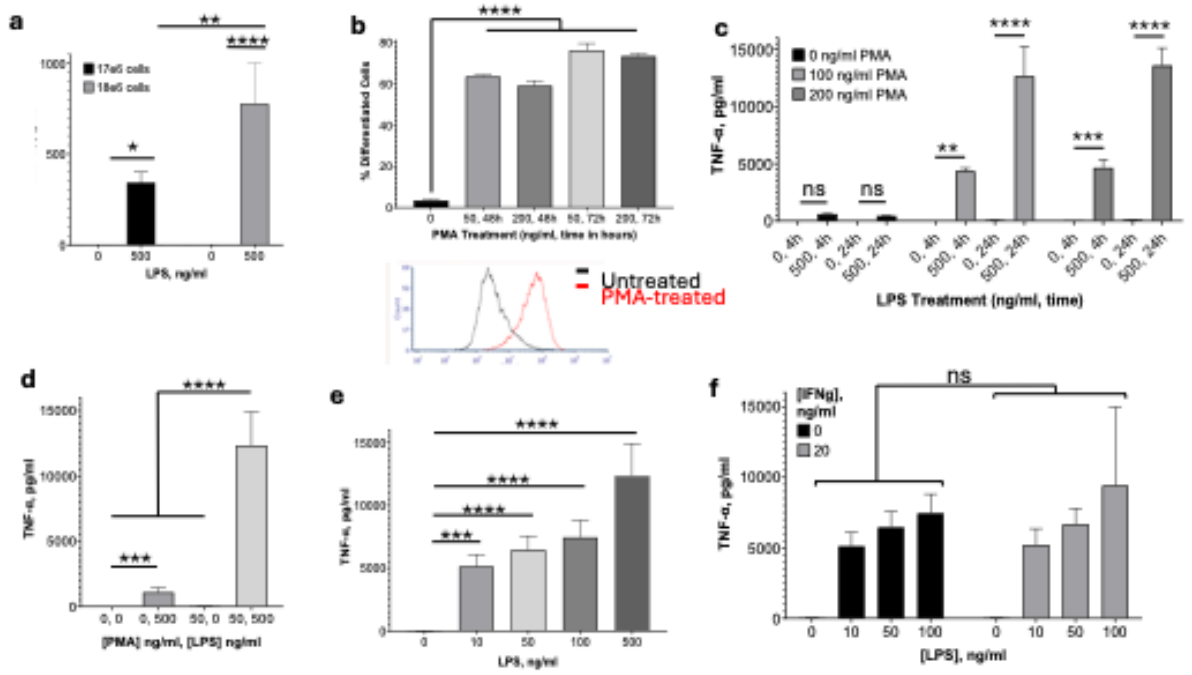

Figure 2.3 THP-1 human macrophages secrete more TNF-α upon lipopolysaccharide (LPS) treatment than THP1 monocytes. (a) Seeding a higher number ($18x10^6$, denoted 18e6) of THP1 monocytes/T150 cm^2 flask significantly increases TNF-α secretion upon activation with 500 ng/ml LPS compared with seeding $17x10^6$ (17e6) THP1 monocytes/flask. (b) Flow cytometric quantification and representative image (below) of THP1 macrophages after differentiation with phorbol 12-myristate 13-acetate (PMA) at different concentrations and times; percent differentiated cells was determined by quantifying the relative CD11b-PE antibody expression per cell measured by mean fluorescence intensity (MFI). (c) TNF-α secretion of non-activated and LPS-activated THP1 monocytes and macrophages at 4 h and 24 h. (d) Comparison of TNF-α secretion levels of THP1 monocytes and macrophages differentiated with 50 ng/ml PMA for 48 h, and subsequently activated with LPS. (e) Comparison of TNF-α secretion levels from THP1 macrophages differentiated with 50 ng/ml PMA for 72 h and subsequently activated with different concentrations of LPS for 48 h. (f) Comparison of TNF-α secretion levels from THP1 macrophages differentiated with 50 ng/ml PMA for 72 h and subsequently activated with different concentrations of LPS and/or interferon-gamma (IFNg) for 48 h. Not significant (ns), *p<0.05, **p<0.01, ***p<0.001, ***p<0.0001, mean (SD); n=3-6, two-way ANOVA followed by Tukey's post-hoc test (a,c,d,f) and n=3-12, one-way ANOVA followed by Tukey's post-hoc test (b,d,e).

I then verified these THP1 macrophage EVs first by characterizing them via NTA (Figure 2.4a,b). Next, TEM images showed distinctive individual particles of THP1 macrophage EVs of a size range of approximately 100-150 nm in diameter, representative of EVs (Figure 2.4c,d). Immunoblotting showed EVs from non-activated and LPS-activated Raw264.7 cells expressed the EV biomarkers Alix and GAPDH (Figure 2.4e).

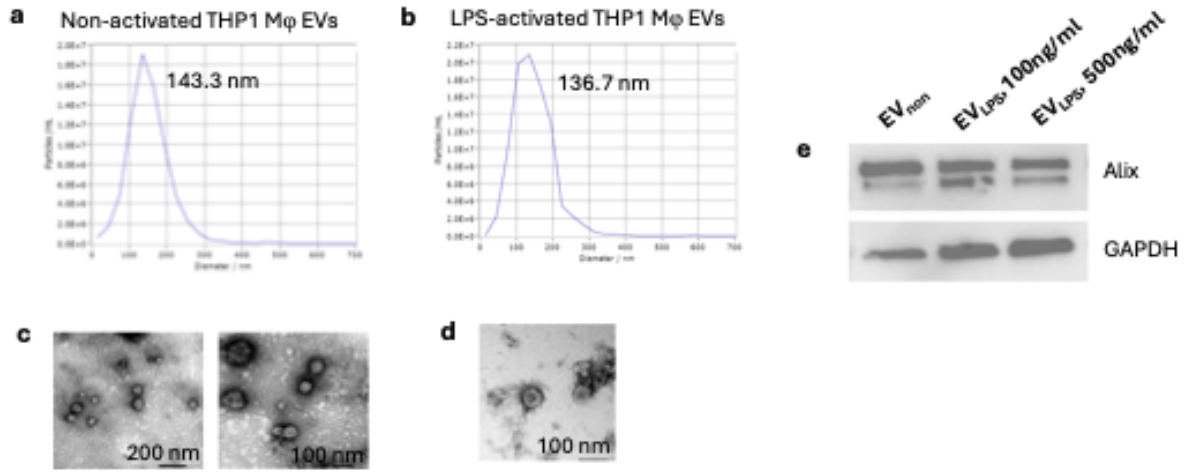

Figure 2.4 Characterization of extracellular vesicles (EVs) from THP1-differentiated macrophages (Mφ) that are non-activated or activated with lipopolysaccharide (LPS). (a,b) Size distribution curves of EVs from non-activated (a) and LPS-activated (b) THP1 macrophages. (c,d) Transmission electron microscopy (TEM) images of EVs from non-activated (c) and LPS-activated (d) THP1 macrophages; X30k scale bar, 200 nm; X50k scale bar, 100 nm. (e) Immunoblot analysis of EVs from non-activated and LPS-activated THP1 macrophages.

I was very excited to advance my studies using macrophages derived from a human leukemia cell line to more physiologically relevant monocytes and macrophages derived from induced pluripotent stem cells (iPSCs), to characterize EV communication with iPSC-derived 3D human colonic organoids (HCOs). However, reviewers of my F31 fellowship application for this project pointed out that it is very difficult to replicate the complexity of the tumor microenvironment in culture, and strongly recommended an in vivo model. So, I shifted my investigations into primary bone marrow-derived macrophages (BMDMs) from mice.

We harvested primary BMDMs from the bone marrow of C57Bl/6 mice and cultured them in 10 ng/ml M-CSF in DMEM supplemented with 10% FBS and antibiotics for 5-7 d. To confirm activation, I stimulated the BMDMs with different concentrations of LPS for 1 h (all not detected, data not shown), 12 h (Figure 2.5a), and 4 d (Figure 2.5b), and quantified optimal activation levels over time with assays measuring cell secretion of RNS.

I then seeded BMDMs with or without 100 ng/ml LPS and isolated EVs via differential ultracentrifugation. EVs from non-activated and LPS-activated BMDMs were counted, characterized and imaged in the NTA (Figure 2.6a,b). TEM images showed individual particles of approximately 120-150 nm in diameter, representative of EVs (Figure 2.6c,d). Immunoblotting verified EVs from non-activated and LPS-activated BMDMs to express the EV biomarker Alix (Figure 2.6e).

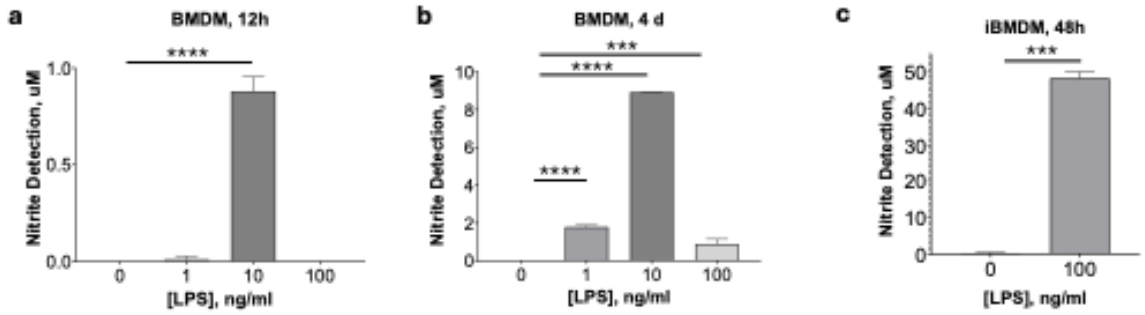

Figure 2.5 Reactive nitrogen species (RNS) are secreted by primary bone marrow derived macrophages (BMDMs) and immortalized BMDMs (iBMDMs) treated with lipopolysaccharide (LPS) at different concentrations and timepoints. (a,b) BMDMs were treated with different concentrations of LPS for 12 h (a) and 4 days (b). mean (SD), n=3, one-way ANOVA followed by Tukey's post-hoc test. iBMDMs were treated with 0 or 100 ng/ml LPS for 48 h. ***p<0.001, ****p<0.0001, mean (SD), n=12, unpaired t-test.

The number of EVs I was able to obtain from harvesting bone marrow was extremely low making the experiments impractical, considering the large number of EVs required. So, Dr. Meena Sudhakaran suggested I try immortalized BMDMs. Dr. Andrew Olive generously provided me with a vial of J2-immortalized iBMDM cells, which turned out to be essential for my in vitro and in vivo experiments. First, I stimulated the iBMDMs with different concentrations of LPS and quantified RNS nitrite secretion (Figure 2.5c). I found these iBMDM cells secreted approximately 5 times more nitrite than the BMDMs secreted after 4 d (Figure 2.5). This is most likely due to the concentration of cells seeded; the BMDMs were cultured at a lower density meaning there was a lower cell-to-media ratio and fewer cells were present to secrete RNS into the conditioned medium (CM) used for NO detection. In the literature, these iBMDM cells are reportedly similar to BMDM cells with regards to morphology, biomarker expression, and metabolism through M1 and M2 polarization states[128, 129].

Next, iBMDM EVs were counted, characterized and imaged in NTA (Figure 2.7a,b). TEM images showed individual particles of approximately 100-150 nm in diameter, representative of EVs (Figure 2.7c,d). Immunoblotting verified EVs from non-activated and LPS-activated iBMDMs to express the EV biomarkers Alix, Flot1, and CD81 (Figure 2.7e). The observed increase in Flot1 expression and decrease in CD81 expression in EVs after LPS stimulation may reflect changes in the subpopulations of EVs being secreted during inflammation, specifically an increase in microvesicle secretion (which contain more Flot1) and a decrease in exosomes (typically CD81-rich)[130].

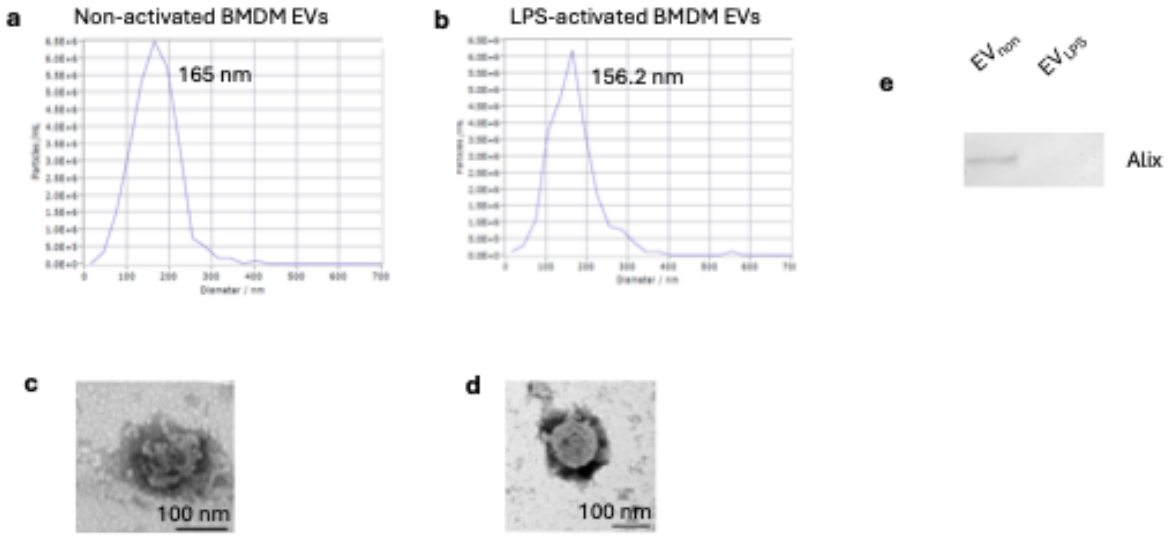

Figure 2.6 Characterization of extracellular vesicles (EVs) from primary bone marrow-derived macrophages (BMDMs) that are non-activated or activated with lipopolysaccharide (LPS). (a,b) Size distribution curves of EVs from non-activated BMDMs (a) and LPS-activated BMDMs (b). (c,d) Transmission electron microscopy (TEM) images of EVs from non-activated (c) and LPS-activated (d) BMDMs; X50k scale bar, 100 nm. (e) Immunoblot analysis of EV biomarkers in EVs from non-activated and LPS-activated BMDMs.

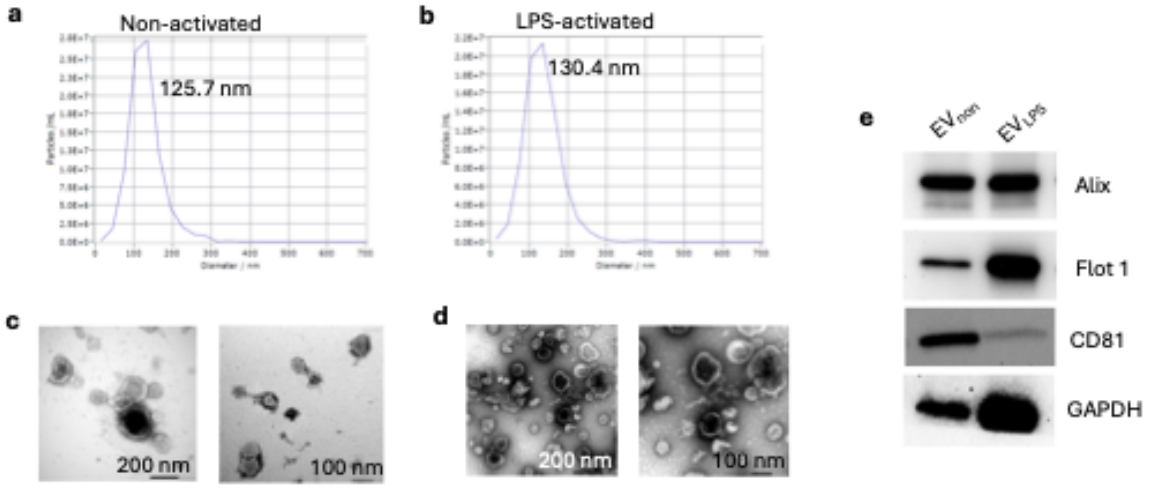

Figure 2.7 Characterization of extracellular vesicles (EVs) from immortalized bone marrow-derived macrophages (iBMDMs) that are non-activated or activated with lipopolysaccharide (LPS). (a,b) Size distribution curves of EVs from non-activated (a) and LPS-activated iBMDMs (b). (c,d) Transmission electron microscopy (TEM) images of EVs from non-activated (c) and LPS-activated (d) iBMDMs; X30k scale bar, 200 nm; X50k scale bar, 100 nm. (e) Immunoblot analysis of EVs from non-activated and LPS-activated iBMDMs.

EVs from LPS-activated macrophages express protein profiles distinct from EVs from non-activated macrophages

Next, I wanted to know if there was a difference in protein contents between EVs from non-activated and LPS-activated macrophages. I also compared the protein profiles of soluble factors (SFs), which I defined as the cell-secreted free-floating proteins and other soluble factors remaining in the supernatant after ultracentrifuge isolation of EVs from conditioned medium (CM). To test my hypothesis that EVs from LPS-activated macrophages mediate colitis-associated cancer, I performed proteomics analysis comparing protein contents in EVs from LPS-activated iBMDM EVs with EVs from non-activated iBMDM EVs. I was particularly interested in proteins that may be involved in proinflammatory and pro-tumorigenic signaling effects. So, I profiled the protein contents of non-activated and LPS-activated iBMDM and THP1 macrophage EVs and SFs via mass spectrometry, with generous help from Dr. Maryam Sayadi with the data analysis.

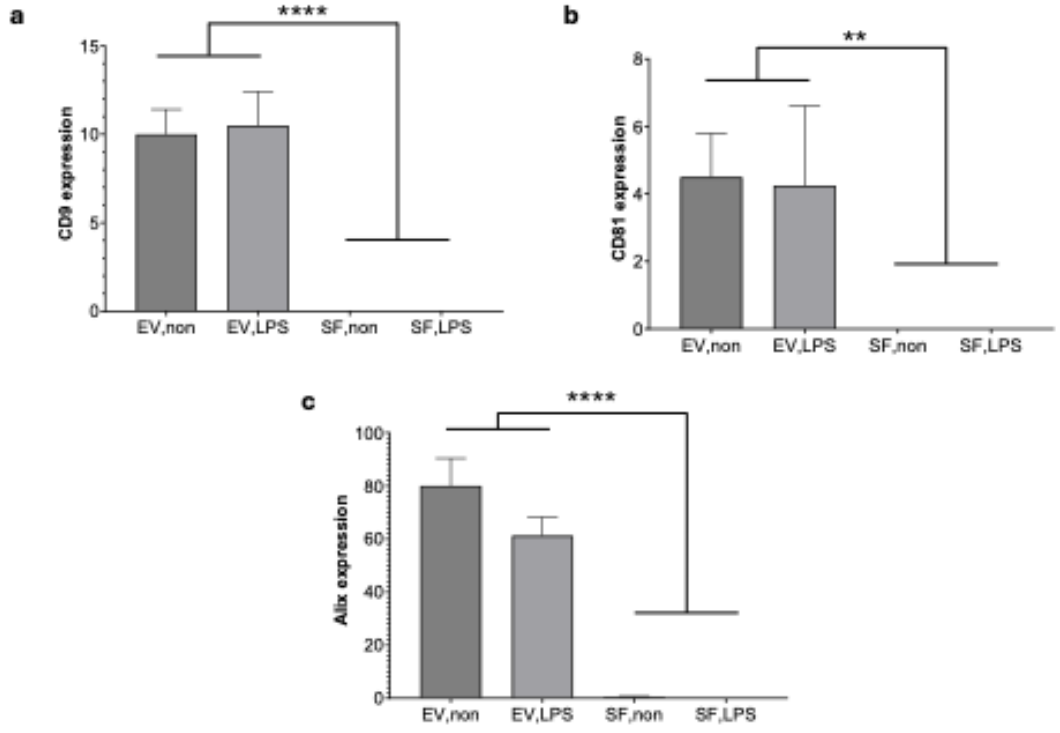

Figure 2.8 Mass spectrometry detected presence of biomarkers of extracellular vesicles (EVs) expressed on EVs from non-activated and LPS-activated immortalized bone marrow-derived macrophages (iBMDMs) but not soluble factors (SFs) as expected. (a-c) Expression of tetraspanin CD9 (a), tetraspanin CD81 (b), and multi-pass membrane protein Alix (c) on EVs from non-activated iBMDMs (EV,non), EVs from LPS-activated iBMDMs (EV,LPS), SFs from non-activated iBMDMs (SF,non), and SFs from LPS-activated iBMDMs (SF,LPS) as detected by mass spectrometry. **p<0.01, ****p<0.0001, mean (SD), n=4, one-way ANOVA followed by Tukey's post-hoc test.

Analyzing this data, I first looked at expression levels of several individual EV biomarkers. As expected, EVs from both non-activated and LPS-activated iBMDMs expressed known biomarkers of EVs including the tetraspanins CD9, CD81, and the multi-pass membrane protein Alix, whereas mass spectrometry did not detect these EV biomarkers in SFs secreted from iBMDMs (Figure 2.8).

Next, we compared expression levels of all proteins identified in mass spectrometry analysis between two conditional groups at a time. EVs from LPS-activated iBMDMs (denoted EV_{LPS}) contained a significant number of differentially expressed proteins as compared to EVs from non-activated iBMDMs (EV_{non}), as seen by the purple and green bars remaining separate on Figure 2.9a. Principal component (PC) analysis confirmed the differential expression of population of proteins present in these conditions were significantly different from each other as visualized by the PC graph in Figure 2.9e. We then generated a volcano plot showing the significantly up- and down-regulated proteins in EVs from LPS-activated iBMDMs relative to EVs from non-activated iBMDMs (Figure 2.9f). We also compared relative large-scale protein expression of SFs from iBMDMs that were non-activated and LPS-activated (Figure 2.9b). Surprisingly, we found that overall, these protein populations were not significantly different as can also be visualized in PC analysis (Figure 2.9g). Because this is the fraction that theoretically contains cell-secreted proteins such as cytokines, that are being investigated at therapeutic targets in the clinic, we ran a volcano plot to show up- and down-regulated proteins expressed in SF_{LPS} as compared with SF_{non} (Figure 2.9h). Heat map analysis also showed that SFs and EVs have different protein profiles compared with each other, when secreted by either LPS-activated or non-activated iBMDMs (Figure 2.9c,d).

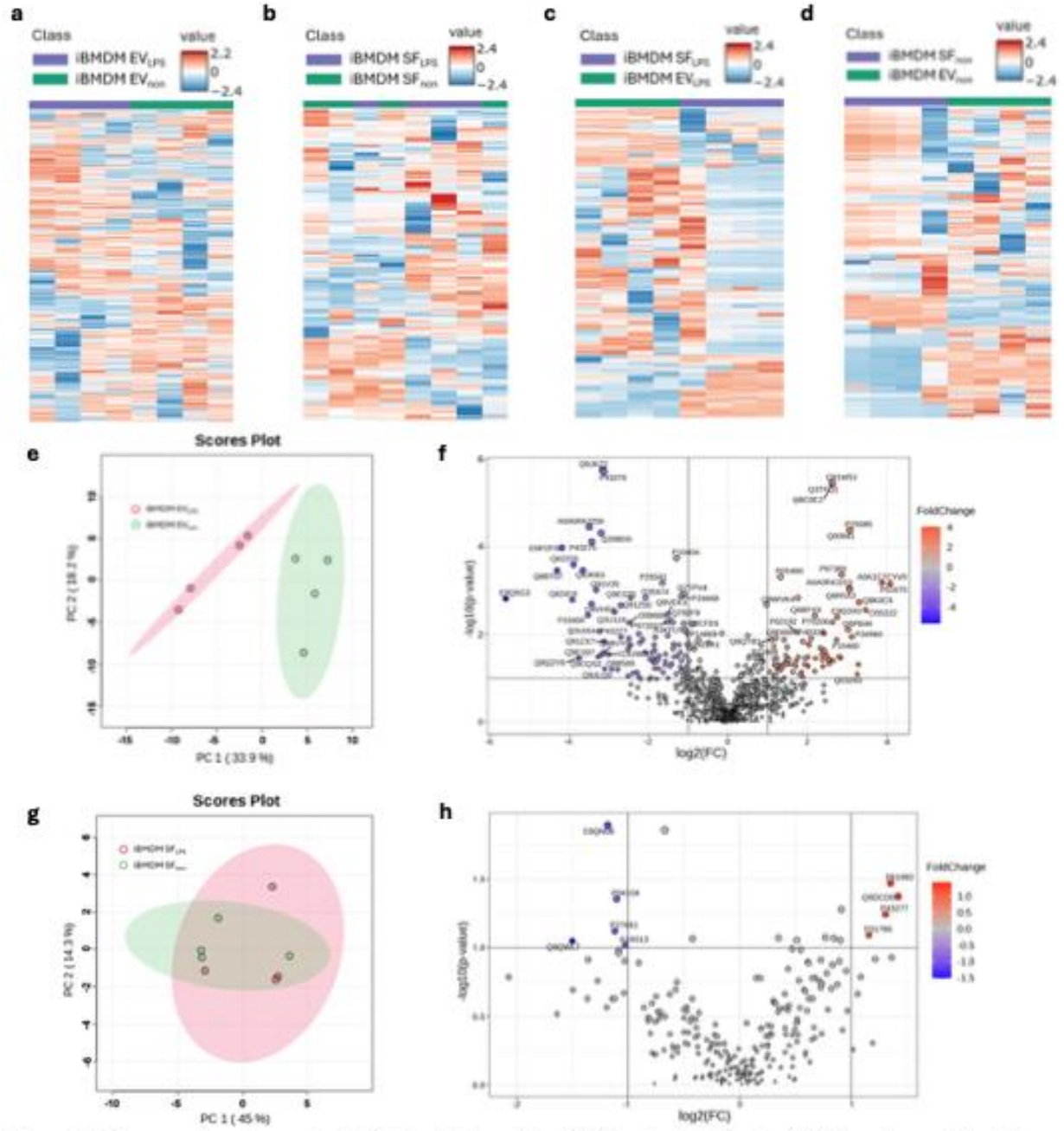

Figure 2.9 Mass spectrometry analysis of extracellular vesicles (EVs) and soluble factors (SFs) from immortalized bone marrow-derived macrophages (iBMDMs) that are non-activated or activated with 100 ng/ml lipopolysaccharide (LPS). (a) Heat map showing differentially expressed proteins in EVs from LPS-activated iBMDMs (EV_{LPS}) and EVs from non-activated iBMDMs (EV_{non}). (b) Heat map showing limited differential expression of proteins in SFs from LPS-activated iBMDMs (SF_{LPS}) compared with SFs from non-activated iBMDMs (SF_{non}). (c) Heat map showing differential expression of proteins in SF_{LPS} compared with EV_{LPS}. (d) Heat map showing differential expression of proteins in SF_{non} compared with EV_{non}. (e) Principal component (PC) analysis of proteins from EV_{LPS} and EV_{non}. (f) Volcano plot showing up- (red) and down-regulated (blue) proteins expressed in EV_{LPS} relative to EV_{non} as reference; fold change set to 2, $p < 0.1$. (g) PC analysis of proteins from SF_{LPS} and SF_{non}. (h) Volcano plot showing up- (red) and down-regulated (blue) proteins expressed in SF_{LPS} relative to SF_{non}; fold change set to 2, $p < 0.1$.

a

Category	Term	RT	Genes	Count	%	P-Value	Benjamini
KEGG_PATHWAY	Proteasome	RT		7	4.0	2.0E-5	1.5E-3
KEGG_PATHWAY	Prion disease	RT		14	8.0	2.0E-5	1.5E-3
KEGG_PATHWAY	Endocytosis	RT		14	8.0	2.1E-5	1.5E-3
KEGG_PATHWAY	Alzheimer disease	RT		15	8.6	2.2E-4	1.1E-2
KEGG_PATHWAY	Epstein-Barr virus infection	RT		11	6.3	4.5E-4	1.9E-2
KEGG_PATHWAY	Lysosome	RT		8	4.6	1.2E-3	4.4E-2
KEGG_PATHWAY	Phagosome	RT		9	5.2	1.5E-3	4.6E-2
KEGG_PATHWAY	Amyotrophic lateral sclerosis	RT		13	7.5	1.7E-3	4.6E-2
KEGG_PATHWAY	Parkinson disease	RT		10	5.7	5.0E-3	1.2E-1
KEGG_PATHWAY	Spinocerebellar ataxia	RT		7	4.0	7.3E-3	1.6E-1
KEGG_PATHWAY	Leishmaniasis	RT		5	2.9	1.0E-2	1.8E-1
KEGG_PATHWAY	Coronavirus disease - COVID-19	RT		9	5.2	1.1E-2	1.8E-1
KEGG_PATHWAY	Huntington disease	RT		10	5.7	1.1E-2	1.8E-1
KEGG_PATHWAY	Pathways of neurodegeneration - multiple diseases	RT		13	7.5	1.2E-2	1.8E-1
KEGG_PATHWAY	Bacterial invasion of epithelial cells	RT		5	2.9	1.4E-2	1.9E-1
KEGG_PATHWAY	Viral carcinogenesis	RT		8	4.6	2.0E-2	2.7E-1
KEGG_PATHWAY	Viral life cycle - HIV-1	RT		4	2.3	3.8E-2	4.7E-1
KEGG_PATHWAY	Aminoacyl-tRNA biosynthesis	RT		4	2.3	4.6E-2	5.4E-1
KEGG_PATHWAY	Necroptosis	RT		6	3.4	6.2E-2	6.9E-1
KEGG_PATHWAY	Platelet activation	RT		5	2.9	6.5E-2	6.9E-1
KEGG_PATHWAY	Tuberculosis	RT		6	3.4	6.8E-2	6.9E-1
KEGG_PATHWAY	Biosynthesis of amino acids	RT		4	2.3	7.1E-2	6.9E-1
KEGG_PATHWAY	Osteoclast differentiation	RT		5	2.9	8.2E-2	7.6E-1

b

Protein ID	Protein Name	FC (EV)	FC (MC38)
P16460	ASS1	2.8254	1.3753
P13020	GNS	-1.5571	-1.3

Figure 2.10 Mass spectrometry shows extracellular vesicles (EVs) from lipopolysaccharide (LPS)-activated immortalized bone marrow-derived macrophages (iBMDMs) express upregulated levels of argininosuccinate synthase 1 (ASS1) and downregulated levels of gelsolin (GSN) protein relative to non-activated iBMDM EVs. (a) Functional annotation chart showing pathway enrichment analysis determined a list of signaling pathways (Terms) found to be differentially expressed in LPS-activated iBMDM EVs relative to non-activated iBMDM EVs via the KEGG database; also shown in table includes related terms (RT) i.e. related pathways, the number of proteins detected that participate in a particular pathway (count), percent involved proteins / total proteins (%), p-value showing significance, and Benjamini correction refers to false discovery rate. (b) Proteins of interest differentially expressed in LPS-activated iBMDM EVs and MC38 colon cells treated with LPS-activated iBMDM EVs; table shows fold change (FC) of expression in LPS-activated iBMDM EVs compared with non-activated iBMDM EVs (FC(EV)) and FC of expression in MC38 cells treated with EVs from LPS-activated iBMDMs compared with MC38 cells treated with EVs from non-activated iBMDMs (FC(MC38)).

We performed Pathway Enrichment Analysis on this data and discovered several pathways significantly up- or down-regulated in EV_{LPS} (Figure 2.10a) suggesting many potential therapeutic targets. Of these, we chose to investigate proteins that were found to be up- and down-regulated in LPS-activated iBMDM EVs and similarly in a colon cancer cell line (MC38) that was treated with these iBMDM EVs (see Chapter 3, Figure 3.9-3.12). Interestingly, Argininosuccinate synthase (ASS1) was detected to be upregulated in LPS-activated iBMDM EVs, and Gelsolin (GSN) was detected to be downregulated in EVs from LPS-activated iBMDMs relative to EVs from non-activated iBMDMs (Figure 2.10b). These proteins are also known to play a role in colitis-associated cancer.

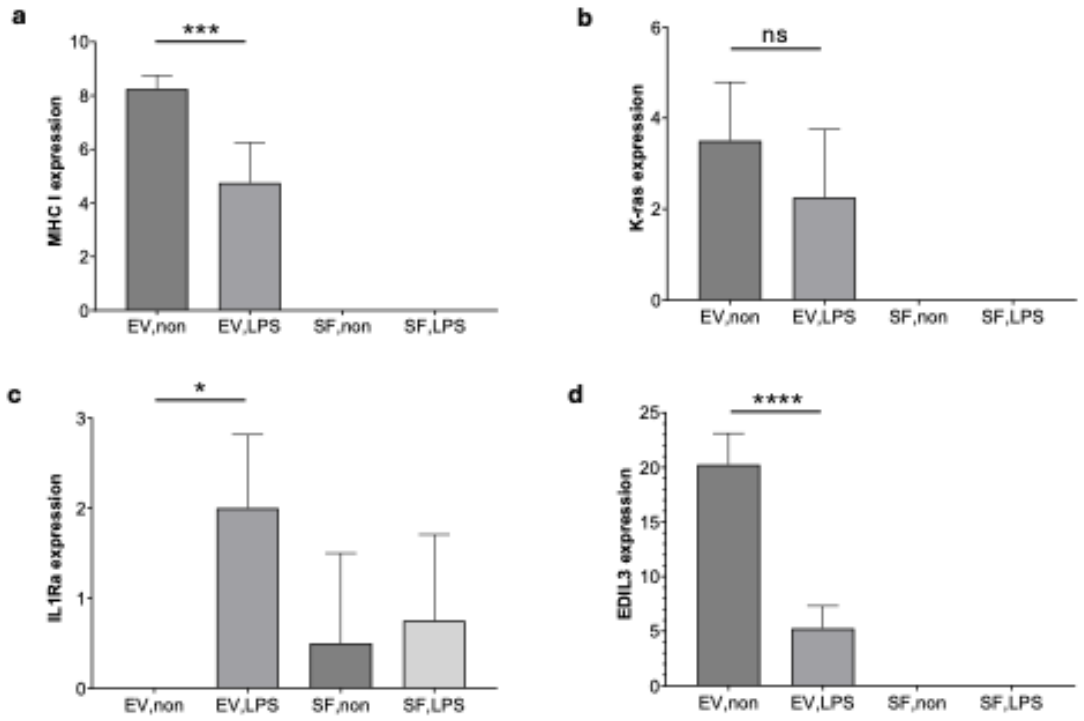

Figure 2.11 Comparison of mass spectrometry detected expression of markers involved in colitis-associated cancer on extracellular vesicles (EVs) and soluble factors (SFs) from non-activated and LPS-activated immortalized bone marrow-derived macrophages (iBMDMs). (a-d) Expression of major histocompatibility complex I (MHC I, a), K-ras (b), interleukin 1 receptor antagonist (IL1Ra, c), and EGF like repeats and discoidin domains 3 (EDIL3, d) on EVs from non-activated iBMDMs (EV,non), EVs from LPS-activated iBMDMs (EV,LPS), SFs from non-activated iBMDMs (SF,non), and SFs from LPS-activated iBMDMs (SF,LPS) as detected by mass spectrometry. Not significant (ns), *$p<0.05$, ***$p<0.001$, ****$p<0.0001$, mean (SD), n=4, one-way ANOVA followed by Tukey's post-hoc test (a,b,d significance only shown between groups containing non-zero values).

From these mass spectrometry data, we also investigated relative expression levels of several markers previously reported to mediate or be associated with inflammation and colitis-associated cancer, namely major histocompatibility complex I (MHC I), K-ras, interleukin 1 receptor antagonist (IL1Ra), and EGF like repeats and discoidin domains 3 (EDIL3). Notably, mass spectrometry detected EVs from LPS-activated iBMDMs to contain downregulated expression of MHC I and EDIL3, and upregulated expression of IL1Ra (Figure 2.11). No significant change was detected in K-ras expression levels between EVs from non-activated and LPS-activated iBMDMs. Mass spectrometry results detected MHC I, K-ras, and EDIL3 proteins to be expressed in EVs from iBMDMs but not detectable by mass spectrometry in SFs (Figure 2.11).

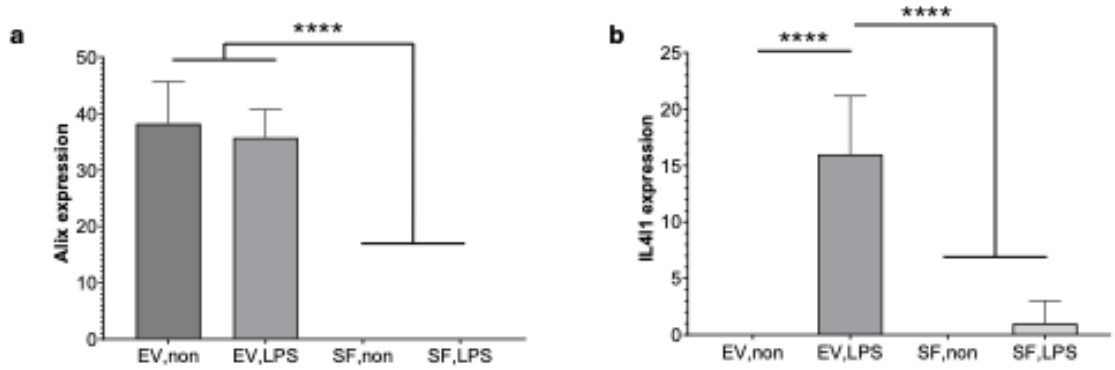

Figure 2.12 Mass spectrometry detected presence of biomarkers of extracellular vesicles (EVs) expressed on EVs from non-activated and LPS-activated THP1-derived macrophages but not soluble factors (SFs) as expected. (a) Expression of multi-pass membrane protein Alix on EVs from non-activated THP1 macrophages (EV,non), EVs from LPS-activated THP1 macrophages (EV,LPS), SFs from non-activated THP1 macrophages (SF,non), and SFs from LPS-activated THP1 macrophages (SF,LPS) as detected by mass spectrometry. (b) Expression of interleukin-4-induced-1 (IL4I1), that can facilitate colon cancer progression, in all conditions. *p<0.05, **p<0.01, ***p<0.001, ****p<0.0001, mean (SD), n=4, one-way ANOVA followed by Tukey's post-hoc test.

We also performed mass spectrometry analysis on EVs and SFs from THP1-differentiated macrophages with and without LPS activation. This data showed the EV biomarker Alix to be expressed in EVs from both non-activated and LPS-activated THP1 macrophages, but not in SFs from either condition (Figure 2.12a). Furthermore, we looked at another protein reported to facilitate colitis-associated cancer, namely interleukin-4-induced-1 (IL4I1). Mass spectrometry detected a significantly upregulated expression of IL4I1 in EVs from THP1 macrophages activated with LPS as compared to EVs from non-activated THP1 macrophages (Figure 2.12b). Expression of IL4I1 was not detectable in EVs or SFs from non-activated THP1 macrophages, but one sample of the SFs from LPS-activated THP1 macrophages showed slightly, but not significantly, elevated expression.

EVs from iBMDMs induce short-term colonic inflammation in APC$^{min/+}$ mice

Next, to determine the effects of injecting these inflammatory EVs orthotopically into the colons of mice, we consulted with Dr. Stephan Rogalla, a gastroenterologist at Stanford University with research expertise in advanced endoscopic techniques and early disease detection in vivo. The small diameter, thinness, and lack of visibility of the murine rectal submucosa[131] makes it challenging to inject. So, Dr. Rogalla generously hosted me at Stanford where we performed endoscopy-guided injections to visualize injections and ensure successful injection into the rectal submucosa specifically.

Interestingly, a group in Montreal investigated the oncogenic potential of cancer patient sera on fibroblasts in culture. They found that exosomes from the serum of breast cancer patients were taken

up by BRCA1 K/O fibroblasts at significantly (~6.6 times) higher rates than wildtype (WT) fibroblasts, and they concluded that tumor suppressor genes may block uptake of transformation-promoting EVs[132]. Colon cancer EVs were also found to increase transformation in BRCA K/O fibroblasts[133]. In colitis-associated colon cancer, two of the most common tumor suppressor gene mutations occur in the TP53 gene and the adenomatous polyposis coli (APC) gene in sequence[8]. The $APC^{min/+}$ mouse strain is heterozygous for an APC mutation, highly susceptible to spontaneous intestinal adenoma formation and a well-established model for colonic tumorigenesis[134] involving inflammation[135].

Dr. Rogalla generously provided several wildtype (WT) C57Bl/6J mice and $APC^{min/+}$ mice (16 weeks old) for my experiments. We injected WT and $APC^{min/+}$ mice with 100 µl saline (PBS), or EVs from iBMDMs that were non-activated or LPS-activated into the rectal submucosa three times over the span of one week. Prior to injection, fecal matter was cleaned out for visualization, and the inside of the rectum was sufficiently lubricated with a needle-less syringe containing PBS before inserting the bronchoscope containing a camera and an injection needle. The length of the tube holds approximately 3 ml of fluid, so the tube was front loaded to avoid wasting EV solution. We took up 50-100 µl of fluid from the head of the endoscope and inserted the endoscope into the mouse. Mice that experienced abdominal swelling caused by perforations were immediately humanely euthanized (this partially accounts for the low sample size in our experiments). Figure 2.13 shows images of successful injections, where the needle was inserted into the rectal submucosa (left images) and fluid was injected (right images). After injections on day 7, mice in the following treatment groups remained eligible for characterization: WT mice injected with PBS (n=4), WT mice injected with EVs from LPS-activated iBMDMs (n=1), $APC^{min/+}$ mice injected with PBS (n=2), $APC^{min/+}$ mice injected with EVs from non-activated iBMDMs (n=1), and $APC^{min/+}$ mice injected with EVs from LPS-activated iBMDMs (n=4). 16-week-old $APC^{min/+}$ mice are not easily available and increasing the sample size in these studies was not feasible.

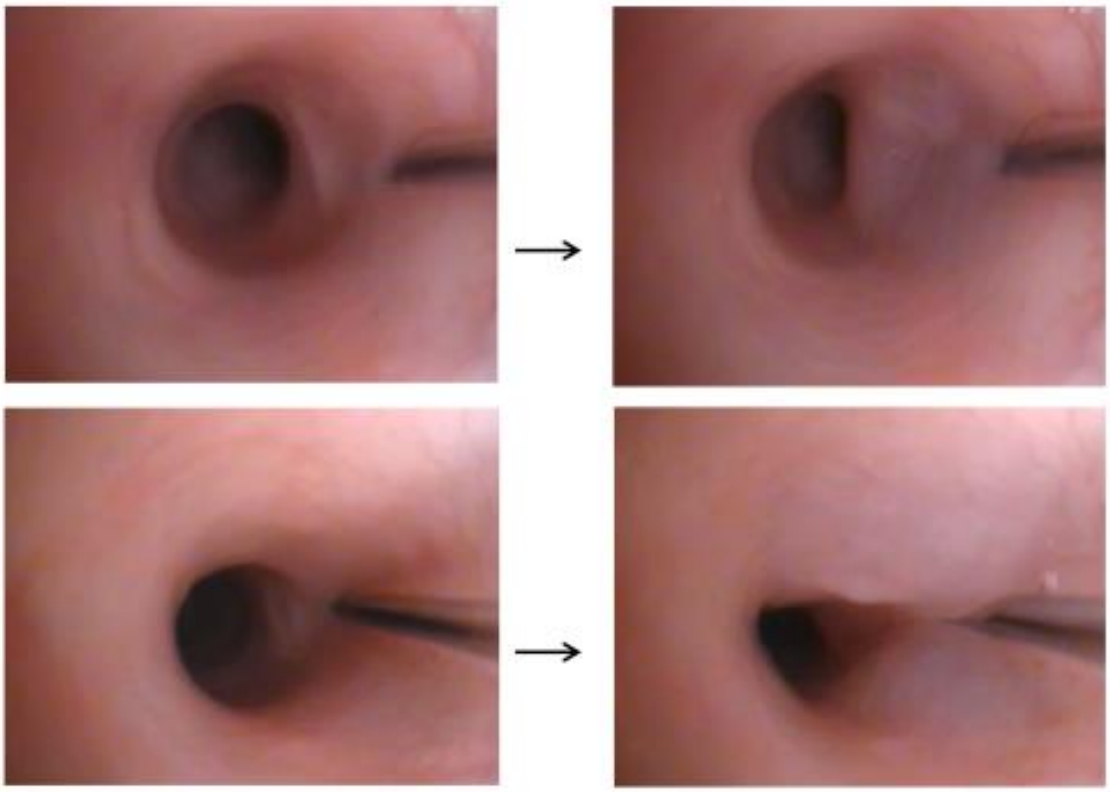

Figure 2.13 Endoscopy images showing before (left) and after (right) injecting 100 µl of treatment into the rectal submucosa of mice; guided by pediatric bronchoscope.

One week post injection, mice were sacrificed and the colon tissues were harvested for analysis. Dr. Victoria Watson, DVM , PhD, DACVP (College of Veterinary Medicine, Michigan State University) performed histopathology analyses on inflammatory changes in these tissues. H&E sections showed inflammatory effects of iBMDM EVs on $APC^{min/+}$ mouse colons (Figure 2.15) but not WT mice (Figure 2.14). Specifically, no change was found in inflammation score, submucosa depth, thickness of muscularis mucosa, or of the lamina propria in WT mice (Figure 2.14d-g). Notably, despite a limiting sample size, there were significant increases in inflammation score of colons from $APC^{min/+}$ mice injected with non-activated and LPS-activated iBMDM EVs relative to PBS controls (Figure 2.15d), indicating that the injections themselves were not inducing inflammation, and that macrophage-secreted EVs have a proinflammatory effect regardless of whether the cells have been stimulated with LPS. We concluded that the preexisting APC tumor suppressor mutation allowed for LPS-activated macrophage EVs to have a proinflammatory effect on the mouse colons even in the short time span of 1 week. The lack of effects

in WT mice may be due to short-term protective immune mechanisms that combat macrophage EV effects. In clinical cases of colitis-associated cancer, it may take years for tumors to form; one week may not have been long enough to induce an effect in WT mice. However, the first "hit", i.e., the underlying APC^{min} mutation, appears to have allowed for proinflammatory signaling effects induced by the iBMDM EVs. An increased sample size and further immunophenotyping characterization will be helpful in identifying the exact mechanism for why non-activated iBMDM EVs and LPS-activated iBMDM EVs both played proinflammatory roles. More in-depth histopathological analyses of the $APC^{min/+}$ mouse colon tissue showed that injections of EVs from non-activated and LPS-activated iBMDMs mildly increased thickening of the submucosa, a hallmark of colonic inflammation (Figure 2.15e). Thickness of the muscularis mucosa was very mildly increased in $APC^{min/+}$ mouse colons injected with LPS-activated iBMDM EVs (Figure 2.15f), and no significant change was seen in lamina propria depth (Figure 2.15g).

Tables 2.2 and 2.3 show even deeper characterization of inflammation in these EV-injected mice. Other methods we utilized to quantitatively and qualitatively describe tissue inflammation included crypt architecture, muscle thickening, luminal bacteria, epithelial injury, and degree of inflammatory cell infiltration (descriptions and scores in Table 2.2), as well as description of inflammatory cells found present in the tissue section and a description of histological effects from this inflammatory infiltrate (Table 2.3). In $APC^{min/+}$ mice, rare, clear regions with loss of crypts was found in the non-activated iBMDM EV-injected condition, whereas one of the four LPS-activated iBMDM EV-injected mice showed a more severe crypt loss (score of 1). None of the WT mice showed changes in crypt architecture, and none of the mice of either genotype showed signs of muscle thickening (Table 2.2). There were few or many clusters of luminal bacteria found in the WT mice, however, most of the $APC^{min/+}$ mice appeared to have rare or no luminal bacteria present (Table 2.2). Epithelial injury (% of mucosa length) was found in the colon tissue from $APC^{min/+}$ mouse injected with non-activated iBMDM EVs (Figure 2.15b), with the injury (likely an ulcer) spanning appx 19% of the length of the mucosa.

We used non-injected WT mice as reference for relatively normal amounts of inflammation in this study (Table 2.3). In $APC^{min/+}$ mice injected with PBS, lymphocytes were mostly within normal limits, with mucus in lumen, and one mouse showed a couple of dilated lymphatics in deep mucosa and one nodular aggregate of gut-associated lymphatic tissue (GALT). This seemed to be relatively similar to the WT mice. $APC^{min/+}$ mice injected with non-activated iBMDM EVs interestingly showed presence of neutrophils and less so macrophages, lymphocytes and plasma cells in the submucosa as well as in the muscle/serosa (Table 2.3). $APC^{min/+}$ mice injected with EVs from LPS-activated iBMDMs exhibited dilated vessels in the deeper mucosa of a couple of tissues, one of which also had dilated crypts. Three of four

of these mice had a GALT aggregate or a large region of GALT (Table 2.3). WT mice injected with PBS or EVs from LPS-activated iBMDMs also contained some GALT aggregates, low numbers of lymphocytes and plasma cells, and a few mildly dilated blood vessels.

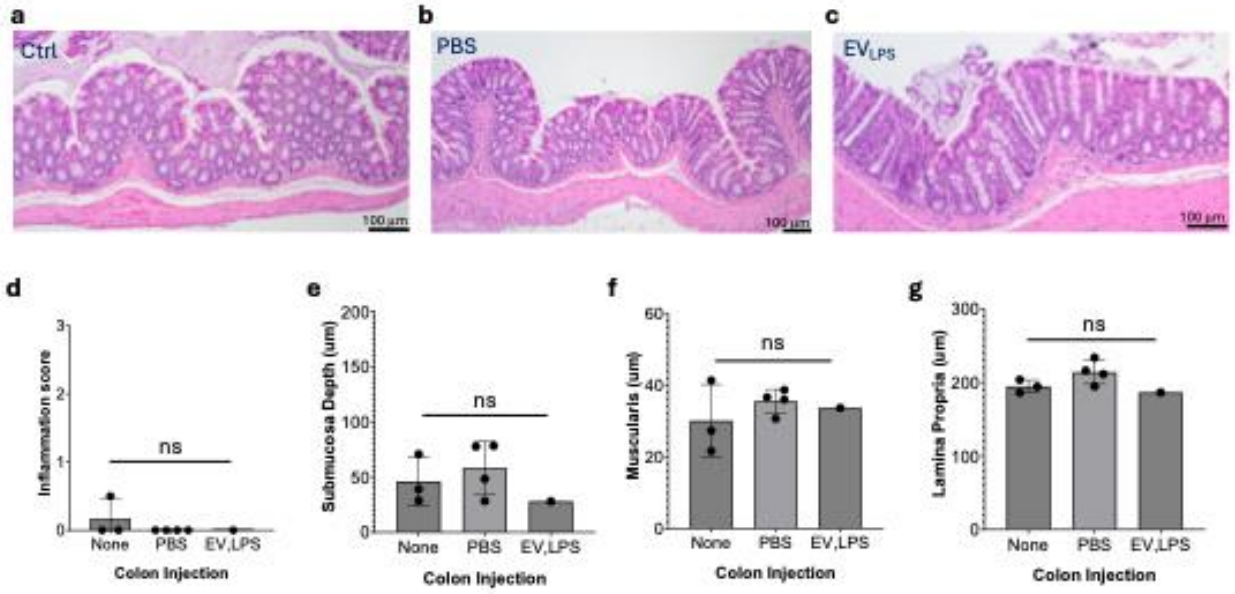

Figure 2.14 Rectal submucosal injections of extracellular vesicles (EVs) from immortalized bone marrow-derived macrophages (iBMDMs) activated with lipopolysaccharide (LPS) do not increase short-term colonic inflammation in wildtype (WT, C57Bl/6) mice. (a-c) Representative H&E-stained images of WT mouse colon with no injections (a, Ctrl) or injected with PBS (b) or LPS-activated iBMDM EVs (c); X10 scale bar, 100 μm. (d-g) Pathological quantifications showing inflammation score (scale 0-3, d), depth of submucosa in μm (e), muscularis mucosa thickness in μm (f), and depth of mucosal lamina propria in μm (g). Not significant (ns), n=1-4, one-way ANOVA followed by Tukey's post-hoc test.

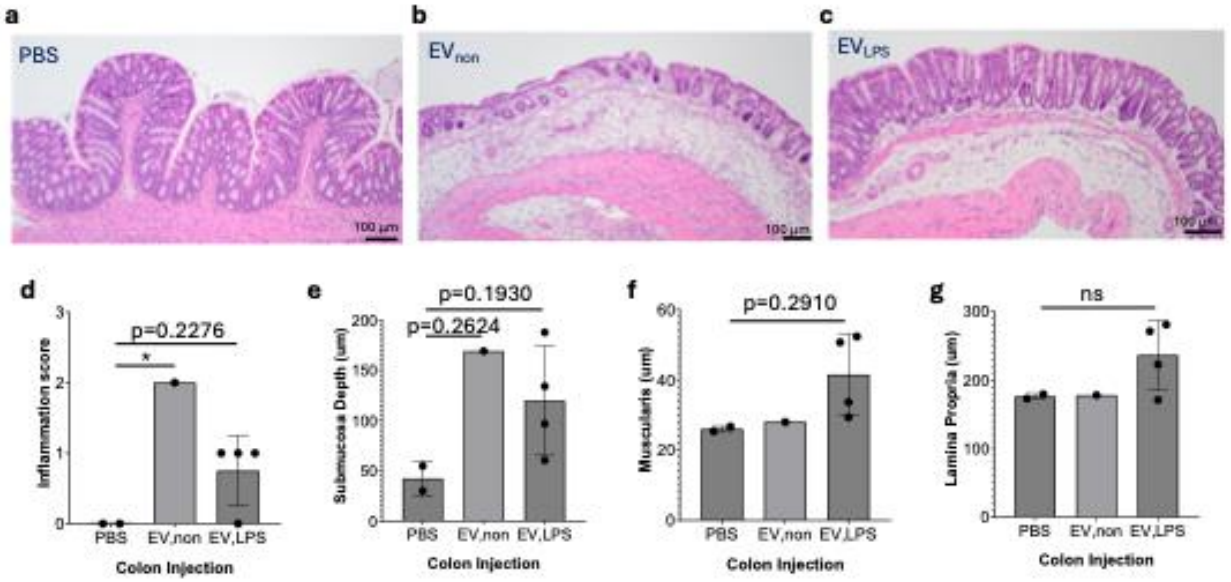

Figure 2.15 Rectal submucosal injections of extracellular vesicles (EVs) from immortalized bone marrow-derived macrophages (iBMDMs) activated with lipopolysaccharide (LPS) increased colonic inflammation in mice with APC^{min} mutation. (a-c) Representative H&E-stained images of colons from APC^{min} mice injected with PBS (a), non-activated iBMDM EVs (EV_{non}, b), and LPS-activated iBMDM EVs (EV_{LPS}, c); X10 scale bar, 100 μm. (d-g) Pathological quantifications showing inflammation score (scale 0-3, d), depth of submucosa in um (e), muscularis mucosa thickness in um (f), and depth of mucosal lamina propria in um (g). Not significant (ns), *$p<0.05$; n=1-4, one-way ANOVA followed by Tukey's post-hoc test (p-values shown for $p<0.3$).

Table 2.2 Scale or description of crypt architecture, muscle thickening, luminal bacteria, epithelial injury, and degree of inflammatory cell infiltration from histopathology analysis of H&E-stained colon tissues of given injection conditions. $APC^{min/+}$ mouse model (APC^{min}), wild type (WT), saline (PBS), extracellular vesicles (EVs), extracellular vesicles from non-activated macrophages (EV_{non}), lipopolysaccharide (LPS), extracellular vesicles from LPS-activated macrophages (EV_{LPS}).

Mouse	**Condition**	**Crypt architecture (0 - 3)** **0: normal** **0.5: rare, clear regions with loss of crypt** **3: severe crypt distortion, loss of entire crypts**	**Muscle thickening (0 – 3)** **0: base of crypt sits on muscularis mucosae** **3: marked muscle thickening**	**Luminal bacteria**	**Epithelial injury (% of mucosa length)**	**Degree of inflammatory cell infiltration (0 – 3)** **0: normal** **3: dense inflammatory infiltrate**
APC^{min}	PBS	0	0	none	0	0
APC^{min}	PBS	0	0	rare	0	0
APC^{min}	EV_{non}	0.5	0	none	19.178	2
APC^{min}	EV_{LPS}	1	0	rare	0	1
APC^{min}	EV_{LPS}	0	0	none	0	0
APC^{min}	EV_{LPS}	0	0	none	0	1
APC^{min}	EV_{LPS}	0	0		0	1
WT	No injection	0	0	none	0	0
WT	No injection	0	0	few clusters	0	0
WT	No injection	0	0	none	0	0.5
WT	PBS	0	0	none	0	0
WT	PBS	0	0	few clusters	0	0
WT	PBS	0	0	many clusters	0	0
WT	PBS	0	0	rare	0	0
WT	EV_{LPS}	0	0	few clusters	0	0

Table 2.3 Description of inflammatory infiltrate and inflammation from histopathology analysis of H&E-stained colon tissues of given injection conditions. Phosphate buffered saline solution (PBS), extracellular vesicles (EV), non-activated iBMDMs (non), lipopolysaccharide (LPS), within normal limits (WNL), plasma cells (PC), lamina propria (LP), gut-associated lymphatic tissue (GALT), submucosa (SM).

Mouse	Condition	Inflammation	Description
APCmin	PBS	mostly lymphocytes WNL	Couple of dilated lymphatics in deep mucosa, one nodular aggregate of GALT, strands of mucus in lumen
APCmin	PBS	mostly lymphocytes WNL	Mucus in lumen
APCmin	EV_{non}	SM contains scattered neutrophils, fewer macrophages and lymphocytes and PC, similar population in muscle/serosa	
APCmin	EV_{LPS}	low numbers of lymphocytes in LP, perivasc mixed mononucs in SC, mixed inflammation in serosa	Dilated vessels in deeper mucosa and SM. Dilated crypts, large region of GALT
APCmin	EV_{LPS}	low numbers of lymphocytes and PC in LP	One GALT aggregate
APCmin	EV_{LPS}	aggregate of neutrophils in lumen, mild increase PC in LP	Dilated vessels in deeper mucosa
APCmin	EV_{LPS}	low numbers of lymphs in LP, perivasc mixed mononucs in SC, mixed inflammation in serosa, few neutrophils in lumen	Large region of GALT
WT	No injection	mostly lymphocytes WNL	Few minimally dilated lymphatics in deep mucosa, couple of dilated lymphatics in submucosa, mucus in lumen, 1 nodule GALT
WT	No injection	mostly lymphocytes WNL	Mucus in lumen
WT	No injection	low numbers lymphs in LP, very rare neutrophils	Mucus in lumen, few mildly dilated lymphatics in deep mucosa
WT	PBS	low numbers of lymphocytes in LP	Dilated blood vessels focally in SM
WT	PBS	low numbers of lymphocytes and PC in LP	Dilated blood vessels focally in SM
WT	PBS	low numbers of lymphocytes and PC in LP	One GALT aggregate, one dilated lacteal SM
WT	PBS		One large GALT aggregate, few dilated lacteals at base of mucosa
WT	EV_{LPS}	low numbers of lymphocytes in LP	Clusters of bacteria in mucus in lumen, mesenteric fat in section

We cannot directly compare thickness and size of colon tissues between WT (C57Bl/6) and $APC^{min/+}$ mice due to their significant size difference. To quantitatively compare the inflammatory response of $APC^{min/+}$ mice to WT mice upon rectal submucosal injections of iBMDM EVs, we compared the fold change in submucosa depth, muscularis thickness, and depth of lamina propria (Figure 2.16). We found that $APC^{min/+}$ mice exhibited a moderately increased thickness in tissue from each of these parameters.

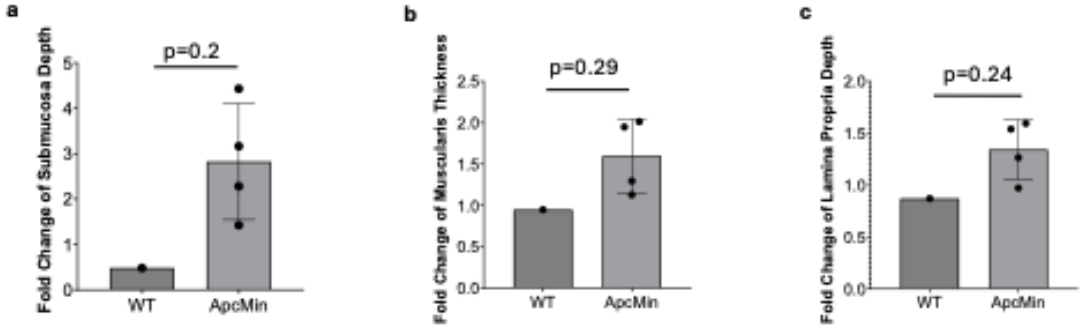

Figure 2.16 Rectal submucosal injections of extracellular vesicles (EVs) from immortalized bone marrow-derived macrophages (iBMDMs) activated with lipopolysaccharide (LPS) increased colonic inflammation in mice with APC^{min} mutation but not WT mice. (a) Fold change of submucosal depth measured in colons from mice injected with LPS-activated iBMDM EVs (EV_{LPS}) relative to control mice of same mutation status injected with PBS. (b) Fold change of muscularis mucosa thickness in colons from mice injected with EV_{LPS} relative to control mice of same mutation status injected with PBS. (c) Fold change of depth of mucosal lamina propria in colons from mice injected with EV_{LPS} relative to control mice of same mutation status injected with PBS. P-values are shown for $p<0.3$; n=1-4, unpaired t-test.

Overall, we found EVs from LPS-activated macrophages differentially expressed proteins that are thought to play a role in colitis-associated cancer, and EVs from iBMDMs increased colonic inflammation in mice with an underlying mutation in the APC tumor suppressor gene within one week.

DISCUSSION

I conclude from the data presented in this chapter that lipopolysaccharide (LPS) activation induces macrophages to secrete extracellular vesicles (EVs) with unique protein contents, some of which are known to mediate colitis-associated cancer, and that macrophage-secreted EVs have inflammatory effects in vivo on colonic epithelium. I discovered LPS-activated macrophages differentially upregulated and downregulated expression of EV proteins (as a model for macrophages active in the context of colitis) relative to non-activated macrophages that may facilitate colitis-associated carcinogenesis.

In chronic ulcerations, breakage in the intestinal lining allows for luminal contents such as bacteria and bacterial components (e.g., LPS) to enter the mucosa, and in response the number of

macrophages increases in this environment[136]. Because there are significantly fewer macrophages and thus macrophage-secreted EVs present in homeostatic conditions, we expect that the proteins upregulated in EVs from LPS-activated macrophages, as compared to those in EVs from non-activated macrophages, will have a stronger effect in mediating colitis-associated cancer.

Differential macrophage activation

Toll-like receptors (TLRs) are a family of innate immune receptors known as pattern recognition receptors (PRRs) because they recognize and bind to pathogen-associated molecular patterns (PAMPs) present on common microbes and induce an innate immune response[137]. Gram-negative lipopolysaccharide (LPS) is the main activator of TLR4, and induces intestinal inflammation[138]. Importantly, LPS-induced TLR4 signaling has been shown to increase colitis-associated carcinogenesis, cancer progression and metastasis[139]. Moreover, TLR4 is overexpressed in patients with colitis-associated cancer, and promotes colitis-associated neoplasia in mice[140]. TLR4 signaling utilizes accessory proteins such as CD14 and LBP to activate a series of transcription factors including nuclear factor kappa-light-chain-enhancer of activated B cells (NF-κB), activator protein-1 (AP-1), and signal transducer and activator of transcription 3 (STAT3), resulting in increased production of factors such as nitric oxide synthase 2 (iNOS) and tumor necrosis factor-alpha (TNF-α). LPS/TLR4-induced secretion of iNOS and TNF-α has been shown to be upregulated in colitis-associated cancer patients[141]. Importantly, LPS also induces negative regulatory pathways of inflammation including anti-inflammatory IL-10 signaling[142]. TLR4 also induces activity of the cyclooxygenase-2 (COX2) enzyme, which, which given the substrate arachidonic acid, increases prostaglandin E2 (PGE_2) production[143]. Both COX2 and PGE_2 have been highly implicated in driving colitis-associated cancer, and elevated expression of COX2 prevalent in CRC tissue is associated with worse prognosis[14]. Selective COX2 inhibitors and non-steroidal anti-inflammatory drugs have been of the most promising chemopreventive therapeutics in patients with colitis at risk of cancer[14]. However, these studies have been inconsistent for decades[18], suggesting there are other signaling mediators involved. This is why we decided to investigate the role of another signaling factor known to mediate colitis and colon cancer—extracellular vesicles (EVs).

Many studies have looked at EVs from macrophages that had been activated with LPS in combination with interferon-gamma (IFNγ). IFNγ is recognized by the IFNγ-receptor (IFNGR) heterodimer on macrophages and colonic epithelial cells. The signaling response includes activation of the STAT1 transcription factor and consequent secretion of proinflammatory cytokines and iNOS[144]. IFNγ has been shown to be necessary for the development of colitis in DSS-treated mice[145]. IFNγ strongly augments the inflammatory effects of LPS through various proposed mechanisms including increasing CD14

expression[146] and/or by promoting TLR4-induced NF-κB activation[147]. For example, stimulating Mono-Mac-6 monocytes with LPS and IFNγ in combination resulted in secretion of threefold-increased levels of TNF-α as compared to stimulation with LPS alone[146]. However, IFNγ has also been shown to negatively regulate the LPS response by repressing TLR4-activated STAT3 induction of anti-inflammatory IL-10 production[148]. This suggests that treating macrophages with LPS in conjunction with IFNγ may affect macrophage signaling and potentially macrophage-secreted EV components and signaling effects. In this chapter, I focused on characterizing EVs from macrophages activated with LPS alone. I used mass spectrometry to identify differential expression of proteins in secreted EVs from macrophages upon LPS activation. We identified two main proteins were of interest—argininosuccinate synthase 1 and gelsolin—as they were differentially expressed in EVs from LPS-activated immortalized bone marrow-derived macrophages (iBMDMs) and in MC38 colon cancer cells treated with these EVs (chapter 3). Both of these proteins have a known role in facilitating colitis-associated cancer.

Argininosuccinate Synthase 1

ASS1 is an enzyme active in the urea and citrulline NO cycles that utilizes ATP to convert citrulline and aspartate into argininosuccinate. It is the rate-limiting enzyme for arginine biosynthesis and subsequent nitric oxide (NO) synthesis[149]. Arginine plays an important role in intestinal epithelial cell growth and repair[150], metabolism[151], and immune function[149]. Arginine availability can also regulate activity of nitric oxide synthase 2 (iNOS)[152]. Interestingly, iNOS, which produces NO from arginine (product of ASS1), is over-expressed in colitis-associated cancer[153]. In the normal colonic epithelium NO can serve as a homeostatic regulator, but if it is chronically upregulated it can initiate and maintain IBD[154] and promote colorectal cancer (CRC)[153, 155]. Specifically, endogenous NO expressed in enterocytes alleviates colitis and colitis-associated cancer, whereas immune cell-derived NO activates macrophages and increases inflammation[156]. These divergent effects of NO depend on specific co-factors; enterocyte-derived NO is typically produced with NO synthase-stabilizing BH4 and anti-inflammatory cytokines that regulate apoptosis and epithelial barrier integrity (by upregulating tight junction proteins), while immune cell-derived NO is secreted with pro-inflammatory cytokines, NF-kB activation, and increased ROS—factors that collectively promote DNA damage and transformation[153, 155, 156].

ASS1 is upregulated in hyperproliferative intestinal epithelium[150], an important early step in cancer development and progression. ASS1 is also upregulated during colitis in enterocytes, which express a shift from oxidative phosphorylation to glycolysis[157]. In contrast, inhibiting arginine synthesis ameliorates colitis and colitis-associated cancer[156]. Colorectal cancer has been characterized by ASS1 overexpression, which is regulated by proinflammatory cytokines[156, 158]. Inhibition of ASS1 also lowers

levels of fumarate, reported as a tumor-suppressive metabolite, which decreases glycolytic activity, lipid metabolism, and proliferation in human SW620 CRC cells[151].

Notably, ASS1 is upregulated in APC-mutated mouse intestinal epithelium organoids and human CRC cell lines[150]. Notably, ASS1 only contributes to growth of APC-mutated organoids under low-arginine conditions[150], but this is not the case in mice with intestinal APC & ASS mutations, probably due to liver (wt) compensation. This idea of compensation is reflected in human CRC cell studies. Because ASS1 is a predictive biomarker for sensitivity to arginine deprivation therapy[159], heightened expression of ASS1 in CRC makes it a poor candidate for arginine deprivation therapy[160]. However, this is likely due to ornithine transcarbamylase (OTC), which converts ornithine into citrulline (needed for ASS to make arginine); inhibiting OTC, which is only expressed in liver and intestinal cells, makes CRC become arginine auxotrophic and thus a potential candidate for arginine deprivation therapy[160, 161]. Prior to OTC activity in the Urea cycle, arginase 1 (Arg1) competes with iNOS to convert arginine instead into ornithine[152]. Serum arginase is a marker of disease progression in colorectal cancer patients, and inhibiting Arg1 in CT26 colon cancer cells decreased migration and metastasis[162]. Interestingly, tumor associated macrophages (TAMs) have been found to express varying proportions of iNOS (M1 marker) and Arg1 (M2 marker) depending on cancer type and stage[163].

Moreover, EVs from LPS-activated iBMDMs are not the only myeloid cell-derived EVs that increase expression of enzymes that regulate arginine metabolism. Granulocytic myeloid-derived suppressor cells (g-MDSCs, $Ly6G^+$ $CD11b^+$) isolated from Lewis lung adenocarcinoma mouse tumors contained Arginase-1 (Arg1) activity, implying murine g-MDSC-secreted EVs contain Arg1[44]. This suggests that EVs from active myeloid cell subtypes may cooperatively regulate (or, in disease, dysregulate) enzymes involved in arginine metabolism in recipient cells.

Gelsolin

We found GSN was downregulated in EVs from LPS-activated iBMDMs (EV_{LPS}) relative to EVs from non-activated iBMDMs (EV_{non}). This correlates with clinical findings; GSN is decreased in colon cancer tissues [164], low fecal GSN has been proposed as a biomarker for inflammatory bowel disease [165], and low serum GSN levels has been proposed as a diagnostic biomarker colon cancer[164].

GSN is an actin-binding protein involved in capping, severing and monomer binding [166]. GSN functions as a tumor suppressor in several ways. Secreted GSN downregulated expression of MMP2 and MMP9[164], and upregulating in vitro expression of GSN in human colon cancer cells decreased their proliferation and invasiveness[167]. GSN inhibits STAT3 signaling, which is thought to be required for colitis-associated cancer[168, 169]. Moreover, tumor-educated macrophages have been shown to decrease GSN expression in

cancer cells. After co-culture with gastric cancer cells, U937 leukemia monocytes secrete CCL5 that signals via the CCR5/Jak2/STAT3 pathway to increase DNA methyltransferase-1 (DNMT1) expression in recipient gastric cancer cells, leading to DNA hypermethylation of the GSN promoter, effectively reducing GSN expression and increasing cell migration[170].

Aside from scavenging bacteria and clearing apoptotic cells, macrophages secrete many mediators that regulate colonic epithelial homeostasis including growth factors for epithelial growth, IL-10 to maintain immune tolerance to constitutive exposure to the gut microbiome, TNF-α to support epithelial barrier integrity, and BMP2 and C1q to support enteric neurons and peristalsis [171]. In response to acute injury via radiation, macrophages were found to secrete EVs containing Wnt5a, Wnt6 and Wnt9a that promote intestinal epithelial tissue repair[172].

Expression of GSN in EVs from non-activated macrophages elucidates another potential mechanism through which macrophage EVs regulate homeostasis in the absence of colitis or cancer. In healthy colonic tissue, the harsh luminal environment necessitates rapid turnover of epithelial cells; this increased rate of proliferation and migration exposes colonic epithelial cells to an increased risk of mutation and consequent carcinogenesis[173]. It is therefore possible that these rapidly proliferating colonic epithelial cells require additional externally derived tumor suppressive signals. In theory, upregulated GSN in EVs from non-activated macrophages may play a role in protecting rapidly proliferating and migrating colonic epithelial cells from uncontrolled proliferation and migration. The downregulation of these protective signals in EVs from LPS-activated macrophages (representing colitis) may potentially result in uncontrolled proliferation and migration/invasion, and thus indirectly facilitate colitis-associated transformation. Further studies are necessary to verify GSN and ASS1 in EVs and signaling effects in recipient colonic epithelial cells.

Other proteins

Major histocompatibility complex I (MHC I) was also detected to be decreased in EV_{LPS} relative to EV_{non}. MHC I is involved in antigen presentation to CD8 T cells; downregulation of MHC I may be due to changes in antigen processing[174]. This means EV_{LPS} may promote decreased antigen presentation, which implies a decreased anti-tumor T cell response.

EGF like repeats and discoidin domains 3 (EDIL3) plays a role in embryonic angiogenesis [175]. Watanabe *et al*. developed a predictive model for cancer development in colitis patients through a screen for 20 mutations in nonneoplastic mucosa in colitis patients[176]. Increased expression of EDIL3 in nonneoplastic tissue of colitis patients was found to be a predictor for colon cancer[176], and EDIL3

promotes CRC[175]. However, we detected EDIL3 to be downregulated in EV_{LPS} relative to EV_{non}, suggesting EV_{LPS} contains both pro-tumorigenic and anti-tumorigenic signals.

Mass spectrometry also detected increased levels of interleukin 1 receptor antagonist (IL1Ra) in EV_{LPS} relative to EV_{non}. As an antagonist for proinflammatory IL-1 cytokines prevalent in colitis, IL1Ra prevents an excessive inflammatory response to pathogens in colitis[177]. Increased IL1Ra reduces the incidence of CAC in AOM/DSS mice[178], but serum concentrations of IL1Ra were found to be increased in CRC patients[179], possibly due to a response to increased IL-6 levels[180]. This shows that EV_{LPS} also may upregulate anti-tumor factors due to the complexity of signaling within inflammation and especially within chronic colitis.

In conclusion, we detected a significantly different protein content in EVs from LPS-activated iBMDMs (modeling EVs from macrophages in colitis) compared to EVs from non-activated iBMDMs (modeling EVs from macrophages in homeostasis). Increased levels of pro-tumorigenic ASS1 in EVs from LPS-activated macrophages reveals one potential mechanism, by which these EVs may directly facilitate, or at least contribute to, colitis-associated cancer. On the other hand, increased levels of the tumor suppressive GSN in EVs from non-activated macrophages may contribute to protecting the healthily functioning colon from uncontrolled proliferation and transformation. Removal of this protective factor GSN in EVs from LPS-activated macrophages may thus indirectly promote colitis-associated cancer formation. However, it is important to note that there are significantly fewer macrophages (and thus fewer macrophage-secreted EVs) present in the non-inflamed colon[136]. This suggests that decreased GSN, EDIL3, and MHC I may play a weaker role in facilitating disease progression than upregulated expression of ASS1 and IL1Ra in EVs. In this case, the downregulated expression of these proteins in EVs from LPS-activated macrophages may not be causal, but may be considered for diagnostic and prognostic purposes. Alternatively, macrophages may not be the major producers of GSN and its tumor suppressor function is generally provided by other cell types.

Interleukin-4-induced-1 in EVs from human macrophages

IL4I1 is an enzyme that regulates the immunometabolism that is induced by IL-4[181]. CRC tumors contained increased expression of IL4I1 relative to normal tissue[181]. Mass spectrometry data showed increased expression of IL4I1 in EVs from THP1 macrophages activated with LPS. LPS induced THP1 macrophages to package increased levels of the pro-regenerative M2 marker IL4I1 into their EVs at an increased amount compared with non-activated THP1 macrophage EVs. This suggests EVs from LPS-activated human macrophages carry pro-tumorigenic proteins, and have the potential to promote

tumorigenesis in the context of LPS-driven inflammation, e.g., colitis in human patients. This supports the clinical relevance of our findings.

Inflammatory effects of macrophage EVs in APC$^{min/+}$ mouse colons

The adenomatous polyposis coli (APC) gene-encoding protein acts as a tumor suppressor mainly by negatively regulating beta-catenin in the Wnt signaling pathway. APC mutations resulting in loss of function (LOF) are common in colitis-associated cancer as well as in sporadic colon cancer; however, mutations in APC typically occur prior to the adenoma stage in sporadic cancer, and after occurrence of dysplasia in colitis-associated cancer[8]. Re-expression of APC in colon cancer cells decreased anchorage-independent growth capacity and tumor formation capacity in mice[182]. Methylation of the APC gene has been shown to contribute to field cancerization[183]. Moreover, heterozygous APC$^{min/+}$ mice with one mutated allele develop adenomas in the small intestine[184]. APC^{min} mutations have been associated with field cancerization effects downstream in the large intestine in mice and humans[185, 186] similar to colitis [187, 188]. Furthermore, the APC^{min} mutation has been shown to contribute to increased tumorigenesis in mice with colitis; for example, heterozygous APC$^{min/+}$ mice treated with DSS had an increased incidence of colitis-associated dysplasia and cancer[189]. Mice with heterozygous APC$^{min/+}$ and *Muc2* (Winnie) mutations have also been used as a model for colitis-associated cancer in mice[190]. Furthermore, patients with familial adenomatous polyposis (FAP) develop multiple adenomas/polyps throughout the colon and rectum, and most often have a mutation in the APC gene[191]. Clinical studies showed the COX inhibitor sulindac and the COX2 inhibitor celecoxib decreased the number and size of polyps in FAP patients[192-195]. Because COX2 mediates inflammation[196], this suggests that inflammation is involved in the process of tumorigenesis following the initial APC gene mutations. Hence, we used the APC$^{min/+}$ mouse as a model for inflammation-associated carcinogenesis.

We found EVs from LPS-activated and non-activated iBMDMs increased colonic inflammation in APC$^{min/+}$ mutated mice. Most notably, the submucosa was thickened, and there was an increase in inflammatory cell infiltrate into the colon tissue. This suggests that macrophages secrete EVs that communicate with resident cells of the colonic epithelium to induce recruitment of immune cells and inflammatory infiltrate. Further studies were conducted in the next chapter to elucidate and characterize the immune cells involved in this response. Using a similar colonoscope-guided injection technique, Slater *et al*. performed local microinjections of primary neutrophil EVs (containing myeloperoxidase) into mouse colons, and found that neutrophil EVs inhibited repair of mechanically-induced colon wounds[197]. Yet another group performed endoscopy-guided microinjections of EVs from neutrophils containing proinflammatory microRNAs miR-23a and miR-155 that also inhibited colonic

epithelium repair in mice with mechanically-induced superficial wounds or with DSS-induced colitis[198]. These microRNAs targeted histones, effectively increasing colonic epithelial cell accumulation of double-stranded breaks (DSB)[198]; DSB repair has been shown to mediate CAC[199]. Thus, EVs from myeloid cell subtypes can mediate acute colonic inflammation; this strengthens our hypothesis that myeloid-derived EVs, including EVs from LPS-activated macrophages, can mediate ulcerative colitis.

However, iBMDM-derived EVs did not have a microscopically detectable impact upon injection into WT mice. This may be due to the short experimental duration of one week with only three EV injections, or the predisposition of $APC^{min/+}$ mice to inflammation that predated the injection of EVs. This suggests that a pre-existing step (field effect) in multi-step tumorigenesis, e.g., a tumor suppressor mutation, may potentiate colon tissue susceptibility to inflammatory signals from macrophage EVs. Evidently, healthy WT tissue is less susceptible to macrophage EV signaling; however, we found a mutation in the APC tumor suppressor gene was able to potentiate macrophage EV-induced inflammatory cell-recruiting signals and increased susceptibility to inflammation. This is of note because chronic inflammation also induces field cancerization in the process of immunocarcinogenesis, so our data suggest that chronic inflammation in the gut may increase colon tissue susceptibility to macrophage EV-induced inflammatory signals that possibly mediate immunocarcinogenesis.

It is important to note that the macrophage cells utilized to produce EVs for this mouse study have been immortalized with myc and raf oncogenes. This implies that these iBMDMs exist in a cancer-like state and are not normal cells. Of note, although proteins encoded by oncogenes have been demonstrated in EVs from cancer cells, mass spectrometry did not detect myc or Braf protein expression in the EVs from these macrophages. The field cancerized-like state in aged $APC^{min/+}$ mice may explain why there were also inflammatory effects in the $APC^{min/+}$ mice injected with non-activated iBMDM EVs. Another possibility is that M0 macrophage derived EVs may induce low levels of inflammation when administered at high concentrations. Furthermore, differential activation/treatment of macrophages has been shown to influence the number and size of secreted EVs[200, 201]. Because there are fewer numbers of macrophages, and consequently macrophage-derived EVs, present in the normal, non-inflamed colon [136], injecting the same number of EVs from non-activated macrophages may not be representative of "homeostatic" conditions. A further limitation is that the small number of mice due to low survival rate from the submucosal injections reduced statistical power and significance.

Signaling pathways involved in processes in chronic inflammation such as damage and regeneration, have been shown to be very similar to many processes in neoplastic transformation. Because immune EVs have been shown to affect different cells of the epithelium, this suggests that

inflammatory EVs may also have pro-tumorigenic effects. Hence, I wanted to see whether these inflammatory EVs may exert pro-tumorigenic effects on colonic epithelial cells.

CHAPTER 3:

EXTRACELLULAR VESICLES FROM LIPOPOLYSACCHARIDE-ACTIVATED MACROPHAGES INCREASE GROWTH, ANCHORAGE-INDEPENDENT GROWTH, AND PRO-TUMORIGENIC IL-17 PATHWAY PROTEIN EXPRESSION IN COLON CANCER CELLS AND ALTER THE TUMOR IMMUNE MICROENVIRONMENT

INTRODUCTION

At the biochemical level, there is a huge overlap between mechanisms and pathways involved in epithelial repair during inflammation and cancer development[202, 203]. Intestinal epithelial cell growth, for instance, is a highly regulated homeostatic process; the rates of cell division and cell death are in dynamic equilibrium with stem cells at the base of the crypts differentiating into epithelial cells to replace those that have died and sloughed off the tissue surface. After damage to the tissue, lost stem cells are repopulated by increased division of existing stem cells[204] and by dedifferentiation of progenitor cells[205], and intestinal cells undergo hyperproliferation[150]. This process when repeated multiple times and more so, when accelerated by mutagens, results in oncogenesis, where the surviving stem cells have acquired genetic and/or epigenetic mutations that prevent the homeostatic negative feedback regulation of proliferation and migration/invasiveness and thus become cancer stem cells[150]. Macrophage-secreted extracellular vesicles (EVs) have been demonstrated to mediate many processes involved in inflammation, tissue regeneration, and tumorigenesis.

Inflammation and tumor-related effects of macrophage-secreted EVs

Macrophages secrete EVs that affect immune and non-immune cells in the colon, and may promote both inflammation and cancer. For example, IL-4 and IL-13-treated THP1 macrophage EVs promote growth, migration, and invasion of CRC cells[75]. SW480 CRC conditioned medium-treated THP1 macrophages secrete EVs that also promote growth, invasion and migration of CRC cells[75]. IL-4-treated human peripheral blood mononuclear cell-derived macrophages secrete EVs that promote ovarian tumor growth[70]. IL-4-activated primary macrophage EVs co-cultured with primary human $CD4^+$ T cells induce a higher proportion of immunosuppressive regulatory T (T_{reg}) cells than EVs from primary human monocytes or macrophages stimulated with IFNγ and LPS together [70]. IL-4-treated THP1 EVs increase migration and invasion of pancreatic adenocarcinoma (PDAC) cells[71]. IL-4-treated THP1 macrophage EVs also reduce apoptosis rate and increase transformation and viability of SKOV3 epithelial ovarian adenocarcinoma cells[72]. CD68 and CD163-expressing macrophages harvested from CRC patient tissues (considered TAMs) secrete EVs that upregulate migration and invasion in CRC cells in vitro and when injected intravenously (i.v.) into nude mice[55].

In mouse cells, IL-4-treated primary peritoneal macrophage EVs reduce colon injury when injected i.v. into mice with DSS-induced colitis by reducing apoptosis and TNF-α, IL-1β and MCP-1 expression, and increasing IL-10 expression[73]. The same IL-4-treated primary mouse peritoneal macrophage EVs administered to LPS-stimulated mouse colon cells (in-vitro model of UC) increased

colon cell viability and IL-10 secretion, and decreased apoptosis and proinflammatory TNF-α, IL-1β and MCP-1 cytokine expression[73].

M1-like macrophage EVs have been shown to induce proinflammatory and antitumor downstream effects. For example, GM-CSF and 1 μg/ml LPS-treated PBMC-derived macrophage-secreted EVs expressed EV markers as well as F4/80 and iNOS[206]. These LPS-activated PBMC macrophage EVs were administered onto glioblastoma and macrophage cell-containing spheroids and increased production of TNF-α, IL-6, IFNγ, IL-1β cytokines, and ROS, which increased cytotoxicity of cancer cells[206]. GM-CSF and LPS-activated PBMC macrophage EVs were injected i.v. into mice with glioblastoma, and had anti-tumor effects as compared to M0 macrophages through immunomodulation, i.e., they decreased the CD163/iNOS M2/M1 ratio[206]. GM-CSF and LPS-activated PBMC macrophage EVs that were engineered to better target the cancer also increased ROS, decreased oxygen availability in tumors, and decreased Ki67 proliferation in vivo[206]. EVs from THP1 macrophages treated with 100 ng/ml LPS inhibited migration and invasion of endometrial stroma cells from patients with endometriosis[80]. IFNγ and LPS-treated THP1 macrophages secrete EVs that suppress migration and invasion of trophoblast cells[83]. IFNγ and LPS-stimulated THP1 macrophage-secreted EVs increase expression of MMP1, MMP9, and MMP13 in chondrocyte cells, and activate the Wnt/β-catenin signaling pathway[84]. IFNγ and LPS-stimulated rat bone marrow-derived macrophage-secreted EVs when injected into rat jaws, increase hyperplasia, edema, and cartilage degradation in addition to upregulating inflammatory MMP1, MMP9, IL-6, IL-1β, and TNF-α expression[84].

In mouse cells, IFNγ and LPS-treated Raw264.7 macrophage-secreted EVs activated the TLR4-NFκB pathway in recipient Raw264.7 cells, and increased CD86 and iNOS expression[207]. It was also shown that 100 ng/ml LPS-treated Raw264.7 macrophage-secreted EVs induced increased expression of iNOS, CD86, IL-6, IL-1β, and TNF-α M1 markers, and downregulated Arg1, CD163, CD206, and IL-10 M2 markers in recipient Raw264.7 macrophages[80]. EVs from Raw264.7 macrophages treated with IFNγ and LPS decreased cell viability, increased apoptosis, and decreased EMT in CRC cells[79]. In mice, IFNγ and LPS-treated Raw264.7 EVs injected into CT26 tumors decreased tumor size, increased IL-10, and decreased PD-L1 and MMP-2[79]. EVs from J774A.1 monocyte/macrophage cells treated with 1 μg/ml LPS decreased melanoma cell viability and proliferation in spheroids[82]. IFNγ and LPS-treated primary mouse bone marrow-derived macrophages (BMDMs) secreted EVs that decreased viability, proliferation, and VEGF expression/angiogenesis in myocardial microvascular endothelial cells in vitro and in vivo[86].

M1-like macrophage EVs have been shown to increase inflammation and inhibit tumor progression in vitro and in vivo[79, 82, 86]. However, the effects of M1-like macrophage EVs appear to be

context-dependent. IFNγ and LPS-treated J774A.1 cell EVs decreased expression of both the M1 marker iNOS and the M2 marker CD206 when injected in calvarial tissue, whereas IL-4-treated J774A.1 cell EVs increased CD206 expression[91]. High glucose-treated THP1 macrophages expressed increased IL-1β and IFNα and decreased IL-10, in a similar fashion to THP1 macrophages treated with IFNγ and LPS[208]. Interestingly, these M1-like high glucose-treated THP1 macrophage EVs increase expression of the M2 markers CD163 and IL-10 in recipient THP1 macrophages[208]. High glucose-treated THP1 macrophage EVs also induce a hyperphosphorylation of pro-tumorigenic AKT in recipient muscle cells[208]. Furthermore, IFNγ and LPS-activated THP1 macrophages EVs increase proliferation and migration of vascular smooth muscle cells via cell signaling pathways that inactivate cyclin-dependent kinase inhibitors in vitro, and IFNγ and LPS-activated Raw264.7 macrophage EVs promoted hyperplasia of smooth muscle cells in vivo[94].

Experimental Setup

In this chapter, I characterize the functional effects of EVs from LPS-activated macrophages on colon cells in vitro and colon tumor progression. Preliminary data from the Contag Lab was performed at Stanford University by Dr. Masamitsu Kanada and an undergraduate student, Marilyn Zhang, who together revealed that the addition of EVs from U937 human monocytes treated with prostaglandin E2 (PGE_2) to MCF10A human breast cells increased cell growth, reduced roundness, and increased nuclear:cytoplasmic ratio (M. Kanada, M. Zhang, unpublished).

Developing an appropriate model to study EV signaling in colitis-associated cancer required balancing biological complexity with experimental feasibility. After evaluating human cells lines, attempting human induced pluripotent stem cell (iPSC)-derived organoids, and primary murine cells and tissues, I selected immortalized bone marrow-derived macrophages (iBMDMs) that were either unstimulated or lipopolysaccharide (LPS)-activated to represent homeostatic and colitic conditions, respectively. These cells were functionally similar to primary cells, and translatable to in vivo preclinical studies.

In our experiments, we found that EVs from LPS-activated iBMDMs had a pro-tumorigenic effect on tumor cells in vitro, yet decreased tumor growth in vivo. We characterized in vitro culture cells and TME-residing immune cells to elucidate the effects of iBMDM EVs on tumor progression and better understand how EVs from macrophages active in colitis can influence tumor progression. Tumorigenesis is a complex process, and EVs are heterogeneous entities capable of widespread biodistribution, efficient cellular uptake, with abundant molecular cargo that may activate a number of pathways. The effects of adding EVs to cells and tissues may, in different circumstances, appear paradoxical. Resolving

the influence of macrophage EVs on the various pathways involved in colitis-associated cancer is the focus of this chapter.

Keywords: ulcerative colitis, colitis-associated cancer, extracellular vesicles, lipopolysaccharide, tumor microenvironment, tumor immune microenvironment

METHODS

Cell Culture

Mouse MC38 colon cancer cells (Kerafast), CT26 colon cancer cells (ATCC, Cat. No. CRL-2638), and human Caco2 colon cancer cells (ATCC, Cat. No. HTB-37) were cultured as directed by the manufacturer. For bioluminescence imaging (BLI) and quantification, Caco2 and 4T1 cells were stably transfected with a Sleeping Beauty transposon plasmid with a bidirectional promoter driving 1) a Blasticidin-resistance marker linked to eGFP and 2) firefly luciferase-2 (fLuc) genes (LuBiG), as previously described[111]. MC38 cells were stably transfected with akaLuc[209] for in vivo studies.

Cell Viability

Cell viability was assessed using the crystal violet staining assay[210] to quantify total biomass per well. After cell treatment, wells were washed and fixed with methanol for 15 min at room temperature. Cells were then stained with 0.5% crystal violet in 25% methanol for 20 min. Finally, wells were washed three times with PBS taking care to not allow cells to dry to avoid dark splotches. Finally, absorbance (optical density) was acquired at 570 nm using the SpectraMax M3 Spectrophotometer (Molecular Devices).

Cell Counting Kit-8 Assay

Cell viability was assessed using the Cell Counting Kit-8 (CCK-8) assay (Sigma Aldrich, Cat. No. 96992) to quantify metabolic activity per well[211], according to manufacturer's protocol. In brief, CT26 colon cancer cells were seeded in 96-well plates (Corning) at a density of 500 cells per well in medium supplemented with 1% pen/strep and 10% EV-depleted FBS for 24 h to settle and adhere. Thereafter, cells were treated with different concentrations of non-activated or LPS-activated macrophage-derived EVs for 48 h. Finally, CCK-8 solution equal to 1/10 the volume of the media was added to wells, and cells were incubated for 1 h at 37 deg C. Absorbance (optical density) was acquired at 450 nm, with 600 nm reads as reference, using the SpectraMax M3 Spectrophotometer (Molecular Devices) and SoftMax Pro software (Version 7.0.2, Molecular Devices).

Cellular confluence

Cellular confluence was assessed in real time using the Incucyte® S3 Live-Cell Analysis System (Sartorius). MC38, CT26, and Caco2-LuBiG colon cancer cells were seeded in 96-well plates (Corning) at a density of 500 cells per well in medium supplemented with 1% pen/strep and 1-10% EV-depleted FBS for

24 h to settle and adhere. Thereafter, cells were treated with different concentrations of non-activated or LPS-activated macrophage-derived EVs, placed in the Incucyte® System, and incubated at 37°C and 5% CO_2. The software was adjusted to take 4 images per well every 12 h over the 96 h period of treatment. The Incucyte® System phase contrast software provided an average percent confluence for each well. Cell proliferation is quantified by counting the number of phase objects overtime. Occupied area (% of confluence) represents cell confluency and growth rate imaged over time.

Functional Metabolism

Basal measurements of oxygen consumption rate (OCR), extracellular acidification rate (ECAR), and lactate-linked proton efflux rate (PER) were obtained in real-time using the Seahorse XFe-96 Extracellular Flux Analyzer (Agilent Technologies) according to manufacturer[212-214]. Prior to running the assay, the cell culture medium was washed with and replaced by the Seahorse XF DMEM medium (pH 7.4) supplemented with 25 mm d-glucose and 4 mm Glutamine. The Seahorse plates were equilibrated in a non-CO2 incubator for 1 h prior to the assay. The Seahorse ATP rate and cell energy phenotype assays were run according to manufacturer's instruction and all reagents for the Seahorse assays were sourced from Agilent Technologies. Wave software (Version 2.6.1) was used to export Seahorse data directly as means ± standard deviation (SD).

Soft agar transformation assay

CT26 and Caco2 cells were seeded in an agar layer at a density of 500 cells per well in a 24-well plate in 200 µl of complete media with 0.3% agar on top of a 0.5% layer of agar in medium supplemented with 2% EV-depleted FBS and 1% antibiotics. Medium (untreated control), different concentrations of non-activated and LPS-activated macrophage-derived EVs, and 5% EV-depleted FBS (positive control) were added to the agar layer containing the cells. Soft agar plates were then left at room temperature for 30 min before being incubated at 37°C and 5% CO_2. After two weeks, the cell colonies in the wells were fixed in 70% ethanol and stained with 200 µl of 0.01% crystal violet. Colonies were counted using the BioTek Cytation 3 imaging plate reader using Gen5 3.04 software (BioTek Instruments, Inc., Winooski, VT, USA) and only colonies greater than 25 µm were recorded.

Protein extraction

MC38 cells were seeded at a density of 50,000 cells per 60 mm dish in complete medium (4.5 ml DMEM + 1% EV-depleted FBS + 1% pen/strep) on day 0. The following day, 500 µl of appropriate concentration of EVs in complete medium were administered. After 48 h of incubation, cells were washed and detached from plates with 4 mM EDTA treatment. Cells were washed once in PBS and centrifuged at 2000g for 5 min. Cells were then resuspended in modified RIPA (mRIPA) buffer containing 0.1% SDS and

Halt Protease and Phosphatase Inhibitor Cocktail (Thermo Fisher, Cat. No. 78440) for gentle cell lysis. Samples were placed on a shaker for 30 min at 4°C, and then subjected to 2 freeze-thaw cycles, from -80°C to RT. Samples were centrifuged at 16,000g for 20 min at 4°C to remove cell debris, and supernatant containing proteins was collected for characterization. Protein concentrations were determined by the Pierce BCA Protein Assay Kit (Thermo Fisher, Cat. No. 23225) using albumin standards according to the manufacturer's protocol.

Protein Gel Electrophoresis & Immunoblotting

5-20 µg protein was mixed with 4X sample buffer (Expedeon, Cat. No. NXB31010), 10X reducing buffer (Thermo Fisher, Cat. No. NP004) and deionized water to a volume of 10-20 µl, and samples were subsequently heated at 90°C for 5 min. Samples and Precision Plus Protein All Blue Standards (BioRad, 1610373) were loaded into Mini-PROTEAN TGX Stain-free Precast gels (BioRad, 4568093) and run with Tris/Glycine SDS Running Buffer (BioRad, 1610732) in the BioRad Mini-PROTEAN Tetra System at 100V for 60-80 min.

PVDF membranes were soaked in methanol for 2 min, washed in DI water and soaked in 1X Trans-Blot Turbo Transfer Buffer (BioRad, 10026938) for 2 min. Filter paper was also soaked in Transfer buffer for 2 min. Blot and gel were then arranged in the following order: bottom (anode), filter paper, membrane, gel, filter paper, top (cathode), as current moves directionally from cathode toward anode. Semi-dry membrane transfer was performed in the BioRad Trans-Blot Turbo Transfer System using the StandardSD protocol (25V, 1.0A, 30 min).

Membranes were blocked in 3-5% non-fat dry milk in TBST for 1 h at RT, or overnight at 4°C. Membranes were stained with primary antibody in blocking buffer (BioRad, 12010020) overnight at 4°C. All antibodies used are listed in Table A.1. Membranes were then washed 3 times for 3 min with TBST and subsequently stained with secondary antibody in blocking buffer for 1-2 h at RT. Blots were again washed 3 times for 3 min with TBST. Blots were incubated in HRP substrate for 1 min using the Pierce ECL Western Blotting Substrate kit (Thermo Fisher, 32209) and imaged in the ChemiDoc MP Imaging System (BioRad). Blots were quantified using ImageJ software.

LC/MS/MS Proteomic Analysis of MC38 Cells*

*Protocol was written with Dr. Douglas Whitten, adapted from Pierce TR0049.0 (www.piercenet.com)

Cell proteomics sample preparation: Four volumes of ice-cold 100% acetone were added to 1 volume of protein solution, and samples were incubated overnight at -20°C. Samples were then pelleted at 14,000g for 10min and washed with 80% acetone/20% water and re-centrifuged. Supernatants were removed and samples placed in a fume hood to allow the residual acetone to evaporate (5-10 min).

Samples were resuspended in 100 µl of 100 mM Tris in water (pH 8.5) and stored at -20°C until further use.

Proteolytic digestion: Protein solutions (100 ul) were mixed with 100 mM Tris-HCl (pH 8.5) supplemented with 6% (w/v) sodium deoxycholate (SDC). Samples were reduced and alkylated by adding tris(2-carboxylethyl)phosphine (TCEP) and chloroacetamide at 10 mM and 40 mM, respectively, and incubating for 5 min at 45°C with shaking at 2000 rpm in an Eppendorf ThermoMixer C. Trypsin, in 50 mM ammonium bicarbonate, was added at a 1:100 ratio (wt/wt) and the mixture was incubated at 37°C overnight with shaking at 1500 rpm in the Thermomixer. The final volume of each digest was ~300 ul. After digestion, SDC was removed by phase extraction using ethyl acetate[113]. The samples were acidified to 1% TFA and subjected to C18 solid phase clean up using StageTips[114] to remove salts.

LC/MS/MS Analysis of MC38 cell lysates: An injection of 5 µl was automatically made using a ThermoFisher EASY-nLC 1200 nanoflow chromatography instrument using a ThermoFisher Acclaim PepMap RSLC 0.1mm x 20mm C18 trapping column and washed for ~5 min with buffer A (99.9% Water/0.1% Formic Acid). Bound peptides were then eluted over 35 min onto a Thermo Acclaim PepMap RSLC 0.075 mm x 500 mm resolving column with a linear gradient of 5% to 28% buffer B in 24 min (buffer B = 80% Acetonitrile/0.1% Formic Acid/19.9% Water). After the gradient elution the column was washed with 90% buffer B for the duration of the run at a constant flow rate of 300 nl/min. Column temperature was maintained at a constant temperature of 50°C using an integrated column oven (PRSO-V2, Sonation GmbH, Biberach, Germany). Eluted peptides were sprayed into a ThermoScientific Q-Exactive HF-X mass spectrometer for data independent acquisition using a FlexSpray spray ion source. Survey scans were taken in the Orbi trap (15000 resolution, determined at m/z 200) over mass range of 395-1005 m/z. Fixed windows of 12 m/z (50 total) were sequentially scanned and fragmented by HCD acquired in the Orbitrap at 45,000 resolution (determined at 200 m/z). Window placements were generated using Skyline[215].

Data analysis: Acquired spectra were processed in the MSU RTSF Proteomics Facility using DIA-NN[216], v1.8.1, using the Robust LC (high precision) quantitation strategy with RT-dependent cross-referencing and Deep Learning enabled in library-free mode against a FASTA file of all *M. musculus* protein sequences downloaded from UNIPROT (www.uniprot.org, downloaded on 20230131). Search parameters were optimized by DIA-NN and results filtered at a precursor FDR of 1%. Mascot parameters for all databases were as follows: allow up to 1 missed tryptic sites, fixed modification of Carbamidomethyl Cysteine, variable modification of Oxidation of Methionine.

RNA isolation

MC38 cells were seeded at a density of 50,000 cells per 60 mm dish in complete medium (4.5 ml DMEM + 1% EV-depleted FBS + 1% pen/strep) on day 0. The following day, 500 µl of appropriate concentration of EVs in complete medium were administered. After 24 or 48 h of incubation, cells were washed and RNA was isolated using the RNeasy mini kit (Qiagen, 74104) according to the manufacturer's protocol. Residual DNA was removed from samples using the on-column RNase-free DNase set (Qiagen, 79254), and samples were treated with DNase solution for 30 minutes (min) at room temperature (RT). RNA concentration was measured using a Qubit 2.0 fluorometer according to manufacturer's protocol (ThermoFisher, Q32866), and RNA integrity of samples was determined using the Agilent 4200 TapeStation analyzer. RNA integrity numbers (RIN) of all samples were greater than 9.7.

qRT-PCR

Reverse transcription was carried out with 500 ng of RNA using the High-Capacity cDNA Reverse Transcription kit (Applied Biosystems, 4368814) following the manufacturer's instructions. SYBR-Green qRT-PCR was carried out on diluted cDNA using SYBR Green PCR Master Mix (Applied Biosystems, 4309155), and triplicate PCR reactions were run on the BioRad CFX96 Real-Time System with a C1000 Touch Thermal Cycler according to manufacturer's protocols. Signals from SYBR-Green probes were normalized using the housekeeper gene GAPDH, and the average $2\Delta\Delta Ct$ values were calculated. Fold change relative to the respective control was determined. The primers for mouse transcript detection are listed in Table A.3.

In Vivo Tumor Studies

Six-week-old female B6(Cg)-Tyrc-2J/J (B6 Albino, The Jackson Laboratory, Strain #000058) mice (n = 3-5 mice per group) with an average weight of 19 grams (g) were used according to procedures approved by the Institutional Animal Care and Use Committee at Michigan State University (PROTO202100276). Non-activated and LPS-activated iBMDM-derived EVs ($2–8\times10^{11}$ particles/ml) in 100 µl PBS were injected subcutaneously (s.c.) into the right flank every day for 1 week prior to tumor induction. Primary tumors were established by s.c. injecting 2×10^{5} MC38 cells suspended in 100 µl PBS into the right flank. 100 µl EVs were s.c. injected until the emergence of the primary tumor; 20-25 µl EVs were subsequently injected intratumorally (i.t.) after tumor emergence every other day until tumor diameter reached 10 mm. Tumor growth in all mice was monitored by digital caliper measurements. Mice with MC38 tumor cells expressing the pLenti-CMV: Flag-Akaluc_SV40:PuroR plasmid (Addgene plasmid #183048) encoding for AkaLuc (Far-Red Firefly luciferase) and puromycin resistance expression under the constitutively expressed CMV promoter were monitored for tumor cell bioluminescence using the In Vivo Imaging

System (IVIS, PerkinElmer) in the IQ Imaging Core Facility. For bioluminescence (BLI) imaging, each mouse was injected intraperitoneally (i.p.) with 5 mM TokeOni AkaLumine-HCl substrate (Sigma, 808350) in 100 µl PBS 20-25 minutes prior to imaging. Mice were anesthetized for imaging using isoflurane (2%–3%). Following the final imaging timepoint, mice were sacrificed using 5% carbon dioxide or cervical dislocation under anesthesia (3% isoflurane), and underwent post-mortem dissection to remove tumors.

Tissue dissociation and flow cytometric staining

After euthanization, tumors were resected and dissociated using a combination of mechanical and enzymatic dissociation strategies. Tumors were cut up into small pieces with a sterile razor and incubated in 10 ml of dissociation medium comprising RPMI with 25 mM HEPES buffer (Sigma Aldrich), 1 mg/ml Collagenase I (Thermo, 178018029), and 100 U/ml DNase I (Worthington Biochemical Corporation LS002139). Enzymatic digestion was undertaken on an orbital shaker (70 rpm) in a 5% CO_2 incubator at 37°C for 45-60 minutes. Afterwards, the medium containing dissociated tissue was filtered through a 70 µm filter into a 50 ml conical tube. Undigested tissue pieces were pushed through the filter with the thumb press of a syringe plunger, and the filter was further washed with PBS without calcium or magnesium (Corning, Cat. No. 45000-446). Centrifugation at 350 x g for 10 minutes was used to sediment cells, which were resuspended in PBS + 2% BSA and counted for flow cytometry and FACS. Following tumor digestion, 1×10^6 cells from each sample (n=3 or 4 per group) were collected for staining in a polypropylene 96-well round bottom plate. Staining steps were performed in 100 µl volumes in the dark at 4°C. Samples were incubated with Zombie NIR Fixable Viability dye (1:750, Biolegend, 423105) for 15 minutes. Thereafter, cells were washed once with flow buffer (0.5% bovine serum albumin in calcium and magnesium-free PBS solution) and incubated with TruStain FcX PLUS (anti-mouse CD16/32) Antibody (BioLegend, 156603; 0.25 µg/sample) in 50 µl for 10 minutes. A 2x antibody mixture containing True-Stain Monocyte Blocker (5 uL/test, Biolegend 426102) was added to the cell suspension (to total 100 ul) for a 30-min incubation to block non-specific binding of cyanine dyes. Antibodies included were: BV605 CD45 (1:300, Biolegend, 103139), AF700 CD11b (1:400, Biolegend, 101222), BV785 F4/80 (1:300, Biolegend, 123141), BV421 CD86 (1:200, Biolegend, 105031), APC CD206 (1:200, Biolegend, 141707), PerCP MHCII (1:200, Biolegend, 107623), SparkBlue 550 CD3 (1:100, Biolegend, 100259), APC-Fire 810 CD4 (1:100, Biolegend, 100479), BB700 CD8a (1:100, Biolegend, 566410), PE-Dazzle 594 CD11c (1:500, Biolegend, 117347), BV510 Ly6C (1:200, Biolegend, 128033), PacBlue Ly6G (1:250, Biolegend, 127612), and BUV737 CD31 (1:200, BD Bioscience, 612802); antibodies used are also listed in Table A.1. After surface marker staining, cells were washed and incubated with 1x Protein Transport Inhibitor Cocktail

(eBioscience, 00-4980-03) for 1 h. Fixation and permeabilization was subsequently performed using the Foxp3/Transcription Factor Staining Buffer Set, (Invitrogen eBioscience, 00-5523-00). Specifically, cells were resuspended in eBioscience Fixation/Permeabilization solution for 10 minutes. Cells were washed and resuspended in eBioscience Permeabilization Buffer with BV650 IL-4 (1:1200, BD Bioscience, 564004), APC-Fire750 IFNg (1:500, Biolegend, 505859), PE-Cy7 Arg1 (1:400, ThermoFisher, 25-3697-80), BUV 615 iNOS (1:500, ThermoFisher, 366-5920-82), AF647 IL-17a (1:200, Biolegend, 506911), and PE FoxP3 (1:40, Biolegend, 320007) for 30 mins incubation.

Thereafter, cells were washed twice, resuspended in 100 µl flow buffer, and passed through 40 µm FlowMi filters for flow cytometry analysis. The Cytek Aurora spectral flow cytometer (Cytek Biosciences, CA, USA) in the MSU Core Flow Cytometry facility was used for sample analyses, using the Cytek SpectroFlo software (version 3.0.3) for data collection. Fluorescence minus one (FMO) samples were used to guide gating strategies, and the flow cytometry data was analyzed with the software FCS Express (DeNovo Software, CA, USA; version 7.12.0005).

Statistical analysis

Statistical analyses were performed using Prism software (10.1.1, GraphPad Inc.). For experiments with three or more groups, statistical significance was determined using one-way ANOVA followed by Tukey's post-hoc test. For experiments comparing two groups, significance was determined using an unpaired t-test. All in vitro data are expressed as mean +/- standard deviation (SD); $p<0.05$ was considered a significant finding. Tumor volume data is expressed as mean +/- standard error; all other in vivo data studies are expressed as mean +/- SD, where $p<0.05$ is considered significant.

RESULTS

Due to the complex and contradictory anti- and pro-tumor effects of extracellular vesicles from M1-like macrophages reported in different contexts, to model colitis I wanted to investigate how differential activation of macrophages influences functional effects of secreted EVs on colon cells in culture. Verified EVs secreted by Raw264.7 macrophages activated with 50 ng/ml lipopolysaccharide (LPS) in combination with 20 ng/ml interferon-gamma (IFNγ) were administered to CT26 colon cancer cells; cell counting kit-8 assay was performed to measure metabolic activity as a surrogate for cell viability (specifically, cellular dehydrogenase activity which is directly proportional to the number of living cells)[211]. I found that EVs secreted by Raw264.7 cells activated by LPS plus IFNγ decreased cell growth of CT26 cells, in a concentration dependent manner relative to CT26 cells treated with EVs from non-activated Raw264.7 cells (Figure 3.1a). Soluble factors (SFs, small soluble molecules present in the supernatant after the final step of ultracentrifuge isolation and concentration of EVs, e.g., free-floating

proteins and metabolites) from LPS plus IFNγ-activated Raw264.7 cells also decreased cell growth in CT26 cells (Figure 3.1a). Murine 4T1 breast cancer cells, also derived from Balb/c mice, were generously provided by Dr. Michael Bachmann who had previously transfected these 4T1 cells with the LuBiG plasmid containing genes encoding blastocidin resistance, GFP, and luciferase (4T1-LuBiG), as previously described[111, 217]. 4T1-LuBiG cell expression of luciferase allows for bioluminescence imaging (BLI); the BLI assay comprises the same number of cells seeded per well before incubation with EV treatment for 48 h. At the end of treatment, cells are treated with luciferin that together with ATP allows the luciferase enzyme to produce bioluminescence, which can be quantified by the In Vivo Imaging System (IVIS) as an indicator of metabolic activity per well. These bioluminescence quantification data can be used as a surrogate for cell growth measurement provided the appropriate controls are measured as well. Along with secreted SFs, the LPS and IFNγ-activated Raw264.7-secreted EVs also mildly decreased cell growth of 4T1-LuBiG cells at a concentration of 4×10^5 Raw264.7-derived EVs administered per 4T1-LuBiG cell seeded per well at the start of the experiment relative to untreated cells (Figure 3.1b).

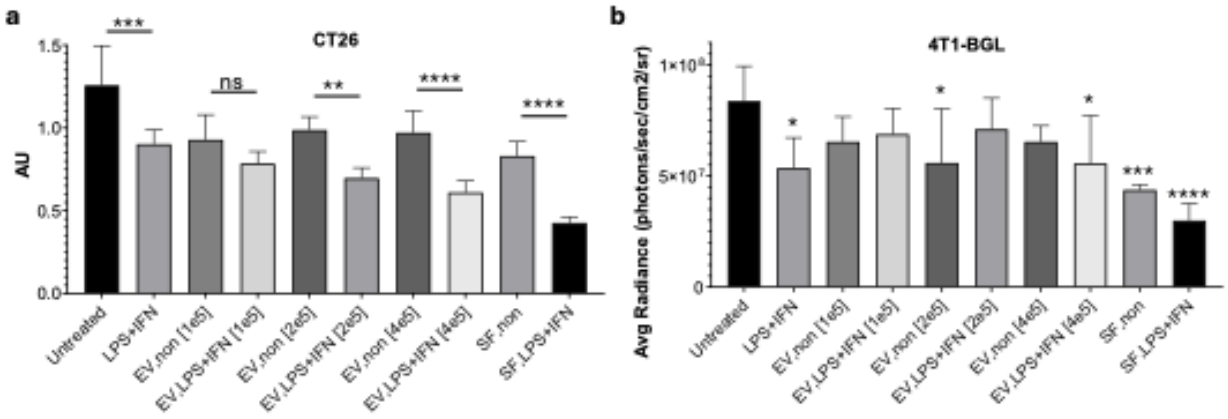

Figure 3.1 Extracellular vesicles (EVs) and soluble factors (SFs) secreted from Raw264.7 macrophages activated with lipopolysaccharide (50 ng/ml LPS) and interferon gamma (20 ng/ml IFNg) decreased growth rate of recipient CT26 colon cancer cells and 4T1 breast cancer cells after 48 h. (a) Cell counting kit-8 colorimetric assay showed decreased metabolic activity per well measured in arbitrary units (AU) as a surrogate for cell growth in CT26 cells treated with EVs and SFs from LPS and IFNg-activated macrophages ($EV_{LPS+IFN}$, $SF_{LPS+IFN}$) compared to EVs and SFs from non-activated macrophages (EV_{non}, SF_{non}) in a dose-dependent manner [# macrophage EVs/CT26 cell seeded]. (b) Bioluminescence imaging (BLI) of luciferin reaction with luciferase stably expressed in 4T1 cells (4T1-LuBiG) quantified average radiance as an indicator of metabolic activity and a surrogate for cell growth; 4T1-LuBiG cells treated with $SF_{LPS+IFN}$ and $EV_{LPS+IFN}$ at a concentration of [4×10^5] macrophage EVs/4T1 cell seeded showed decreased cell growth relative to untreated. Not significant (ns), *p<0.05, **p<0.01, ***p<0.001, ****p<0.0001, mean (SD), n = 6, one-way ANOVA followed by Tukey's post-hoc test (b, significance values compared with untreated control group). Concentrations are expressed in scientific notation (e.g., [2e5] = [2×10^5]); in graph labels, text after the comma appears as subscript (e.g., EV,LPS+IFN = $EV_{LPS+IFN}$).

EVs from LPS-activated macrophages increased proliferation of colon cells

To compare how the activation state of macrophages affects the signaling effects of secreted EVs, I administered EVs from non-activated Raw264.7 cells and EVs from Raw264.7 cells activated with 500 ng/ml LPS only onto 4T1-LuBiG cells. I found that EVs from LPS-activated Raw264.7 cells increased cell growth of 4T1-LuBiG cells after 48 h as measured by crystal violet biomass assay (Figure 3.2a). I later discovered an IncuCyte imaging system at MSU, with the capability for live cell imaging to conduct label-free proliferation assays over time in the incubator. I repeated this EV transfer study and measured proliferation over time, and confirmed that EVs from LPS-activated Raw264.7 cells increased cell growth kinetics of 4T1-LuBiG cells relative to cells treated with EVs from non-activated Raw264.7 macrophages; this change in growth started around 36 h and was detected until at least 60 h post EV-treatment (Figure 3.2b).

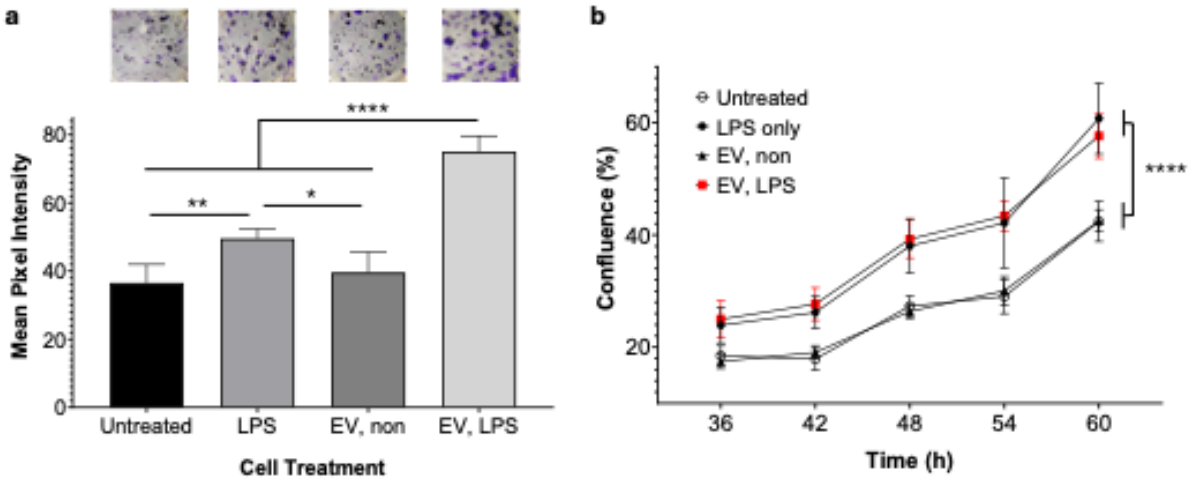

Figure 3.2 Extracellular vesicles (EVs) from Raw264.7 macrophages activated with lipopolysaccharide (LPS) increased growth rate of 4T1 breast cancer cells. (a) Crystal violet assay quantification showing increased cell biomass as a surrogate for cell growth in 4T1 cells treated with EVs from LPS-activated macrophages (EV_{LPS}) after 48 h compared to untreated, 500 ng/ml LPS (LPS), or non-activated macrophages (EV_{non}); representative well images above. (b) IncuCyte imaging and quantification of 4T1 cells treated with each condition over time shows similar results. *p<0.05, **p<0.01, ****p<0.0001, mean (SD), n = 5-6, one-way ANOVA (a) or two-way ANOVA (b) followed by Tukey's post-hoc test. In graph labels, text after the comma appears as subscript (e.g., EV,LPS = EV_{LPS}).

I then wanted to see if this was also the case in other cell types. Specifically, I wanted to see if this was translatable to human cells, which may have greater implications for clinical translatability. First, I administered EVs from THP1 monocytes treated with either 1 μM prostaglandin E2 (PGE_2) or 1 μg/ml LPS onto Caco2 colon cancer cells containing the LuBiG transposon expressing luciferase (Caco2-LuBiG). PGE_2 is a proinflammatory lipid mediator produced by cyclooxygenase (COX)-2 from arachidonic acid. PGE_2 activates macrophages through different E prostanoid (EP) receptors, resulting in increased intracellular cAMP and produces immunosuppressive activity, e.g., inhibits bacterial killing, TNF-α secretion, and ROS production[218]. Both COX-2 and PGE_2 have been shown to play a role in colitis-associated cancer[14]. Although PGE_2 was previously reported to promote tumor growth in LS174T colon cancer cells [219], I found 1 μM PGE_2 treatment did not change cell growth of Caco2 tumor cells after 48 h (Figure 3.3a). I also found that EVs from THP1 monocytes that were stimulated with PGE_2 did not influence Caco2 cell growth rate after 48 h treatment (Figure 3.3a). Treating Caco2-LuBiG cells directly with bacterial lipopolysaccharide (LPS) also did not impact cell growth, nor did EVs from non-activated THP1 monocytes. Interestingly, EVs from LPS-activated THP1 monocytes significantly increased growth of Caco2-LuBiG cells after 48 h (Figure 3.3a). Thus, signaling via the PGE_2 pathway cannot substitute for signaling via the LPS-TLR4 pathway in this culture model. This further confirmed my hypothesis that activation of macrophages and context of EV secretion influences functional signaling effects in recipient cells. I also administered previously verified EVs from THP1-differentiated macrophages onto Caco2-LuBiG cells and found an even higher increase in cell growth over 48 h in Caco2-LuBiG cells treated with EVs from LPS-activated THP1 macrophages as compared with non-activated THP1 macrophages (Figure 3.3b).

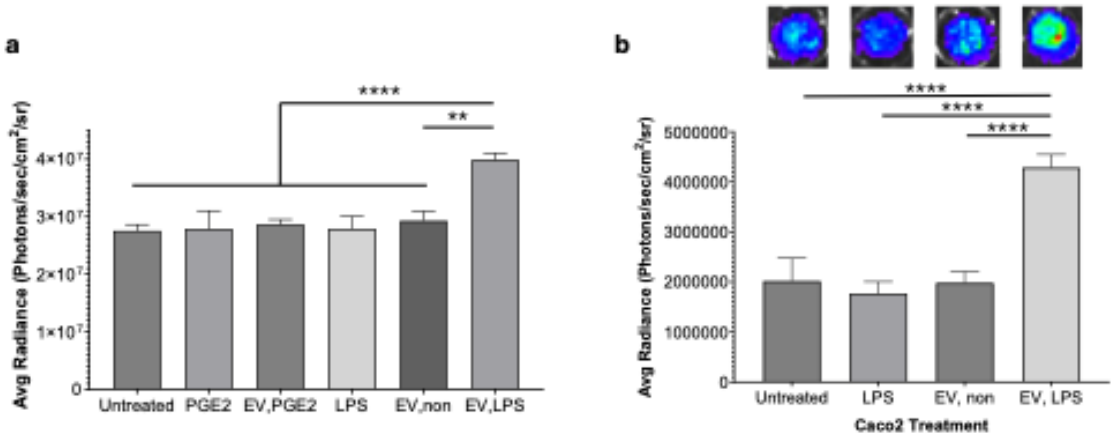

Figure 3.3 Extracellular vesicles (EVs) from lipopolysaccharide (LPS)-activated THP1 monocytes and macrophages increase growth rate of Caco2 colon carcinoma cells expressing luciferase (Caco2-LuBiG) after 48 h. (a) Caco2-LuBiG cells express more total ATP levels per well (a surrogate for cell growth) when treated with EVs from THP1 monocytes stimulated with 1 µg/ml LPS (EV_{LPS}) as compared to Caco2-LuBiG cells treated with 1 µg/ml LPS (LPS), 1 µM prostaglandin E_2 (PGE2), EVs from untreated THP1 monocytes (EV_{non}), or EVs from PGE_2-treated THP1 monocytes (EV_{PGE2}). (b) Caco2-LuBiG cells express more total ATP levels per well (cell growth) when treated with EVs from THP1 macrophages activated with 500 ng/ml LPS (EV_{LPS}) as compared to Caco2-LuBiG cells treated 500 ng/ml LPS (LPS) or EVs from non-activated THP1 macrophages (EV_{non}); representative well images above. **p<0.01, ****p<0.0001, mean (SD), n = 3 or 6, one-way ANOVA followed by Tukey's post-hoc test. In graph labels, text after the comma appears as subscript (e.g., EV,LPS = EV_{LPS}).

Caco2-LuBiG cells were also found to express more bioenergetic ATP levels in cell lysates when treated with EVs from LPS-activated THP1 macrophages (EV_{LPS}) as compared to Caco2-LuBiG cells treated with EVs from non-activated THP1 macrophages (EV_{non}) or 500 ng/ml LPS (LPS); Caco2-LuBiG cells also express more bioenergetic ATP levels in cell lysates when treated with SFs from LPS-activated THP1 macrophages (SF_{LPS}) as compared to SFs from non-activated THP1 macrophages (SF_{non}) (Figure 3.4a).

I also ran crystal violet assay on Caco2-LuBiG cells treated with EVs and SFs from non- and LPS-activated THP1 macrophages. I found Caco2-LuBiG cells treated with [2×10^5] and [4×10^5] EVs from LPS-activated THP1 macrophages induced a modest increase in Caco2-LuBiG cell growth over 48 h, possibly due to the high percentage of FBS (20%) supplemented in the medium as the growth factors present in fetal bovine serum could increase growth rate, where it is not as likely for another factor to be able to further increase growth rate (Figure 3.4b). Surprisingly, the crystal violet assay did not detect a difference in cell growth of Caco2-LuBiGs treated with SFs from LPS-activated THP1 macrophages relative to SFs from non-activated THP1 macrophages (Figure 3.4b). To investigate whether this cell

growth may be due to increased metabolic activity, Seahorse assays were used to measure extracellular acidification rate (ECAR), an indicator of glycolytic activity, as well as the oxygen consumption rate (OCR), indicating mitochondrial activity in Caco2-LuBiG cells treated with EVs and SFs from THP1 macrophages. I found that EVs from LPS-activated THP1 macrophage significantly decreased ECAR and thus glycolysis of recipient Caco2-LuBiG cells in a concentration dependent manner, i.e., at a concentration of [4×10^5] THP1 EV/cell but not [2×10^5] EV/cell as measured on the Agilent Seahorse (Figure 3.4c). Surprisingly, non-activated THP1 macrophage EV increased ECAR relative to untreated Caco2 cells. There is a similar yet insignificant trend in ECAR in Caco2-LuBiG cells treated with SFs from LPS-activated THP1 macrophages as compared to SFs from non-activated THP1 macrophages (Figure 3.4c). Glycolysis has been thought to be generally upregulated in cancer cells; however, there is increasing evidence that this metabolic reprogramming is not because of any impairment of mitochondrial oxidative phosphorylation (OXPHOS), and that various cancers have different energy metabolic pathways since glycolysis and OXPHOS are both cooperative and competitive [220]. The caveat to the Seahorse study results is that normalization of ECAR and OCR were done with a separate plate for crystal violet staining; this does not account for potential cell loss in the Seahorse plate, though we did not observe any cell loss when observing all the wells under brightfield microscopy and the plates appeared similar. Future experiments utilizing the IncuCyte live cell imager to confirm confluence and normalize to cell number will provide more accurate measures of metabolic activity.

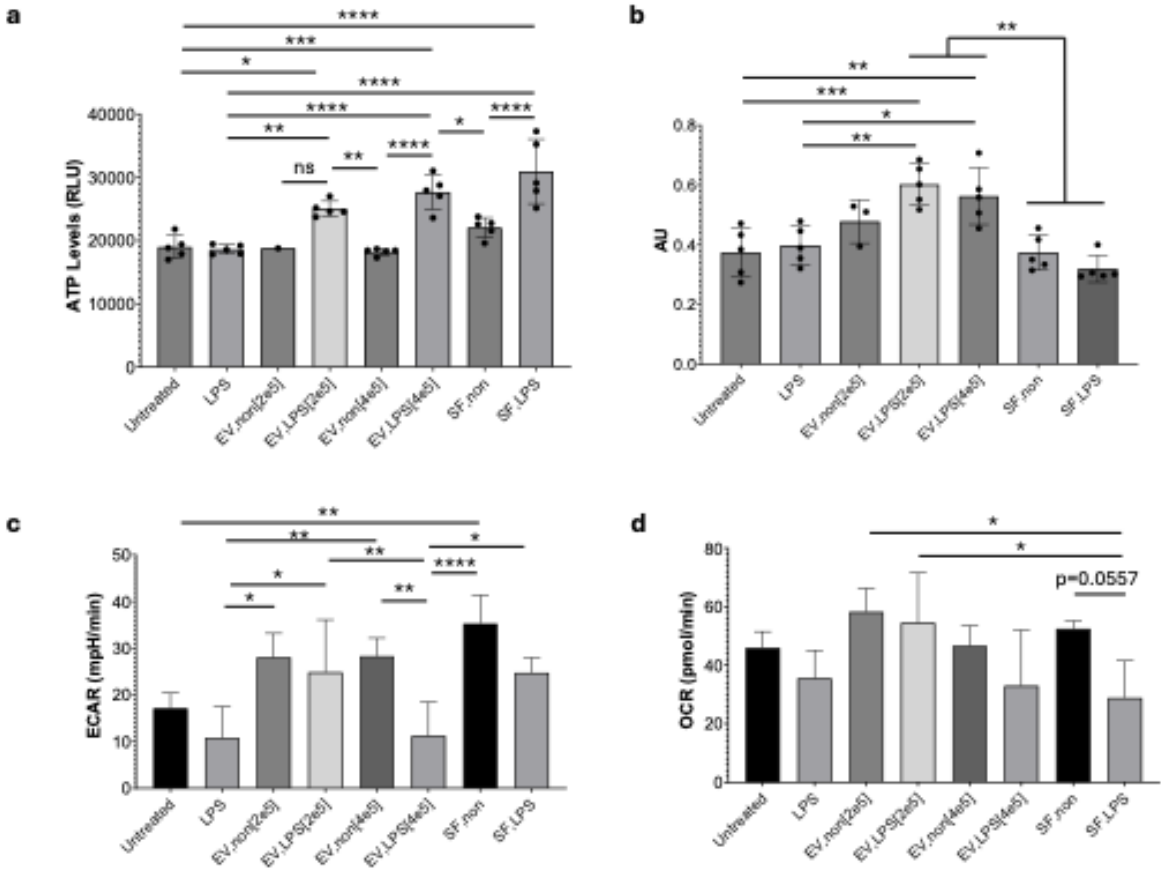

Figure 3.4 Extracellular vesicles (EVs) and soluble factors (SFs) secreted by THP1 macrophages activated with lipopolysaccharide (LPS) increased ATP levels and decreased extracellular acidification rate (ECAR) in Caco2 colon carcinoma cells expressing luciferase (Caco2-LuBiG) after 48 h. (a) Bioenergetic ATP levels expressed in Caco2-LuBiG cells treated with EVs and SFs from non-activated and LPS-activated THP1 macrophages or 500 ng/ml LPS (LPS). (b) Crystal violet assay shows a moderately increased cell growth in Caco2 cells treated with EV_{LPS} at a concentration of [2×10^5] and [4×10^5] macrophage EV/Caco2-LuBiG cell seeded relative to select conditions. (c,d) Extracellular acidification rate (ECAR, c) and oxygen consumption rate (OCR, d) of Caco2-LuBiG cells treated with EVs and SFs from non- and LPS-activated THP1 macrophages. Not significant (ns), *p<0.05, **p<0.01,***p<0.001, ****p<0.0001, mean (SD), n = 3-6 (a,b) and n=5 (c,d), one-way ANOVA followed by Tukey's post-hoc test. Concentrations are expressed in scientific notation (e.g., [2e5] = [2×10^5]); in graph labels, text after the comma appears as subscript (e.g., EV,LPS = EV_{LPS}).

Next, I characterized changes in cell growth kinetics induced by EVs from primary bone marrow-derived macrophages (BMDMs), since Raw264.7 and THP1 cells are both leukemia-derived cell lines. After confirming BMDM activation from LPS treatment and verifying secretion of EVs (Figure 2.5-2.6), I administered EVs from BMDMs that were a) not activated or b) activated with either 10 or 100 ng/ml LPS onto MC38 mouse colon cancer cells (both from C57Bl/6 mice). When MC38 cells were co-cultured with BMDM EVs in medium supplemented with 10% EV-depleted fetal bovine serum (FBS), I did not observe any change in cell growth rate of MC38 cells (Figure 3.5a). However, when I co-cultured MC38s with EVs from BMDMs in medium supplemented with 1% EV-depleted FBS, I found that LPS-activated BMDM EVs induced increased growth rate in MC38 cells not at 36 h, but significantly at the 60 h time point (Figure 3.5b). Even though 10 ng/ml LPS induced higher secretion of nitric oxide in BMDMs than 100 ng/ml LPS (Figure 2.5), EVs from BMDMs activated with 100 ng/ml LPS increased growth rate of recipient MC38 cells more than did EVs from BMDMs activated with 10 ng/ml LPS (Figure 3.5b). From this, I concluded that culture medium supplemented with 10% FBS potentially causes the culture medium to become enriched in growth factors such that the rate of cell growth in this medium is already at a maximum and cannot be significantly increased by external signals.

Experiments with primary cells were very impactful for my study, but isolating EVs from BMDMs quickly proved extremely challenging because primary BMDMs do not replicate in culture after harvesting, and use of EV from these cells was impractical. To overcome this problem, Dr. Andrew Olive (MSU) generously provided J2-immortalized BMDMs (iBMDMs), in which the J2 virus introduced v-myc and v-raf/mil oncogenes[106]. I discovered that EVs from LPS-activated iBMDMs induced a similar increase in MC38 cell growth rate in a concentration-dependent manner (Figure 3.5c). I repeated this study several times and saw significantly increased cell growth rates around 48-96 h post EV administration.

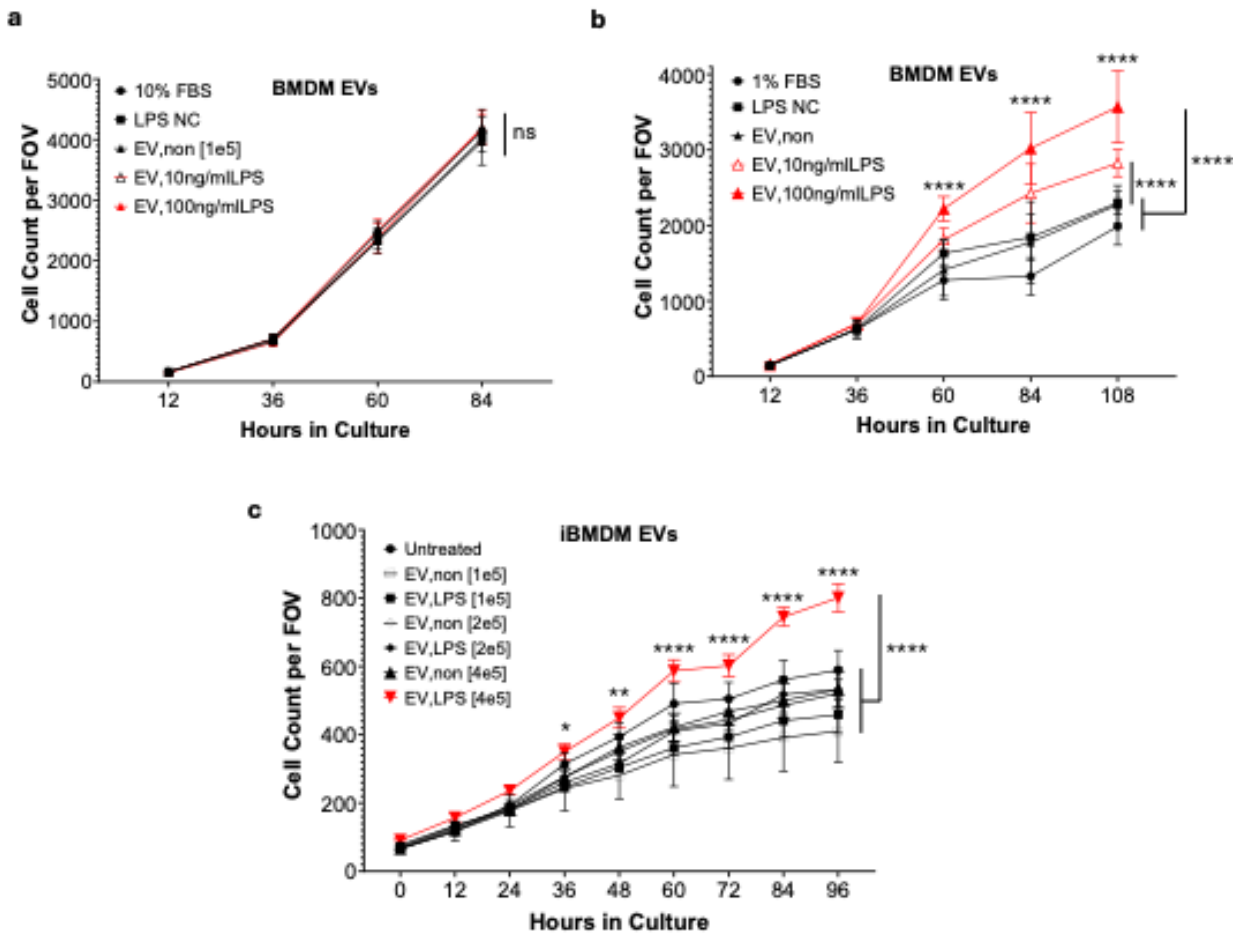

Figure 3.5 Growth kinetics of MC38 colon cells treated with extracellular vesicles (EVs) from primary bone marrow-derived macrophages (BMDMs) and immortalized BMDMs (iBMDMs) that were non-activated or activated with lipopolysaccharide (LPS) in different concentrations of fetal bovine serum (FBS) depleted of EVs. (a) Growth rate is unchanged in MC38 cells cultured in 10% FBS that were treated with EVs from BMDMs that were non-activated (EV_{non}) or activated with 10 ng/ml LPS ($EV_{10ng/mlLPS}$) or 100 ng/ml LPS ($EV_{100ng/mlLPS}$) at a concentration of [1×10^5] BMDM EVs per MC38 cell seeded. (b) Growth rate of MC38 cells cultured in 1% FBS that were treated with EVs from BMDMs that were EV_{non} or $EV_{10ng/mlLPS}$ or $EV_{100ng/mlLPS}$ at a concentration of [1×10^5] BMDM EVs/MC38. (c) Growth rate of MC38 cells that were treated with EVs from iBMDMs that were EV_{non} or $EV_{10ng/mlLPS}$ or $EV_{100ng/mlLPS}$ at different EV concentrations [# iBMDM EVs/MC38]. Not significant (ns), *p<0.05, **p<0.01, ****p < 0.0001, mean (SD), n = 6, two-way ANOVA followed by Tukey's post-hoc test (values on right of graph compare all timepoints between groups; values on top of EV_{LPS} conditions are compared per timepoint to EV_{non} condition). LPS negative control (NC) treatment was to control for EV treatments i.e. ~7 µl of EV volume was administered of EV_{LPS} and of 100 ng/ml LPS to confirm that residual endotoxin was not responsible for effects in growth kinetics. Concentrations are expressed in scientific notation (e.g., [2e5] = [2×10^5]); in graph labels, text after the comma appears as subscript (e.g., EV,LPS = EV_{LPS}).

EVs from LPS-activated macrophages increase anchorage-independent growth and pro-tumorigenic IL-17 signaling protein expression in colon cells

Because proliferation and metabolic reprogramming is also characteristic of inflammation, I wanted to test if EVs from LPS-activated macrophages may induce transformational changes in recipient cells. I found that EVs from LPS-activated Raw264.7 cells increased CT26 colony formation in soft agar at two different concentrations of EVs (Figure 3.6a). From this I concluded that LPS-activated macrophage EVs increase the anchorage-independent growth capacity of transformed CT26 cells. I also performed soft agar assays on MC38 colon cancer cells treated with EVs from non-activated and LPS-activated iBMDMs. Relative to non-activated iBMDM EVs, MC38 cells treated with EVs from LPS-activated iBMDM EVs grew increasingly anchorage-independently in a concentration-dependent manner (Figure 3.6b,c). Surprisingly, non-activated iBMDM EVs decreased colony formation relative to untreated transformed cells, which may imply that non-activated macrophage EVs also play a role in negatively regulating colon cancer cell growth in 3D cultures and therefore, possibly, in vivo too.

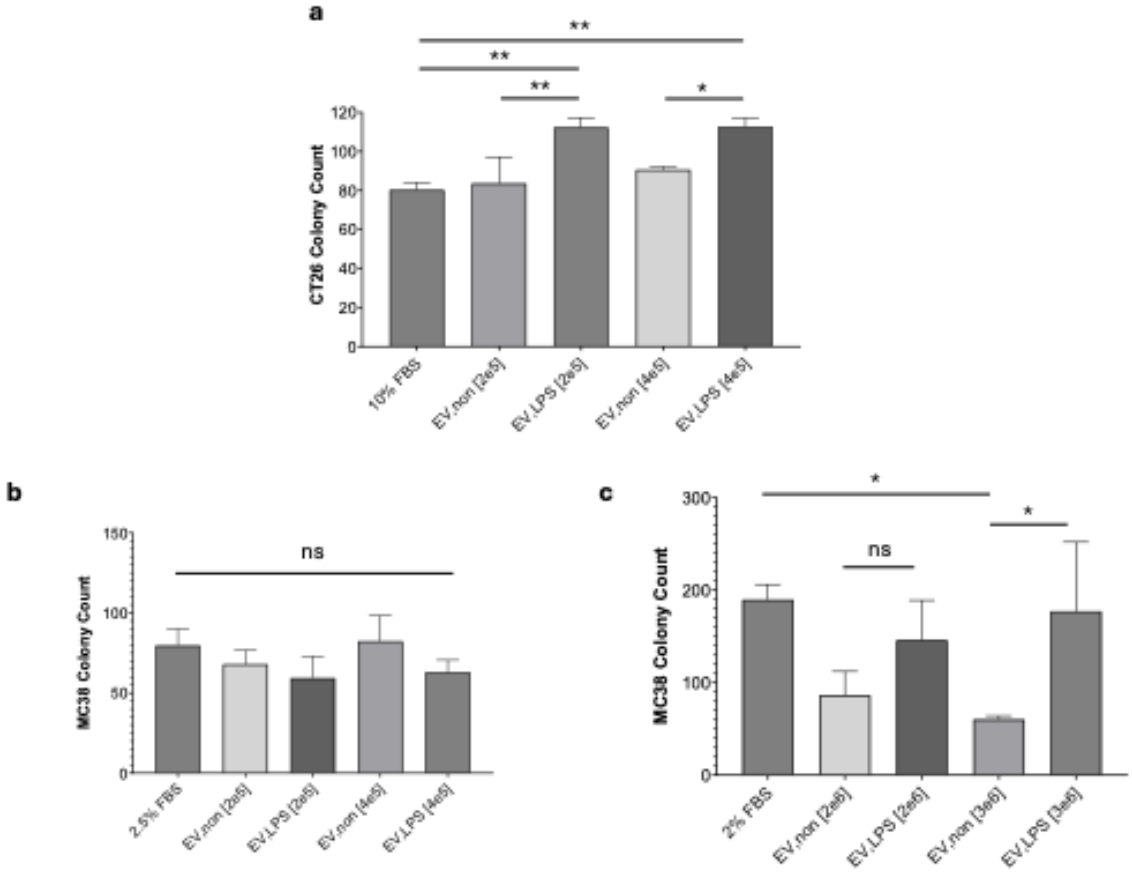

Figure 3.6 Extracellular vesicles (EVs) from lipopolysaccharide (LPS)-activated macrophages increase anchorage-independent growth in soft agar of colon cancer cells. (a) Anchorage-independent growth of CT26 cells is increased when treated with EVs from LPS-activated Raw cells (EV_{LPS}) as compared with EVs from non-activated Raw cells (EV_{non}) at concentrations of [2×10^5] and [4×10^5] macrophage EVs/cell. (b) Anchorage-independent growth of MC38 cells is not changed when treated with EVs from non-activated and LPS-activated immortalized bone marrow-derived macrophages (iBMDMs) at a concentration of [2×10^5] and [4×10^5] macrophage EVs/cell. (c) LPS-activated iBMDM EVs (EV_{LPS}) increased anchorage-independent MC38 growth relative to non-activated iBMDM EVs (EV_{non}) in a dose-dependent manner. Not significant (ns), *p<0.05, **p<0.01, mean (SD), n = 3, one-way ANOVA followed by Tukey's post-hoc test. Concentrations are expressed in scientific notation (e.g., [2e5] = [2×10^5]); in graph labels, text after the comma appears as subscript (e.g., EV,LPS = EV_{LPS}).

Next, I wanted to investigate what signals could be contributing to the increase growth rate of colon cells in response to LPS-activated macrophage EVs. In collaboration with the MSU Proteomics Core and Dr. Maryam Sayadi, we performed a mass spectrometry analysis to identify differentially expressed proteins in MC38 cells treated with EVs from non-activated iBMDMs (EV_{non}) and EVs from LPS-activated iBMDMs (EV_{LPS}) at two different concentrations. Heat maps showed significantly different protein expression levels at a population level between EV_{LPS}-treated MC38 cells and EV_{non}-treated MC38 cells at

concentrations of [2×10^5] and [4×10^5] iBMDM EVs per recipient MC38 cell seeded initially in experiment (Figure 3.7a,d). Principal component (PC) analysis confirmed the differential expression of protein profiles between EV_{LPS}-treated MC38 cells and EV_{non}-treated MC38 cells at [2×10^5] EV/cell (Figure 3.7e) and [4×10^5] EV/cell (Figure 3.7g). Heat map analysis also showed us that there were no significant differences in protein profiles between MC38s treated with EV_{non} between the differing concentration treatments of [2×10^5] vs [4×10^5] EV/cell (Figure 3.7c), or in MC38s treated with EV_{LPS} at [2×10^5] vs [4×10^5] EV/cell (Figure 3.7d).

To visualize and identify differentially expressed proteins from this massive amount of data, we made volcano plots of proteins that are up- and downregulated in MC38s treated with EV_{LPS} relative to EV_{non} as reference, with fold change threshold set to 2, and $p < 0.1$ at both EV treatment concentrations (Figure 3.7f,h). Pathway enrichment analysis (PEA) revealed the IL-17 signaling pathway to be upregulated in EV_{LPS}-treated MC38s based on a significant number of upregulated proteins involved in IL17 signaling (Figure 3.8a). The IL-17 signaling pathway has been identified as a pro-tumorigenic molecular mechanism involved in colitis-associated cancer[188, 221]. The three proteins identified to be upregulated and significantly involved in this pathway in EV_{LPS}-treated MC38 cells (Figure 3.8) include Fos-related antigen 1 (Fra-1), Prostaglandin-endoperoxide synthase 2 (Ptgs2 or COX2), and CCAAT/enhancer binding protein-beta (C/EBPβ). These proteins were verified to be expressed in EV-treated MC38 proteins via immunoblotting (Figure 3.8e-g), and the same trend is observed upon quantification, although immunoblotting analysis was not sensitive enough to allow quantification at the level needed for determining statistical significance of the observed differences (Figure 3.8h-j).

Next, we investigated various other proteins previously reported to facilitate colitis-associated cancer. We found nuclear factor-kappa B NF-κB1, NF-κB2, and cyclin-dependent kinase-1 (CDK1) protein levels to be significantly upregulated in MC38 cells treated with EVs from LPS-activated macrophages (EV_{LPS}) relative to EVs from non-activated macrophages (EV_{non}) at [2×10^5] and [4×10^5] macrophage EVs/MC38 cell and untreated (Figure 3.9a-c). We also investigated signal transducer and activator of transcription (STAT) factors prevalent in colitis associated cancer. Mass spectrometry detected STAT1 to be significantly downregulated in EV_{LPS}-treated MC38 proteins relative to EV_{non} treatment and untreated, with no changes detected in STAT3 or STAT6 (Figure 3.10d-f). The selective downregulation of STAT1 without changes in STAT3 or STAT6 suggests that EVs from LPS-activated macrophages may preferentially affect interferon signaling pathways rather than IL-6 family and/or IL-4/IL-13 pathways[222]. This may provide a molecular basis for macrophage EV-induced changes in colon cell growth in

monolayer and soft agar indicating anchorage-dependent and anchorage-independent growth rates, respectively.

Mass spectrometry also detected a moderately increased expression of the tumor suppressor p53 protein in MC38 cells treated with $EV_{LPS}[2\times10^5]$, $EV_{non}[4\times10^5]$, and $EV_{LPS}[4\times10^5]$ relative to untreated (Figure 3.10a). A moderately decreased level of the Mothers against decapentaplegic homolog 2 (SMAD2) transcription factor was detected in MC38 cells treated with $EV_{LPS}[4\times10^5]$ relative to $EV_{non}[2\times10^5]$ and untreated (Figure 3.10b). There was a mildly increased level of p38 (MAPK14) expression detected in MC38 cells treated with $EV_{LPS}[4\times10^5]$ relative to $EV_{non}[2\times10^5]$, and no change was detected in cell division cycle regulator cyclin A2, cell movement regulator β-catenin 1, immune escape-promoting CD47, or antigen presentation machinery MHC I protein expression between MC38 treatment conditions (Figure 3.10c-i).

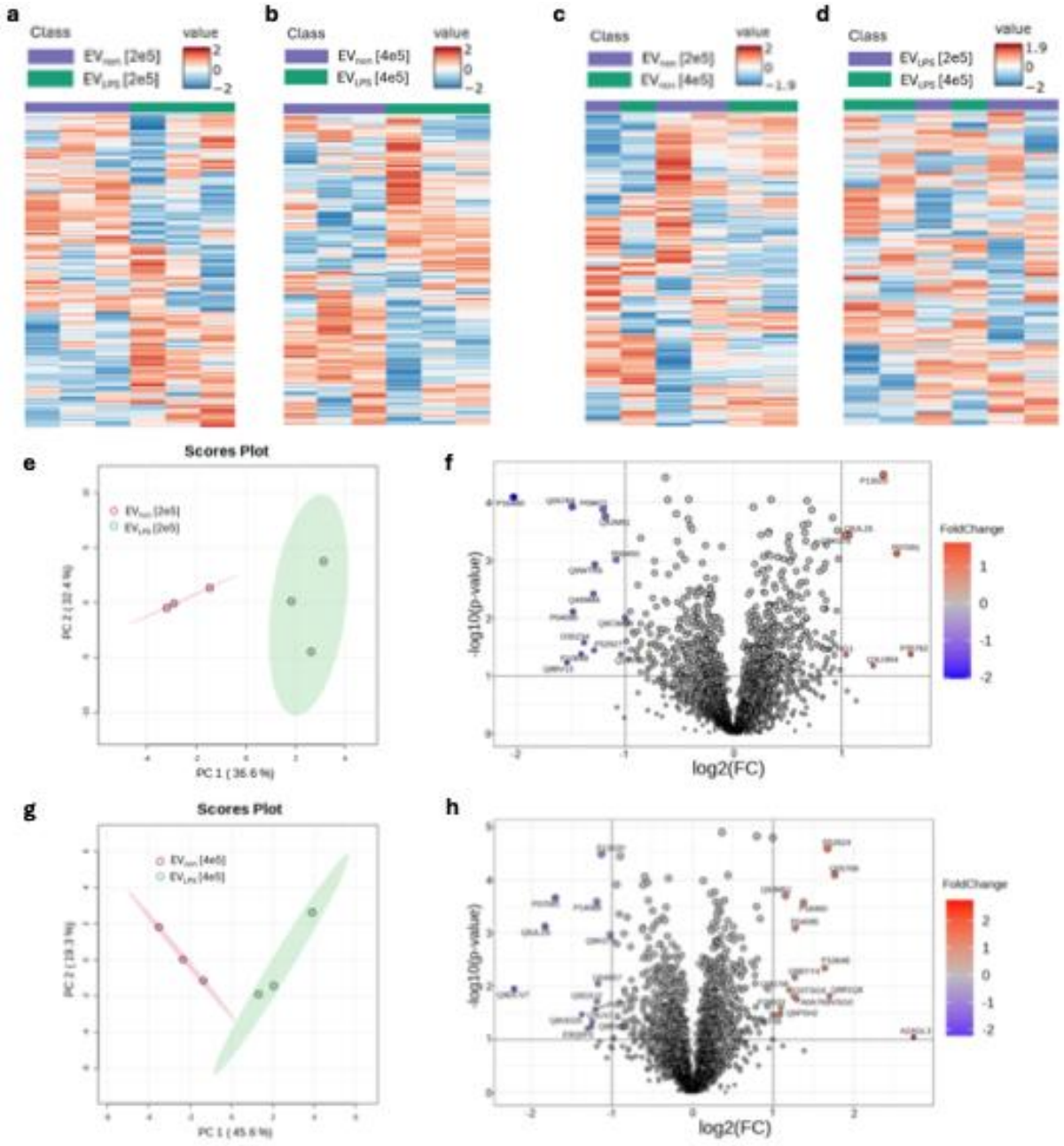

Figure 3.7 Mass spectrometry analysis of MC38 colon cells treated with extracellular vesicles (EVs) from non-activated and lipopolysaccharide (LPS)-activated immortalized bone marrow-derived macrophages (iBMDMs). (a,b) Heat maps showing differentially expressed proteins in MC38 cells treated with EVs from non-activated iBMDMs (EV_{non}) and EVs from LPS-activated iBMDMs (EV_{LPS}) at (a) [2×10^5] or (b) [4×10^5] iBMDM EVs/MC38 cell seeded. (c,d) Heat maps showing differentially expressed proteins in MC38s treated with (c) EV_{non} or (d) EV_{LPS} at [2×10^5] and [4×10^5]. (e) Principal component analysis (PCA) of proteins from MC38s treated EV_{non} and EV_{LPS} at [2×10^5]. (f) Volcano plot showing up- (red) and down-regulated (blue) proteins expressed in MC38s treated with EV_{LPS} relative to EV_{non} at [2×10^5]; fold change set to 2, $p < 0.1$. (g) PCA of proteins from MC38s treated with EV_{non} and EV_{LPS} at [4×10^5]. (h) Volcano plot showing up- (red) and down-regulated (blue) proteins in MC38s treated with EV_{LPS} relative to EV_{non} at [4×10^5]; fold change set to 2, $p < 0.1$.

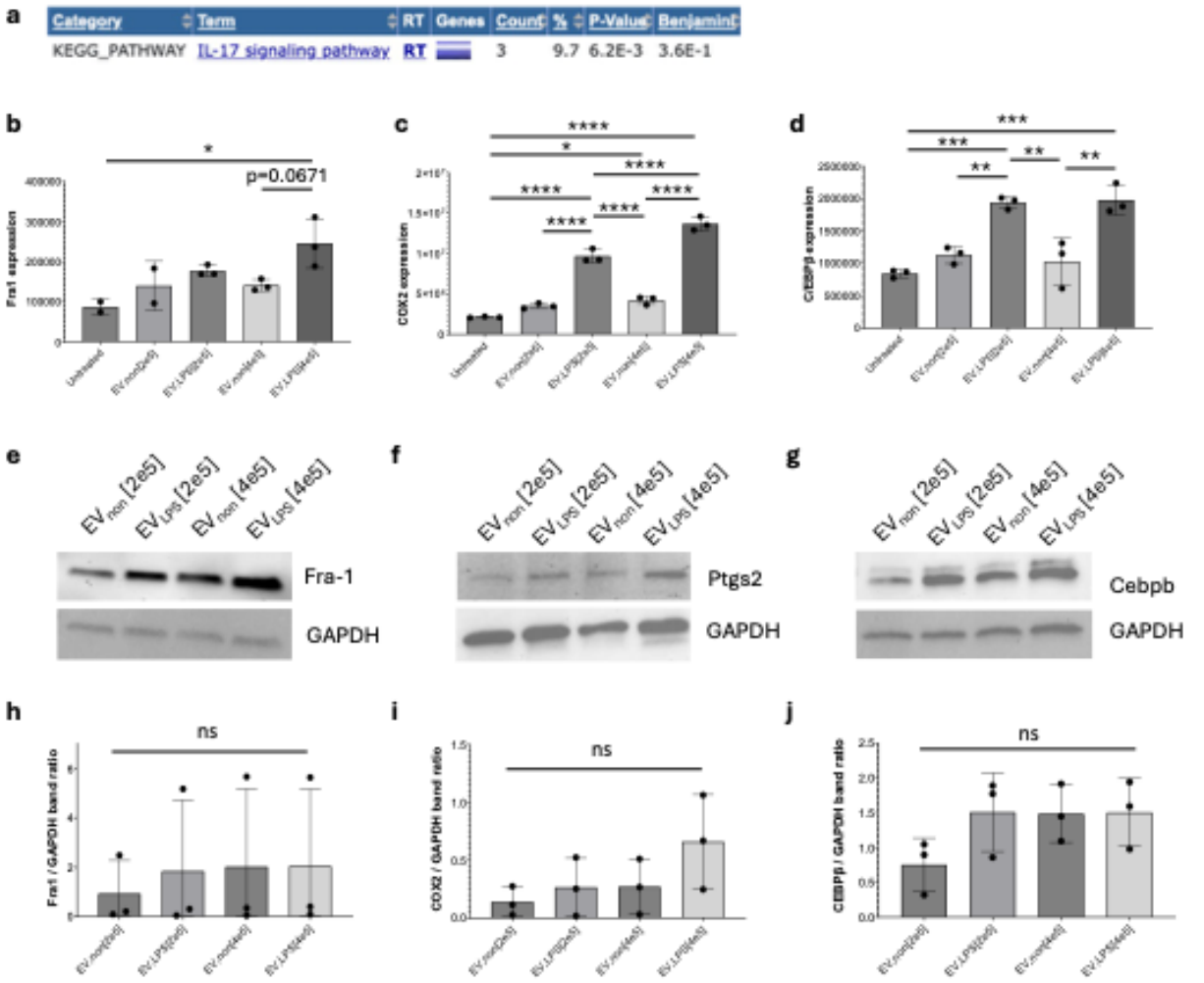

Figure 3.8 Pathway enrichment analysis (PEA) revealed MC38 colon cells treated with extracellular vesicles (EVs) from lipopolysaccharide (LPS)-activated immortalized bone marrow-derived macrophages (iBMDMs) express increased protumorigenic IL17 signaling pathway proteins as compared with MC38 cells treated with EVs from non-activated iBMDMs (EV_{non}). (a) Functional annotation chart showing PEA-determined a list of signaling pathways (terms) found to be differentially expressed in MC38s treated with LPS-activated iBMDM EVs (EV_{LPS}) relative to MC38s treated with EV_{non} via the KEGG database; also shown in table includes related terms (RT) i.e. related pathways, the number of proteins detected that participate in a particular pathway (count), percent involved proteins / total proteins (%), p-value showing significance, and Benjamini correction referring to false discovery rate (FDR); significance in PEA determined via FDR analysis. (b-d) Protein expression of Fos-related antigen 1 (Fra1, b), Prostaglandin-endoperoxide synthase 2 (Ptgs2, c), and CCAAT/enhancer binding protein-beta (Cepbp, d) in MC38 cells treated with EV_{non} and EV_{LPS} at a concentration of [2×10^5] and [4×10^5] iBMDM EVs/MC38 cell seeded. (e-g) Immunoblotting confirmed presence of Fra1 (e), Ptgs2 (f), and Cebpb (g) proteins expressed in MC38s treated with EV_{non} and EV_{LPS} at [2×10^5] and [4×10^5] EV/cell. (h-j) Quantification of respective western blots bands of Fra1 (h), Ptgs2 (i), and Cebpb (j) proteins expressed in MC38s treated with EV_{non} and EV_{LPS} at [2×10^5] and [4×10^5] EV/cell. Not significant (ns), mean (SD), n=3, significance determined via one-way ANOVA followed by Tukey's post-hoc test. Concentrations are expressed in scientific notation (e.g., [2e5] = [2×10^5]); in graph labels, text after the comma appears as subscript (e.g., EV,LPS = EV_{LPS}).

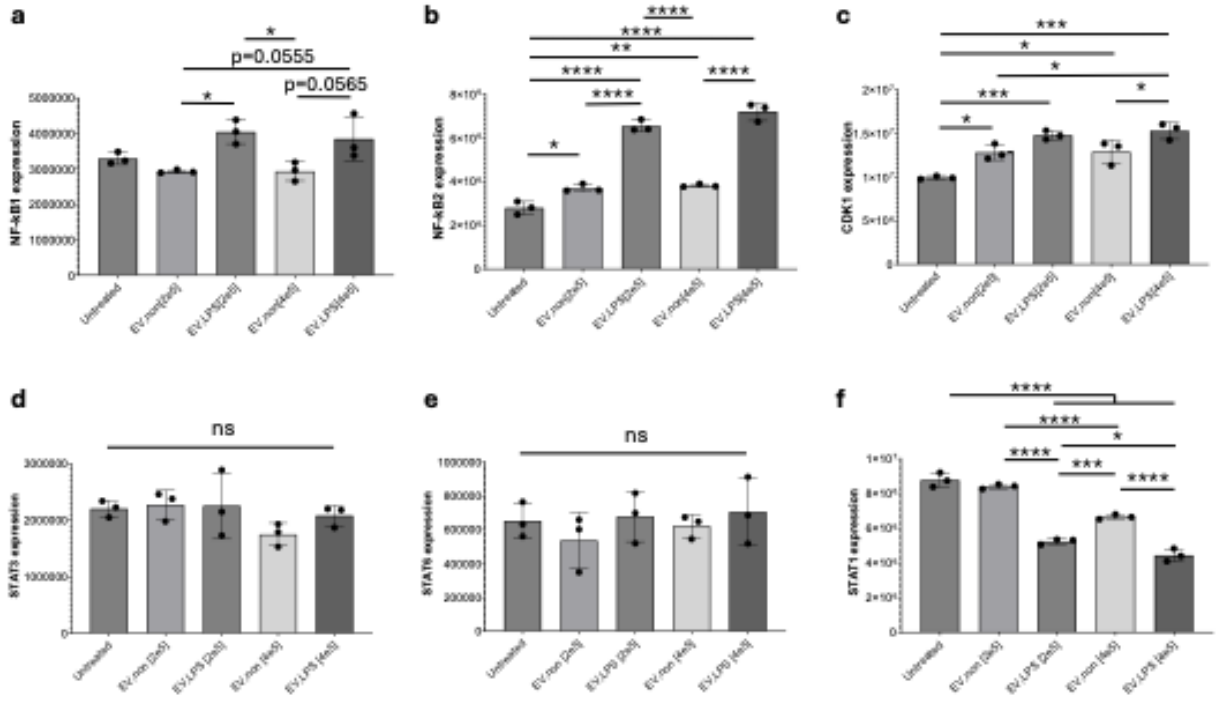

Figure 3.9 Mass spectrometry revealed that MC38 colon cells treated with extracellular vesicles (EVs) from lipopolysaccharide (LPS)-activated immortalized bone marrow-derived macrophages (iBMDMs) express differential levels of proteins involved in the progression of colitis-associated cancer. (a-c) MC38 cells treated with EVs from LPS-activated iBMDMs (EV_{LPS}) have increased levels of nuclear factor-kappa B1 (NF-kB1, a), NF-kB2 (b), and cyclin-dependent kinase-1 (CDK-1, c) protein compared to MC38 cells treated with EVs from non-activated iBMDMs (EV_{non}) at concentrations of [2×10^5] and [4×10^5] iBMDM EVs per MC38 cell seeded. (d,e) Changes in STAT3 (d) and STAT6 (e) expression levels were not detected in MC38 cells treated with EV_{LPS} and EV_{non}. (f) STAT1 expression was decreased in MC38 cells treated with EV_{LPS} compared to EV_{non} at both concentrations; conditions described in Table 3.1. Not significant (ns), *p<0.05,**p<0.01, ***p<0.001, ****p<0.0001, mean (SD), n=3, significance determined via one-way ANOVA followed by Tukey's post-hoc test. Concentrations are expressed in scientific notation (e.g., [2e5] = [2×10^5]); in graph labels, text after the comma appears as subscript (e.g., EV,LPS = EV_{LPS}).

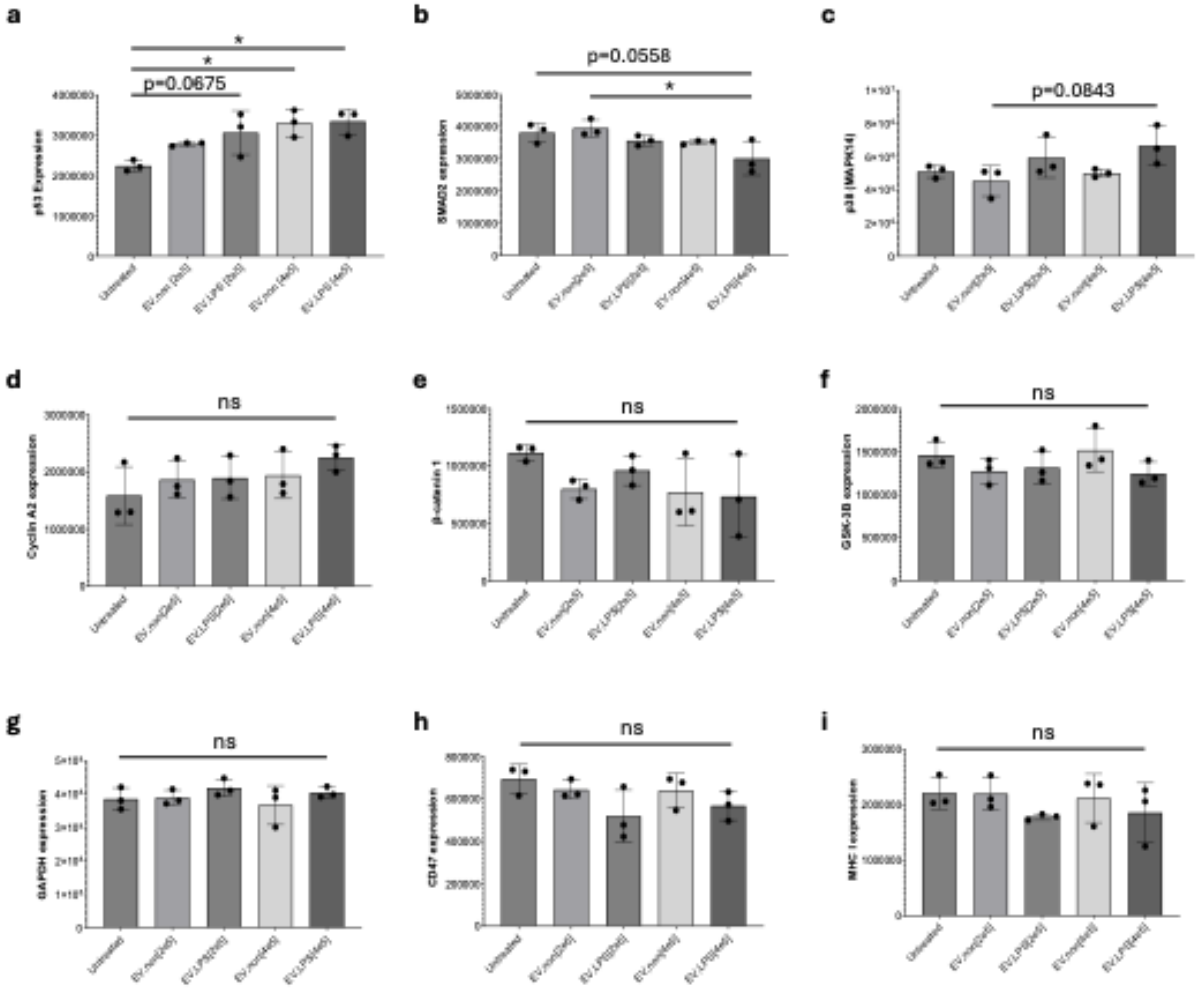

Figure 3.10 Mass spectrometry detected moderately differentially expressed proteins in MC38 cells treated with extracellular vesicles (EVs) from lipopolysaccharide (LPS)-activated immortalized bone marrow-derived macrophages (iBMDMs) and EVs from non-activated iBMDMs (EV_{non}). (a) p53 expression was mildly increased in MC38s treated with EVs from LPS-activated iBMDMs (EV_{LPS}) and EV_{non} at concentrations of [2×10^5] and/or [4×10^5] iBMDM EVs per MC38 cell seeded, relative to untreated. (b) MC38 cells treated with EV_{LPS} at [4×10^5] iBMDM EVs/cell (EV_{LPS}[4e5]) expressed moderately decreased levels of SMAD2 relative to untreated MC38s. (c) MC38 cells treated with EV_{LPS}[4e5] expressed moderately decreased levels of p38 (MAPK14) compared to MC38 cells treated with EV_{non}[2e5]. (d-i) Expression of Cyclin A2 (d),B-catenin-1 (e), glycogen synthase kinase-3 beta (GSK-3B, f), glyceraldehyde 3-phosphate dehydrogenase (GAPDH, g), CD47 (h), and MHC I (i) protein levels was unchanged between MC38 treatment conditions; conditions described in Table 3.1. Not significant (ns), *p<0.05, mean (SD), n=3, significance determined via one-way ANOVA followed by Tukey's post-hoc test. Concentrations are expressed in scientific notation (e.g., [2e5] = [2×10^5]); in graph labels, text after the comma appears as subscript (e.g., EV,LPS = EV_{LPS}).

Normal cell survival and proliferation is typically anchorage-dependent and mediated by signaling pathways including integrin signaling and growth factor pathways[223]. Anchorage-independent

growth is the ability of transformed cells to grow in the absence of "anchoring" signals from a solid surface; this is a hallmark of carcinogenesis[224]. So, dissecting the signaling pathways in recipient colon cells that mediate their EV_{LPS}-induced increase in anchorage-independent growth in soft agar is crucial to understanding the molecular mechanism(s), by which EVs from LPS-activated macrophages drive inflammation-mediated tumorigenesis. Anchorage-independent growth is required for cancer cells to detach from the basement membrane and invade the underlying connective and muscular tissues[225]. Uncontrolled proliferation, invasion, and metastasis are three hallmarks, i.e., key defining features, of cancer cells. Invasion and metastasis require cell migration, for which epithelial lineage cells need to undergo the process of epithelial-to-mesenchymal transition (EMT)[226]. During EMT, cellular gene expression shifts away from epithelial cell markers, such as E-cadherin, towards upregulated expression of mesenchymal markers including vimentin, N-cadherin, and the transcription factors Snail, Slug, Twist, and ZEB1[227]. This is why I next attempted to test whether EMT was involved in EV_{LPS}-induced MC38 increase in anchorage-independent growth (required for invasion) and increased cell growth (potentially mediated by proliferation).

I isolated RNA from MC38 cells treated with EV_{LPS} and EV_{non} at concentrations of [2×10^5] and [4×10^5] iBMDM EVs/MC38 cell seeded. My first attempt at RNA isolation using TRIzol chloroform extraction produced RNA of abysmal quality, i.e., Tapestation analysis showed RNA integrity number (RIN) values of less than 5 across the board (RIN scale: 1-10, with ≥8 ideal for most applications). I tried to be very careful to not take up DNA after phase separation, but in consulting with Dr. Kevin Childs we decided quality may be impacted from trace amounts of phenol remaining in the RNA-containing supernatant that interfered with RNA quality. After re-running the experiment and isolating RNA via column extraction using Qiagen's RNeasy kit, Tapestation results showed the quality of my RNA to have a RIN $\geq$ 9.7 in every sample. After that, I was confident to send these RNA samples for sequencing and proceed with performing RT-qPCR.

Then, we characterized differential mRNA expression of a panel of epithelial and mesenchymal biomarkers via RT-qPCR in MC38 cells treated with EV_{LPS} and EV_{non} at different concentrations. We found that MC38s treated with EV_{LPS} at a concentration of [2×10^5] iBMDM EV/MC38 cell expressed decreased levels of E-cadherin (Ecad) and Snail mRNA as compared with untreated MC38s after 24 h (Figure 3.11a). MC38s treated with EV_{non}[2×10^5] expressed increased levels of vimentin (Vim), N-cadherin (Ncad) and Twist mRNA as compared with other conditions after 24 h (Figure 3.11a). MC38s treated with EV_{LPS} at a concentration of [2×10^5] iBMDM EV/MC38 cell expressed increased levels of Ecad, Slug, and ZEB1 mRNA as compared with other select treatment conditions after 48 h (Figure 3.11b).

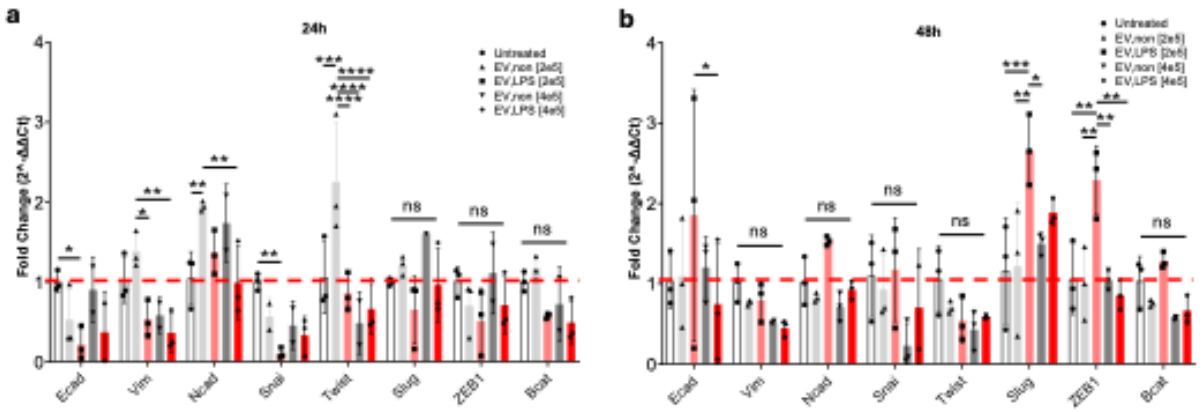

Figure 3.11 MC38 colon cells treated with high concentration of extracellular vesicles (EVs) from lipopolysaccharide (LPS)-activated immortalized bone marrow-derived macrophages (iBMDMs) express increased N-cadherin (Ncad) and Snail mRNA levels as compared with MC38 cells treated with higher concentration [4×10^5 iBMDM EV/MC38 cell seeded] EVs from non-activated iBMDM EVs (EV_{non}) after 24 h (a) but not 48 h (b). Not significant (ns), mean (SD), n=3, significance determined via one-way ANOVA followed by Tukey's post-hoc test. Concentrations are expressed in scientific notation (e.g., [2e5] = [2×10^5]); in graph labels, text after the comma appears as subscript (e.g., EV,LPS = EV_{LPS}).

Colon explants undergo autophagy in culture

I next attempted to treat colon explants with primary BMDM EVs in ex vivo cultures in the hopes of developing a more physiologically relevant model. Harvested colon explants underwent autophagy when cultured ex vivo (Figure 3.12a,b). I was able to mildly mitigate loss of some crypt structures by supplementing medium with epidermal growth factor (EGF) and Insulin-Transferrin-Selenium (ITS); however, there was still autophagy present (Figure 3.12c).

Because the TP53 gene encoding the pro-apoptotic transcription factor p53 is commonly mutated in early colitis-associated cancer and thus its protein product becomes functionally inactivated, I wanted to investigate whether EVs or SFs from LPS-activated BMDMs (representing colitis) exhibit anti-apoptotic effects and mitigate the autophagy found in colon tissue explants. Colon tissue biopsies treated with approximately [9×10^4] LPS-activated BMDM EVs per colon cell did not exhibit any preserved crypt structure or cell viability as compared to non-activated iBMDM EVs (Figure 3.13). SFs from LPS-activated BMDMs also did not improve autophagy and loss of cell viability/crypt structure as compared to SFs from non-activated BMDMs (Figure 3.14). Thus, a low concentration of macrophage EVs or SFs did not demonstrate a significantly protective effect against this tissue degradation.

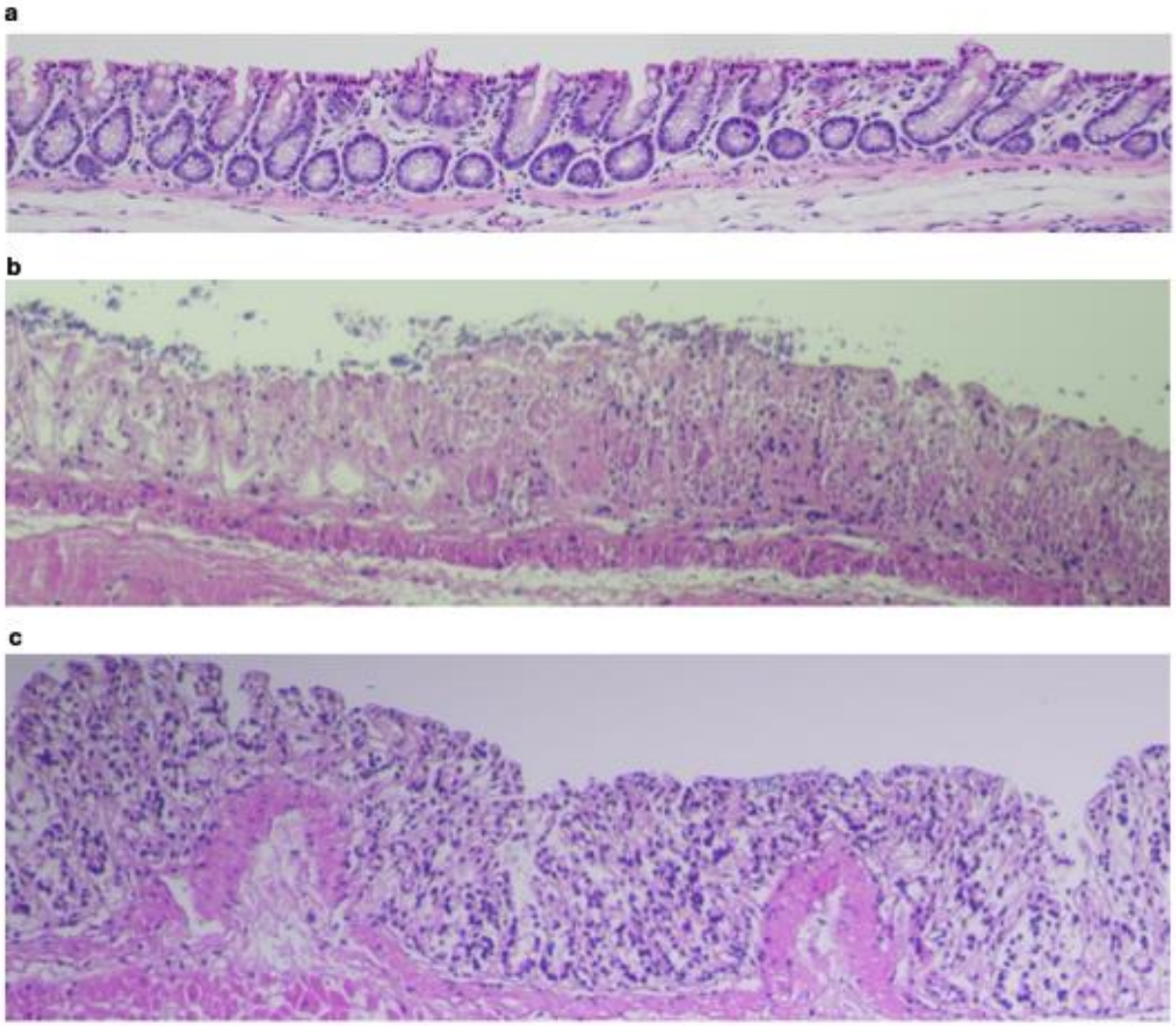

Figure 3.12 Crypt morphology of mouse colon explants cultured ex vivo show culture conditions may mildly mitigate autophagy after 3 days. (a) Colon tissue was H&E stained immediately after harvesting. (b) Colon tissue cultured for 3 d in DMEM medium supplemented with 2% penicillin/streptomycin antibiotics. (c) Colon tissue cultured for 3 d in DMEM/F12 medium supplemented with 100 ng/ml EGF, ITS, and 2% antibiotics. Images taken at 10X magnification.

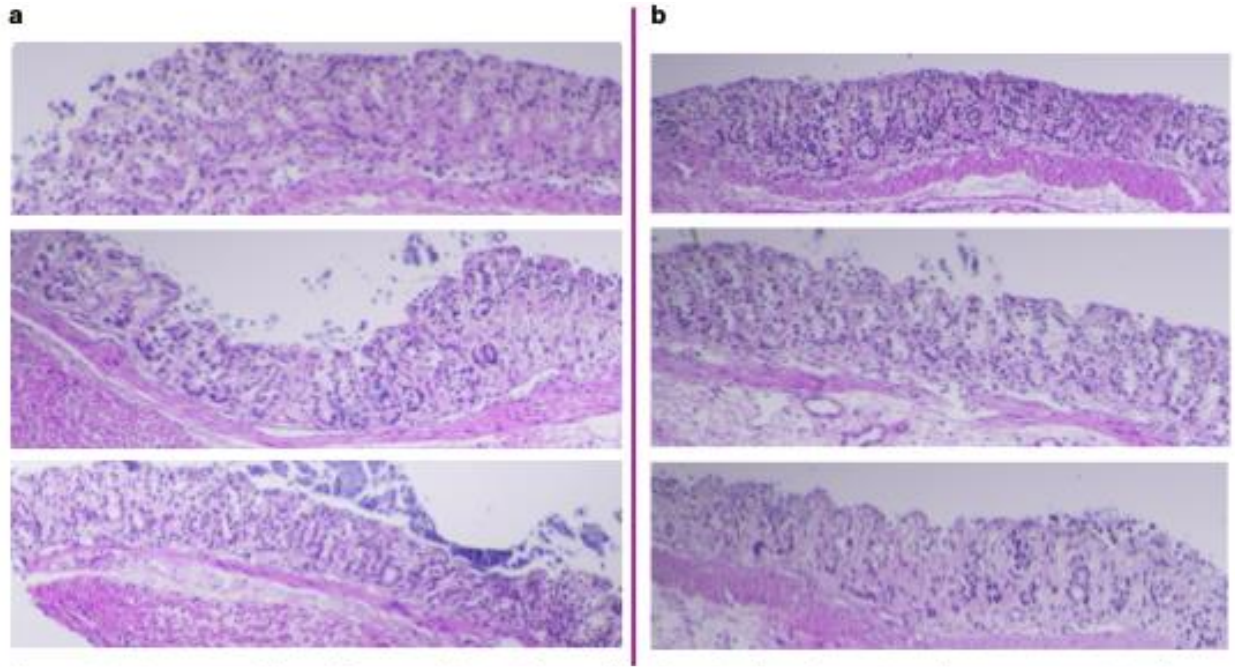

Figure 3.13 Crypt morphology of mouse colon explants cultured ex vivo show that primary bone marrow-derived macrophage (BMDM)-secreted extracellular vesicles (EVs) did not significantly reduce autophagy. (a) H&E stains showing colon explants from three different mice co-cultured with EVs from non-activated BMDMs for 48 h (concentration: [9×10^4] EVs/cell). (b) Colon explants from three different mice co-cultured with EVs from BMDMs activated with 100 ng/ml lipopolysaccharide (LPS) also did not reduce autophagy of colon explants cultured ex vivo (concentration: [9×10^4] EVs/cell). Images taken at 10X magnification.

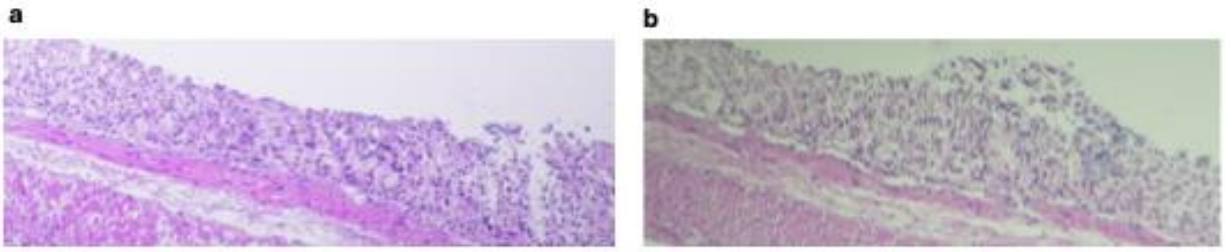

Figure 3.14 Crypt morphology of mouse colon explants cultured ex vivo show that primary bone marrow-derived macrophage (BMDM)-secreted soluble factors (SFs) did not significantly reduce autophagy in colon explants. (a) H&E stains showing colon explants cultured with SFs from non-activated BMDMs for 48 h. (b) Colon explants cultured with SFs from BMDMs activated with 100 ng/ml lipopolysaccharide (LPS) also did not reduce autophagy of colon explants. Images taken at 10X magnification.

EVs from LPS-activated iBMDMs mediate myeloid cell differentiation and activation in the tumor immune microenvironment

After elucidating the functional effects of EVs from LPS-activated macrophages on colonic epithelial cells in culture, I wanted to characterize effects of EV_{LPS} on predisposing colon tissue to tumor induction and progression. First, we subcutaneously (s.c.) injected 100 µl saline (PBS) or EVs from LPS-activated iBMDMs into the right flank of BL6-albino mice for 7 d prior to injection of MC38 cells or MC38 cells expressing the akaLuciferase protein (MC38-akaLuc). Akaluciferase is a novel luciferase protein with higher signal intensity than D-luciferase[228, 229]; however, luciferase has been reported to be immunogenic and affect tumor growth[230, 231]. Mouse experimental conditions are described in Figure 3.15 and Table 3.1.

I injected MC38-akaLuc tumor-bearing mice intraperitoneally (i.p) with substrate Akalumine-HCl and performed bioluminescence imaging (BLI) using the In Vivo Imaging System (IVIS) every other day for 38 d post tumor induction. I found that there was no significant difference between the average radiance of MC38-akaLuc tumor-bearing mice injected with EVs from LPS-activated iBMDMs before tumor induction as compared to MC38-akaLuc tumor-bearing mice injected with PBS before tumor induction (Figure 3.16a). However, I deem this as not a representative model because the size of the tumors were not very proportional to the BLI signal intensities (Figure 3.16d). This could be because non-akaLuc expressing MC38 cells survived and proliferated, or because the tumor cells suppressed expression of akaLuc. Regardless, I decided against using this model because of the high variability within groups and the potential for akaLuc immunogenicity to interfere with our dependent variable measuring tumor growth due to immunogenicity of EVs from LPS-activated iBMDMs. We did not see a difference in tumor mass of MC38-akaLuc tumor-bearing mice injected with EVs from LPS-activated iBMDMs before tumor induction as compared with MC38-akaLuc tumor-bearing mice injected with PBS before tumor induction (Figure 3.16c).

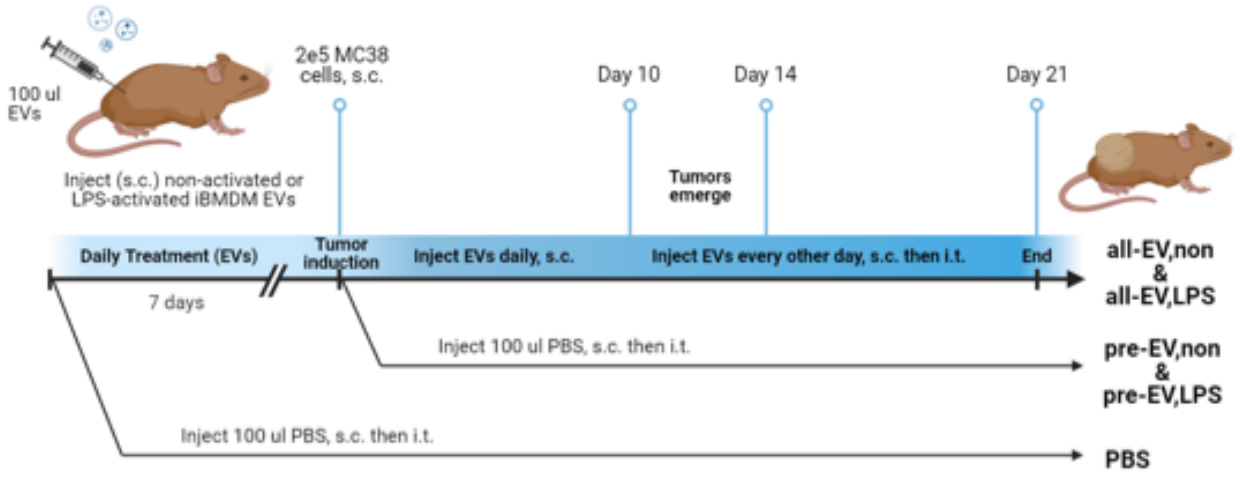

Figure 3.15 Graphic showing our mouse model of colitis-associated cancer (CAC) and injection conditions. Colitis-associated cancer (CAC), extracellular vesicles (EVs), subcutaneous (s.c.), intratumoral (i.t.).

Table 3.1 Extracellular vesicle (EV)-treated MC38 tumor experimental conditions; 100 µl volume per injection. Tumors were induced with 2×10^5 MC38 colon cancer cell injection on day 0, and tumors emerged around day 10-14. Abbreviation (abbv), phosphate buffered saline (PBS), immortalized bone marrow-derived macrophages (iBMDM), extracellular vesicles (EVs), non-activated iBMDM EVs (EV_{non}), lipopolysaccharide (LPS), LPS-activated EVs (EV_{LPS}), subcutaneous (s.c.), intratumoral (i.t.).

Description of Condition	**Abbv**	**Day -7 to 0**	**Day 0**	**Day 0 to 10 (daily)**	**Day 11 to 21 (every 2 d)**
Saline ctrl	PBS	PBS, s.c.	MC38, s.c.	PBS, s.c.	PBS, i.t.
Tumor site preconditioned with EVs from non-activated iBMDMs	pre-EV_{non}	EV_{non}, s.c.	MC38, s.c.	PBS, s.c.	PBS, i.t.
Tumor site preconditioned with EVs from LPS-activated iBMDMs	pre-EV_{LPS}	EV_{LPS}, s.c.	MC38, s.c.	PBS, s.c.	PBS, i.t.
Tumor site preconditioned and injected all through experimental duration with EVs from non-activated iBMDMs	all-EV_{non}	EV_{non}, s.c.	MC38, s.c.	EV_{non}, s.c.	EV_{non}, i.t.
Tumor site preconditioned and injected all through experimental duration with EVs from LPS-activated iBMDMs	all-EV_{LPS}	EV_{LPS}, s.c.	MC38, s.c.	EV_{LPS}, s.c.	EV_{LPS}, i.t.

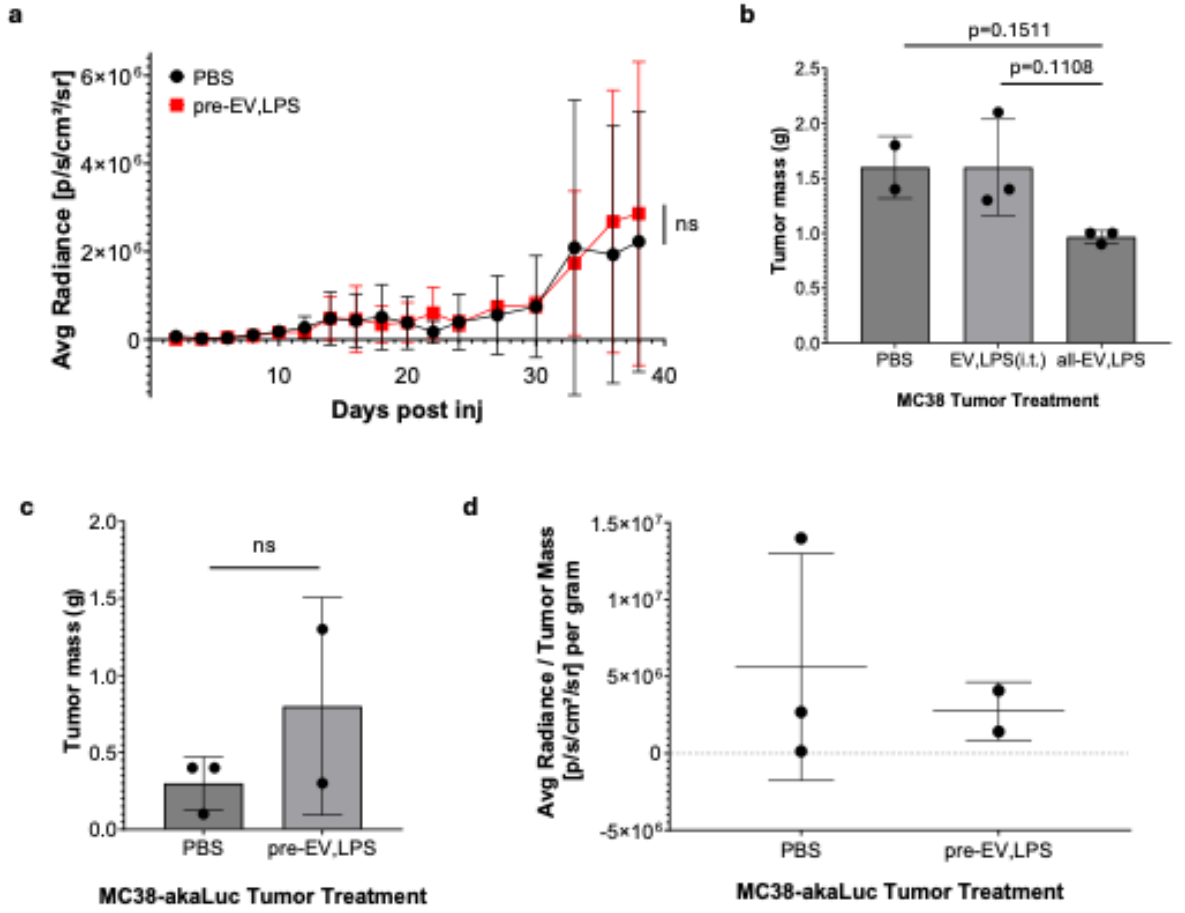

Figure 3.16 MC38 tumors labeled with akaLuciferase (akaLuc) did not express proportional radiance signal to tumor mass ratio. (a) Bioluminescence imaging (BLI) of MC38-akaLuc tumor-bearing mice showed no difference in radiance between mice injected with PBS and mice injected before tumor induction with extracellular vesicles (EVs) from immortalized bone marrow-derived macrophages (iBMDMs) activated with lipopolysaccharide (LPS). (b) Tumor mass of unlabeled MC38 tumor-bearing mice 21 days after tumor induction shows decreased tumor mass in mice injected before and after tumor induction with EVs from LPS-activated iBMDMs (all-EV_{LPS}) compared with mice injected with PBS and mice injected with EVs from LPS-activated iBMDMs intratumorally (i.t.) after tumor emergence on day 14 (EV,LPS(i.t.)). (c) Tumor mass of MC38-akaLuc tumor-bearing mice injected with EVs from LPS-activated iBMDMs before tumor induction (pre-EV_{LPS}) compared to mice injected with PBS before tumor induction. (d) Graph depicting the high variability of average radiance of MC38-akaLuc tumor-bearing mice per gram of tumor mass (day 38). Not significant (ns), mean (SD), n=2-3, two-way ANOVA (a) or one-way ANOVA (b) followed by Tukey's post-hoc test; unpaired t-test (c). In graph labels, text after the comma appears as subscript (e.g., pre-EV,LPS = pre-EV_{LPS}).

Interestingly, unlabeled MC38 tumor-bearing mice injected with EVs from LPS-activated iBMDMs before and after tumor induction harbored smaller tumors than MC38 tumor-bearing mice injected with PBS or EVs from LPS-activated iBMDMs intratumorally (i.t.) after tumor emergence on day

14 (Figure 3.16b). This was a modest effect, and contrary to what we were expecting based on our in vitro data that had suggested EVs from LPS-activated iBMDMs exerted a pro-tumorigenic effect. So, I hypothesized that EVs from iBMDMs interact with the tumor immune environment to impact tumor growth.

I thus repeated this pilot study with more cohorts including an immunophenotyping flow cytometry panel. We injected 100 µl saline (PBS, subcutaneous, s.c.), non-activated iBMDM EVs, or LPS-activated iBMDM EVs into the tumor site (flank) of BL6-albino mice for either 7-d prior to injection of MC38 cells, and/or 3 weeks post tumor induction (mouse experimental conditions are described in Figure 3.15 and Table 3.1).

We found that mice injected with LPS-activated iBMDM EVs (EV_{LPS}) before and after tumor induction (all-EV_{LPS}) developed tumors that were significantly larger than those in mice injected with non-activated iBMDM EVs (EV_{non}) before and after tumor induction (Figure 3.17a). Mice injected with EV_{non} before and after tumor induction (all-EV_{non}) produced the smallest group of tumors at endpoint day 22; in fact, two of these mice actually did not develop tumors sizable enough for resection or characterization by day 22. Similar to the pilot study, we also found mice injected with EV_{LPS} before tumor induction (pre-EV_{LPS}) developed tumors that were significantly smaller than those in mice injected with PBS (Figure 3.17b). However, the caveat to this latter finding is that one mouse from the pre-EV_{LPS} condition was excluded from these measurements due to its tumor being too large by day 17.

Three mice had to be excluded from the tumor volume measurements due to premature death (Table 3.2). One mouse from the all-EV_{LPS} condition stopped breathing after day 10 anesthesia exposure (<1 min, 2% isoflurane) and EV injections. All of the mice from this condition had erythema apparent surrounding the site of EV injection; we decided to inject mice only every other day after this occurrence. One mouse from the pre-EV_{LPS} condition developed a tumor that grew rapidly, and this mouse was humanely sacrificed on day 17. This also occurred with one PBS-injected mouse on day 20. On endpoint day 22, there were 4 mice with tumors too small to dissociate for flow cytometric analysis. This included 1 pre-EV_{LPS} injected mouse, 2 all-EV_{non} injected mice, and 1 all-EV_{LPS} injected mouse. Consequently, a total of seven mice were excluded from the flow cytometry study, to render a sample size of 2-4 in each group. The exclusion of these mice from the flow cytometry analysis represents a limitation in our study, particularly for the pre-EV_{LPS} group where early sacrifice of a mouse with an unusually aggressive tumor may have removed an important data point. Further studies with larger cohorts may provide more robust validation of these initial findings.

Immunophenotyping performed via flow cytometry (gating strategies shown in Table 3.3) showed no difference in the numbers of infiltrating $CD45^+$ nucleated hematopoietic cells present in the tumor microenvironment (TME) of mice between conditions (Figure 3.18a). Of the $CD45^-$ population, we did not detect significant differences in numbers of $CD31^+$ endothelial cells, indicating that vessel cell growth was not changed between conditions (Figure 3.18c).

Of the $CD45^+$ cell population, we found no difference in numbers of $CD11b^+$ myeloid cells between tumor conditions (Figure 3.18b). We did, however, find that tumors from mice injected with EV_{LPS} before and after tumor induction (all-EV_{LPS}) contained a significantly decreased number of $CD11b^+F4/80^+$ macrophages relative to all other conditions (Figure 3.19a). This may be due to an increased presence of other $CD11b^+$ myeloid cells that do not express F4/80, as can be seen by the population shift in the flow cytometry plot comparing CD11b and F4/80 expression in all-EV_{LPS} mouse tumors (Figure 3.19b-f).

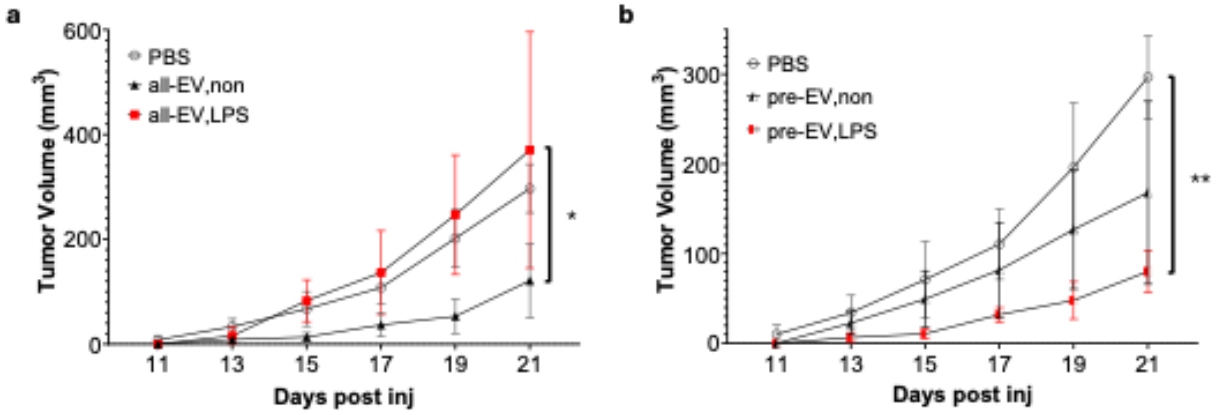

Figure 3.17 Tumor volumes of mice that survived for entirety of 22-day experiment. (a) Caliper measurements show bigger tumor size in mice injected with extracellular vesicles (EVs) from lipopolysaccharide (LPS)-activated macrophages in tumor site before and after tumor induction (all-EV_{LPS}) compared to EVs from non-activated macrophages (all-EV_{non}). (b) Tumor size is smaller in mice injected with EVs from LPS-activated macrophages in tumor site before tumor induction (pre-EV_{LPS}) relative to EVs from non-activated macrophages (pre-EV_{non}); mouse conditions are described in Table 3.2. *p<0.05, **p<0.01, mean (SEM), n = 2–4, one-way ANOVA followed by Tukey's post-hoc test. In graph labels, text after the comma appears as subscript (e.g., pre-EV,LPS = pre-EV_{LPS}).

Table 3.2 Mice that died before day 22 were excluded from the MC38 tumor study; conditions described in Table 3.2. Extracellular vesicles (EVs), lipopolysaccharide (LPS), EVs from LPS-activated macrophages (EV_{LPS}), mice injected with EV_{LPS} before and after tumor induction i.e. all throughout experiment (all-EV_{LPS}), mice preconditioned with EV_{LPS} injections prior to tumor induction (pre-EV_{LPS}).

Mouse No.	Condition	Day of death	Reason
1	All-EV_{LPS}	Day 11	Had excessive erythema, stopped breathing after weak response to anesthesia
2	Pre-EV_{LPS}	Day 17	Tumor too large + used for dissociation practice
3	PBS	Day 20	Randomly selected from group; used for dissociation practice. Excluded from study

Table 3.3 Flow cytometry gating strategy for cell types in the MC38 tumor microenvironment and summary of experimental findings.

Cell Type	Markers	Differential expression	Figures
Nucleated hematopoietic cells	$CD45^+$	ns	3.19
Endothelial cells	$CD45^-$ $CD31^+$	ns	3.19
Myeloid cells	$CD45^+$ $CD11b^+$	ns	3.19
Macrophages	$CD45^+$ $CD11b^+$ $F4/80^+$	Downregulated in all-EV_{LPS}	3.20
M1-like cells	$CD45^+$ $CD11b^+$ $CD86^+$	Downregulated in all-EV_{LPS}	3.21
M2-like cells	$CD45^+$ $CD11b^+$ $CD206^+$	ns	3.22
Tumor-associated macrophages (TAMs)		Downregulated in pre-EV_{LPS} and all-EV_{LPS}	3.24
Granulocytic myeloid-derived suppressor cells (g-MDSCs)	$CD45^+$ $CD11b^+$ $Ly6G^+$ $Ly6C^{med}$	Upregulated in all-EV_{LPS}	3.23
Monocytic myeloid-derived suppressor cells (m-MDSCs)	$CD45^+$ $CD11b^+$ $Ly6G^-$ Ly6C+	Moderately downregulated in all-EV_{LPS}	3.23
Neutrophils	$CD45^+$ $CD11b^+$ $Ly6G^+$ $F4/80^-$	Upregulated in all-EV_{LPS}	3.25
Dendritic cells	$CD45^+$ $CD11c^+$	Downregulated in all-EV_{LPS}	3.26
D1-like cells	$CD45^+$ $CD11c^+$ $CD86^+$	Moderately downregulated in all-EV_{LPS}	3.27
D2-like cells	$CD45^+$ $CD11c^+$ $CD206^+$	ns	3.27
pan T-cells	$CD45^+$ $CD11b^-$ $CD3^+$	ns	3.28
Helper T cells	$CD45^+$ $CD11b^-$ $CD3^+$ $CD4^+$	ns	3.28
Cytotoxic T lymphocytes	$CD45^+$ $CD11b^-$ $CD3^+$ $CD8^+$	ns	3.28

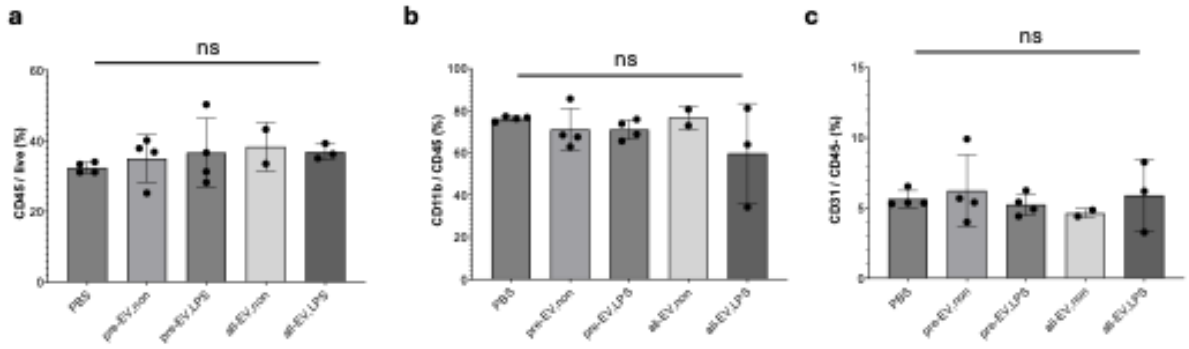

Figure 3.18 Flow cytometric quantification shows that extracellular vesicles (EVs) from non-activated and lipopolysaccharide (LPS)-activated macrophages do not affect numbers of nucleated hematopoietic cells (a), total myeloid cells (b), and endothelial cells (c) in the tumor microenvironment; conditions are described in Table 3.2. Not significant (ns), mean (SD), n = 2–4, one-way ANOVA followed by Tukey's post-hoc test. In graph labels, text after the comma appears as subscript (e.g., pre-EV,LPS = pre-EV_{LPS}).

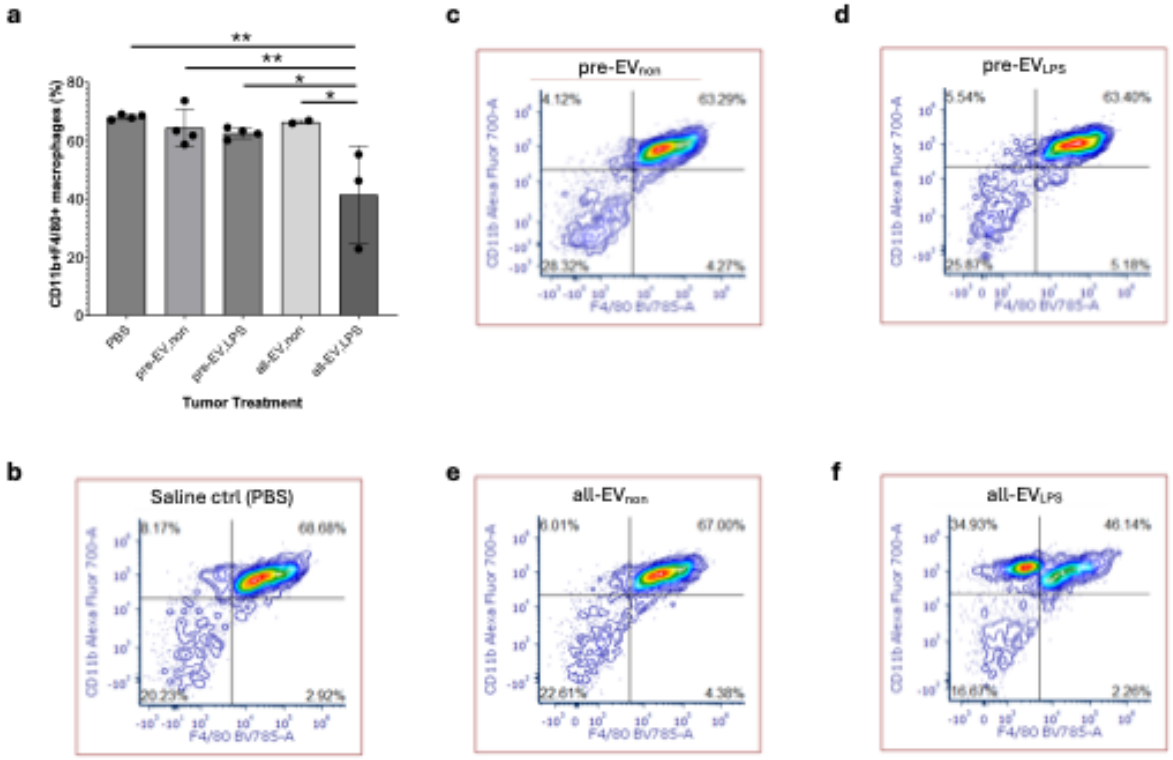

Figure 3.19 Flow cytometric quantification shows that extracellular vesicles (EVs) from lipopolysaccharide (LPS)-activated macrophages decrease numbers of macrophages in the tumor microenvironment. (a) Flow cytometric quantification showing decreased macrophage numbers in tumors of mice injected with EVs from LPS-activated macrophages before and after tumor induction (all-EV_{LPS}). (b-f) Representative flow cytometry images of each condition, as described in Table 3.2. *p < 0.05, **p<0.01, mean (SD), n = 2–4, one-way ANOVA followed by Tukey's post-hoc test. In graph labels, text after the comma appears as subscript (e.g., pre-EV,LPS = pre-EV_{LPS}).

We also found that CD86, a common M1 macrophage marker, was significantly downregulated in CD11b$^+$ myeloid cells from tumors of mice injected with all-EV$_{LPS}$ compared with all other conditions (Figure 3.20a,c-g). This can also be seen to a lesser extent in CD11b$^+$F4/80$^+$ macrophages (Figure 3.20b). We did not detect significant changes in expression of CD206, a common M2 macrophage marker (Figure 3.21).

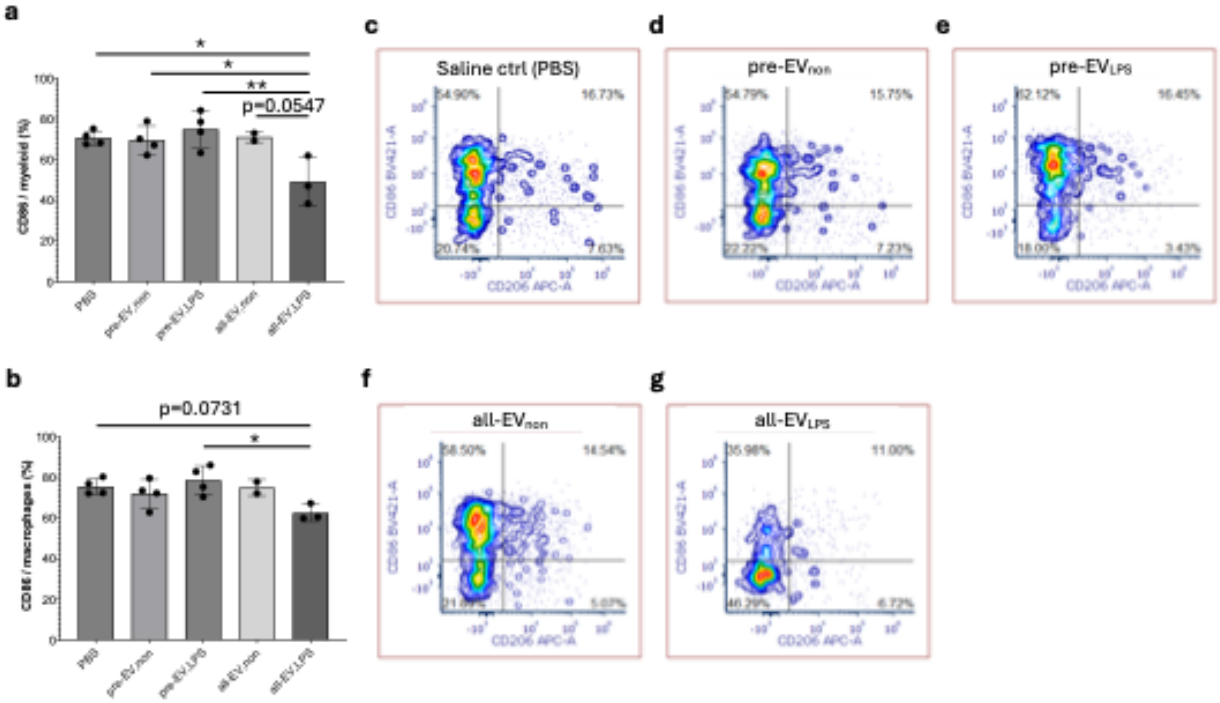

Figure 3.20 Flow cytometric quantification shows that extracellular vesicles (EVs) from lipopolysaccharide (LPS)-activated macrophages decrease CD11b$^+$ myeloid cell and CD11b$^+$F4/80$^+$ macrophage expression of the M1-like polarization marker CD86 in the tumor microenvironment. (a) Flow cytometric quantification shows decreased numbers of M1-like myeloid cell numbers in mice injected with EVs from LPS-activated macrophages before and after tumor induction (all-EV$_{LPS}$) relative to all conditions. (b) Quantification shows moderately decreased numbers of CD86$^+$ M1-like macrophage numbers in mice injected with all-EV$_{LPS}$ relative to select conditions. (c-g) Representative flow cytometry images of CD86 and CD206 expression in myeloid cells from each condition, as described in Table 3.2. *p<0.05, **p<0.01, p<0.10 values are given, mean (SD), n = 2–4, one-way ANOVA followed by Tukey's post-hoc test. In graph labels, text after the comma appears as subscript (e.g., pre-EV,LPS = pre-EV$_{LPS}$).

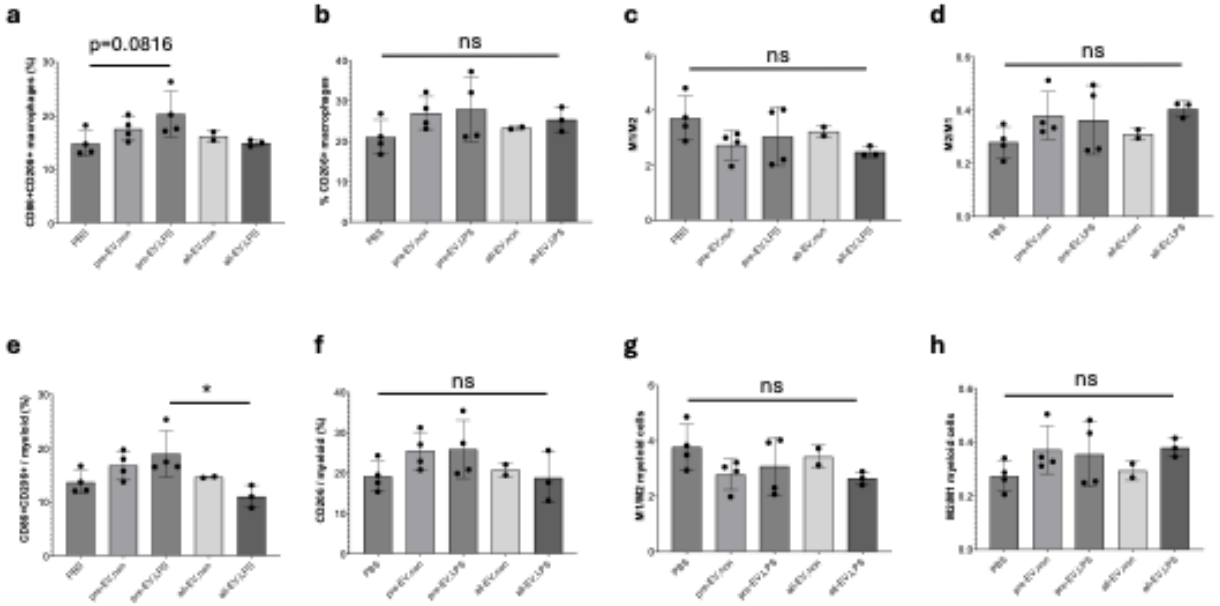

Figure 3.21 Flow cytometric quantification shows that extracellular vesicles (EVs) from lipopolysaccharide (LPS)-activated macrophages injected before tumor induction (pre-EV_{LPS}) moderately increased number of cells expressing both M1-like (CD86) and M2-like (CD206) polarization markers in $CD11b^{+}F4/80^{+}$ macrophage (a) and $CD11b^{+}$ myeloid (e) cell populations relative to select conditions. EVs do not significantly affect $CD11b^{+}F4/80^{+}$ macrophage or $CD11b^{+}$ myeloid cell expression of the M2-like marker CD206 (b,f), $CD86^{+}/CD206^{+}$ proportions of M1/M2 cells (c,g), or $CD206^{+}/CD86^{+}$ proportions of M2/M1 cells (d,h) in the tumor microenvironment; conditions are described in Table 3.2. Not significant (ns), *p<0.05, p<0.10 values are given, mean (SD), n = 2–4, one-way ANOVA followed by Tukey's post-hoc test. In graph labels, text after the comma appears as subscript (e.g., pre-EV,LPS = pre-EV_{LPS}).

Because of the increase in non-macrophage $CD11b^{+}$ myeloid cells in all-EV_{LPS} mouse tumors relative to all other conditions, we further investigated other myeloid cell populations that could be involved in this differential response to EVs from LPS-activated macrophages. Myeloid-derived suppressor cells (MDSCs) develop during altered myeloid differentiation in both pathological conditions like cancer as well as certain physiological states[232-234]. MDSCs are characterized by their potent immunosuppressive activities, including inhibition of anticancer activity of T cells and NK cells, promoting tumor immune evasion[235]. The two groups of MDSCs include monocytic-MDSCs (m-MDSCs) that are morphologically and phenotypically similar to monocytes, and granulocytic-MDSCs (g-MDSCs) which are similar to immature neutrophils[232, 236]. These groups can be differentiated based on phenotypic features, e.g., expression levels of surface Ly6C and Ly6G markers[237]. Specifically, g-MDSCs can be defined as $CD11b^{+}Ly6G^{+}Ly6C^{lo}$, and m-MDSCs as $CD11b^{+}Ly6G^{-}Ly6C^{hi}$ expressive cells[238], as seen in Table 3.3.

Interestingly, we discovered a significantly increased number of polymorphic mononuclear/granulocytic myeloid-derived suppressor cells (g-MDSCs) present in the all-EV_{LPS} injected mouse tumors relative to all other conditions (Figure 3.22a). We also found a moderately downregulated number of monocytic MDSCs (m-MDSCs) present in the all-EV_{LPS} mouse tumors relative to select conditions (Figure 3.22b). This suggests there is a differential response of MDSC subtypes to EVs from LPS-activated macrophages, either directly or indirectly. Additionally, because MDSCs are immature myeloid subtypes, the increased recruitment of g-MDSCs in tumors treated with all-EV_{LPS} suggests a potential for EVs from LPS-activated macrophages in regulating myeloid cell differentiation in the TME.

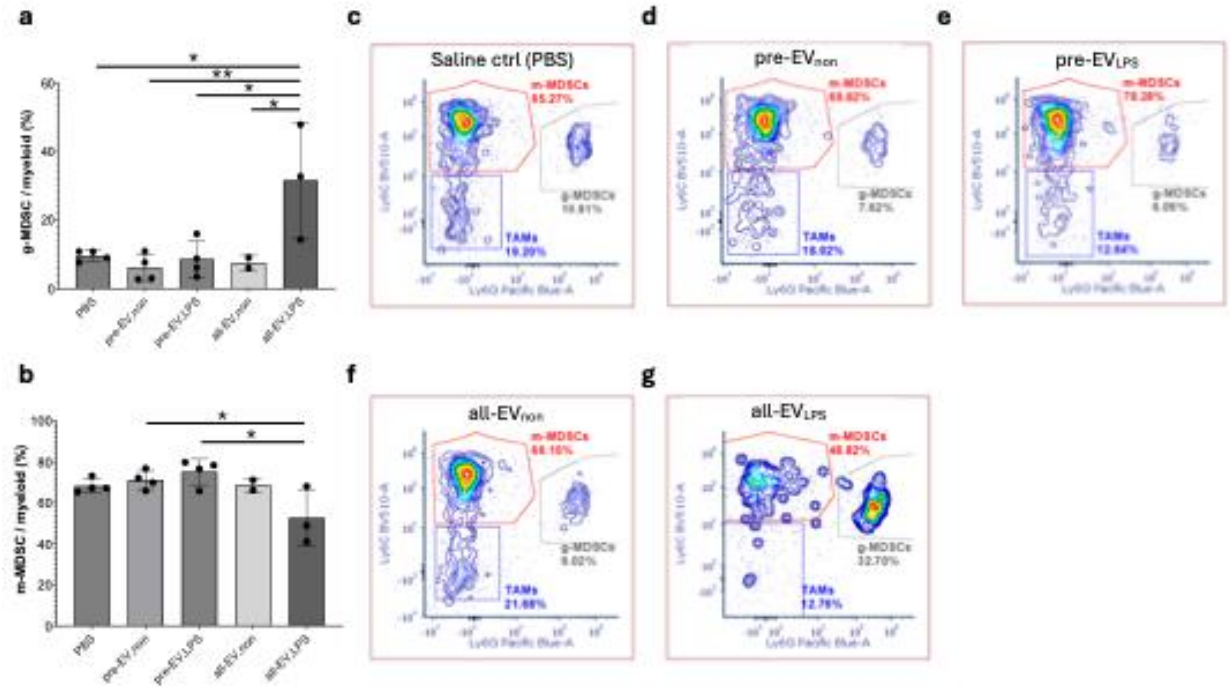

Figure 3.22 Extracellular vesicles (EVs) from lipopolysaccharide (LPS)-activated macrophages increased granulocytic myeloid-derived suppressor cell (g-MDSC) numbers in the tumor microenvironment. (a) Quantification showing increased numbers of g-MDSCs in mice injected with EVs from LPS-activated macrophages before tumor induction (pre-EV_{LPS}) and both before and after tumor induction (all-EV_{LPS}). (b) Quantification showing moderately decreased numbers of monocytic-MDSCs (m-MDSCs) in all-EV_{LPS} mice relative to select conditions. (c-g) Representative flow cytometry images of each condition, as described in Table 3.2. *p< 0.05, **p<0.01, mean (SD), n = 2–4, one-way ANOVA followed by Tukey's post-hoc test. In graph labels, text after the comma appears as subscript (e.g., pre-EV,LPS = pre-EV_{LPS}).

Furthermore, tumor-associated macrophages (TAMs) can originate from monocyte/macrophages or m-MDSC to become partially or fully pro-tumorigenic via various mechanisms, as TAM populations in tumors are heterogeneous[234, 236]. We found a decreased expression of TAMs in pre-EV_{LPS} and all-EV_{LPS} conditions (Figure 3.23). Note that percentages shown on flow cytometry graphs (panels c-g) are from one representative sample, while the quantitative analysis in panel b represents the mean values across all biological replicates (n = 2-4). TAMs present also expressed a slightly increased level of CD206 pro-regenerative M2 marker (Figure 3.23c). This is intriguing, as it suggests that EVs from LPS-activated macrophages injected prior to tumor cell induction signal to the epithelium to later impact the recruitment and/or differentiation of TAMs in the subsequently occurring TME. The newfound potential for EVs to induce changes in the epithelium prior to tumor induction that subsequently affects myeloid cell differentiation or recruitment during tumor development suggests that macrophage EVs may play a significant mechanistic role in colitis-induced field cancerization.

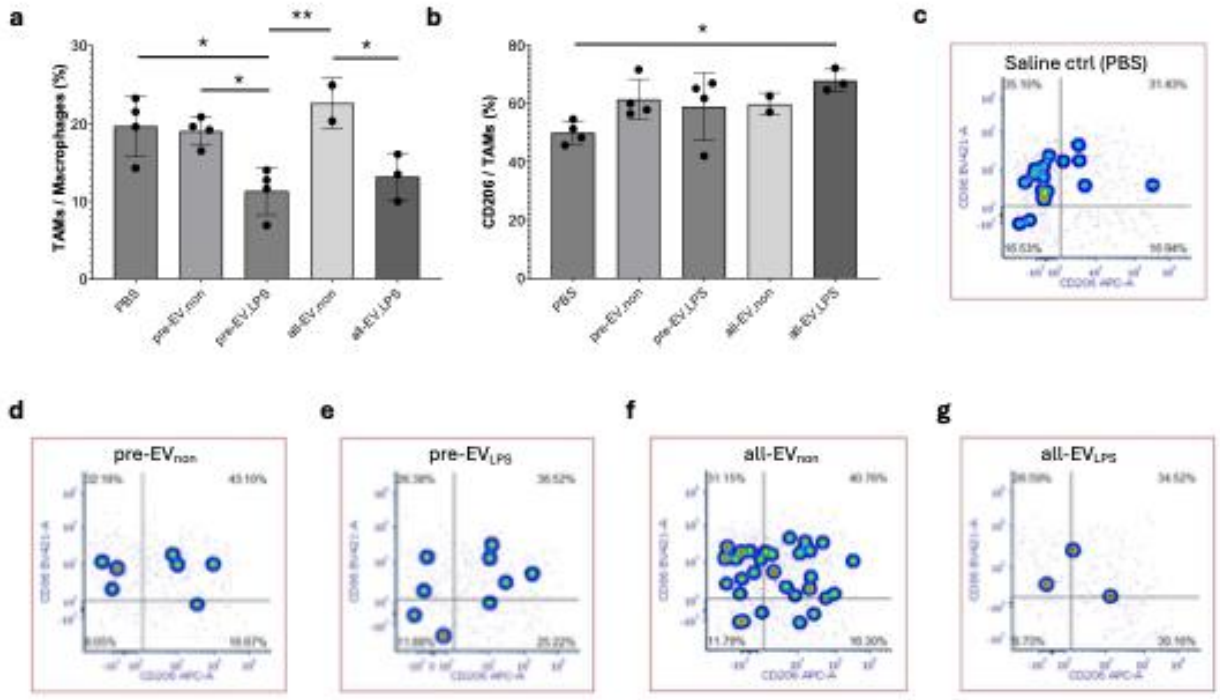

Figure 3.23 Extracellular vesicles (EVs) from lipopolysaccharide (LPS)-activated macrophages decrease Ly6G$^-$Ly6C$^-$CD11b$^+$F4/80$^+$ tumor-associated macrophages (TAMs) and increased M2-like CD206 expression in TAMs in the tumor microenvironment. (a) Flow cytometric quantification showing decreased numbers of TAMs in mice injected with EVs from LPS-activated macrophages before tumor induction (pre-EV$_{LPS}$) and both before and after tumor induction (all-EV$_{LPS}$). (b) TAMs were also decreased in mice injected with pre-EV$_{LPS}$ and all-EV$_{LPS}$. (c) Quantification showing increased proportions of Ly6C$^+$ and/or Ly6G$^+$ macrophages (non-TAMs) in mice injected with pre-EV$_{LPS}$ and all-EV$_{LPS}$ relative to controls. (d) Tumors in mice injected with all-EV$_{LPS}$ contained an increased number of M2-like CD206$^+$ TAMs relative to saline-injected control tumors. (e-i) Representative flow cytometry images of CD86 (ns) and CD206 expression in TAMs from each condition, as described in Table 3.2. Not significant (ns), *p<0.05, **p<0.01, mean (SD), n = 2–4, one-way ANOVA followed by Tukey's post-hoc test. In graph labels, text after the comma appears as subscript (e.g., pre-EV,LPS = pre-EV$_{LPS}$).

I then proceeded to further characterize the tumor-residing macrophages that were not defined as TAMs (i.e., CD11b$^+$F4/80$^+$ cells expressing Ly6C and/or Ly6G). Similar to Figure 3.23a, Figure 3.24a shows that of the F4/80$^+$CD11b$^+$ macrophages present in the TME, there were a significantly upregulated proportion of macrophages that were not Ly6C$^-$Ly6G$^-$ TAMs, i.e., that expressed Ly6C and/or Ly6G, present in tumors treated with pre-EV$_{LPS}$ and all-EV$_{LPS}$. I will henceforth refer to this Ly6C and/or Ly6G expressing CD11b$^+$F4/80$^+$ macrophage population as “non-TAM macrophages”. It may be important to avoid labeling TAMs as “pro-tumor” and non-TAM macrophages as “anti-tumor” without

deeper characterization. Importantly, we found these non-TAM macrophages to express lower levels of M1 marker CD86 in tumors treated with all-EV_{LPS} (Figure 3.24b, e-i). Thus, EVs from LPS-activated macrophages may signal directly to cells in the TME and facilitate the polarization of non-TAM macrophages. Decreased expression of M1 markers suggests decreased anti-tumor activity of these macrophages and thus a potential for tumors to progress faster, however, further characterization of these macrophages is required to elucidate the signaling mechanism and effects on tumorigenesis. We also found a modest increase in CD206 (M2 marker) expression on non-TAM macrophages in tumors treated with pre-EV_{LPS} relative to saline controls (Figure 3.24c,d). This suggests that EVs from LPS-activated macrophages present in the tissue environment prior to tumor induction/formation (e.g., in colitis prior to carcinogenesis) may induce changes in cells of the microenvironment preceding tumor induction/formation (potentially similar to premalignant environments), which promotes subsequently induced tumors to upregulate M2-like pro-regenerative markers in non-TAM macrophages. Thus, EVs from LPS-activated macrophages present in the tissue prior to tumor induction may induce changes in the colon tissue, which later effectively downregulate TAM expression and/or infiltration in subsequently emerging tumors; along with predisposing tissues to induce a decrease in TAM marker expression and an increase in M2 marker expression in non-TAM macrophages in the TME, the continued presence of EVs from LPS-activated macrophages in the TME after tumor emergence also decreases M1 activity in all myeloid subsets.

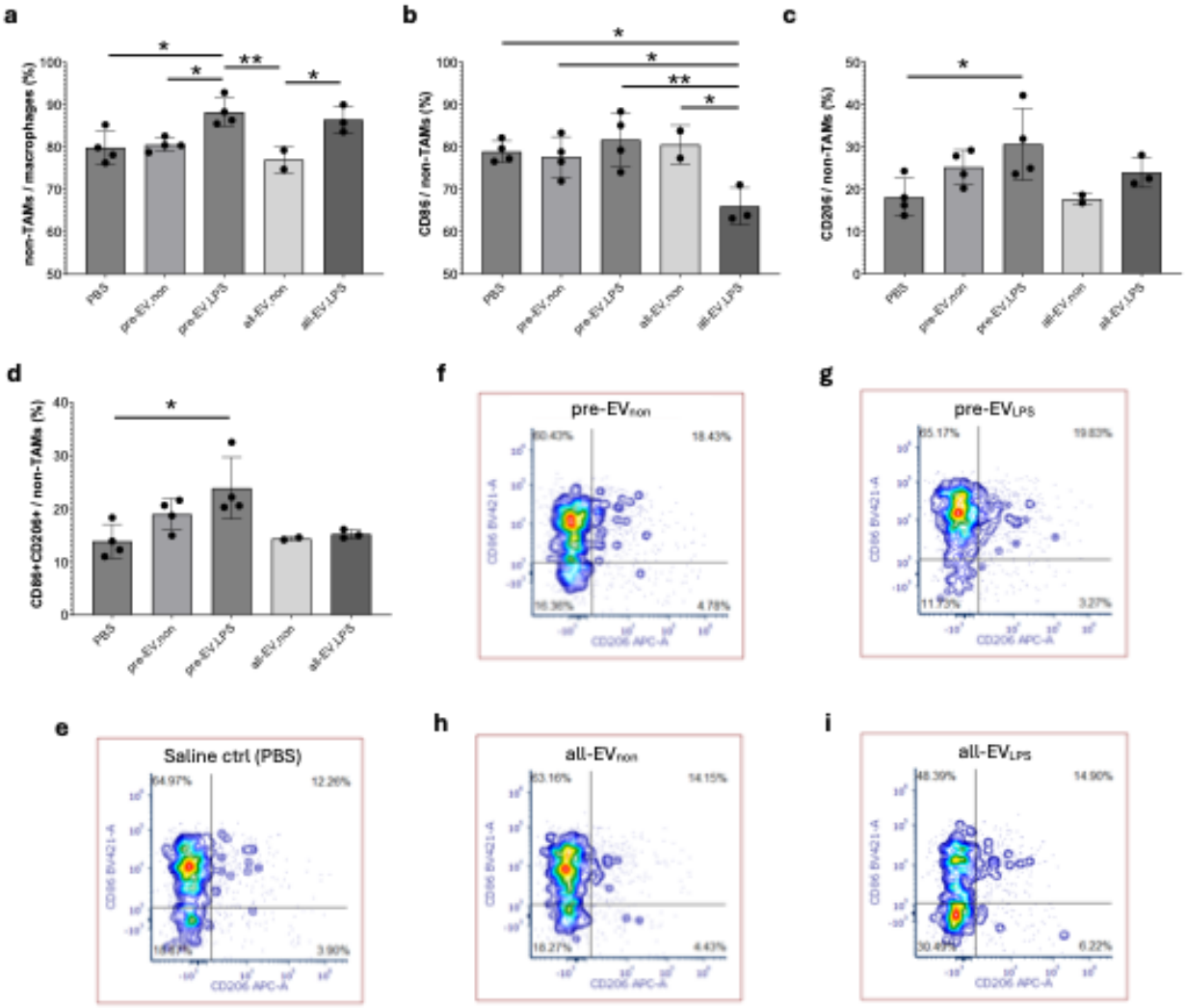

Figure 3.24 Extracellular vesicles (EVs) from lipopolysaccharide (LPS)-activated macrophages increase proportion of macrophages that are not tumor-associated macrophages (non-TAMs) in the tumor microenvironment. (a) Flow cytometric quantification showing increased proportions of $Ly6C^+$ and/or $Ly6G^+$ macrophages in mice injected with EVs from LPS-activated macrophages before tumor induction (pre-EV_{LPS}) and both before and after tumor induction (all-EV_{LPS}) relative to controls. (b-g) Representative flow cytometry images of CD86 (ns) and CD206 expression in non-TAMs from each condition, as described in Table 3.2. Not significant (ns), *p<0.05, **p<0.01, mean (SD), n = 2–4, one-way ANOVA followed by Tukey's post-hoc test. In graph labels, text after the comma appears as subscript (e.g., pre-EV,LPS = pre-EV_{LPS}).

Phenotypically very similar to g-MDSCs (and thus difficult to differentiate), neutrophils were defined here as $Ly6G^{+}F4/80^{-}$ myeloid cells. Neutrophils were found to be significantly upregulated in all-EV_{LPS} injected mice relative to all other conditions (Figure 3.25). Neutrophil recruitment is mediated commonly by chemokines in colitis, and they have also been found to secrete IL-6, which promotes colitis-associated cancer[178].

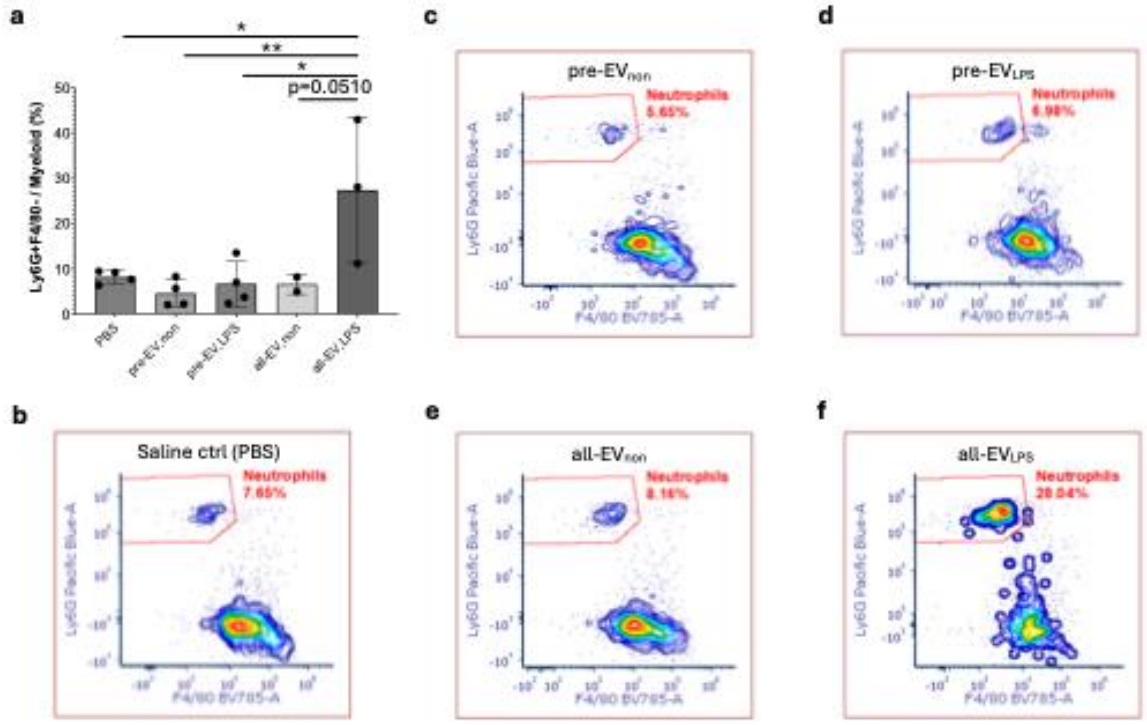

Figure 3.25 Extracellular vesicles (EVs) from lipopolysaccharide (LPS)-activated macrophages increase neutrophil infiltration into the tumor microenvironment. (a) Flow cytometric quantification showing increased numbers of neutrophils in mice injected with EVs from LPS-activated macrophages in tumor site before and after tumor induction (all-EV_{LPS}) relative to all other conditions. (b-f) Representative flow cytometry images of each condition, as described in Table 3.2. *$p < 0.05$, **$p<0.01$, mean (SD), n = 2–4, one-way ANOVA followed by Tukey's post-hoc test. In graph labels, text after the comma appears as subscript (e.g., pre-EV,LPS = pre-EV_{LPS}).

In pre-EV_{LPS} mice, tumor-residing $Ly6G^{+}F4/80^{-}$ cells termed neutrophils expressed increased CD86 proinflammatory marker relative to all other conditions (Figure 3.26a). We see a similar trend in g-MDSC expression of CD86 (Figure 3.26i). Also, pre-EV_{LPS} injected mouse tumor neutrophils expressed moderately increased CD206 pro-regenerative marker relative to PBS control (Figure 3.26b), but there was no difference in CD206 expression between conditions in g-MDSCs (Figure 3.26j). This increase in CD86 expression is not present in tumors from all-EV_{LPS} mice. This suggests that EVs from LPS-activated macrophages present in the tissue environment prior to tumor induction/formation (e.g., in colitis prior to tumorigenesis) may induce changes in cells of the microenvironment preceding tumor induction/formation (potentially similar to premalignant environments), which promotes subsequently induced tumors to upregulate N1-like proinflammatory markers in neutrophils, and M1-like proinflammatory markers in g-MDSCs. Thus, EVs from LPS-activated macrophages present in the tissue prior to tumor induction may induce changes in tissue, which later effectively upregulate neutrophil and g-MDSC expression of CD86 in subsequently emerging tumors.

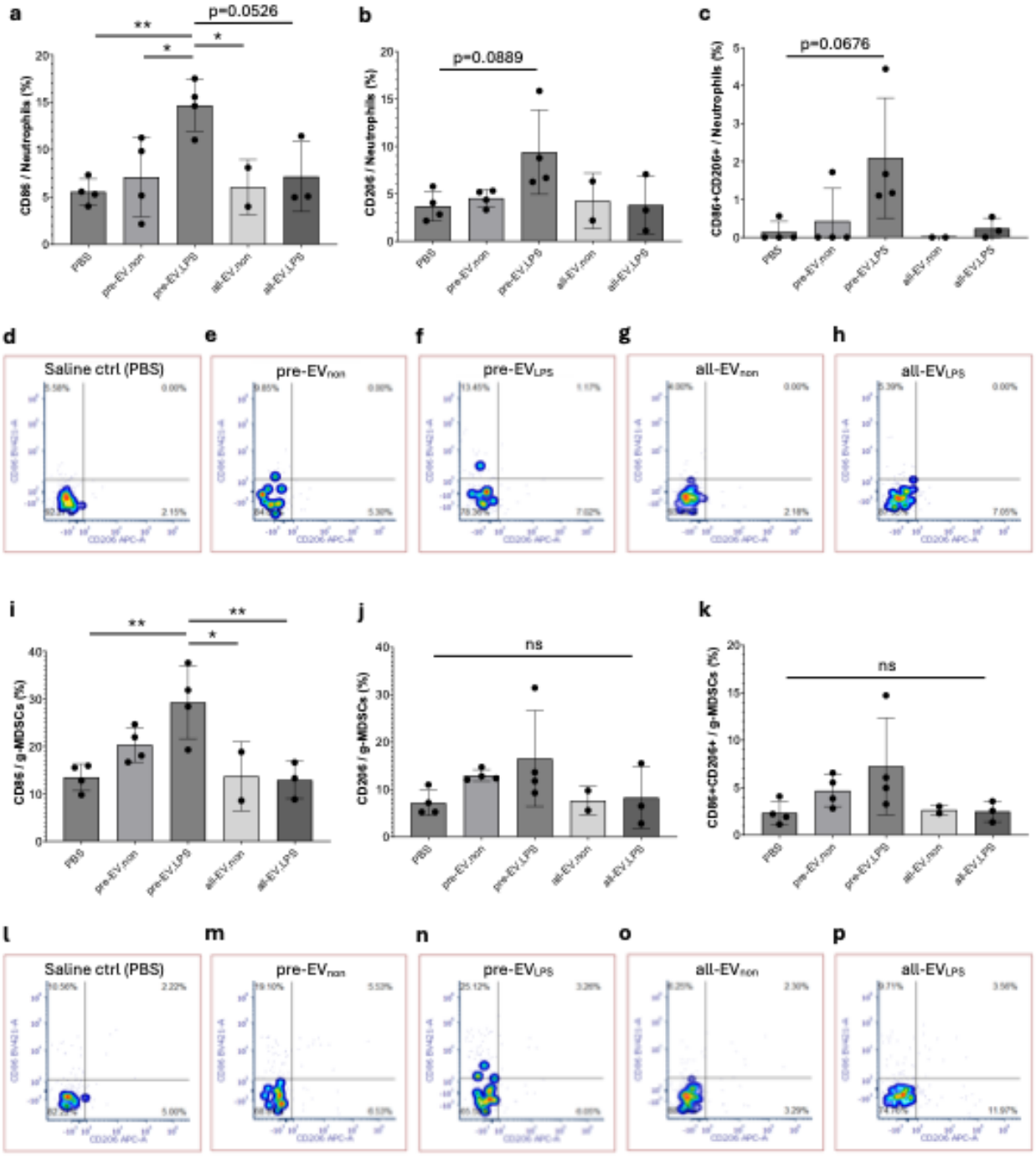

Figure 3.26 Flow cytometric quantification shows that extracellular vesicles (EVs) from lipopolysaccharide (LPS)-activated macrophages injected before tumor induction (pre-EV_{LPS}) increased neutrophil and g-MDSC expression of pro-inflammatory CD86 marker. (a-c) Flow cytometric quantification showing proportion of neutrophils expressing CD86 (a), CD206 (b), or both (c) in each condition, and representative flow cytometry images (d-h); conditions are described in Table 3.2. (i-k) Quantification showing proportion of g-MDSCs expressing CD86 (i), CD206 (j), or both (k) in each condition, and representative flow cytometry images (l-p). Not significant (ns), *p<0.05, **p<0.01, p values indicated for p<0.10, mean (SD), n = 2–4, one-way ANOVA followed by Tukey's post-hoc test.

We next looked at CD11c$^+$ dendritic cells (DCs), which we found present at significantly decreased numbers in all-EV$_{LPS}$ mice relative to all other conditions (Figure 3.27a). Of the DCs, we found a moderately decreased amount of CD86 expressing D1-like DCs in the all-EV$_{LPS}$ treated mouse tumors (Figure 3.28a), and no significant changes in the D2 marker CD206 (Figure 3.28b,c). Within the CD11c DC populations, there was a moderately decreased number of MHCII-expressing DCs (Figure 3.27b). MHCII is utilized by DCs to present antigens to CD4 T helper cells; however, we detected no significant differences between groups in CD3 pan-T cell numbers, CD4 T helper cell numbers, or CD8 cytotoxic T lymphocytes present in the tumor microenvironment after 22 days (Figure 3.29). It is important to note that many of these tumors were still relatively small implying early-stage malignancy.

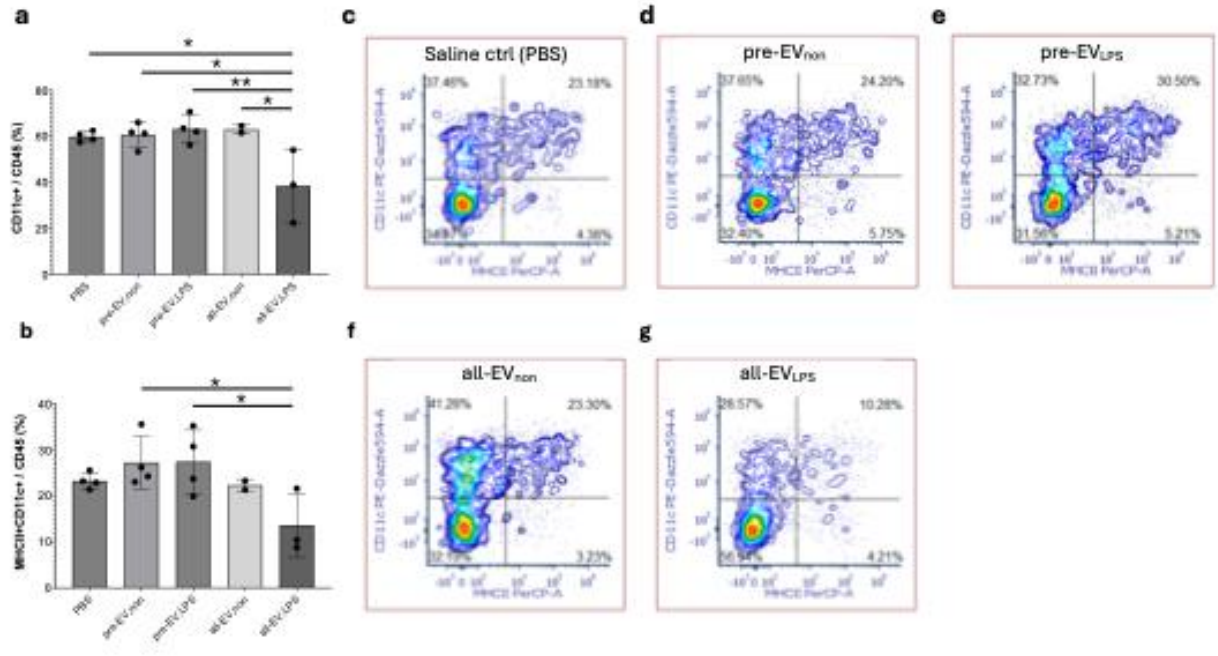

Figure 3.27 Extracellular vesicles (EVs) from lipopolysaccharide (LPS)-activated macrophages decrease CD11c$^+$ dendritic cell (DC) number in the tumor microenvironment. (a) Flow cytometric quantification showing decreased numbers of CD11c$^+$ DCs in mice injected with EVs from LPS-activated macrophages in tumor site before and after tumor induction (all-EV$_{LPS}$) relative to all other conditions. (b) Quantification showed moderately decreased numbers of MHCII-expressing DCs in mice injected with all-EV$_{LPS}$ relative to select conditions. (c-g) Representative flow cytometry images of each condition, as described in Table 3.2. *$p < 0.05$, **$p<0.01$, mean (SD), n = 2–4, one-way ANOVA followed by Tukey's post-hoc test. In graph labels, text after the comma appears as subscript (e.g., pre-EV,LPS = pre-EV$_{LPS}$).

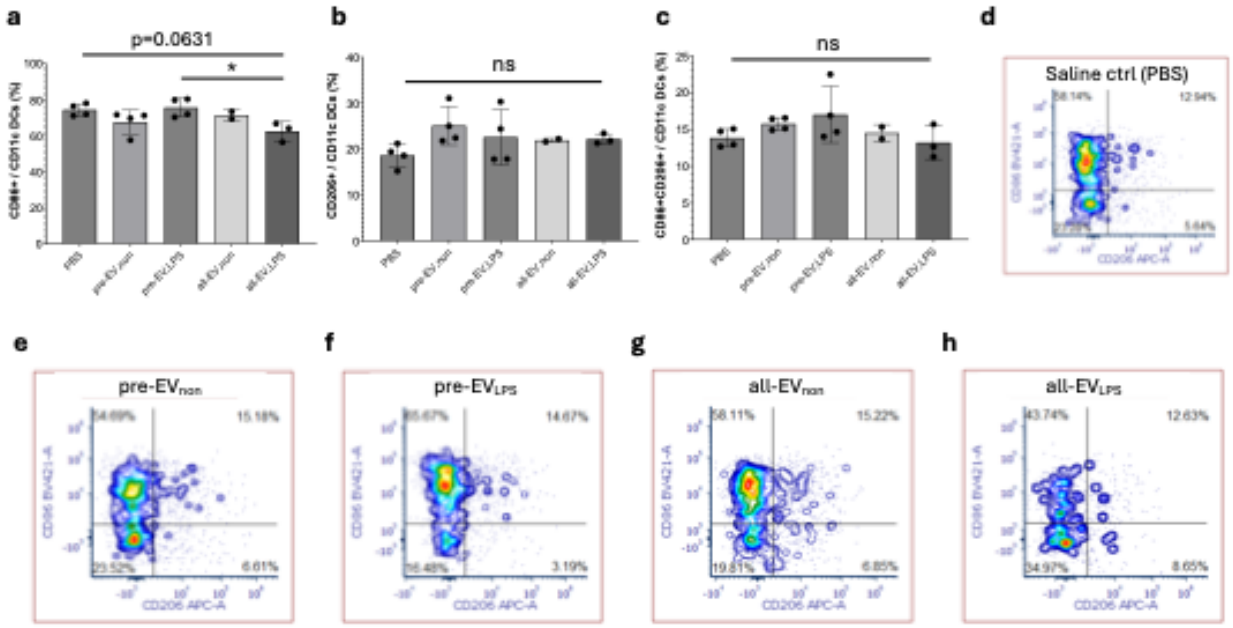

Figure 3.28 Extracellular vesicles (EVs) from lipopolysaccharide (LPS)-activated macrophages decrease CD86⁺ dendritic cells (DCs) in the tumor microenvironment. (a) Flow cytometric quantification showing moderately decreased numbers of CD86⁺ (D1) DCs in mice injected with EVs from LPS-activated macrophages in tumor site before and after tumor induction (all-EV_{LPS}) relative to select conditions. (b,c) Quantification showed no change in CD206⁺ (D2) DC populations (b) or CD86⁺CD206⁺ DC populations in tumors between conditions. (d-h) Representative flow cytometry images of CD86 (D1) and CD206 (D2) expression in DCs from tumors of each condition, as described in Table 3.2. Not significant (ns), *p < 0.05, mean (SD), n = 2–4, one-way ANOVA followed by Tukey's post-hoc test. In graph labels, text after the comma appears as subscript (e.g., pre-EV,LPS = pre-EV_{LPS}).

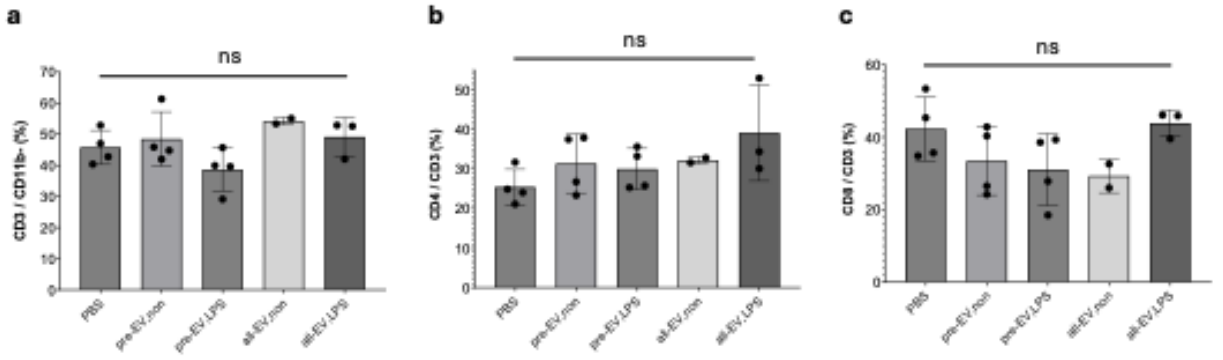

Figure 3.29 Flow cytometric quantification shows that extracellular vesicles (EVs) from non-activated and lipopolysaccharide (LPS)-activated macrophages do not affect numbers of CD3⁺ T cells (a), proportion of CD4⁺/CD3⁺ T helper cells (b), or proportion of CD8⁺/CD3⁺ cytotoxic T cells (c) in the tumor microenvironment; conditions are described in Table 3.2. Not significant (ns), mean (SD), n = 2–4, one-way ANOVA followed by Tukey's post-hoc test. In graph labels, text after the comma appears as subscript (e.g., pre-EV,LPS = pre-EV_{LPS}).

Here, we have shown that LPS-activated macrophage EVs promote colon cell growth in 2D cultures and anchorage-independent growth in soft agar, and upregulate pro-tumorigenic IL-17 signaling protein expression. In vivo, LPS-activated macrophage EVs increased tumor growth when injected before and after tumor induction, and influenced myeloid cell development and immune recruitment. Namely, LPS-activated macrophage EVs decreased tumor numbers of $F4/80^+$ macrophages, $Ly6C^-Ly6G^-$ TAMs, m-MDSCs and DCs, whereas they increased the numbers of tumor-associated g-MDSCs and neutrophils. We also found LPS-activated macrophage EVs had a moderate impact on decreasing expression of CD86 M1 marker in $CD11b^+$ myeloid cells, $F4/80^+$ macrophages and DCs.

DISCUSSION

The colonic epithelium provides a complex barrier to maintain a healthy homeostatic relationship between the microbiome in the gut lumen and its underlying connective tissue and host immune cells. The immune environment in the intestine is unique in that immune cells normally display tolerance towards bacteria in the gut lumen[239] unless the barrier function is disrupted and/or pathogenic bacteria invade. This implies that macrophages are differentially activated in this context.

Culture models of colitis and cancer lack components of the complexity of chronic inflammation and tumorigenesis. However, in order to understand intercellular signaling within these complex systems, it is sometimes advantageous to isolate and characterize individual signaling components in a more manageable in vitro system. This reductionist approach is pursued with the intention of applying the knowledge about individual signaling components back into the bigger picture and the complexities of the living body.

We modeled macrophage activation in colitis in vitro by treating macrophages with bacterial lipopolysaccharide (LPS). This has previously been used as an in vitro model for macrophage and colonic cell activity in colitis[56, 73]. Moreover, administration of LPS onto intestinal epithelial cells or intraperitoneal (i.p.) injection of LPS into mice have also been used as models for intestinal inflammation[240]. To ensure LPS was not directly affecting the colon cells as has been previously reported to occur in vivo [241], we included colon cell treatments using the same LPS concentration as was used to stimulate EV-donor macrophage cells and/or negative controls of that concentration and amount of EVs added to ensure that residual LPS in administrated EVs was not contributing to the observed effects. However, it may actually be more representative to include LPS in addition to colon cell treatment with EVs from LPS-activated macrophages, because the colonic epithelial cells would be exposed to all of these factors at once in the environment of colitis. In fact, Guo *et al*. performed Gene Ontology (GO)

enrichment analyses and found that dysplasia in colitis is strongly associated with LPS and increased immune cell infiltration into the mucosa [242].

Our assays characterizing the functional signaling effects of LPS-activated macrophage extracellular vesicles (EVs) showed increased recipient colon cell growth in 2D monolayer cultures, anchorage-independent growth of transformed cells in 3D soft agar, and upregulated pro-tumorigenic IL-17 signaling pathway protein expression in vitro. This suggests that LPS-activated macrophage EVs (EV_{LPS}) have a potentially pro-tumorigenic role when taken up by recipient colonic epithelial cells. Interestingly, we also observed minor increases in colon cell growth and pro-tumorigenic protein expression between conditions treated with increased numbers of EVs from non-activated macrophages. This may indicate that the number of macrophages present to secrete EVs may affect colonic epithelial tissue. Indeed, inflamed colonic tissue recruits a higher number of macrophages[136]. Thus, a more representative future model may take this proportional number of EVs into account for experimental design. However, for initial proof of concept we chose to use equal numbers of EVs from macrophages in non-activated and LPS-activated conditions.

Epithelial/Mesenchymal Transition

EVs from LPS-activated macrophages (2×10^5 per MC38 cell) triggered a temporal shift in mesenchymal markers in MC38 cells. At 24 h, decreased Vimentin and Twist suggest a transient mesenchymal-epithelial transition (MET), while by 48 h, increased Slug and ZEB1 implicates an epithelial-to-mesenchymal transition (EMT). Although these changes were moderate, this MET/EMT fluctuation may be relevant to metastasis, where cells undergo EMT for dissemination followed by MET for colonization at distant sites[243].

However, most likely, the moderate and contradictory changes we found in EMT (e.g., mesenchymal marker mRNA levels increasing along with epithelial marker E-cadherin mRNA levels increasing) in our culture model imply that there may be an alternative signaling mechanism involved in the pro-tumorigenic effects of LPS-activated macrophage EVs on colon cells. RNA sequencing analysis (in progress) may be a more sensitive method to further elucidate EV_{LPS}-induced pro-tumorigenic signaling effects in colon cells.

IL17 Signaling

Aside from serving as a physical barrier segregating the gut lumen from the submucosa, colonic epithelial cells importantly mediate (i.e., deliver signals) between microbiome components (e.g., LPS) and immune cells (e.g., macrophages)[244]. Functions of colonic epithelial cells include secreting cytokines and chemokines to recruit host immune cells and activate or induce immune tolerance in them, as well

as responding to factors produced by immune cells that can consequently impact proliferation, migration, differentiation and barrier function of colonic epithelial cells[245]. In colonic epithelial cells, the complex IL-17 signaling cascade induces activation of transcription factors including NF-κB, ERK, CCAAT-enhancer-binding protein β (C/EBPβ), and the activator protein-1 (AP-1) complex to upregulate expression of inflammatory mediators such as cyclooxygenase-2 (COX2) and IL-6[246]. Interestingly, IL-17 increased NF-κB and ERK1/2-driven COX2 expression in cancer cell lines, which in turn increased secretion of pro-inflammatory prostaglandin E2 (PGE_2); conditioned medium from IL-17-stimulated cancer cells was administered to macrophages which secreted increased levels of IL-10 and decreased levels of iNOS and TNF-α[247]. However, direct treatment of macrophages with IL-17 did not induce this pro-regenerative/M2-like macrophage profile, suggesting that the pro-tumorigenic effects of IL-17 signaling may occur through pre-cancerous epithelial cells and not macrophages[247]. AP-1 is a heterodimeric transcription factor, often comprised of c-Fos and c-Jun, that responds to stimuli such as cytokines and growth factors and regulate genes involved in many cellular processes associated with cancer progression such as proliferation, migration and invasion [248]. Fos-related antigen 1 (Fra-1), encoded by the FOSL1 gene, is a member of the Fos family of AP-1 subunits involved in IL-17 signaling in colon cells[249]. AP-1 subunits have been found to form heterodimers with C/EBPs to bind unique DNA sequences[250]. C/EBPβ influences many cell processes, including glycolysis and growth in colon cancer cells[251].

IL-17 signaling has been found to exert a pro-tumorigenic role in colorectal cancer (CRC)[252]. Elevated IL-17 levels are found in IBD patient mucosa[253] and serum[254], CRC patient tissues, and is associated with poor CRC prognosis[255]. The IL-17 signaling pathway and its inducer, IL17A, also play important roles in colitis-associated cancer. IL17A-K/O mice treated with azoxymethane and dextran sodium sulfate (AOM/DSS, a common model for colitis-associated cancer[256]) developed fewer tumors and had lower inflammation and proliferation scores than WT mice[257]. Another study found IL17A-deficient mice treated with AOM/DSS to also express decreased levels of IL-6, IFN-γ, and TNF-α cytokines, as well as downregulated levels of beta-catenin, p-STAT3, cyclin D1, cyclin-dependent kinase 2 (CDK2), cyclin E, Glycogen synthase kinase 3-β (GSK3-β) and p-Akt as compared with WT mice[221]. In the DSS-induced colitis model, IL17A-K/O mice also had a reduced inflammatory response, G-CSF and MCP-1 production, and mortality as compared to WT mice[258]. Likewise, in the TBNS-induced colitis model, IL17-K/O mice exhibited reduced colonic inflammation, IL-6 and MIP-2 production, and myeloperoxidase activity[259]. Ablation of IL-17 in $APC^{min/+}$ mice significantly reduced intestinal tumor development[260]. Interestingly, IL-17 treatment of HT29 CRC cells increased secretion of neutrophil-recruiting chemokines

CXCL1, CXCL2, CXCL5, CXCL6 and IL-8, as well as the Th17-recruiting chemokine CCL20[261]. IL-17 was also found to promote colon cancer cell secretion of VEGF and IL-6, both of which are known to promote colitis-associated cancer[255].

In CRC patient tissues, IL-17 was found to be secreted mainly by tumor-resident macrophages and Th17 cells[255], suggesting that macrophages are a main contributor of promoting IL-17 signaling to surrounding cells. In parallel, we found EVs from LPS-activated macrophages to promote IL-17 signaling in recipient MC38 colon cancer cells. Specifically, we found that EV_{LPS} increased MC38 cell expression of three integral proteins that play a role in IL-17 signaling, namely COX2, C/EBPβ, and Fra-1.

Cyclooxygenase-2

In colitis-associated cancer (CAC) tissues, COX2 was found to be overexpressed throughout early and later stages of neoplastic progression[262]. Overexpression of COX2 has been shown to play an important role in colon carcinogenesis and cancer progression[263]. Caco2 colon cancer cells transfected to constitutively express COX2 expressed increased levels of matrix metalloproteinase (MMP)-2, secretion of prostaglandin E2 (PGE_2), and cell invasiveness[264], as well as increased secretion of VEGF and tumor-associated angiogenesis[265]. COX2 produces PGE_2, which mediates inflammation in colitis and promotes colon cancer[14]. For example, PGE_2 increases the motility of CRC cells through the phosphatidylinositol 3-kinase (PI3K)/Akt signaling pathways[266]. PGE_2 induces CRC cell expression of Bcl2, resulting in increased resistance to apoptosis, and increased colony formation of CRC cells in monolayer cultures[267]. COX2-produced PGE_2 can also promote tumor immune evasion by regulating myeloid-derived suppressor cells (MDSCs), macrophages, and dendritic cells[219]. Prostaglandin J2, another product of COX2, increases proliferation of COX-depleted CRC cells[268].

In select studies, non-steroidal anti-inflammatory drugs (NSAIDs) have been found to reduce the incidence of cancer in colitis patients by inhibiting COX2 activity[269]. For example, inhibiting COX2 via celecoxib decreased the number and size of adenomatous polyps in FAP patients harboring the APC mutation[195]. In mice, inhibiting COX2 in CRC cells that overexpress COX2 reduced tumorigenesis[270]. In APC-mutated mice, the number of polyps was decreased in mice with genetic COX2-K/O [263, 271] and in mice treated with the COX inhibitor sulindac[272]. However, the effects of NSAIDs and selective COX2 inhibitors have been inconsistent[18], and long-term use of NSAIDs results in adverse effects, such as GI bleeding[273]. Our discovery that EVs from LPS-activated macrophages increase recipient colon cancer cell expression of COX2 suggests that EVs from macrophages in colitis signal to colonic epithelial cells to increase expression of COX2. This elucidates a potential therapeutic target to effectively reduce COX2 overexpression and chemoprevention of colitis-associated dysplasia or CAC.

CCAAT-enhancer-binding protein β

C/EBPβ is a transcription factor that regulates many cell processes involved in inflammation and cancer including proliferation, cell differentiation, migration, and metabolic activity[274]. C/EBPβ is commonly upregulated in CAC patients[275]. Interestingly, repressing C/EBPβ downregulates expression of dual specificity phosphatase 6 (DUSP6), which consequently alleviates LPS-induced intestinal inflammation in colonic epithelial cells and in mice[240]. Another group discovered that treating Caco2 colon cells with 1 μg/ml LPS for 24 h increased expression of C/EBPβ[276]. Pharmacologically inhibiting C/EBPβ in this culture model decreased expression of the gluconeogenesis-regulating enzyme phosphoenolpyruvate carboxykinase 1 (PCK1) and the receptor tyrosine kinase ligand ephrin A1 (EFNA1)[276], both of which have been shown to be overexpressed and promote CRC [277, 278]. Inhibiting C/EBPβ and thus transcription of PCK1 and EFNA1 restored the expression of integral components of the epithelial barrier, i.e., claudin-1, occluding and ZO-1[276]. Upregulated C/EBPβ activity also has been found to regulate colon cancer progression. For example, C/EBPβ inhibition of the Farnesoid X Receptor (FXR) in colon cancer cells allows for increased extracellular acidification rate (ECAR, an indicator for glycolytic activity) and growth advantage[251]. In colon cancer cells, C/EBPβ can also upregulate the serine protease inhibitor Serpin Family A Member 1 (SERPINA1), which activates the STAT3 pathway, consequently increasing cellular proliferation and migration[279]. Treating colon cancer cells with the stress hormone epinephrine upregulates C/EBPβ and downstream TRIM2, and consequently downregulates p53; whereas inhibiting C/EBPβ decreases EMT proteins and restores p53 levels[280]. Thus, the upregulation of C/EBPβ found in MC38 colon cells treated with EVs from LPS-activated macrophages (EV_{LPS}) relative to non-activated macrophages suggests that EV_{LPS} could promote colon cancer progression in the context of colitis.

Fos-related antigen 1

Fra-1 is a member of the Fos family that can dimerize with Jun proteins to form the activator protein 1 (AP-1) transcription factor complex, involved in regulating many genes implicated in tumorigenesis[281]. Fra-1 is reported to be upregulated in CAC patient tissues[275], as well as in active IBD tissue samples[282], CRC[283], and invasiveness of CRC metastases[249]. Inhibiting Fra-1 in CRC cells mitigates EMT, migration and invasion induced by the IL-6/STAT3/Fra-1 signaling axis[249].

However, in K-ras mutated HCT116 colon cancer cells, overexpression of Fra-1 decreases cellular proliferation and migration; the authors concluded that in IBD, this may indicate decreased damage repair ability and increased IBD recurrence[282]. DSS-induced colitis resulted in increased Fra-1 expression in mice[284]. Takada *et al*. injected LPS i.p. into WT mice and mice overexpressing Fra-1, and found that

Fra-1 overexpression in mice caused a reduction in expression of NF-kB, resulting in decreased anti- and proinflammatory cytokine secretion and increased tolerance to LPS exposure and DSS-induced colitis[284]. We detected both Fra-1 and NF-kB levels to be elevated in MC38 colon cells treated with EVs from LPS-activated macrophages. This suggests that although the upregulation of Fra-1 by EV_{LPS} treatment may potentially mediate cell migration and invasion in colitis and colon cancer, its interactions with other nuclear factors may also influence Fra-1 signaling in colitis-associated cancer.

Signal transducer and activator of transcription 1

We also discovered that, relative to controls, MC38 cells treated with EVs from LPS-activated macrophages (EV_{LPS}) expressed decreased levels of STAT1, although STAT3 and STAT6 were unchanged between conditions. STAT1 is a member of several signaling pathways activated by a number of ligands (e.g., interferon alpha, interferon gamma, epidermal growth factor, platelet derived growth factor, interleukin 6, and IL-17). It has an established role as a tumor suppressor in the early stages of colitis-associated cancer through its regulation of proliferation, apoptosis, and immune cell signaling[285]. After AOM/DSS treatment to induce CAC, relative to WT mice, STAT1-deficient mice exhibited increased inflammation and tumor development, and the spleens of these mice had increased accumulation of $Ly6G^{+}Ly6C^{-}CD11b^{+}$ myeloid cells and production of IL-17 and IL-22 [286]. It would be fascinating to further investigate the mechanism by which EVs from LPS-activated macrophages decrease STAT1 levels in colon cancer cells.

Nuclear factor-kappa B

NF-κB is a heterodimeric transcription factor complex that is upregulated in colitis patients[287] and thought to be the main link between inflammation and carcinogenesis in CAC[288]. The subunits of NF-κB are conserved and include: Rel (c-Rel), RelA (p65), RelB, NF-κB1 (p50 and its precursor p105), and NF-κB2 (p52 and its precursor p100)[289]. Interestingly, we found significantly increased levels of NF-κB1 (P25799) and NF-κB2 (Q9WTK5) in MC38 cells treated with EVs from LPS-activated macrophages.

Classic canonical NF-κB1 is a dual-address transcription factor that is activated by TLR ligands and cytokines, such as TNF-α and IL-1β, which induce phosphorylation of IKKβ, thus freeing NF-κB1 so that it can migrate from the cytoplasm to the nucleus and induce specific gene expression[290]. Deleting IKKβ in intestinal epithelial cells decreased tumor incidence but not size, whereas deleting IKKβ in myeloid cells decreased tumor size and expression of proinflammatory cytokines that the authors suggest may "serve as tumor growth factors" [288]. NF-κB2 p100 precursor subunit preferentially binds RelB in the cytoplasm; upon stimulation with factors reported to promote CAC and/or CRC such as LPS[139], lymphotoxin β[291], CD40L[292], B cell activating factor (BAFF)[293], or receptor activator of nuclear

factor kappa beta (RANKL)[294], the NF-κB-inducing kinase (NIK) and inhibitory-κB Kinase α (IKKα) cleaves p100 into p52, allowing nuclear translocation of RelB:p52 dimers to activate transcription of many genes involved in proliferation, migration, and inflammation[295]. This highly regulated process often becomes uncontrolled in CAC[296]. Thus, the elevation of NF-κB1 and NF-κB2 found in MC38 cells treated with EVs from LPS-activated macrophages suggests yet another pathway through which EV_{LPS} may induce inflammation and tumorigenesis.

Cyclin-dependent kinase-1

EVs from LPS-activated macrophages induced recipient MC38 cells to upregulate expression of CDK1 as detected by mass spectrometry. CDK1 is a cell cycle regulator and its activity has been shown to be highly elevated in CRC tissues and promote CRC cell proliferation and tumor progression[297]. Upregulated CDK1 can result in uncontrolled proliferation, which increases the risk of mutation, characteristic of tumorigenesis. Inhibiting CDK1 in $BRAF^{V600E}$ CRC cells increased their sensitivity to MEK/ERK inhibitors[298]. This elucidates the potential mechanism, by which EVs from LPS-activated macrophages increase recipient colon cell growth. Further studies investigating the contents of EVs that upregulate CDK1 in colon cells may reveal novel therapeutic target(s) to prevent uncontrolled proliferation in patients with colitis at risk of cancer.

Other regulators

EVs from LPS-activated macrophages significantly decreased the expression of the tumor suppressor gene SMAD2 in MC38 cells treated with a concentration of [4×10^5] EVs per colon cell, relative to EVs from non-activated macrophages at a lower concentration of [2×10^5] EV/cell. We suggest this finding to be significant because there are fewer macrophages present in the non-inflamed colon, and thus there would be fewer macrophage EVs present to signal to colon cells[136]. Importantly, downregulated expression of SMAD2, a member of the tumor-suppressive TGF-β signaling pathway, have also been found in tissues undergoing colitis-associated dysplasia as compared to benign colitis tissue[299].

Mass spectrometry detected that, relative to untreated condition, MC38 cells treated with EVs from macrophages expressed increased levels of p53 protein regardless of LPS activation status or concentration of EV treatment. The tumor suppressive function of p53 lies mainly in regulating transcription of many genes involved in apoptosis[300]. Overexpression of p53 may be due to increased activity or due to mutation[300], so we cannot draw functional conclusions from this finding. However, p53 is commonly mutated early in colitis-associated cancer[301] and overexpressed in CRC patient tissues[302]. EV_{non} and EV_{LPS}-induced increase in p53 expression of recipient MC38 cells may suggest that macrophage

EVs (regardless of activation status) deliver signals to colonic epithelial cells that require upregulation of apoptosis. However, because MC38 cells have mutations in the TP53 gene, this regulation does not occur normally. It would be interesting to investigate nuclear localization/p53 activity in EV-treated CT26 cells, as these have a wild-type TP53 gene but a tumorigenic mutation in the KRAS oncogene.

Lastly, mass spectrometry detected increased levels of mitogen-activated protein kinase 14 (MAPK14, p38α) in MC38 cells treated with higher concentration of EV_{LPS} relative to a lower concentration of EV_{non}. This may be physiologically relevant because they are fewer macrophages in homeostatic tissues relative to colitis, and these macrophages may secrete lower amounts of EVs per cell[136]. The complex effects of MAPK14 involve regulating intestinal barrier function in homeostasis; however, MAPK14 suppresses DSS-induced inflammation and transformation, whereas MAPK14 promotes proliferation and survival of colon tumor cells[303] and inhibiting MAPK14 decreased CRC progression and metastasis in vitro and in vivo[304]. Further studies would be necessary to deduce the exact role of MAPK14 in this context.

Overall from our mass spectrometric proteomics analyses, we found that EVs from LPS-activated macrophages increased colon cell expression of pro-tumorigenic IL-17 signaling proteins, levels of NF-κB and CDK1, while they decreased STAT1 levels. This unveils a potential mechanism, by which EV_{LPS} increases cell growth in monolayer culture and leads to anchorage-independent growth, and suggests that macrophage EVs in colitis have the potential to promote CAC.

In vivo experimental model

In my mouse study, preconditioning tumor sites (s.c. flank) with macrophage-derived EVs for 7 days before MC38 tumor cell induction was carried out to model EVs from macrophages in colitis (LPS-activated macrophages) compared to EVs from macrophages in homeostatic conditions (non-activated macrophages) prior to tumor emergence. In the preconditioned mice, following tumor induction, we injected PBS as a control for EV injections in the mice exposed to macrophage EVs throughout the duration of tumor growth (see Table 3.4 for description of conditions and abbreviations). Macrophage EVs injected only before tumor induction served to determine whether macrophage EVs predispose tissues to cancer, and to model active colitis occurring before tumorigenesis (where the colitis is in the latent stage during tumor progression). Injecting macrophage EVs throughout duration of tumor growth modeled colitis occurring actively throughout tumorigenesis in colitis-associated cancer.

Progressing into my in vivo studies, I wanted to answer the following questions:

1. Do EVs from macrophages in colitis precondition a tissue site and promote tumorigenesis?
2. Do EVs from macrophages in colitis affect tumor progression?

Albeit non-orthotopic, our feasible murine model has given us clues toward answering these questions. My data demonstrates that the dialog between macrophages and colon cells through EV signaling is an intrinsic part of the inflammatory response. I have also shown that EVs from LPS-activated macrophages (EV_{LPS}) decreased macrophage numbers, decreased the proportion of TAMs, decreased DC numbers, and increased recruitment of g-MDSCs and neutrophils in the TME. Orthotopic injections of EV_{LPS} into mouse models of colitis-associated cancer (CAC) will help further elucidate macrophage EV signaling effects during colitis and their role in colitis-associated tumorigenesis.

Cancer occurs in a subset of patients with colitis, and risk of cancer increases with disease duration and severity/extent of disease[305]. However, when and why these cancers emerge is a complex process that has only been partially elucidated. For example, some colitis patients experience latent stages in between chronic ulcerations. Some nanoscopic biomarkers of field cancerization have been detected to occur downstream of colitis, in distal regions of the colon. For this reason, I hypothesize that in CAC patients, regions of the colon affected by colitis that are upstream of the tumor contain macrophages that are not considered tumor-associated macrophages, but are still secreting pro-tumorigenic EVs that are effectively signaling to the downstream TME. The broader implication is that EVs from macrophages in colitis have the potential to induce field cancerization and mediate immunocarcinogenesis.

Inflammation is reported to involve, first, M1 macrophage activation for pathogen destruction, and subsequently, M2 macrophage activation to resolve the inflammation. There are differentially activated populations during active colitis and latent stages, and macrophages during these different stages may secrete EVs that differentially mediate pro- or anti-tumorigenic signals. I designed my experimental model to also address the question of how EVs from macrophages in colitis or homeostasis may mediate tumor formation during active periods of colitis (modeled by all-EV_{LPS}) as compared to latent stages in between ulcerations/inflammatory episodes in colitis (modeled by pre-EV_{LPS}).

In our pilot study to compare tumor growth in mice injected with EVs from LPS-activated macrophages before tumor induction (pre-EV_{LPS}) and after tumor emergence (EV_{LPS}(i.t.)) relative to saline (PBS) injections, we found that pre-EV_{LPS} mice developed smaller tumors than other conditions after 21 days. This was the opposite effect than we expected, as EVs from LPS-activated macrophages (EV_{LPS}) had increased growth and pro-tumorigenic protein expression in colon cells in vitro.

So, I hypothesized that EVs from LPS-activated macrophages were somehow affecting the tumor immune microenvironment. For example, STAT3 has been shown to be a necessary factor in the development of AOM/DSS-induced CAC in mice[168], and accelerates tumorigenesis in CRC[306]. However,

Irey *et al*. found that STAT3 inhibitors induced breast cancer cells to secrete factors that signal to macrophages, inducing expression of pro-tumor factors including TNF-α/NF-κB, EMT, IL-6/STAT3, IL-2/STAT5, and secretion of pro-tumorigenic COX2/PGE_2 which may play a role in tumor resistance to targeted therapies[307]. Deleting STAT3 in murine myeloid cells reduced formation of tumors in AOM/DSS-treated mice[308], but inhibiting STAT3 in intestinal epithelial cells increased invasiveness of CRC cells and of tumor cells in $APC^{min/+}$ mice (unlike sporadic CRC where APC loss is typically the initiating mutation[309], in colitis-associated cancer, APC mutations generally occur at later stages of tumorigenesis)[310]. So, I hypothesized that EV_{LPS} signal to tumor macrophages and other immune cells to promote tumorigenesis. This may occur either directly or indirectly; injected macrophage EVs may be directly taken up by tumor-residing macrophages, or taken up by epithelial or stromal cells which then secrete factors that signal to immune cells to exhibit an anti-tumor effect. This is why I proceeded to perform immunophenotyping in a more extensive study; conditions for this study are described in Figure 3.15 and Table 3.1.

In the mice that survived for the entirety of the full 22-day experimental study, we found that mice treated with EVs from LPS-activated macrophages before and after tumor induction (all-EV_{LPS}) had larger tumors on average than mice treated with EVs from non-activated macrophages before and after tumor induction (all-EV_{non}) but not PBS control. However, mice treated with EVs from LPS-activated macrophages before tumor induction (pre-EV_{LPS}) had smaller tumors on average than PBS-treated control mice but not significantly different from mice treated with EVs from non-activated macrophages before tumor induction (pre-EV_{non}). This may suggest that tissue exposure to macrophage-secreted EVs in colitis ongoing throughout the entire process of tumor initiation and progression may promote tumorigenesis, whereas tissue exposed to macrophage EVs from colitis that then undergoes a latent phase without active inflammation just before tumor emergence may instead suppress subsequently occurring tumorigenesis. This observation parallels the classic multistage carcinogenesis model first described by Dr. Yamagiwa and colleagues, where continuous exposure to chemical carcinogens is required for tumor development, while breaks in promotion early on lead to tumor regression[311]. This was elaborated upon by Dr. Robert A. Weinberg in The Biology of Cancer, who demonstrated that carcinogenesis requires sustained promotional signaling (such as ongoing chronic inflammatory signals) to progress to malignancy[22].

The finding that pre-EV_{LPS} decreased tumor size and all-EV_{LPS} increased tumor size also suggests that prior to tumor induction or emergence, EV_{LPS} signals induce changes in non-cancer tissues that affect subsequently occurring tumorigenesis differently from EV_{LPS} directly signaling to the TME. This can be compared to the theory of field cancerization, whereby signals from chronic inflammation predispose

tissues to subsequently occurring tumorigenesis. However in this case, EV_{LPS} administered only before tumor emergence appears to "predispose" tissues to mildly suppress tumor growth. This could occur through EV-recipient non-cancer epithelial or stromal cells signaling to later emerging tumor cells, or to immune cells in the subsequently occurring TME.

However, a confounding factor that weakens these findings is that one mouse in the pre-EV_{LPS} group developed a tumor that grew too fast and was thus sacrificed on day 17 of study. This tumor was used for dissociation practice for single cell RNA sequencing studies on these mice (data not shown). Also, one mouse in the all-EV_{LPS} group died after anesthesia probably due to excessive erythema around the site of EV injection inducing weakness and low energy.

Macrophages

Tumors of mice injected with all-EV_{LPS} contained a lower number of $CD11b^+F4/80^+$ macrophages than all other conditions. A decreased number of macrophages in mouse tumors treated with all-EV_{LPS} relative to all-EV_{non} may signify that activated macrophage-secreted EVs decrease the macrophage population in the TME, or promote non-macrophage cells. Interestingly, in Figure 3.20f, you can see an increase in the population of $CD11b^+$ myeloid cells that do not express the F4/80 macrophage-specific marker. Thus, LPS activation of macrophages may induce secretion of EVs that deliver signals to (i.e., mediate) other types of CD11b myeloid cells that are not macrophages.

The decrease in the number of macrophages in all-EV_{LPS} tumors also occurred relative to pre-EV_{LPS} tumors. This suggests that EV_{LPS} does not predispose tissues to change the numbers or recruitment of tumor-residing macrophages, but EV_{LPS} can signal directly to the TME to decrease the macrophage number. Moreover, the $CD11b^+$ myeloid cell population, and to a lesser extent $CD11b^+F4/80^+$ macrophages, present in the tumors of mice injected with all-EV_{LPS} expressed decreased levels of the M1 marker CD86. This shows that EV_{LPS} can facilitate tumor-residing myeloid cell and macrophage polarization either directly (EV_{LPS} could be taken up by myeloid cells) or indirectly (EV_{LPS} could be taken up by stromal/cancer cells which secrete factors to affect myeloid cell polarization). Future EV tracking studies would be useful to analyze this signaling mechanism.

Within the $CD45^+$ nucleated hematopoietic cell population of tumor cells, macrophages were defined as $CD11b^+F4/80^+$ cells and tumor-associated macrophages (TAMs) were defined as $CD11b^+F4/80^+Ly6C^{lo}Ly6G^-$ [312]. In the tumor microenvironment (TME), TAMs can either be derived from monocytes/macrophages or from m-MDSCs [234]. Arguably our most interesting discovery thus far, fewer TAMs were present in tumors of mice injected with pre-EV_{LPS} and all-EV_{LPS}, relative to all other controls (pre-EV_{non}, all-EV_{non}, and PBS). Specifically, preconditioning the tumor site with EV_{LPS} every day for 7 days

prior to tumor induction induced subsequently occurring tumors to harbor fewer TAMs. This means there was an increased proportion of macrophages that expressed Ly6C and/or Ly6G, which I termed "non-TAM" macrophages, present in tumors from pre-EV_{LPS} mice.

The finding that pre-EV_{LPS} tumors harbor fewer TAMs suggests that prior to tumor induction or emergence, EV_{LPS} signals induce changes in non-cancer tissue cells that affect subsequently occurring tumorigenesis differently from EV_{non} signals. In this case, EV_{LPS} administered before tumor emergence appears to "predispose" tissues to later regulate TAM recruitment or differentiation in a subsequently occurring tumor. Thus, in colitis, macrophage-secreted EVs have the potential to induce changes in pre-cancer tissue that affect those cells signaling with macrophages later in tumorigenesis.

Moreover, in these non-TAM macrophages, pre-EV_{LPS} treatment moderately increased CD206 expression relative to PBS controls, and all-EV_{LPS} treatment significantly decreased CD86 expression relative to all other conditions. Thus, EV_{LPS} injection into the TME plays a clear role in facilitating polarization of all tumor-residing macrophages and myeloid cells, i.e., decreasing M1-like macrophage/myeloid cell marker expression in the TME. However, EV_{LPS} injection into tissues before tumor emergence may indirectly affect polarization of non-TAM macrophages by increasing M2-like macrophage cell expression in the TME.

If we assume the theory of tumor macrophage differentiation to be correct, that M1-like macrophages are anti-tumorigenic whereas M2-like macrophages and TAMs are pro-tumorigenic[313], our findings imply that EVs from LPS-activated macrophages exhibit both M1/anti- and M2/pro-tumorigenic effects prior to tumor emergence (decrease pro-tumor TAMs, increase pro-tumor CD206 M2 marker expression in non-TAM macrophages), and after tumor emergence (decrease total macrophage number, decrease CD86 M1 marker expression in macrophages and myeloid cells, increased g-MDSCs, decreased m-MDSCs, decreased proportion of TAMs, increased CD206 marker expression on TAMs, decreased CD86 expression in non-TAM macrophages, increased neutrophil infiltration, decreased dendritic cell number, and decreased MHCII and CD86 expression on dendritic cells). These effects are visualized in Table 3.4.

Box 3.1. Theoretical effects of extracellular vesicles from macrophages activated with lipopolysaccharide.

Myeloid-derived suppressor cells

Dr. Gabrilovich's group has referred to the recent discoveries in myeloid cell subtypes as the "era of increasing myeloid cell diversity"[233]. One of the relatively newer identified cells are MDSCs—first discovered in tumors due to their immunosuppressive functions on T-cells[314]. An excellent visual hierarchy of myeloid cell differentiation has been published[234]. MDSCs are characterized by their pathologically immunosuppressive state[234]. MDSCs have been found to be upregulated in patients with CAC[315]. Circulating MDSC levels are increased in premalignant states including IBD[237] and colon polyposis[233], and are associated with poor patient prognosis in CRC[316].

The immunosuppressive functions of MDSCs are often regulated by STAT3, STAT1, STAT6, NF-κB, COX2, and CEBPβ [233, 238]. Uniquely, g-MDSCs preferentially use ROS, peroxynitrite, Arg 1, and PGE_2, whereas m-MDSCs more often utilize NO, IL-10, TGFβ, and PDL1[233]. In CRC, factors that may recruit or promote MDSC expansion includes GM-CSF, PGE_2, IFNγ, SCF, S100A8/A9, TGF-β, IL-10, IL-12, IL-13, and MMP-9 [317]. We did not detect most CAC-associated cytokines or growth factors expressed in EVs from LPS-activated macrophages; this suggests that EV_{LPS} induce changes in other cell subtypes, which then signal to recruit MDSCs into the TME or affect myeloid cell differentiation within the TME.

In colitis, MDSCs can promote progression of CAC through many signaling mechanisms[318]. During IBD, MDSC-secreted ROS has the potential to damage intestinal epithelial cell DNA and promote colitis-associated cancer[319]. In colitis, MDSCs secrete IL-6, which is critical for tumor development in colitis-associated cancer[168]. MDSCs have been found to secrete inflammatory S100A8/9, which is upregulated in dysplasia and adenoma in colitis-associated cancer and promotes colon cancer[320].

Interestingly, EVs from g-MDSCs have been shown to mediate signaling in colitis and CAC. One group found that g-MDSCs ($Ly6G^+CD11b^+$), derived from murine lewis lung adenocarcinoma tumors, secreted EVs that exhibited Arg1 activity[44]. Notably, injecting (i.p.) g-MDSC EVs into mice with DSS-induced colitis attenuated colonic inflammation[44]. Another study found that recipient CT26 CRC cells expressed increased stemness, colony formation, NF-kB expression, and formed s.c. tumors earlier and faster following treatment with EVs (containing inflammatory S100A9) from g-MDSCs harvested from the spleens of CT26 tumor-bearing mice[321]. Moreover, tumor incidence was increased in AOM/DSS-induced CAC mice after tail vein (i.v.) injection of EVs (containing S100A9) from g-MDSCs harvested from the spleens of mice with CAC[321].

The effects of EVs from g-MDSCs on mice with CRC tumors and CAC can be compared with our newly discovered effects of EV_{LPS} injection preceding CRC tumor induction. We observed a notable increase in g-MDSC cell number in tumors of mice treated with all-EV_{LPS} relative to all other conditions.

This is similar to the previous finding that injected (i.v. via tail vein) AOM/DSS-induced CAC mice with EVs from g-MDSCs; tumor from these mice contained a higher number of g-MDSC cells[321]. This suggests that EVs from LPS-activated macrophages recruit g-MDSCs to the TME similarly to EVs from g-MDSCs. Investigating the mechanism of EV_{LPS} signaling in the TME to recruit g-MDSCs may reveal a therapeutic target to inhibit this recruitment, since g-MDSCs have been shown to be tumor-promoting and are being investigated as therapeutic targets for CRC[322].

Moreover, we found a higher proportion of m-MDSCs present in the TME relative to g-MDSCs. This is different from a study in AOM/DSS-treated mice, which found CAC tumors to contain a higher proportion of g-MDSCs[321]. Also, EVs from g-MDSCs decreased Th1 T cell and increased Treg infiltration into mesenteric lymph nodes in DSS-induced colitis mice[44], while in CAC mice EVs from g-MDSCs increased total CD3 T cell and CD8 T cell numbers[321]. However, we did not detect a difference in T cell recruitment in mice treated with EVs from non-activated or LPS-activated macrophages. This may be because tumors harvested were relatively small in size, preferable for our model of early tumor development. It may also be because our mice harbored MC38 CRC tumors. MC38 tumors are considered to be immunogenic and similar to human CRC in their expression of PD-L1 and responsiveness to immune checkpoint inhibitors, as well as recruiting Treg cells to evade anti-tumor immunity[323].

Of note, all-EV_{LPS} tumors expressed a significant increase in the number of tumor-residing g-MDSCs, whereas pre-EV_{LPS} tumors did not contain different numbers of g-MDSC cells relative to controls. This suggests that EV_{LPS} recruit g-MDSCs only in the presence of a pre-existing tumor, after emergence/induction. Because this is not an orthotopic model, we can make no conclusions as to whether this is due to cell type; because we injected already transformed cells, we cannot make conclusions about the effect of EVs on the process of neoplastic transformation. We can, however, conclude that EV_{LPS} increases recruitment of g-MDSCs into the TME, known to be tumor-promoting.

Furthermore, pre-EV_{LPS} tumor-residing g-MDSCs expressed increased levels of the proinflammatory M1 marker CD86 relative to all other conditions. This strengthens our claim that EV_{LPS} signals induce changes in non-cancer tissue cells that affect subsequently occurring local tumorigenesis. EV_{LPS} administered before tumor emergence appear to "predispose" tissues to later regulate g-MDSC activation and polarize them into M1-like g-MDSCs in a subsequently occurring tumor. However, CD86 expression in g-MDSCs is not increased in all-EV_{LPS} mouse tumors, implying that EV_{LPS} signaling directly to the TME effectively mitigates this proinflammatory M1 phenotype. Thus, in colitis, macrophage-secreted EVs have the potential to induce changes in pre-cancer tissue that can, later in tumorigenesis, signal to

g-MDSCs and mediate their activation status toward an M1 state; furthermore, these changes in pre-cancer tissue may be reversed if EV_{LPS} are continuously administered to the TME.

MDSCs have also been shown to promote tumor neoangiogenesis in CRC[324]. We did not find an increase in $CD31^+$ endothelial cells or neoangiogenesis in our CRC tumors. These findings suggest that angiogenesis may not significantly mediate the increased pro-tumor immune infiltrate observed in our LPS-activated macrophage EV model.

Neutrophils

Neutrophils are classically considered to be proinflammatory cells that destroy pathogens through mechanisms such as phagocytosis and NETosis, but they also subsequently signal to macrophages to turn toward a pro-regenerative polarization state[325], so they may not always be fully proinflammatory or "N1". In fact, tumor-associated neutrophils (TANs) have been shown to promote CRC[326]. For example, HIF2-α in colon tumor epithelial cells promoted CXCL1 secretion, which recruited neutrophils that increased colon carcinogenesis in CAC mice[327]. LPS triggers neutrophils to secrete IL-1β, which induces mononuclear phagocytes, mostly monocytes and macrophages, to secrete IL-6 and promote CAC[178]. In AOM/DSS-treated CAC mice, intestinal epithelial cells produce the transcription factor BATF3 that promotes secretion of CXCL5 to recruit neutrophils, promoting CAC development[328]. In AOM/DSS-treated CAC mice, $Ly6G^+$ neutrophil recruitment was increased in the colonic lamina propria and submucosa through the chemokine CXCL2, and treatment with anti-Ly6G-neutralizing antibodies to inhibit neutrophil recruitment, decreased CAC tumor number and size[329]. However, reducing Ly6G expressing neutrophilic granulocytes in tumors may also deplete functions of MDSCs, so it is unclear which cell subtype is involved in tumor reduction. In this study, Ly6G expressing cells also expressed MMP-9 and neutrophil elastase (NE), both of which are associated with colon cancer progression[330, 331]. However, another group found opposing effects; neutrophil-deficient and depleted mice treated with AOM/DSS (CAC model) or with APC mutation (sporadic CRC model) expressed increased tumor growth and invasiveness, partially mediated by IL-17 signaling and interactions with microbiota[332]. However, this study used LysM-Cre;Mcl1fl/fl mice, so Cre induction kills many cells of the myeloid lineage and not only neutrophils. So, we again face the same challenge in identifying exactly which cell subtype is involved in mediating tumorigenesis in these mice.

It has been suggested that neutrophil cells are too short-lived to be polarized in the TME, so N1 type cells are proposed to be the activated, "bona fide" neutrophils whereas N2 like neutrophil cells in the tumor, sometimes termed TANs, may actually exist as g-MDSCs[238]. Because g-MDSCs are a precursor for neutrophils, they share many characteristics[234]. As in previous studies, I have defined neutrophils as

$CD11b^+F4/80^-Ly6G^+$ expressing $CD45^+$ cells [333], differentiated from g-MDSCs by a defined lack of F4/80 expression.

Of all tumor-residing CD11b myeloid cells, we found an increased proportion of $Ly6G^+F4/80^-$ cells that we termed neutrophils in tumors from all-EV_{LPS} mice relative to all other conditions. This implies that EV_{LPS} can directly or indirectly recruit neutrophils to the TME. This finding is similar to a previous report that administering EVs from neutrophils intra-luminally into the ileum of mice effectively increased neutrophil infiltration[334]. Of note, pre-EV_{LPS} mouse tumor-residing neutrophils expressed increased levels of proinflammatory CD86 (N1) marker relative to all other conditions. This further strengthens our claim that EV_{LPS} signals may induce changes in non-cancer tissue cells that affect subsequently occurring tumorigenesis. EV_{LPS} administered before tumor emergence may thus "predispose" tissues to later regulate neutrophil activation and increase N1-like polarization status in a subsequently occurring tumor. CD86 expression in neutrophils, however, is not increased in all-EV_{LPS} mouse tumors, implying that EV_{LPS} signaling directly to the TME effectively mitigates the recruitment of proinflammatory N1 neutrophils. Thus, in colitis, macrophage-secreted EVs have the potential to induce changes in pre-cancer tissue that can, later in tumorigenesis, signal to neutrophils and shift their activation status toward an N1 state; furthermore, these changes in pre-cancer tissues may be reversed if EV_{LPS} is continuously administered to the TME.

Furthermore, neutrophil-secreted EVs contain myeloperoxidase (MPO) that can inhibit CRC cell migration and proliferation in vitro and inhibited colonic mucosal wound repair in vivo mice[197]. EVs from neutrophils have also been shown to contain proinflammatory microRNAs miR-23a and miR-155, which target histones and effectively promote the accumulation of double-strand breaks (DSBs) in colon tissues with acute wounds and DSS-induced colitis[198]; DSB accumulation can induce genetic and epigenetic alterations, and is characteristic of cancer progression and CAC[199]. Because CRC is accompanied by increasingly accumulating genetic and epigenetic alterations that together with chronic inflammation drive tumorigenesis forward, this suggests that neutrophil EVs have the potential to be the mediator of immunocarcinogenesis in the colon. Neutrophil EVs have also been found to express MMP-9, which aided in cleaving intercellular adhesions to damage CRC cell monolayers[334]. Bui *et al*. reviewed the role of neutrophil-secreted factors, including reactive oxygen species, cytokines, matrix metalloproteinases, and EV-packaged miRs, that drive genomic instability in tissues experiencing chronically recurring tissue injury[335].

Albeit difficult to differentiate from g-MDSCs, neutrophils likely play a prominent role in CAC and tumor progression, and their recruitment to tumors in a CAC model appears to be mediated by EVs from LPS-activated macrophages directly and/or indirectly.

Dendritic cells

DCs are professional antigen presenting cells (APCs) that can engulf proteins from viruses, bacteria, and tumor cells and present these neoantigens to T cells on major histocompatibility complex (MHC) molecules I and II to activate CD8 cytotoxic T lymphocytes (CTLs) and CD4 T helper cells, respectively[336]. The degree of DC infiltration into the TME of CRC has been shown to negatively correlate with tumor stage and metastasis, i.e., lower numbers of infiltrating DCs are associated with more advanced patient tumor stage[337]. In fact, impairing the function of DCs is a key mechanism CRC cells employ for immune escape; for example, loss of DCs have been shown to be a necessary driver of CAC; for example, in T-bet$^{-/-}$RAG2$^{-/-}$ mouse model of CAC, restoring T-bet (transcription factor that mediates Th1 response) function in DCs decreased development of neoplasia[338]. Tumor-associated DCs may further promote tumors by secreting CXCL1 that has been found to induce cell mobility and EMT in CRC cells[339]. DCs have been shown to respond to EVs from intestinal epithelial cells, which can modulate DC growth, maturation, and antigen presentation[40]. In our model, we found fewer DCs in the tumors of mice injected with all-EV_{LPS} relative to all other conditions. It is thus possible that EV_{LPS} exert a tumor-promoting role by decreasing recruitment of DCs. We also found DCs in tumors from all-EV_{LPS} mice to express lower levels of MHC II, suggesting that EVs from LPS-activated macrophages may inhibit maturation of DCs or promote an immature phenotype. Immature DCs (iDCs) express low MHC II levels, tend to be immunosuppressive, and promote CRC[336]. We also found all-EV_{LPS} tumor-residing DCs to express decreased levels of CD86 (D1, proinflammatory) relative to PBS and pre-EV_{LPS} conditions. This means that EV_{LPS} may induce a pro-regenerative (or at least decrease the proinflammatory) phenotype in the remaining population of DCs in the TME.

In summary, we found that EVs from LPS-activated macrophages produced substantial changes in the numbers, activation, and differentiation status of tumor-associated immune cell populations. Further studies that inhibit specific proteins in macrophage EVs implicated in colitis-associated cancer (e.g., ASS1) prior to exposure to colon cancer cells or tumor induction may reveal the mechanisms by which inflammatory EVs predispose colonic tissue to malignant transformation.

Table 3.4 Effects of extracellular vesicles from macrophages on myeloid cells in the tumor immune microenvironment.

Effects from pre-EV_{LPS}	**Effects from all-EV_{LPS}**	**Strength of effects**	**Theoretical effects on tumor immune microenvironment**
	Decrease total macrophage number	Significant	Indeterminate
	Decrease CD86 M1 marker expression in all myeloid cells	Significant	Pro-regenerative
	Decrease CD86 M1 marker expression in macrophage	Moderate; significant relative to PBS and pre-EV_{LPS}	Pro-regenerative
	Increase g-MDSCs	Significant	Immunosuppressive
	Decrease m-MDSCs	Moderate; significant relative to pre-EV_{non} and pre-EV_{LPS}	Indeterminate
Decrease proportion of TAMs	Decrease proportion of TAMs		
	Increased CD206 expression in TAMs	Relative to PBS only	Pro-regenerative
Increase CD206 M2 marker expression in non-TAM macrophages	Decrease CD86 M1 marker expression in non-TAM macrophages		Pro-regenerative
	Increased neutrophil infiltration	Significant	Proinflammatory
	Decreased dendritic cell number	Significant	
	Decreased MHC II expression on dendritic cells	Relative to pre-EV_{non} and pre-EV_{LPS}	Immunosuppressive
	Decreased CD86 expression on dendritic cells	Relative to PBS and pre-EV_{LPS}	

CHAPTER 4:

REVEALING THE ROLE OF IMMUNOMETABOLISM IN POLYLACTIC ACID BIOIMPLANT-DRIVEN CHRONIC INFLAMMATION

INTRODUCTION

Lipopolysaccharide (LPS) regulates the metabolic state of inflammatory cells as a model of immune cell activation in chronic ulcerations leading to mucosal infiltration of gram-negative bacteria. In contrast, I was also interested in investigating chronic inflammation in the absence of bacterial components, i.e., sterile chronic inflammation. Polylactic acid (PLA) is the most widely used biopolymer in medicine, with applications ranging from dissolvable sutures to tissue implants[340]. The main roadblock to PLA usage in clinical therapies is its induction of chronic inflammation[341]. PLA-induced chronic inflammation can occur in a sterile environment and thus serves as a system distinct from lipopolysaccharide (LPS) stimulation, even though implanted PLA can also lead to infections and stimulation of the immune system can be multipartite. In parallel to my research on extracellular vesicle (EV) signaling effects in the environment of chronic inflammation by the bacterial component LPS, I also collaborated on studies examining lactic acid signaling and its inflammatory effects on the microenvironment surrounding tissue implants [104, 342, 343].

The aging and injured population is driving a need for better and more well-tolerated bone implants, and this is interfacing with the field of regenerative medicine to a point where it is conceivable that synthetic bone implants could be created that are designed to eventually be replaced with natural bone through natural and guided regenerative processes. PLA is biodegradable, amorphous or semi-crystalline, flexible and strong, and can be customized with other polymers and embedded drugs, making it an excellent candidate material for bioimplants. The stereochemistry of PLA can affect its structure and degradation products; amorphous PLA (aPLA) is more disordered in structure and degrades faster into more D-lactic acid than semi-crystalline PLA (cPLA), which degrades slower into more L-lactic acid. The chronic inflammation in response to PLA degradation products has long been attributed to tissue acidification. However, many attempts to buffer the implants, including with PLA infused with hydroxyapatite (HA), have not mitigated the chronic stimulation of the immune response. *The following text is exerpted from our manuscript titled "Polylactide Degradation Activates Immune Cells by Metabolic Reprogramming", published in Adv. Sci.[104].*

"Polylactide (PLA) is the most widely utilized biopolymer[340], with applications in nanotechnology, drug delivery, and adult reconstructive surgery for tissue regeneration. However, after surgical implantation, PLA elicits adverse immune responses in up to 44% of human patients, often requiring further interventions[344, 345]. In animals, a 66% incidence of excessive fibrosis with capsules from long-term inflammation which significantly limit implant-tissue integration has been reported[341]. PLA degrades by hydrolysis into d- or l-lactic acid, with semi-crystalline PLA degrading slower and tending to

contain less D-content than amorphous PLA[340, 346]. Adverse responses to PLA are exacerbated by mechanical loading and increasing implant size[347], and occur after prolonged exposure to large amounts of PLA degradation products[344, 348-350]. It is speculated that adverse responses are mediated by PLA degradation reducing pH in surrounding tissue[351], the historical basis of which involved Photobacterium phosphoreum[352]. This bacterium expresses a luciferase whose reduced metabolic activity, measured by bioluminescence, can infer toxicity. In this study, breakdown products (extract) of PLA were obtained either in sterile water or Tris buffer; addition of acidic extract correlated with reduced luminescence. However, the study was not performed on mammalian cells, did not reflect the buffered in vivo microenvironment or simulate prolonged exposure times to accumulated PLA degradation products. Establishing that a decrease in pH correlates with PLA degradation has informed the current strategy in regenerative medicine to neutralize acidic PLA degradation products both in vitro and in vivo using polyphosphazene[353], calcium carbonate, sodium bicarbonate, and calcium hydroxyapatite salts[351], bioglass[354] and composites containing alloys or hydroxides of magnesium[355, 356] despite reports of failures[357]. The lack of a clearly described mechanism of immune cell activation by PLA degradation remains a major obstacle in the safe application of large-PLA-based implants in load-bearing applications as reflected by their paucity in FDA approvals[358], and in soft tissue surgery where neutralizing ceramics cannot be applied[359].

Metabolic reprogramming refers to significant changes in oxidative phosphorylation and glycolytic flux patterns and is a driver of fibrosis and bacterial lipopolysaccharide (LPS)-induced inflammation[360, 361]. Here we set out to establish a molecular mechanism that directly links metabolic reprogramming to inflammation and fibrosis, consequent to cellular interactions with PLA degradation products. Foremost, we develop and validate a bioenergetic model of prolonged immune cell interaction with accumulated PLA degradation products. Only after prolonged exposure to amorphous or semi-crystalline PLA degradation products did macrophages and fibroblasts mechanistically undergo metabolic reprogramming and marked bioenergetic changes, with higher PLA crystallinity delaying onset. Using our model, we observed that PLA breakdown products markedly increase proinflammatory cytokine expression in primary macrophages through lactate signaling. Targeting different glycolytic steps using small molecule inhibitors modulated proinflammatory and stimulated anti-inflammatory cytokine expression by inhibiting metabolic reprogramming and altered bioenergetics in a dose-dependent manner. This process is highly specific and not cytotoxic to surrounding unaffected immune cells. Further, we demonstrate that the use of the small molecule inhibitors imbedded in PLA implants substantiated our hypothesis of controlling the inflammatory response in vivo. Our findings establish a

new biocompatibility paradigm by identifying altered metabolism as a target for immunomodulation of PLA-based implants, fundamentally differing from previous strategies aimed at neutralizing PLA. Therefore, major advances in the use of PLA for human and veterinary applications are anticipated."

Table 4.1 Metabolic drugs used in this study and their mechanism of action. Abbreviations (abbv), oxidative phosphorylation (ox-phos), electron transport chain (ETC).

Target pathway	**Drug name**	**Abbv**	**Mechanism of Action**	**FDA approval**
Glycolysis	3-(3-pyridinyl)−1-(4-pyridinyl)−2-propen-1-one	3PO	inhibits 6- phosphofructo-2-kinase (rate-limiting enzyme of glycolysis)[362]	
Glycolysis	2-deoxyglucose	2DG	inhibits hexokinase (first enzyme in glycolysis)[214]	
Glycolysis	aminooxyacetic acid	a.a.	prevents uptake of glycolytic substrates[363]	used safely in clinical trials for many conditions/diseases[364]
Ox-phos	rotenone	rot	inhibits complex I of the mitochondrial ETC	
Ox-phos	metformin	met	inhibits complex I of the mitochondrial ETC	approved for diabetes[365 366]
Ox-phos	antimycin A	AA	inhibits complex III of the mitochondrial ETC[365]	
Ox-phos	oligomycin	olig.	inhibits complex V of the mitochondrial ETC[365]	

Dr. Chima Maduka formulated the brilliant hypothesis that acidification was not the sole reason for the increased inflammation in PLA implants. He proposed that the breakdown products acts as signaling molecules that activate immune cells by modulating their metabolism.

In my opportune collaboration with Dr. Maduka, we examined immunometabolism and PLA implants. Dr. Maduka made PLA breakdown products (extracts) by incubating PLA beads in serum-containing DMEM medium in a shaker at 37°C for 12 d. Buffering allowed for pH to remain balanced,

unlike previously-made PLA extracts created in water. We cultured immune cells in PLA extracts for prolonged periods (7-12 d) to mimic chronic exposure to PLA breakdown products. We found that ECAR and OCR were upregulated, so we looked for drugs targeting both pathways that could mitigate this inflammatory response to the biomaterials. I helped characterize the effects of aPLA and cPLA on MEFs and BMDMs in vitro. We discovered a mechanism by which PLA extracts induce inflammation in macrophages and fibroblasts. After prolonged exposure, PLA extracts (including L-lactic acid) increased bioenergetic levels and metabolism in macrophages, inducing a proinflammatory response. We also found that this can be effectively mitigated with metabolic inhibitors in vitro. We then progressed into preclinical studies. With Dr. Chima Maduka, Dr. Ashley Makela, and Anthony Tundo, I spearheaded flow cytometric characterization of the immune infiltrate landscape on s.c. implanted aPLA with or without infused glycolytic inhibitor drugs in mouse dermis. We found that aPLA implants increased proinflammatory immune infiltrate, and this was mitigatable with metabolic inhibitors. Notably, HA exacerbates the proinflammatory immune response.

Our studies implicate that chronic immune stimulation by implanted PLA is driven by monomers and oligomers of lactate released into the tissue environment surrounding PLA implants through biodegradation. Since lactate builds up in the hypoxic tumor microenvironment, and lactate signaling has been shown to be involved in tumorigenesis and cancer progression, there may be some parallels between immune stimulation by implanted PLA, and by malignant growth at later stages of disease with relevance to the concept that tumors release EVs that create premetastatic niches. This is analogous to EVs creating premalignant environments, i.e., immunocarcinogenesis.

These findings have huge clinical implications as they reveal a variety of metabolic inhibitors as a potential therapeutic that will allow PLA to be used for bone implants. They also explain why attempting to neutralize PLA implants with HA may not mitigate inflammation. The results and that follow are based on, and in some places where noted are excerpted from, published papers and papers under review on which I am one of the co-authors with Drs. Contag, Maduka, and Makela.

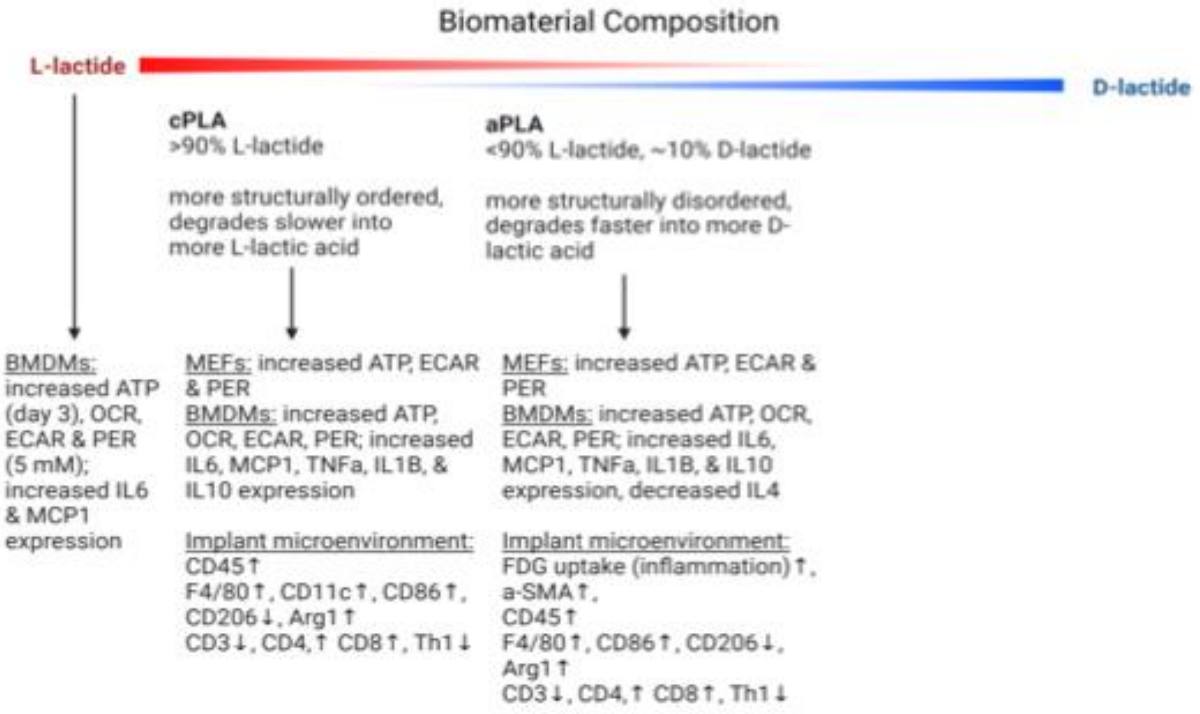

Figure 4.1 Graphical abstract showing effects of amorphous polylactide (aPLA) and semi-crystalline polylactide (cPLA) extracts on fibroblasts (MEFs), macrophages (BMDMs), and the in vivo tissue environment. Created with *BioRender.com*.

METHODS

The following text is excerpted from our manuscript titled "Polylactide Degradation Activates Immune Cells by Metabolic Reprogramming", published in Adv. Sci.[104].

Materials

3-(3-Pyridinyl)−1-(4-pyridinyl)−2-propen-1-one (MilliporeSigma), 2-deoxyglucose (MilliporeSigma) and aminooxyacetic acid (Sigma–Aldrich) were used for glycolytic inhibition and l-lactic acid (Sigma–Aldrich) was used at various concentrations to reproduce the effects of PLA degradation products. Each of these materials were made in complete medium before adding to wells of a 96-well plate.

Cells

Mouse embryonic fibroblast cell line (NIH 3T3 cell line; ATCC) and murine primary bone-marrow-derived macrophages (BMDMs) were used. In each experiment, either 5000 fibroblasts or 50 000 BMDMs were initially seeded. BMDMs were sourced from male and female C57BL/6J mice (Jackson Laboratories) of 3–4 months[213, 367]. NIH 3T3 cells were stably transfected with a Sleeping Beauty transposon plasmid (pLuBIG) having a bidirectional promoter driving an improved firefly luciferase gene (fLuc) and a fusion

gene encoding a Blasticidin-resistance marker (BsdR) linked to eGFP (LuBiG)[368]; enables monitoring of bioenergetic changes in live cells[111, 369]. All cells were cultured in a total of 200 µl complete medium with volumes of extracts specified in figure legends.

Cell Viability

Cell viability was assessed using the crystal violet staining assay[210], at room temperature, as an end-point measure of total biomass generated over the course of the culture period. Briefly, out of 200 µL of medium per well, 150 µL was discarded. To each well, 150 µL of 99.9% methanol (MilliporeSigma) was added for 15 min to kill and fix the cells, then discarded. Afterward, 100 µL of 0.5% crystal violet (25% methanol) was added for 20 min, then the wells were emptied. Each well was washed twice with 200 µL of phosphate-buffered saline for 2 min. Absorbance (optical density) was acquired at 570 nm using the SpectraMax M3 Spectrophotometer (Molecular Devices) and SoftMax Pro software (Version 7.0.2, Molecular Devices).

Bioenergetic Assessment

Bioluminescence was measured using the IVIS Spectrum in vivo imaging system (PerkinElmer) after adding 150 µg mL−1 of d-luciferin (PerkinElmer). Living Image (Version 4.5.2, PerkinElmer) was used for acquiring bioluminescence on the IVIS Spectrum. Standard ATP/ADP kits (Sigma–Aldrich) containing d-luciferin, luciferase, and cell lysis buffer were used to according to manufacturer's instructions. Luminescence at integration time of 1000 ms was obtained using the SpectraMax M3 Spectrophotometer (Molecular Devices) using SoftMax Pro (Version 7.0.2, Molecular Devices).

Functional Metabolism

Basal measurements of oxygen consumption rate (OCR), extracellular acidification rate (ECAR), and lactate-linked proton efflux rate (PER) were obtained in real-time using the Seahorse XFe-96 Extracellular Flux Analyzer (Agilent Technologies) according to manufacturer[212-214]. Prior to running the assay, the cell culture medium was washed with and replaced by the Seahorse XF DMEM medium (pH 7.4) supplemented with 25 mm d-glucose and 4 mm Glutamine. The Seahorse plates were equilibrated in a non-CO2 incubator for 1 h prior to the assay. The Seahorse ATP rate and cell energy phenotype assays were run according to manufacturer's instruction and all reagents for the Seahorse assays were sourced from Agilent Technologies. Wave software (Version 2.6.1) was used to export Seahorse data directly as means ± standard deviation (SD).

Chemokine and Cytokine Measurements

Cytokine and chemokine levels were measured using a MILLIPLEX MAP mouse magnetic bead multiplex kit (MilliporeSigma)[370] to assess for IL-6, MCP-1, TNF-α, IL-1β, IL-4, IL-10, IFN-γ, and 1L-13 protein

expression in supernatants. Data was acquired using Luminex 200 (Luminex Corporation) by the xPONENT software (Version 3.1, Luminex Corporation). Using the glycolytic inhibitor, 3PO, expectedly decreased cytokine values to < 3.2 pg mL−1 in some experiments. For statistical analyses, those values were expressed as 3.1 pg mL−1. Values exceeding the dynamic range of the assay, in accordance with manufacturer's instruction, were excluded. Additionally, IL-6 ELISA kits (RayBiotech) for supernatants were used according to manufacturer's instructions.

Mouse model

Amorphous PLA was compounded with 2DG at 190 °C for 3 min in a DSM 15 cc mini-extruder (DSM Xplore) and pelletizer (Leistritz Extrusion Technology). The in-vitro studies indicate 1 mm 2DG to be an effective concentration. Accordingly, one estimated that 189 mg of 2DG in 10 g of amorphous PLA will approximate effective concentrations after accounting for the potential thermal degradation of 2DG, converting mm to w/w values[371]. Comparable amounts (200 mg) of hydroxyapatite (HA; 2.5 µm particle sizes[372]; Sigma–Aldrich) in were compounded 10 g of amorphous PLA under the same melt-blending thermal conditions. To exclude the effect of melt-blending as a confounder in studies, amorphous PLA controls were processed under the same thermal conditions to make “reprocessed” amorphous PLA. Pellets from melt-blending were made into 1.75 mm diameter filaments using an extruder (Filabot EX2) at 170 °C with air set at 93. For surgical implantation, amorphous PLA filaments were cut into 1 mm lengths; four biomaterials were subcutaneously implanted on the dorsum (back) of each mouse, with two cranially (2.5 cm apart) and two caudally (2.5 cm apart)[353].

PET imaging

Two-month-old female C57BL/6J mice (n = 3 mice per group) with an average weight of 19 g were used according to procedures approved by the Institutional Animal Care and Use Committee at Michigan State University (PROTO202100327). Mice were anesthetized using isoflurane (2%–3%). The back of each mouse was shaved and alternate iodine and alcohol swabs were used as skin disinfectants. Aseptic surgery consisted of incisions through the skin into the subcutis, where biomaterials were inserted into a pouch made with forceps. Afterward, surgical glue (3 m Vetbond) was used to appose the skin. Each mouse received intraperitoneal or subcutaneous pre- and post-operative meloxicam (5 mg kg−1) injections as well as postoperative saline. Sham controls underwent the same procedure without biomaterial implantation. After 6 weeks, the dorsum of mice was shaved to visibly observe sites of surgical implantation. Thereafter, mice were intraperitoneally injected with 4.82 MBq F-18 fluorodeoxyglucose (Cardinal Health) in 200 µL. At 65 min post-dose, mice were euthanized and blood drawn from their hearts. Circular biopsies (12 mm diameter) of full skin thickness, with visible implants

in the center, were recovered. Similar-sized biopsies were collected from mice in the sham group in the region where surgical incision was made. Biomaterial migration from subcutaneous sites only allowed for the recovery of most and not all implants. As such, for obtaining data on the gamma counter (Figure 7a), there were 12 skin biopsies from three mice in the sham group, 8 skin biopsies from three mice (amorphous PLA group), and 10 skin biopsies from three mice (amorphous + 2DG group). Skin biopsies, blood sample and heart organs were weighed, with only skin samples fixed in 4% paraformaldehyde (PFA). Activity in all samples was assessed via gamma counter (Wizard 2, Perkin Elmer) once decayed to a linear range. All injected doses and gamma counter measurements were decay-corrected to the same timepoint to calculate the percent of injected dose taken up per gram of assessed tissue (%ID g−1; Figure 7a).

Immunohistochemistry staining and image analysis

For tissue staining, one skin biopsy per mouse was passed through increasing concentration of 10%, 20%, and 30% sucrose, daily. Using 99.9% methanol (Sigma–Aldrich) on dry ice, tissues were embedded in optimal cutting temperature (O.C.T.) compound (Tissue-Tek) by snap freezing. After equilibration at −20 °C, multiple successive 8 µm sections were obtained using a microtome-cryostat. Sections were routinely stained using hematoxylin and eosin. Two different tissue sections were immunostained using conjugated antibodies as follows: 1) F4/80-FITC (1:100; BioLegend; 123 107), CD11b-PE (1:100; BioLegend; 101 207), CD206-BV421 (1:200; BioLegend; 141 717) and CD86-Alexa Fluor 647 (1:100; BioLegend; 105 019) using ordinary mounting medium; 2) alpha-SMA-eFluor660 (1:150; ThermoFisher Scientific; 50-9760-82), TGF-beta-PE (1:100; ThermoFisher Scientific; 12-9821-82) using DAPI mounting medium. Sections for TGF-beta were permeabilized using 0.1% Triton X in 1× PBS (PBST) for 8 min then washed off with 1x PBS generously. Afterward, blocking buffer (0.5% bovine serum albumin in 1× PBS) was used to cover slides for 30 min. Slides were then incubated in antibodies at 4 °C overnight. Subsequently, slides with tissue sections were washed in 1× PBS, and mounting medium applied. Immunostained sections on slides were imaged using a Leica DMi8 Thunder microscope fitted with a DFC9000 GTC sCMOS camera and LAS-X software (Leica, version 3.7.4). Imaging settings at 20× magnification and 100% intensity were: 1) F4/80-FITC excitation using the 475 laser (filter 535/70; 500 ms); CD11b-PE excitation using the 555 laser (no filter; 500 ms); CD206-BV421 excitation using 395 laser (no filter; 150 ms); CD86-Alexa Fluor 647 excitation using the 635 laser (no filter; 500 ms). 2) alpha-SMA-eFluor660 excitation using the 635 laser (no filter; 500 ms), TGF-beta-PE excitation using the 555 laser (no filter; 500 ms) and DAPI excitation using the 395 laser (535 filter; 500 ms). On the other hand, sections stained with hematoxylin and eosin were imaged at 40× using the Nikon Eclipse Ci microscope

fitted with a CoolSNAP DYNO (Photometrics) and NIS elements BR 5.21.02 software (Nikon Instruments Inc.). Microscope images were prepared and analyzed using ImageJ (version 1.53k). For analyzing immunostained sections, five randomly selected rectangular areas of interest (1644.708 μm2), encompassing cells adjacent to implants, were obtained as mean gray values[373] a tissue section. In the sham group, biopsies were taken from incision sites, and areas without cells were also analyzed. Where derived from n = 2 or n = 3 mice, 10 or 15 data points, respectively were graphically represented to fully reveal inherent variance across samples (Figures 7b–e and 8a,b); only the aPLA + HA group had sections derived from n = 2 mice after one sample was damaged during cryo-sectioning and excluded from analyses. Representative images (16-bit; 0 to 65535) were adjusted to enhance contrast for direct comparison using ImageJ as follows: CD86 (800–11000), CD206 (2000–5000), F4/80 (500–4000), CD11b (800–11000), α-SMA (1300–5000), DAPI (6000–31, 000), and TGF-β (1900–13000).

Statistical analysis

Statistical software (GraphPad Prism) was used to analyze data presented as mean with standard deviation (SD). The significance level was set at $p < 0.05$, and details of statistical tests and sample sizes, which were biological replicates, are provided in figure legends. Exported data (mean, SD) from Wave in Seahorse experiments had the underlying assumption of normality and similar variance and thus were tested using corresponding parametric tests as indicated in figure legends.

The following text includes excerpts from the manuscripts titled “Regulating the proinflammatory response to implanted composite biomaterials comprising polylactide and hydroxyapatite by targeting immunometabolism”, published in Bioactive Materials[342], and “The role of mitochondrial complex I in the proinflammatory response to polylactide implants”, currently submitted to ACS Applied Engineering Materials [343].

Tissue digestion for flow cytometry

Eleven weeks following implantation, mice were shaved around the implanted biomaterial site (or sham site), then euthanized for excision of tissue. Circular biopsies (8 mm diameter) were collected from each mouse and tissues were pooled from the same groups. Tissues were cut with surgical scissors for ∼1 min followed by digestion in an enzyme cocktail containing 0.5 mg/ml Liberase (Sigma-Aldrich), 0.5 mg/mlμ Collagenase Type IV (Stem Cell Technologies), 250 U/ml Deoxyribonuclease I (Worthington Biochemical Corporation) in 25 mM HEPES buffer (Sigma-Aldrich). The tissue/enzyme cocktail was incubated at 37°C with 5% CO_2 on top of an orbital shaker, shaking at 70 rpm for 1 h. Following incubation, 5 ml of the tissue/enzyme cocktail mixture was run through a 70 μm filter into a 50 ml conical tube and the remaining tissues which were not digested were mechanically dissociated against the serrated portion

of a petri dish. The resultant mixture was filtered into the previous 50 ml conical tube. Remaining undigested tissue in the 70 µm filter was again mechanically dissociated with the thumb press of a syringe plunger for optimal extraction of cells. The petri dish was washed with cold Hanks' Balanced Salt Solution without calcium, magnesium and phenol red (ThermoFisher Scientific), followed by filtration into the conical tube. Cells were centrifuged at 350G for 10 min followed by automated counting (Countess Automated Cell Counter, Invitrogen) for flow cytometry.

Flow cytometry

For flow cytometry staining in a polypropylene 96-well round bottom plate (Sigma, cat#P6866), 1 × 106 cells were used. All staining steps were performed in 100 µl volume in the dark at 4 °C. Samples were first incubated with LIVE/DEAD Fixable Blue Dead Cell Stain kit (1:500, Thermofisher, cat#L23105) for 20 min. Thereafter, cells were washed once with flow buffer, followed by incubation with TruStain FcX (anti-mouse CD16/32) Antibody (BioLegend, Cat#101319; 1 µg/sample) in 50 µl volume for 10 min. The following antibodies were mixed together at 2x concentration in 50 µl and added directly to the cell suspension: BV605 CD45 (1:500, Biolegend, cat#103139), AF700 CD11b (1:300, Biolegend, cat#101222), BV785 F4/80 (1:300, Biolegend, cat#123141), BV421 CD86 (1:200, Biolegend, cat#105031), APC CD206 (1:200, Biolegend, cat#141707), PerCP MHCII (1:200, Biolegend, cat#107623), PacBlue Ly6G (1:250, BD Bioscience, cat#127611), SparkBlue 550 CD3 (1:100, Biolegend, 100259), APC-Fire 810 CD4 (1:100, Biolegend, 100479), BB700 CD8a (1:100, Biolegend, 566410), and PE-Dazzle 594 CD11c (1:500, Biolegend, cat#117347). Before fixation and permeabilization (BD Cytofix/Cytoperm kit, BDB554714), cells were washed once, suspended in BD Perm/wash buffer with BV650 IL-4 (1:50, BD Bioscience, cat#564004), APC-Fire750 IFNg (1:80, Biolegend, 505859), and PE-Cy7 Arg1 (1:100, ThermoFisher, 25-3697-80) for 30 mins incubation. Thereafter, cells were washed twice with BD Perm/wash buffer then suspended in a final volume of 100 µl for flow cytometry analysis.

The Cytek Aurora spectral flow cytometer (Cytek Biosciences, CA, USA) was used for sample analyses, using the Cytek SpectroFlo software (version 3.0.3) for data collection. Fluorescence minus one (FMO) samples were used to guide gating strategies, and the flow cytometry data was analyzed with the software FCSExpress (DeNovo Software, CA, USA; version 7.12.0005).

RESULTS

The following text includes excerpts from our manuscript titled "Polylactide Degradation Activates Immune Cells by Metabolic Reprogramming", published in Adv. Sci.[104].

Bioenergetics is altered in fibroblasts after prolonged exposure to PLA extracts

First, we tested effects of amorphous PLA (aPLA) and semi-crystalline PLA (cPLA) extracts on mouse embryonic fibroblasts (MEFs). Firefly luciferase-expressing NIH 3T3 cells (3T3-LuBiG) were generously provided by Dr. Michael Bachmann[368]. Firefly luciferase is an oxidoreductase that requires ATP and molecular O_2 to convert D-luciferin (D-luc) substrate into oxyluciferin, producing luminescence that is detectable by bioluminescence imaging (BLI) via the IVIS. Administering an excess concentration of 150 μg/ml D-luciferin to 3T3-LuBiG cells allows ATP to be the rate-limiting reactant, and cellular ATP levels consequently remain proportional to the amount of bioluminescence quantifiably measured by the IVIS. We discovered that prolonged exposure (7-12 d) of 3T3-LuBiG fibroblasts to cPLA extracts increased bioenergetic (ATP) expression levels (Figure 4.2a).

Next, we confirmed these results on wild-type 3T3 MEFs. After treating 3T3 cells with PLA extracts for 7 or 12 d, the standard ATP assay on lysed cells showed that by day 12, there was a 1.9- and 2.3-fold increase in ATP levels among cells exposed to cPLA and aPLA extract, respectively (Figure 4.2b). The crystal violet assay for cell number measurement[210] in 3T3-LuBiGs showed that cell numbers are similar between groups, and thus cell numbers do not account for the bioenergetic (ATP) level changes measured per well (Figure 4.2c).

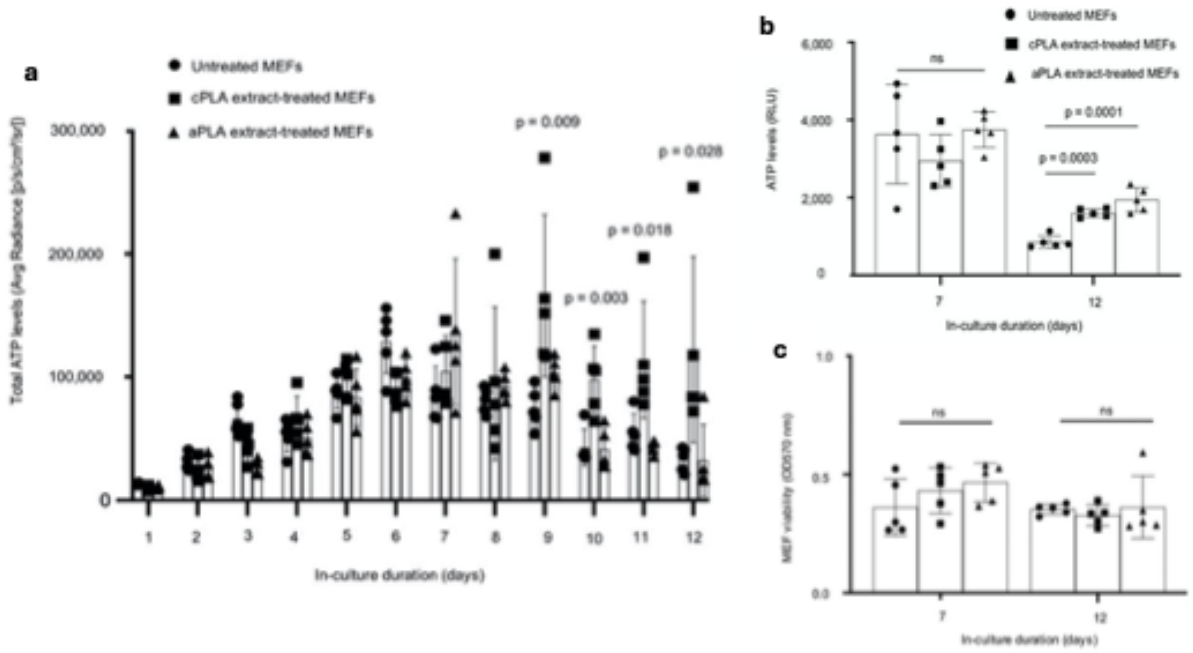

Figure 4.2 Bioenergetic (ATP) levels are elevated in mouse embryonic fibroblasts (MEFs) only after prolonged exposure to polylactide (PLA) degradation products (extract). (a) Using the In Vivo Imaging System (IVIS), ATP levels in live cells are increased in luciferase-expressing MEFs after prolonged exposure to crystalline PLA (cPLA) degradation products, in comparison to controls. (b) Measuring ATP in cell lysates of wild-type MEFs revealed that prolonged exposure to both amorphous PLA (aPLA) and cPLA results in elevated ATP levels. (c) Cell numbers between groups are similar for MEFs. Not significant (ns), mean (SD), n = 5, one-way ANOVA followed by Tukey's post-hoc test; 100 µl of control or PLA extract was used.

Functional metabolism is altered in fibroblasts after prolonged exposure to PLA extracts

To determine the metabolic pathways responsible for the bioenergetic changes we had observed, Seahorse assays were used to measure oxygen consumption rate (OCR), extracellular acidification rate (ECAR), and lactate-linked proton efflux rate (PER) in a customized medium (pH 7.4); this technique has not been previously used to examine PLA-induced adverse responses. PLA extract was removed and washed off the cells prior to running the Seahorse assay at a pH 7.4. Seahorse assays measure ECAR as an index of glycolytic flux, OCR as an index of oxidative phosphorylation, and PER as an index of monocarboxylate transporter function[374] in live cells; and are used to assess for metabolic reprogramming[212-214].

After prolonged exposure of fibroblasts to aPLA and cPLA extracts, glycolytic flux (ECAR; Figure 4.3a,b) is increased by 1.6- and 1.7-fold, respectively. Furthermore, monocarboxylate transporter function is increased in aPLA or cPLA extract-treated fibroblasts by 1.6- and 1.5-fold, respectively (Figure 4.3c,d).

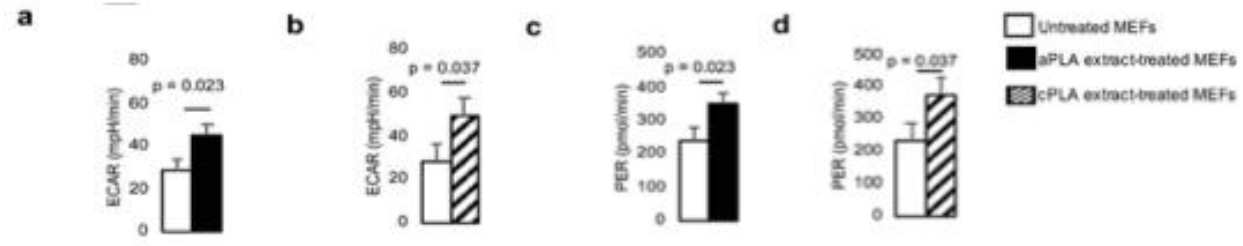

Figure 4.3 Functional metabolism is altered in mouse embryonic fibroblasts (MEFs) after exposure to polylactide (PLA) extracts. a,b) Following exposure to amorphous PLA (aPLA; a) or crystalline PLA (cPLA; b) extracts, extracellular acidification rate (ECAR) is increased. c,d) Proton efflux rate (PER) is elevated in MEFs after exposure to aPLA (c) or cPLA (d) extract. Mean (SD), n = 3, two-tailed unpaired t-test or Brown–Forsythe and Welch ANOVA followed by Dunnett's T3 multiple comparisons test; 100 µl of control or PLA extract was used for 7 days.

Bioenergetic changes in fibroblasts exposed to PLA extracts are modulated with glycolytic inhibitors

We then tested whether this aPLA and cPLA-induced increase in bioenergetic (ATP) levels could be therapeutically targeted. We targeted different steps in the glycolytic pathway using three small molecule inhibitors: 3-(3-pyridinyl)−1-(4-pyridinyl)−2-propen-1-one (3PO), 2-deoxyglucose (2DG) and aminooxyacetic acid (a.a.). Whereas 3PO specifically inhibits 6- phosphofructo-2-kinase which is the rate-limiting glycolytic enzyme,[362] 2DG inhibits hexokinase, the first enzyme in glycolysis,[214] and aminooxyacetic acid prevents uptake of glycolytic substrates[363]. The functions of these drugs are outlined in Table 4.1.

Remarkably, increased bioenergetic (ATP) levels in aPLA or cPLA extract-treated fibroblasts are inhibited by 3PO, 2DG, and a.a. in a temporal and dose-dependent manner (Figure 4.4a,b).

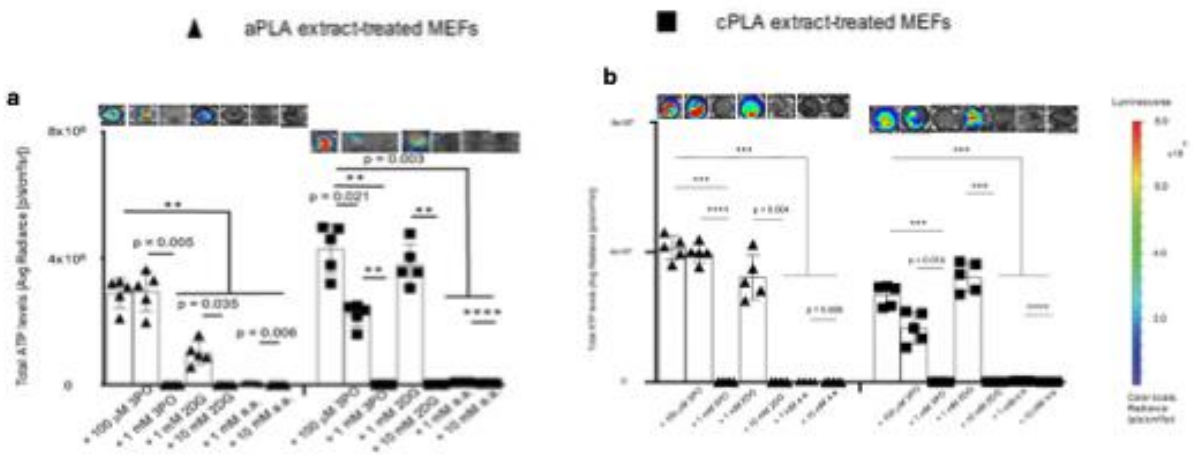

Figure 4.4 Bioenergetic (ATP) levels in mouse embryonic fibroblasts (MEFs) after exposure to aPLA or cPLA extracts are decreased in a dose-dependent manner by 3-(3-pyridinyl)−1-(4-pyridinyl)−2-propen-1-one (3PO), 2-deoxyglucose (2DG) and aminooxyacetic acid (a.a.; representative wells are shown) after (a) 7 days of treatment and (b) 12 days of treatment. **p = 0.002, ****p < 0.0001, mean (SD), n = 5, two-tailed unpaired t-test or Brown–Forsythe and Welch ANOVA followed by Dunnett's T3 multiple comparisons test; 100 µl of control or PLA extract was used for 7 days.

Bioenergetics is altered in macrophages after prolonged exposure to PLA extracts

Next, we utilized mouse primary BMDMs, which, unlike NIH 3T3 cells, do not proliferate in vitro culture[375]. Both ATP[376] and ADP[377] metabolism and ratios are crucial in inflammatory conditions. In BMDMs and consistent with our observations in fibroblasts, we observed marked increases in ATP and ADP levels (Figure 4.5a,b) or ATP/ADP ratios (Figure 4.5c) which were not due to changing glucose levels (Figure 4.5d). Overall, cell numbers could not account for observed bioenergetic changes (Figure 4.5d), excluding changing cell numbers as a confounder in our model.

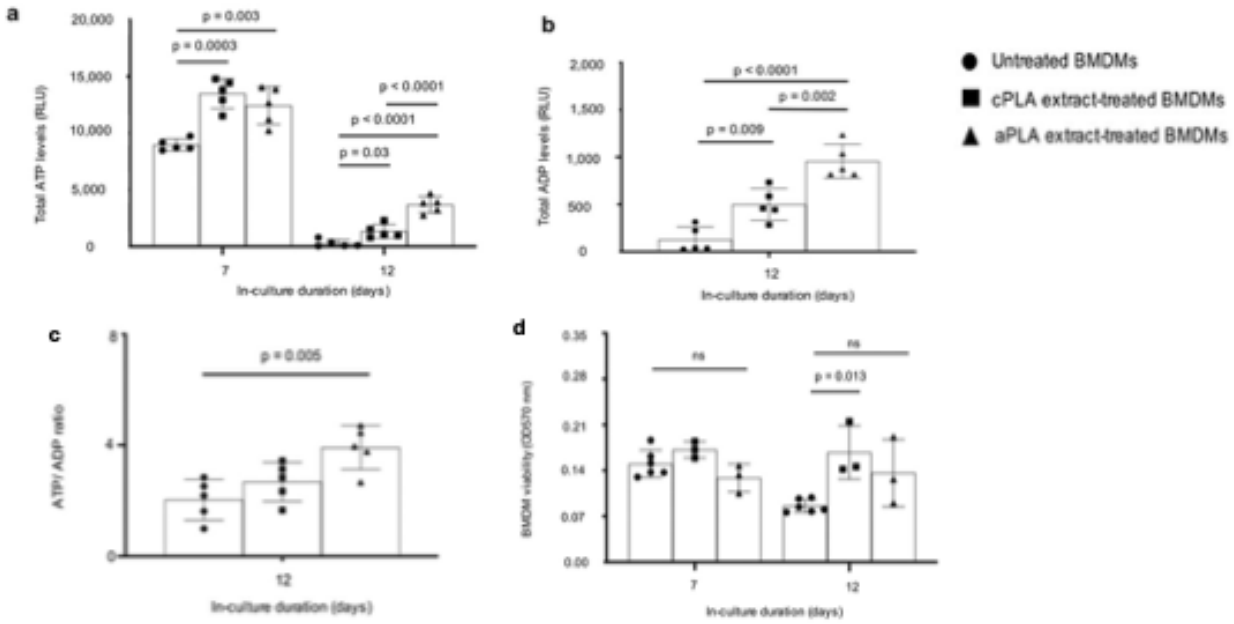

Figure 4.5 Bioenergetics is increased in primary bone marrow-derived macrophages (BMDMs) after prolonged exposure to polylactide (PLA) extracts. (a) ATP levels (b) ADP levels, (c) and ATP/ADP ratios are increased in BMDMs after prolonged exposure to aPLA or cPLA extracts in comparison to controls. (d) Cell numbers between groups are similar for BMDMs. Not significant (ns), mean (SD), n = 5 (a–c), n = 3–6 (d), one-way ANOVA followed by Tukey's post-hoc test; 100 µl of control or PLA extract was used.

Exposure of macrophages to PLA extracts selectively results in metabolic reprogramming, and this can be modulated by glycolytic inhibitors

Primary BMDMs exposed to aPLA extract were metabolically altered, showing a two-fold increase in oxidative phosphorylation (OCR; Figure 4.6a), 3.5-fold increase in glycolytic flux (ECAR; Figure 4.6b), and 3.5-fold increase in monocarboxylate transporter activity (PER; Figure 4.6c) in comparison to untreated BMDMs. Similar amounts (100 µl) of cPLA extract resulted in a 1.6-fold increase in OCR (Figure 4.6d) but no change in ECAR (Figure 4.6e) or PER (Figure 4.6f). However, higher amounts (150 µl) of cPLA extract resulted in 3.2-, 3.8-, and 3.8-fold increases in OCR, ECAR, and PER, respectively (Figure 4.7a–c) compared to controls, suggesting that greater volume of cPLA extract is required for reprogramming than aPLA.

In a dose-dependent manner, glycolytic inhibitors 3PO, 2DG, and a.a. inhibited metabolic reprogramming following exposure to aPLA (Figure 4.6a–c) or cPLA extract (Figure 4.6f). In untreated BMDMs, 2DG and 1 mM a.a. treatment resulted in a compensatory increase in OCR (Figure 4.6g), whereas ECAR and PER were not affected (data not shown).

Under the same experimental conditions, cell viability was not reduced in untreated BMDMs after exposure to glycolytic inhibitors (Figure 4.8a), demonstrating the absence of cytotoxicity[210]. However, when BMDMs were treated with aPLA or cPLA extract, where metabolism was abnormally remodeled, 3PO, 2DG, and a.a. mildly, but selectively, reduced cell viability (Figure 4.8b). Therefore, pharmacologically targeting altered metabolism in primary BMDMs following exposure to PLA extract is highly specific with limited toxicity to immune cells that have normal metabolic profiles.

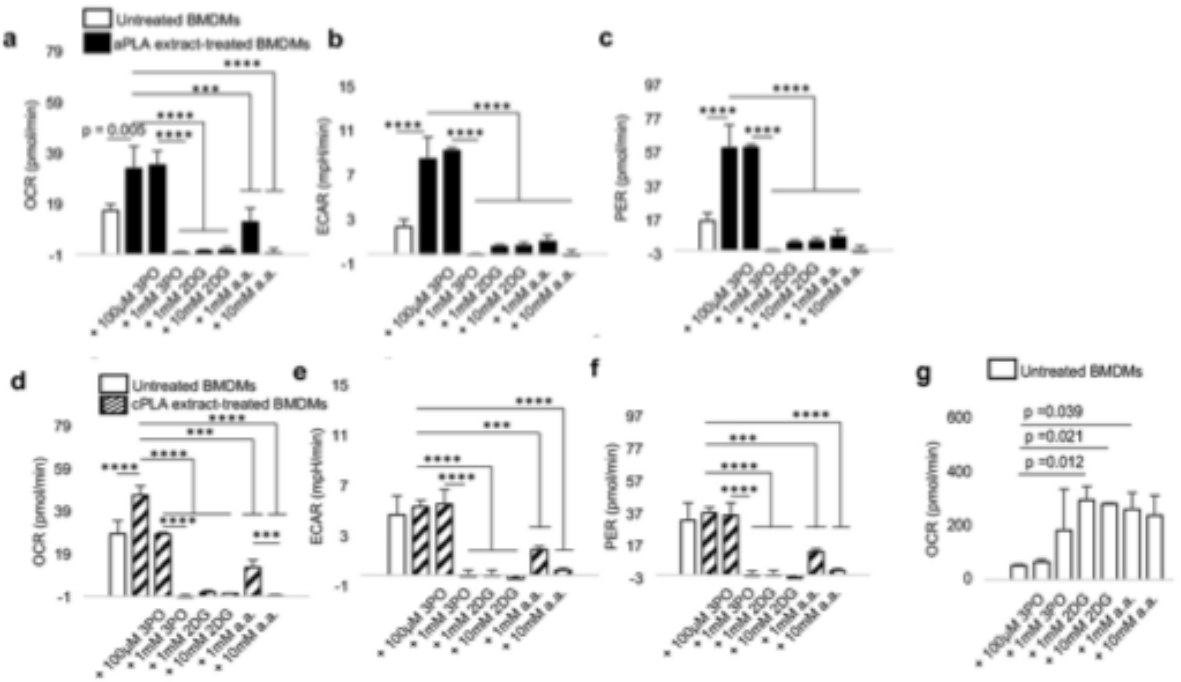

Figure 4.6 Functional metabolic indices are altered in primary bone marrow-derived macrophages (BMDMs) after prolonged exposure to polylactide (PLA) degradation products (extract), and can be modulated by glycolytic inhibitors. a–c) Following exposure to amorphous PLA (aPLA) extract, oxygen consumption rate (OCR) (a), extracellular acidification rate (ECAR) (b), and proton efflux rate (PER) (c) are increased relative to controls, and this abnormal increase can be dose-dependently controlled by various small molecule inhibitors. d–f) OCR (d) and not ECAR (e) and PER (f) are increased relative to controls in groups exposed to crystalline PLA (cPLA) extract, and functional metabolic indices can be controlled by pharmacologic inhibitors of glycolysis. g) Compensatory increase in OCR occurs in untreated BMDMs after treatment with some inhibitors. Not significant (ns), ***p < 0.001, ****p < 0.0001, mean (SD), n = 3, one-way ANOVA followed by Tukey's post-hoc test; 3-(3-pyridinyl)−1-(4-pyridinyl)−2-propen-1- one (3PO), 2-deoxyglucose (2DG) and aminooxyacetic acid (a.a.); 100 µl of control or PLA extract was used for 7 days.

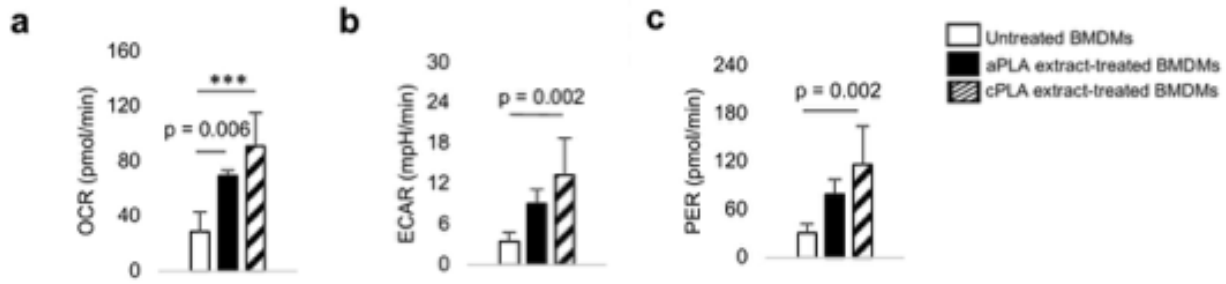

Figure 4.7 Functional metabolic indices are increased in primary bone marrow-derived macrophages (BMDMs) after exposure to cPLA extracts. a-c, Oxygen consumption rate (OCR, a), extracellular acidification rate (ECAR, b) and proton efflux rate (PER, c) are increased following exposure to cPLA extracts. ***p<0.001, mean (SD), n=5, one-way ANOVA followed by Tukey's post-hoc test; 150 µl of control of PLA extract was used on day 7.

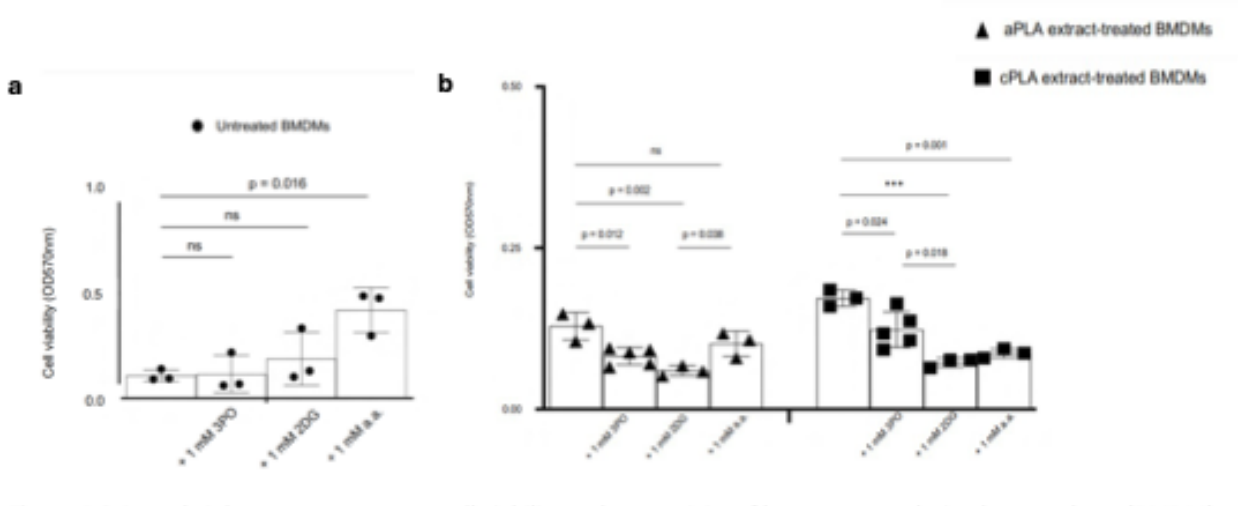

Figure 4.8 Crystal violet assay to measure cell viability and cytotoxicity of bone marrow derived macrophage (BMDM) cells exposed to polylactide (PLA) following treatment with glycolytic inhibitors. (a) Cell viability was not decreased in untreated BMDMs following exposure to glycolytic inhibitors. (b) BMDMs exposed to aPLA or cPLA extracts decreased in cell viability after treatment with glycolytic inhibitors. Not significant (ns), ***p<0.001, mean (SD), n=3 (c), n=3-5 (d), one-way ANOVA followed by Tukey's post-hoc test; 3-(3-pyridinyl)−1-(4-pyridinyl)−2-propen-1- one (3PO), 2-deoxyglucose (2DG) and aminooxyacetic acid (a.a.); 100 µl of control of PLA extract was used on day 7.

The following text includes excerpts from the manuscript titled "The role of mitochondrial complex I in the proinflammatory response to polylactide implants", currently submitted to ACS Applied Engineering Materials [343].

Bioenergetic changes in macrophages exposed to aPLA extracts are modulated by drugs that inhibit mitochondrial respiration

Next, we wanted to see if drugs inhibiting oxidative phosphorylation (ox-phos) could also be effective in mitigating the bioenergetic and metabolic reprogramming effects by PLA extracts on BMDMs. To chemically probe the function of complex I, III and V of the mitochondrial electron transport chain (mETC), we treated macrophage conditions with their respective inhibitors. Rotenone inhibits complex I of the mETC, an effect reproduced by metformin, which is a Food and Drug Administration (FDA)-approved drug prescribed for diabetic patients[365, 366]. Antimycin A and oligomycin inhibit complex III and V, respectively, of the mETC[365].

Compared to untreated controls, exposure to aPLA or cPLA extracts increased ATP levels (Figure 4.9a,b)[104]. Inhibitors of complex I, III and V decreased ATP levels in the aPLA-treated groups (Figure 4.9a), but there were no significant reductions in the cPLA groups (Figure 4.9b). Interestingly, with both rotenone and metformin, inhibition of complex I was dose-dependent in the aPLA-treated group (Fig. 4.9a). Observed bioenergetic changes were not associated with significant changes in cell viability in aPLA or cPLA extract-treated BMDMs, suggesting minimal toxicity (Figure 4.10a,b).

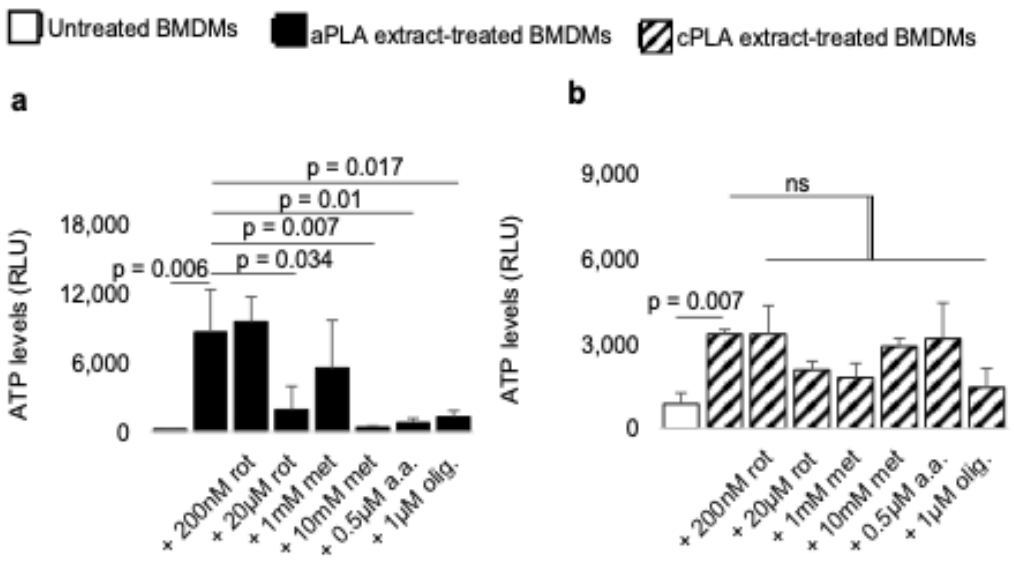

Figure 4.9 Inhibition of mitochondrial respiration differentially affects bioenergetics (ATP levels) in primary bone marrow-derived macrophages (BMDMs) exposed to polylactide (PLA) degradation products (extracts). a, Compared to untreated BMDMs, amorphous PLA (aPLA) extracts increase ATP levels; elevated bioenergetics is reduced by inhibiting of the mitochondrial electron transport chain using rotenone (rot), metformin (met), antimycin A (a.a.) and oligomycin (olig.). b, Increased bioenergetics from exposure to crystalline PLA (cPLA) extracts is not decreased by inhibition of mitochondrial respiration. Not significant (ns), mean (SD), n=3, one-way ANOVA followed by Tukey's post-hoc test; 100 µl aPLA or 150 µl cPLA extract with corresponding controls were used after 7 days in culture.

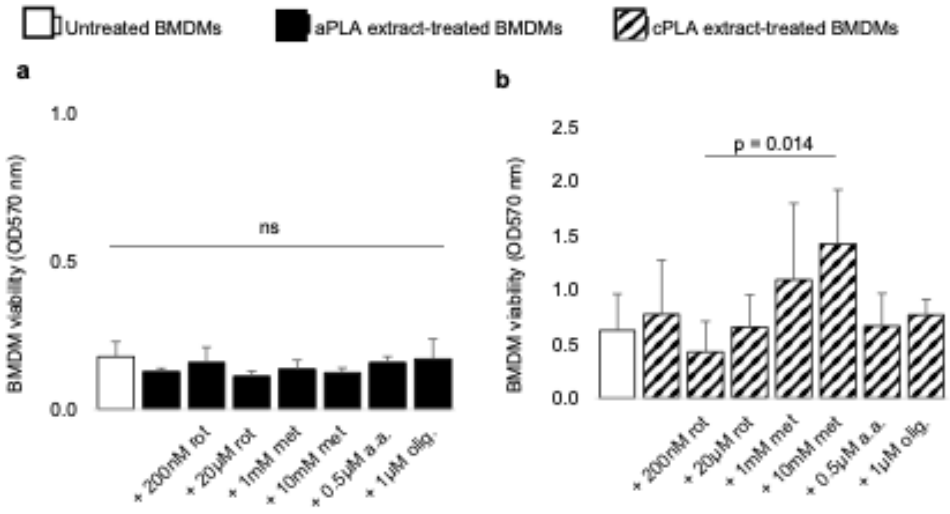

Figure 4.10 Inhibition of the mitochondrial electron transport chain does not reduce primary bone marrow-derived macrophage (BMDM) cell viability. a-b, Compared to untreated BMDMs, exposure to amorphous polylactide (aPLA; a) or crystalline polylactide (cPLA; b) does not affect cell numbers; treatment with inhibitors of mitochondria respiration, including rotenone (rot), metformin (met), antimycin A (a.a.) and oligomycin (olig.) does not reduce cell viability relative to PLA-treated cells. Not significant (ns), mean (SD), n=5, one-way ANOVA followed by Tukey's post-hoc test; 100 µl aPLA or 150 µl cPLA extract with corresponding controls were used after 7 days in culture.

Oxygen consumption rate in macrophages exposed to cPLA extracts is modulated by drugs that inhibit mitochondrial respiration

There was increased OCR in BMDMs exposed to cPLA extracts, which was decreased by chemically inhibiting complex I or V, but not complex III (Figure 4.11a). Interestingly, inhibition of the mETC did not decrease OCR in untreated BMDMs (Figure 4.11c) and BMDMs exposed to aPLA breakdown products (Figure 4.11b). These results suggest that ATP production may be uncoupled from OCR through the mETC, distinct from ATP generation in resting cells under physiological conditions[378].

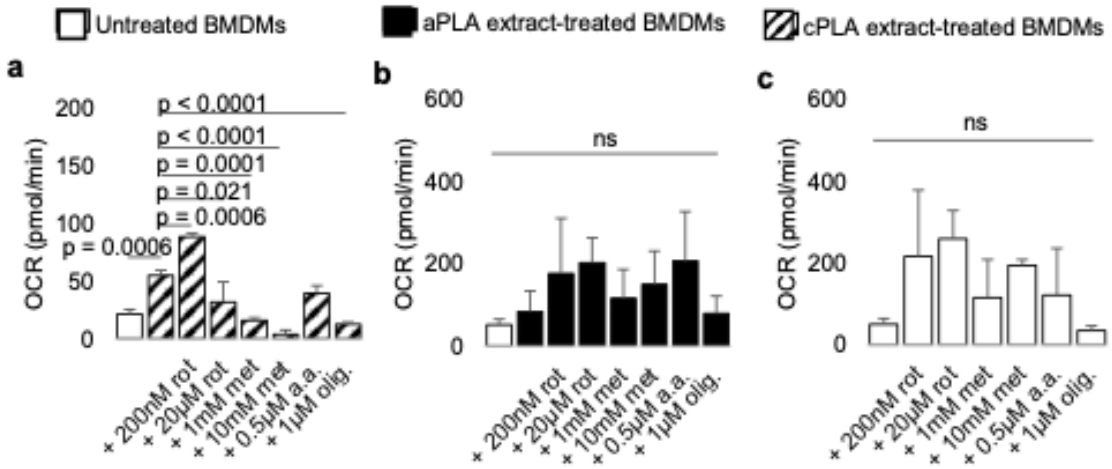

Figure 4.11 Pharmacologically targeting complex I of the electron transport chain (ETC) reduces oxygen consumption rate (OCR) in primary bone marrow-derived macrophages (BMDMs) exposed to crystalline (cPLA) but not amorphous polylactide (aPLA) extracts. a-b, In BMDMs exposed to cPLA (a) but not aPLA (b) extracts, elevated OCR is decreased by inhibition of complex I using rotenone (rot) or metformin (met), or complex V using oligomycin (olig.), but not complex III using antimycin A (a.a.). c, Targeting the ETC using rot, met, a.a. and olig. in untreated BMDMs does not decrease OCR. Mean (SD), n=3, one-way ANOVA followed by Tukey's post-hoc test; 100 µl aPLA or 150 µl cPLA extract with corresponding controls were used after 7 days in culture.

The following text includes excerpts from our manuscript titled "Polylactide Degradation Activates Immune Cells by Metabolic Reprogramming", published in Adv. Sci. [104].

Glycolytic inhibition modulates proinflammatory and stimulates anti-inflammatory cytokine expression in macrophages exposed to PLA extracts

To determine whether glycolytic inhibition affects proinflammatory (IL-6, MCP-1, TNF-α, IL-1β and IFN-γ) and anti-inflammatory (IL-4, IL-10, and 1L-13) protein expression, we used a magnetic bead-based chemokine and cytokine assay[370]. We observed that prolonged exposure of BMDMs to aPLA and cPLA extracts resulted in 228- and 319-fold increases, respectively, in IL-6 protein expression (Figure 4.12a) compared to untreated BMDMs. aPLA extracts increased MCP-1 (Figure 4.12b), TNF-α (Figure 4.12c) and IL-1β (Figure 4.12d) levels by 1.2-, 21-, and 567-fold, respectively. Likewise, cPLA extracts increased MCP-1 (Figure 4.12b), TNF-α (Figure 4.12c), and IL-1β (Fig 4.12d) levels by 4.7-, 27-, and 1378-fold, respectively. Abnormally increased levels of IL-6, MCP-1, TNF-α, and IL-1β were modulated by addition of 3PO, 2DG, or a.a. (Figure 4.12a–d).

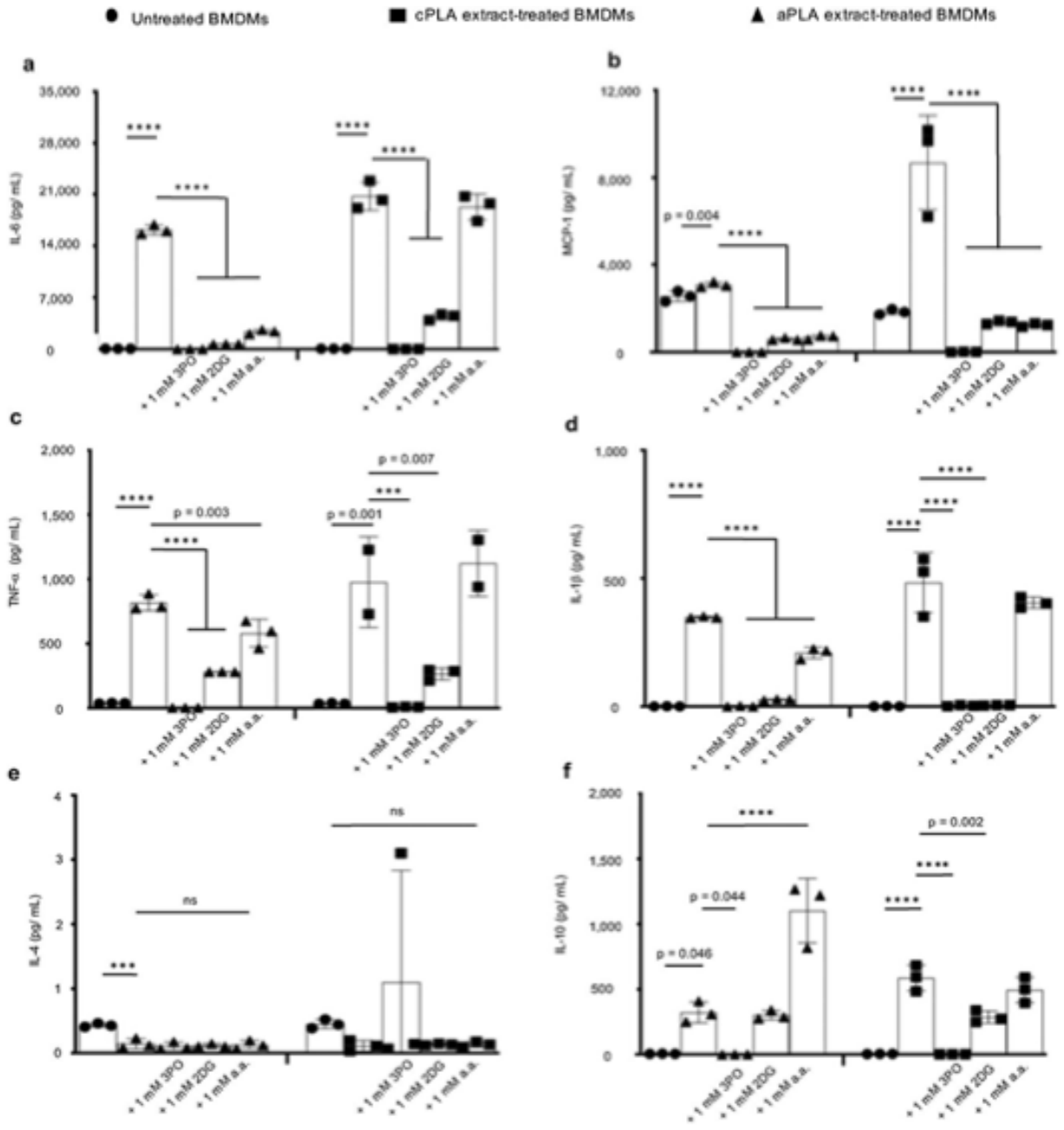

Figure 4.12 In macrophages exposed to PLA extracts, glycolytic inhibitors modulate elevated proinflammatory cytokine expression and stimulate or do not reduce anti-inflammatory cytokine levels. a–d) Following exposure to amorphous PLA (aPLA) or crystalline PLA (cPLA) extract, primary bone marrow-derived macrophages (BMDMs) express elevated levels of IL-6 (a), MCP-1 (b), TNF-α (c), and IL-1β (d) in comparison to untreated BMDMs, and these elevated proinflammatory cytokine levels can be modulated by various small molecule inhibitors of glycolysis. e) Addition of glycolytic inhibitors to PLA does not reduce IL-4 expression. f) Expression of IL-10 is increased by inhibiting glycolysis using aminooxyacetic acid (a.a.) in aPLA. Not significant (ns), ***$p < 0.001$, ****$p < 0.0001$, mean (SD), n = 3 in all except the cPLA group in TNF-α (Figure 6c) where n = 2–3, one-way ANOVA followed by Tukey's post-hoc test; 3-(3-pyridinyl)−1-(4-pyridinyl)−2-propen-1-one (3PO), 2-deoxyglucose (2DG); 100 µl of aPLA or 150 µl of cPLA extract with corresponding controls were used on day 7.

Levels of IFN-γ and IL-13 were unchanged by PLA extract (data not shown) but exposure to aPLA extract decreased IL-4 protein levels by 3-fold (Figure 4.12e) relative to untreated BMDMs. Remarkably, with the exception of 3PO, IL-10 expression was either unchanged (cPLA) or increased by 3.4-fold (aPLA) upon the addition of a.a. (Figure 4.12f) relative to BMDMs exposed to PLA extract.

Short- and long-term exposure of macrophages to L-lactic acid alters bioenergetics, metabolic reprogramming, and cytokine secretion changes in a similar manner to PLA extracts

We exposed BMDMs to various doses of L-lactic acid. We observed that bioenergetic levels are altered in the short-term (day 3; Figure 4.13a) for all doses of L-lactic acid treatment, resulting in a 1.5 to 1.6-fold increase in ATP levels. After prolonged (day 7) exposure to L-lactic acid and even when bioenergetic alterations were not apparent, oxidative phosphorylation (OCR; Figure 4.13b), glycolytic flux (ECAR; Figure 4.13c), and monocarboxylate transporter function (PER; Figure 4.13d) were increased by 2.3-, 2.8-, and 2.8-fold, mechanistically reproducing observations made with aPLA and cPLA extracts in our bioenergetic model. These changes were not dependent on alterations in cell number because L-lactic acid did not affect BMDM viability at day 7 or 12 relative to controls (Figure 4.14). Moreover, similar to aPLA and cPLA, exposure of BMDMs to L-lactic acid resulted in elevated IL-6 protein expression by 2.3-fold (Figure 4.15a). Increased MCP-1 levels in BMDMs also occurred after exposure to L-lactic acid (Figure 4.15b).

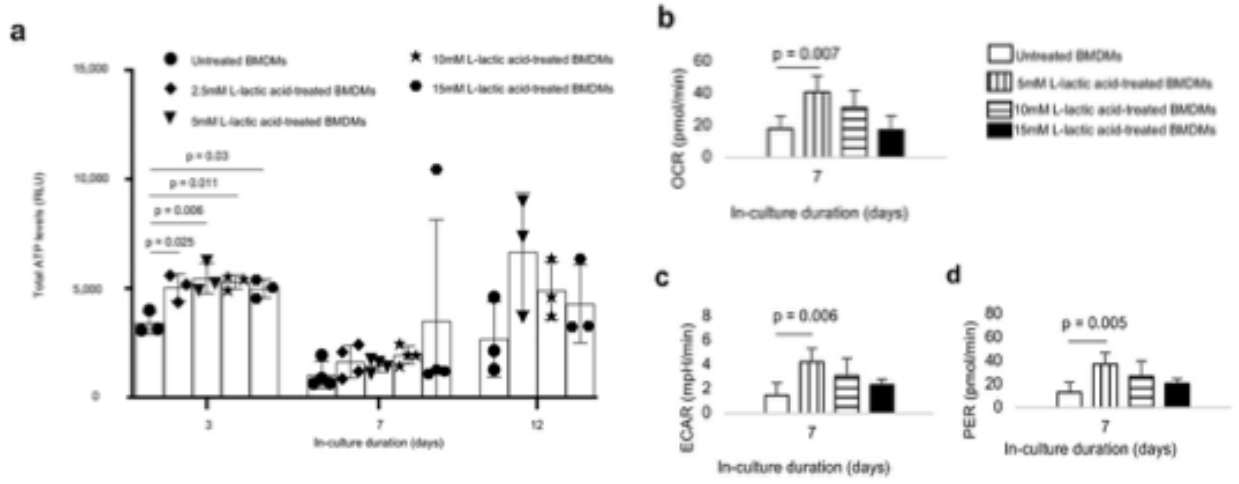

Figure 4.13 Treatment of primary bone marrow-derived macrophages (BMDMs) with L-lactic acid altered bioenergetic (ATP) levels and functional metabolism. a) Treatment with different doses of monomeric L-lactic acid resulted in changes in ATP levels. b–d) Following exposure to L-lactic acid, oxygen consumption rate (OCR, b), extracellular acidification rate (ECAR, c), and proton efflux rate (PER, d) are increased. One-way ANOVA followed by Tukey's post-hoc test, mean (SD), n = 3–4 (a), n = 5 (b–d).

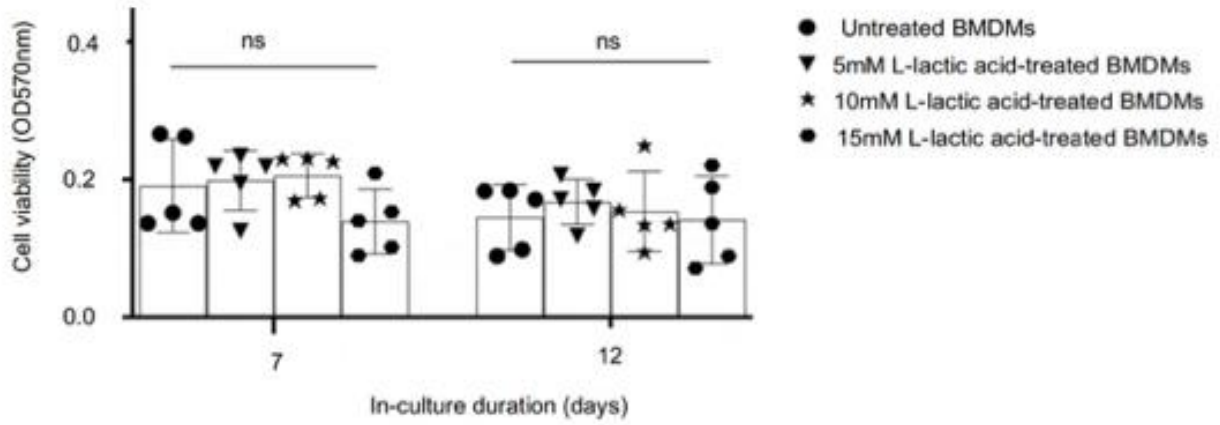

Figure 4.14 Crystal violet assay shows viability of primary bone marrow-derived macrophages (BMDMs) is similar after treatment with L-lactic acid over time. Not significant (ns), one-way ANOVA, mean (SD), n=5.

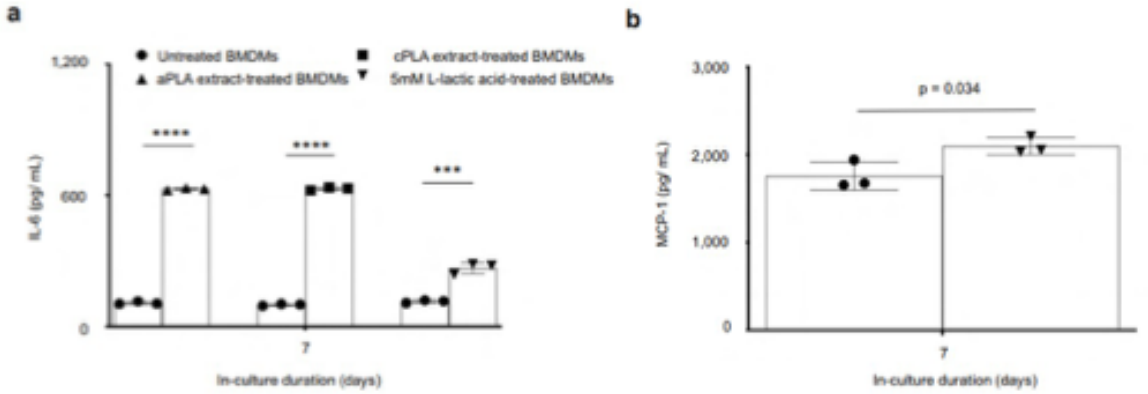

Figure 4.15 IL-6 and MCP-1 protein levels are increased following prolonged exposure of primary bone marrow-derived macrophages (BMDMs) to L-lactic acid in comparison to untreated BMDMs. a, Using ELISA reproduced changes in IL-6 levels following exposure of BMDMs to aPLA, cPLA, or L-lactic acid. b, Similarly, MCP-1 levels are increased after exposing BMDMs to L-lactic acid as measured by the MILLIPLEX assay. ***p<0.001, ****p<0.0001, mean (SD), n=3, two-tailed unpaired t-test; 100 µl of aPLA or 150 µl of cPLA with corresponding controls were used; whereas corresponding controls for PLA were incubated for 12 days, the controls for L-lactic acid were not.

Increased radiolabeled glucose uptake occurs in the PLA microenvironment and drives inflammation in-vivo

Taken together, our in vitro data suggests that metabolic changes drive inflammation arising from PLA degradation. However, in vitro methods for characterizing PLA degradation may not fully simulate the complexity of events in the body. Therefore, we sought to test our hypothesis that metabolic changes drive inflammation in vivo and to test the local efficacy of small molecule metabolic inhibitors. We incorporated 2DG into aPLA by melt-blending at 190°C and compared it to aPLA which had been subjected to similar melt-blending conditions (called reprocessed aPLA). Following melt-blending, extruded (sterile) filaments (1.75 mm diameter, 1 mm long) were subcutaneously implanted on the back (dorsum) of mice. Sham controls underwent similar surgical exposures but were not implanted with any materials. After 6 weeks, mice were intraperitoneally (i.p.) injected with F-18 fluorodeoxyglucose (FDG) and euthanized; using FDG allows for the quantification of metabolic reprogramming and inflammation in vivo[379]. At 65-min post-injection, circular biopsies (12 mm in diameter) of full-thickness skin containing implants were assayed for radioactivity using a gamma counter. Compared to sham controls, skin containing reprocessed aPLA implants had 1.35-fold increase in FDG uptake, which was abolished in skin containing aPLA+2DG implants (Figure 4.16). We observed increased glycolytic dependence in the PLA inflammatory microenvironment using sterile aPLA, which was abrogated by 2DG, one of the glycolytic inhibitors applied in our in vitro studies.

Radiolabeled glucose (FDG) uptake is often used to measure glycolytic dependence, in vivo, such as in some cancers or inflammatory disorders where enhanced glycolysis is pivotal to disease progression[380]. Interestingly, after surgical resection of colorectal and cervical tumors in human patients, chronic, sterile inflammation from PLA-based adhesion barriers elevate FDG uptake, falsely mimicking cancer recurrence[381, 382].

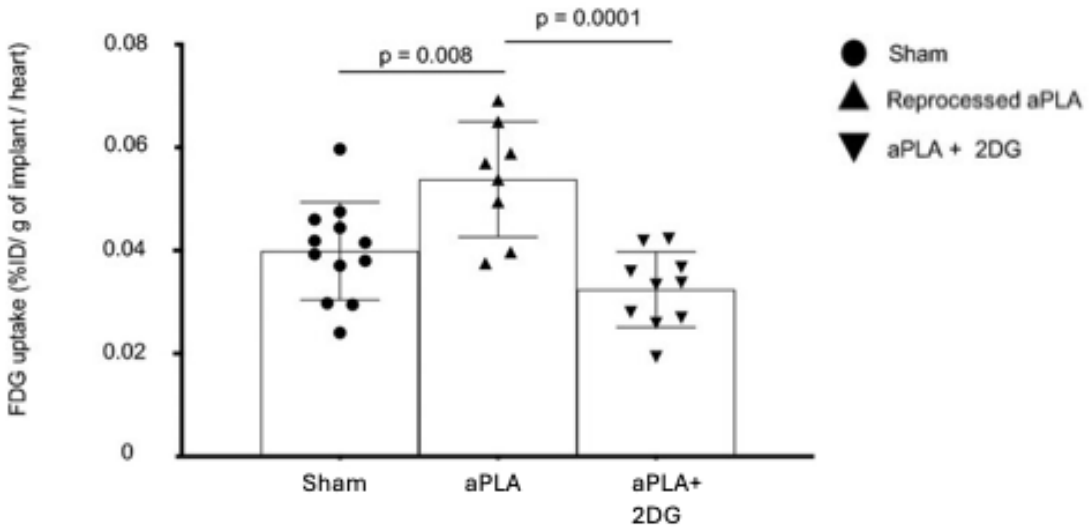

Figure 4.16 Increased radiolabeled glucose uptake occurs in the polylactide (PLA) microenvironment and drives inflammation in vivo. When normalized to heart values, percent injected dose per gram (%ID g−1) of biopsied tissues surrounding amorphous PLA (aPLA) implants show higher F-18 fluorodeoxyglucose (FDG) uptake compared to sham controls; increased FDG uptake is reduced by incorporation of 2-deoxyglucose (2DG). Mean (SD); sham (n = 12), aPLA (n = 8), aPLA + 2DG (n = 10); one-way ANOVA followed by Tukey's post-hoc test.

Fibroblasts are activated in PLA implant microenvironment, and this can be regulated by inhibiting glycolysis

Fibroblasts are a key cellular player of excessive fibrosis around PLA implants,[353, 383] and their activation in myofibroblast phenotype is marked by α-SMA and TGF-β expression[384]. Moreover, metabolic reprogramming is known to play a key role in profibrotic disorders, activating fibroblasts[360]. We next wanted to know if glycolytic inhibitors could affect fibroblast activation in the PLA implant microenvironment. We also wanted to know how this was affected by hydroxyapatite (HA), a mineral commonly used to neutralize acidity in PLA implants[385].

To test this, we performed immunohistochemistry staining of the tissue microenvironment surrounding reprocessed aPLA, aPLA with incorporated 2DG, and aPLA-hydroxyapatite (aPLA+HA) composite biomaterial implants in our mouse model. We observed a 1.4-fold increase in α-SMA intensity with reprocessed PLA compared to sham controls, which was decreased in the aPLA+2DG, but not aPLA+HA group (Figure 4.17a; Figure 4.18). With TGF-β intensity, aPLA+HA was elevated relative to other groups (Figure 4.17b; Figure 4.18). Compared to aPLA+HA, aPLA+2DG revealed 1.4- and 1.8-fold decrease in α-SMA and TGF-β intensities, respectively (Figure 4.17b).

Increased fibroblast activation, measured by α-SMA expression, in the PLA microenvironment was reduced by inhibiting glycolysis using 2DG and not neutralizing acidity using HA. Compared to HA, 2DG reduced both α-SMA and TGF-β expression. This suggests that metabolism, and not acidity, regulates fibroblast activation in the PLA microenvironment.

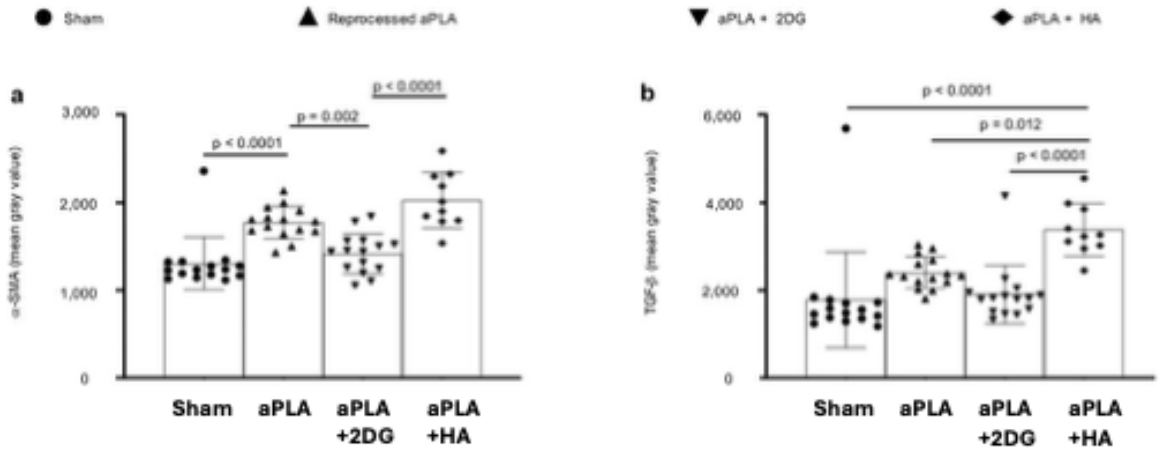

Figure 4.17 Activation of fibroblasts in the polylactide (PLA) microenvironment is regulated by immunometabolism. a) Compared to sham controls, mean fluorescence intensity (MFI) of alpha-smooth muscle actin (α-SMA) is increased following surgical implantation of amorphous PLA (aPLA) or a combination of aPLA and hydroxyapatite (HA), but not a combination of aPLA and 2-deoxyglucose (2DG). b) Compared to other groups, MFI of transforming growth factor-beta (TGF-β) is increased in aPLA + HA. Mean (SD); sham (n = 15), aPLA (n = 15), aPLA + 2DG (n = 15), aPLA + HA (n = 10); one-way ANOVA followed by Tukey's post-hoc test.

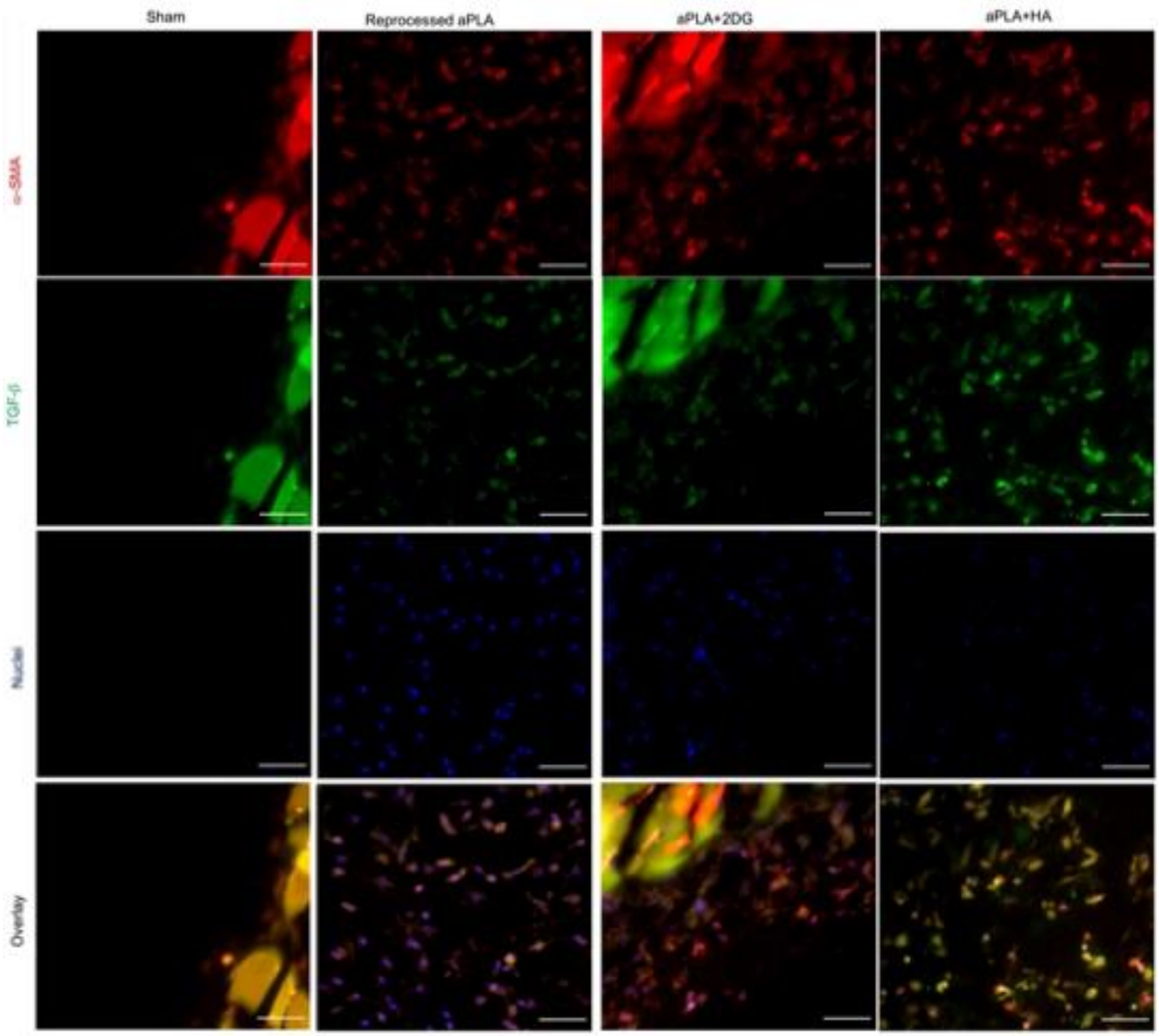

Figure 4.18 Immunohistochemical staining with a-SMA-eFluor 660 and TGF-b-PE using a DAPI mounting medium show fibroblast activation following implantation of amorphous polylactide (aPLA) with and without 2-deoxyglucose (2DG) or hydroxyapatite (HA) when compared to sham controls (scale bars, 50 µm).

The following text includes excerpts from the manuscript titled "The role of mitochondrial complex I in the proinflammatory response to polylactide implants", currently under review at ACS Applied Engineering Materials[343].

PLA implants increase immune infiltration and inflammatory states in the implant microenvironment, and some effects can be modulated by metformin

We then used our s.c. implantation mouse model to test for potential immunomodulatory effects arising from the inhibition of oxidative phosphorylation. We compared reprocessed aPLA and cPLA to respective polymers that incorporated metformin, which chemically inhibits complex I of the mitochondrial ETC (mETC).

In comparison to sham groups, nucleated hematopoietic ($CD45^+$) and macrophage ($F4/80^+$) cell populations were increased around aPLA and cPLA biomaterials (Figure 4.19a-b)[386]. However, the incorporation of metformin did not reduce $CD45^+$ or $F4/80^+$ populations (Figure 4.19a-b). Dendritic ($CD11c^+$) cell populations were elevated in the cPLA but not the aPLA microenvironment (Figure 4.19c)[386]. The incorporation of metformin in either aPLA or cPLA increased dendritic cell numbers compared to aPLA or cPLA alone (Figure 4.19c).

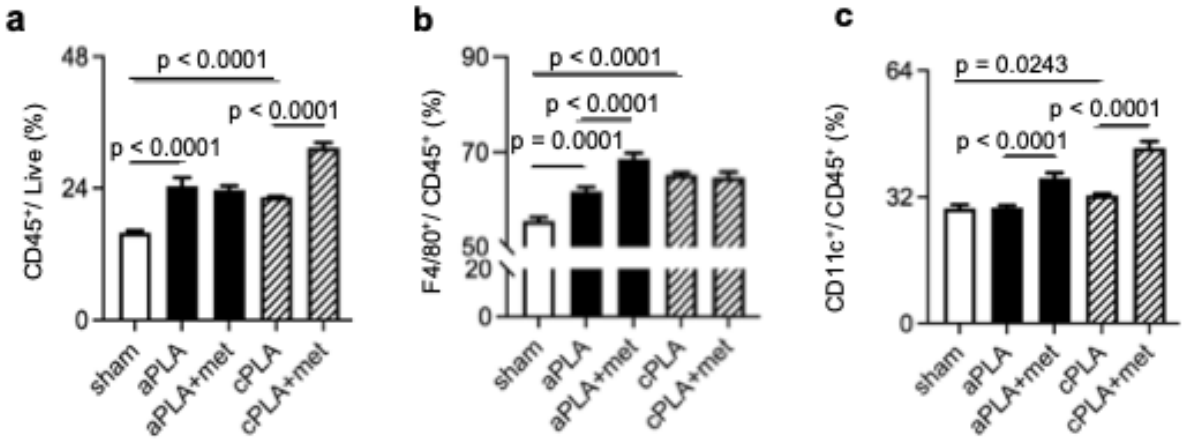

Figure 4.19 Polylactide (PLA) implants increase immune cell infiltrate into implant microenvironment, and this can be modulated by incorporation of metformin. a, Unlike with amorphous PLA (aPLA), the incorporation of metformin (met) in crystalline PLA (cPLA) increases the frequency of nucleated hematopoietic ($CD45^+$) populations in the implant microenvironment. b, With the incorporation of met, there is increased macrophage recruitment in the aPLA and not the cPLA microenvironment. c, The incorporation of met increases the proportion of recruited dendritic ($CD11c^+$) cells in the aPLA and cPLA microenvironment. Mean (SD), one-way ANOVA followed by Tukey's multiple comparison test, n = 3.

We then wanted to test the effects of our implants on macrophage polarization in vivo. We assigned proinflammatory and anti-inflammatory macrophage (F4/80) populations as $CD86^{+}CD206^{-}$ and $CD206^{+}$, respectively[387, 388]. Whereas the fold change of proinflammatory with respect to anti-inflammatory macrophages was increased, the fold change of anti-inflammatory with respect to proinflammatory macrophages was decreased in the aPLA and cPLA microenvironment (Figure 4.20a-b)[386]. The incorporation of metformin neither decreased proinflammatory nor increased anti-inflammatory ratios (Figure 4.20a-b).

Macrophage activation in vivo exists on a continuum of functional phenotypes[389]. For this reason, we also quantified expression of arginase 1 (Arg1), another M2 marker, in the implant microenvironment. Compared to sham groups, Arg1 levels were increased in the biomaterial microenvironment of aPLA and cPLA implants (Figure 4.20c). The seemingly conflicting effects of aPLA and cPLA on macrophage expression of these M2 markers highlights the fact that macrophage response to PLA in vivo is not discretely polarized into wholly proinflammatory M1 or anti-inflammatory M2 phenotypes. Interestingly, the incorporation of metformin increased Arg1 levels in the cPLA but not the aPLA microenvironment (Figure 4.20c).

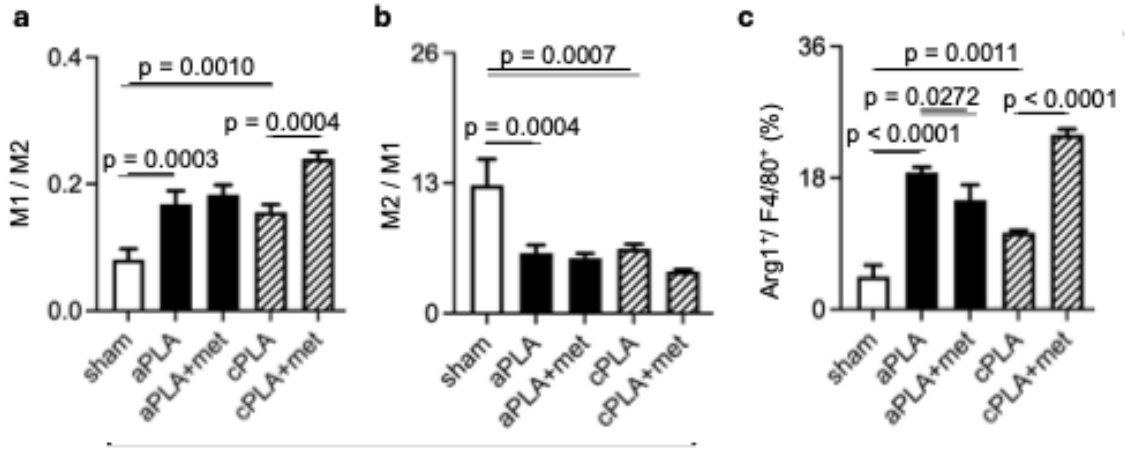

Figure 4.20 The proinflammatory states of macrophages are not reduced by incorporation of metformin in polylactide (PLA) implants. a, The fold change of proinflammatory (M1; $CD86^{+}CD206^{-}$) with respect to anti-inflammatory (M2; $CD206^{+}$) macrophage is neither reduced in the aPLA nor cPLA microenvironment following the incorporation of metformin. b, The fold change of M2 to M1 macrophage is unchanged by the incorporation of metformin. c, Unlike with aPLA, arginase 1 (Arg1) levels are increased by the incorporation of metformin in the cPLA microenvironment. Mean (SD), one-way ANOVA followed by Tukey's multiple comparison test, n = 3.

We also looked at the effects of PLA implants with and without metformin on the polarization states of dendritic cells in vivo. The fold change of proinflammatory (D1) with respect to anti-inflammatory (D2) dendritic cells was increased (Figure 4.21a), and the fold change of D2 with respect to D1 dendritic cells was decreased (Figure 4.21b) around aPLA and cPLA biomaterials[386]. The incorporation of metformin in aPLA or cPLA implants had no effects on anti-inflammatory ratios (Fig. 4.21b). Consistent with observations made with macrophages, the incorporation of metformin in cPLA increased Arg1 levels compared to cPLA alone (Fig. 4.21c).

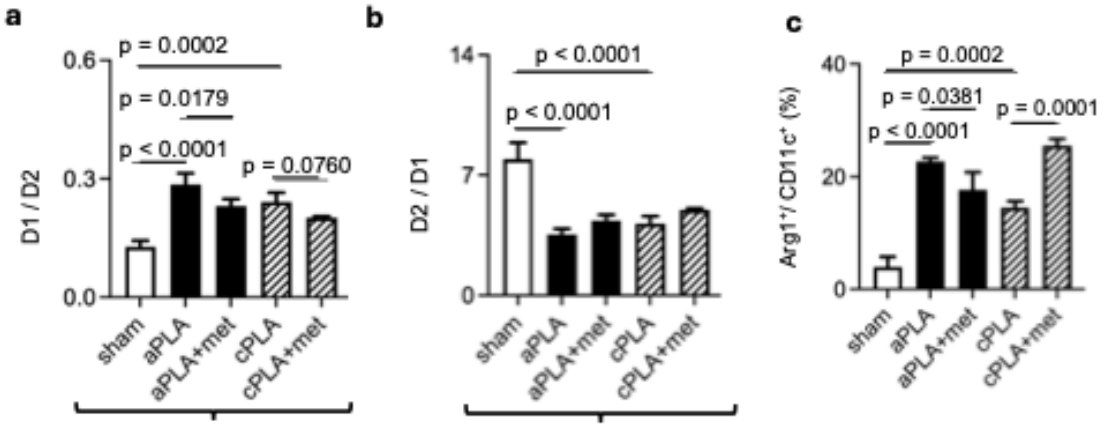

Figure 4.21 The incorporation of metformin affects the polarization states of dendritic cells in the polylactide (PLA) microenvironment. b, The fold change of proinflammatory (D1; $CD86^{+}CD206^{-}$) dendritic cells with respect to anti-inflammatory (D2; $CD206^{+}$) dendritic cells is deceased with incorporation of metformin in the aPLA microenvironment; this difference is not significant with cPLA. h, The fold change of D2 to D1 dendritic cells is unchanged by the incorporation of metformin in aPLA or cPLA implants. i, Unlike with aPLA, Arginase 1 ($Arg1^{+}$) dendritic cell populations are increased by the incorporation of metformin in cPLA implants. Mean (SD), one-way ANOVA followed by Tukey's or Newman-Keul's multiple comparison test, n = 3.

Next, we characterized effects of PLA implants with and without metformin on T cell populations and activation states. We observed that $CD3^{+}$ T cell populations were decreased around aPLA and cPLA implants, and that the inclusion of metformin did not alter T cell frequencies (Figure 4.22a). Among T cells, $CD8^{+}$ cytotoxic T cells as well as $CD4^{+}$ T helper cells were increased around aPLA and cPLA implants, but the addition of metformin did not alter CD4 and CD8 levels (Figure 4.22b-c). Interestingly, the inclusion of metformin in cPLA but not aPLA implants concomitantly elevated IL-4 and IFN-γ cytokine production from T helper cells (Figure 4.22d-e).

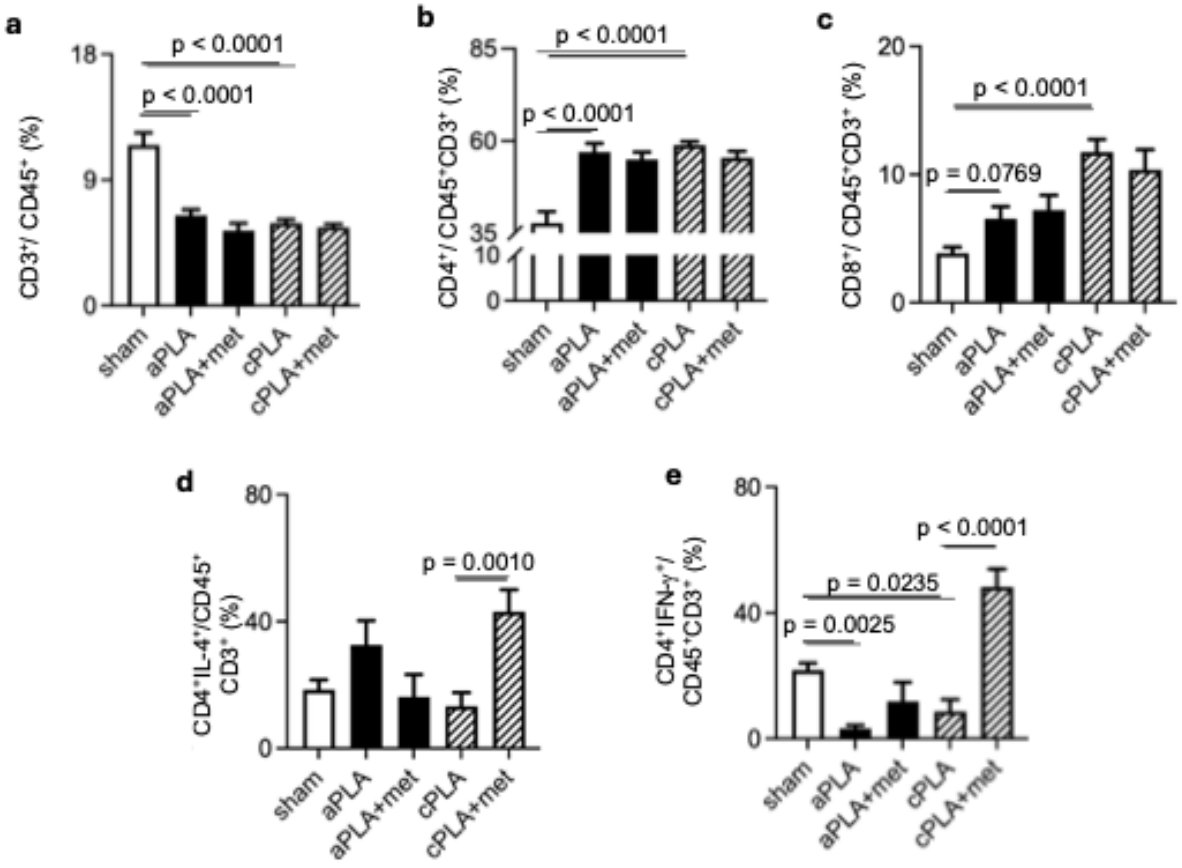

Figure 4.22 Metformin exerts differential effects on the activation states of T-cells in the polylactide (PLA) microenvironment. a, Overall T-cell ($CD3^+CD11b^-$ gated on $CD45^+$ cells) populations are decreased in aPLA and cPLA implants relative to sham surgeries, and this is unchanged by the incorporation of metformin. b-c, Frequencies of T helper lymphocytes ($CD45^+CD3^+CD4^+$ cells; b) and cytotoxic T lymphocytes ($CD45^+CD3^+CD8^+$ cells; c) are increased in aPLA and cPLA implants relative to sham, but this is unaffected by incorporation of metformin in aPLA or cPLA implants. d-e, Unlike with aPLA implants, both T helper 2 cells expressing interleukin-4 (IL-4; d) as well as T helper 1 cells expressing interferon-gamma (IFN-g; e) are increased by incorporation of metformin in cPLA implants. Mean (SD), one-way ANOVA followed by Tukey's multiple comparison test, n = 3.

The following text includes excerpts from the manuscript titled "Regulating the proinflammatory response to implanted composite biomaterials comprising polylactide and hydroxyapatite by targeting immunometabolism", published in Bioactive Materials[342].

aPLA-hydroxyapatite composite biomaterials increase immune infiltration and inflammatory states in the implant microenvironment, and some effects can be modulated by glycolytic inhibitors

Because hydroxyapatite (HA) is so commonly used as a mineral to neutralize the acidic environment produced by PLA implants, we next wanted to test the effects of amorphous polylactide-

hydroxyapatite (aPLA+HA) composite biomaterial implants in vivo, with and without glycolytic inhibition. We utilized our 6-week mouse model with s.q. implanted aPLA+HA biomaterials, with or without incorporated glycolytic inhibitors aminooxyacetic acid (a.a.) or 2-deoxyglucose (2DG) at previously optimized doses[104, 386, 390]. These two small molecule inhibitors act at different steps in glycolysis; a.a. inhibits uptake of glycolytic substrates and glutamine metabolism, 2DG inhibits hexokinase in the glycolytic pathway[391, 392].

Although implantation of aPLA+HA increased overall nucleated hematopoietic ($CD45^+$) cell populations, incorporation of a.a. but not 2DG reduced $CD45^+$ levels (Figure 4.23a). Consistent with prior observations[393, 394], implantation of aPLA+HA increased levels of $F4/80^+$ macrophages[395] relative to sham controls, but incorporation of a.a. or 2DG did not reduce cellular recruitment (Figure 4.23b). We also observed that $CD11c^+$ dendritic cell populations were elevated in the aPLA+HA microenvironment compared to sham controls as previously reported[393, 394], and that incorporation of either a.a. or 2DG reduced these dendritic cell numbers (Figure 4.23c).

Previously, we have observed that, relative to aPLA alone, aPLA+HA does not reduce $Ly6G^+$ neutrophils recruited to the biomaterial microenvironment[386]. Here, we found that, compared to sham controls, aPLA+HA implantation elevated neutrophil levels (Figure 4.23d). Remarkably, incorporating a.a. or 2DG in aPLA+HA modulated this proinflammatory tendency (Figure 4.23d). Elevated neutrophil levels are prevalent in murine bone defects implanted with micron-sized HA particles, an effect that is reduced by using nano-sized HA particles[396]. Reduced neutrophil levels are correlated with the pro-regenerative macrophage phenotype that is necessary to drive bone regeneration[396]. This observation is translationally relevant as HA potently activates human neutrophils in-vitro[354, 397, 398].

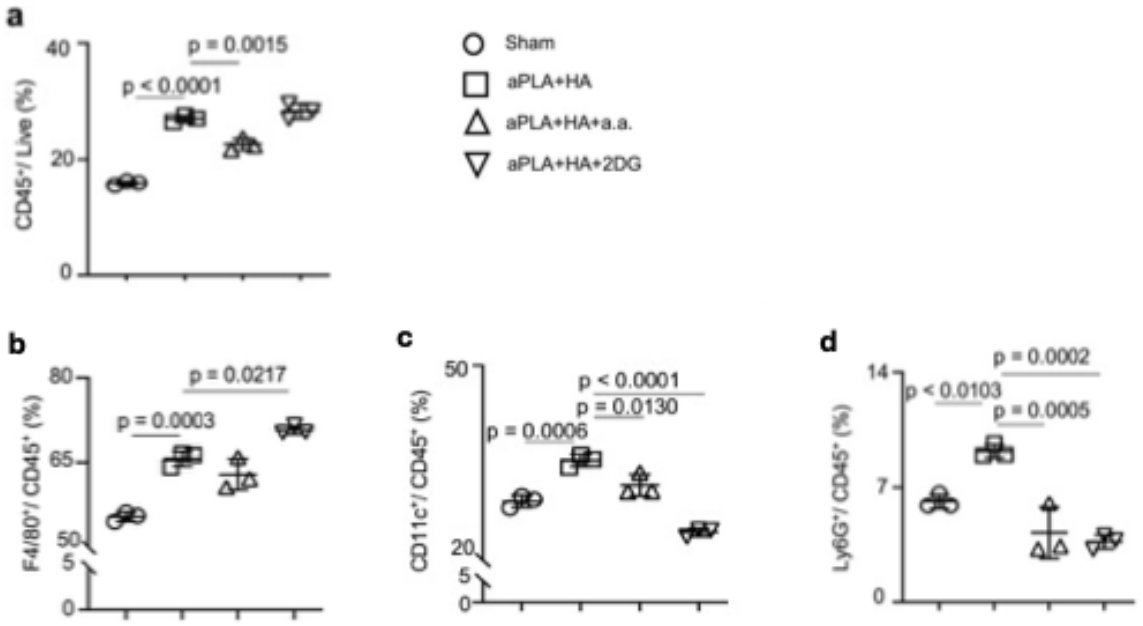

Figure 4.23 The numbers of immune cell populations present in the amorphous polylactide-hydroxyapatite (aPLA+HA) composite biomaterial microenvironment can be differentially affected by targeting different glycolytic steps via metabolic inhibitors. a, Flow cytometry quantification of nucleated hematopoietic ($CD45^+$) cells gated on live cells. b, Flow cytometry quantification of macrophages ($F4/80^+$ cells) gated on live $CD45^+$ cells. c, Flow cytometry quantification of dendritic ($CD11c^+$) cells gated on live $CD45^+$ cells. d, Flow cytometry quantification of neutrophil ($Ly6G^+$) cells gated on live $CD45^+$ cells. One-way ANOVA followed by Tukey's or Newman-Keul's multiple comparison test, n = 3; amorphous polylactide (aPLA), hydroxyapatite (HA), aminooxyacetic acid (a.a.), 2-deoxyglucose (2DG).

To test the effects of aPLA+HA implants on macrophage polarization in vivo, we again designated proinflammatory and anti-inflammatory macrophage (F4/80) populations as $CD86^+CD206^-$ and $CD206^+$, respectively[388, 399]. Relative to sham controls, aPLA+HA elevated proinflammatory (M1)-like and reduced anti-inflammatory (M2)-like macrophage levels as compared to sham controls. Flow cytometric analysis showed an increased fold change of M1 with respect to M2 macrophages; importantly, incorporation of a.a. and 2DG reduced this M1/M2 ratio (Figure 4.24a). Although implantation of aPLA+HA decreased the fold change of M2 to M1 macrophages, our glycolytic inhibitors did not mitigate this to a statistically significant extent (Figure 4.24b).

Also in our $F4/80^+$ macrophages, we observed that aPLA+HA increased Arg1 levels (Figure 4.24c) relative to sham controls, likely from its immunomodulatory capability[396, 400]. Additionally, incorporation of a.a. but not 2DG to aPLA+HA tended to further increase Arg1 levels among macrophages, although this trend was not statistically significant (Figure 4.24c).

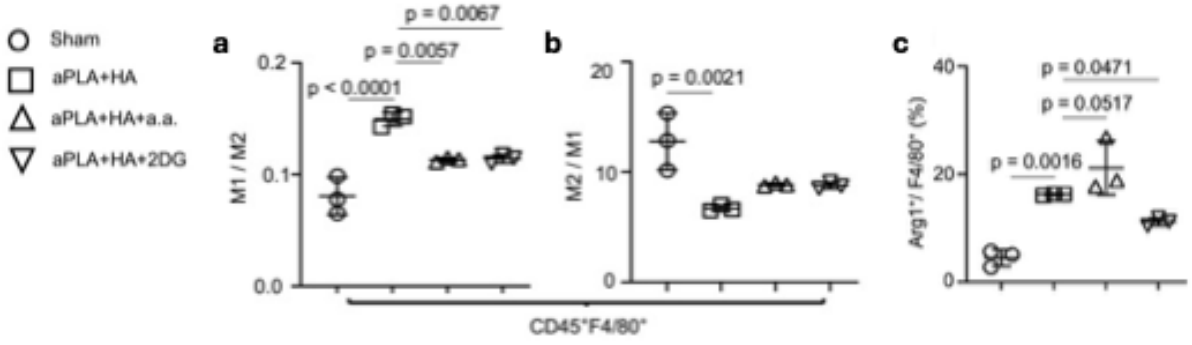

Figure 4.24 Activation states of macrophages in the amorphous polylactide hydroxyapatite (aPLA+HA) composite biomaterial microenvironment are differentially affected by targeting different glycolytic steps. a, Fold change of proinflammatory (M1; $CD86^{+}CD206^{-}$) macrophages with respect to anti-inflammatory (M2; $CD206^{+}$) macrophages. b, Fold change of M2 macrophages with respect to M1 macrophages. c, Quantification of Arginase 1 ($Arg1^{+}$) macrophages. One-way ANOVA followed by Tukey's multiple comparison test, n = 3; amorphous polylactide (aPLA), hydroxyapatite (HA), aminooxyacetic acid (a.a.), 2-deoxyglucose (2DG).

Finally, given that elevated $CD11c^{+}$ dendritic cell numbers in the aPLA+HA microenvironment were reduced by a.a. and 2DG (Figure 4.23c), we then looked at polarization states of dendritic cells. Compared to sham controls, the fold change of proinflammatory (D1) dendritic cells relative to anti-inflammatory (D2) dendritic cells was increased in the microenvironment of aPLA+HA implants; yet, incorporation of a.a. or 2DG did not reduce D1 dendritic cell levels (Figure 4.25a). Furthermore, although the fold change of D2 dendritic cells to D1 dendritic cells was decreased in aPLA+HA compared to sham controls, incorporating a.a. or 2DG did not increase D2 dendritic cell proportions (Figure 4.25b).

Expression of Arg1 among dendritic cells was increased following implantation of aPLA+HA relative to sham controls (Figure 4.25c). Notably, compared to aPLA+HA, incorporating a.a. further elevated Arg1 expression among dendritic cell populations (Figure 4.25c). Increased Arg1 expression in the composite biomaterial microenvironment could arise from inhibition of aspartate-aminotransferase by a.a., which obviates metabolic and transcriptional activation of immune cells into proinflammatory states[401]. Elevated Arg1 is a crucial driver of osteoinduction, creating a pro-regenerative composite biomaterial microenvironment[402].

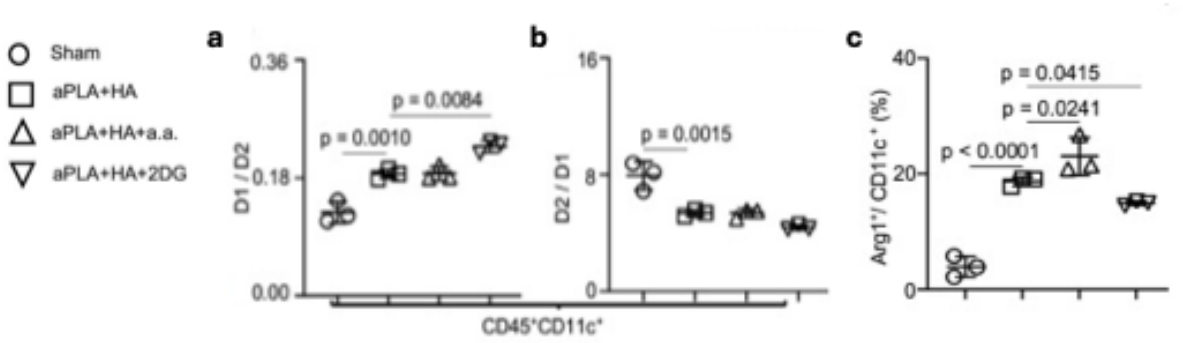

Figure 4.25 Inflammatory states of dendritic cells are affected in the amorphous polylactide-hydroxyapatite (aPLA+HA) composite biomaterial microenvironment. a, Fold change of proinflammatory (D1; $CD86^{+}CD206^{-}$) dendritic cells with respect to anti-inflammatory (D2; $CD206^{+}$) dendritic cells. g, Fold change of D2 with respect to D1 dendritic cells. h, Quantification of Arginase 1 ($Arg1^{+}$) dendritic cells. One-way ANOVA followed by Tukey's or Newman-Keul's multiple comparison test, n = 3; amorphous polylactide (aPLA), hydroxyapatite (HA), aminooxyacetic acid (a.a.), 2-deoxyglucose (2DG).

DISCUSSION

The following text throughout this section includes exerpts from our manuscripts titled the manuscript titled "Polylactide Degradation Activates Immune Cells by Metabolic Reprogramming", published in Adv. Sci.[104]; "Regulating the proinflammatory response to implanted composite biomaterials comprising polylactide and hydroxyapatite by targeting immunometabolism", published in Bioactive Materials[342]; and "The role of mitochondrial complex I in the proinflammatory response to polylactide implants", currently under review at ACS Applied Engineering Materials[343].

Cell responses to PLA extracts

Upon treatment with polylactide (PLA) degradation products (extracts), mouse embryonic fibroblasts (MEFs) expressed increased bioenergetic (ATP) activity, as well as extracellular acidification rate (ECAR) and proton efflux rate (PER). Increased ATP production could implicate a variety of cell processes, including cell growth/metabolic activation. Increased ECAR activity signifies increased glycolytic activity. This occurred as a result of treatment with both amorphous PLA (aPLA) and semi-crystalline PLA (cPLA) extracts, and effects could be mitigated by glycolytic inhibitors in a dose-dependent manner.

Upon treatment with PLA extracts, primary bone marrow-derived macrophages (BMDMs) expressed increased bioenergetic (ATP) activity, as well as increased oxygen consumption rate (OCR), extracellular acidification rate (ECAR) and proton efflux rate (PER). ECAR and PER indicate glycolytic activity whereas OCR indicates mitochondrial activity and macrophage activation. Activation from

treatment with aPLA and cPLA extracts was confirmed with increased expression of proinflammatory cytokines, which could also be mitigated with glycolytic inhibitors as well, suggesting dependence on immunometabolism for immune cell activation.

L-lactic acid as driver of PLA extract-induced chronic inflammation

Lactate is a signaling molecule in immunity[403] and cancer progression[404]. Its role when combined with LPS is conflicting, with reports of proinflammatory and anti-inflammatory effects[405, 406]. However, a stand-alone ability of lactate to activate immune cells is novel, as prior inflammatory and cancer models did not simulate prolonged exposure times, a critical feature of cancer and immune microenvironments. This is significant in that it elucidates a potential mechanism whereby PLA implant breakdown products signal to surrounding cells inducing inflammation; this identifies a therapeutic target that could be used in combination with current treatments to mitigate acidification in the PLA bioimplant environment.

Targeting immunometabolism induced by PLA extracts in vivo

The glycolytic inhibitors 3PO, 2DG, and a.a. effectively mitigated aPLA and cPLA-induced increase in ATP in MEFs, and changes in OCR, ECAR and proinflammatory cytokine secretion of BMDMs in vitro culture. In BMDMs, the ox-phos inhibitors rot, met, AA, and olig also effectively mitigated aPLA-induced ATP increases and cPLA-induced OCR increases. These effects are outlined in Figure 4.26.

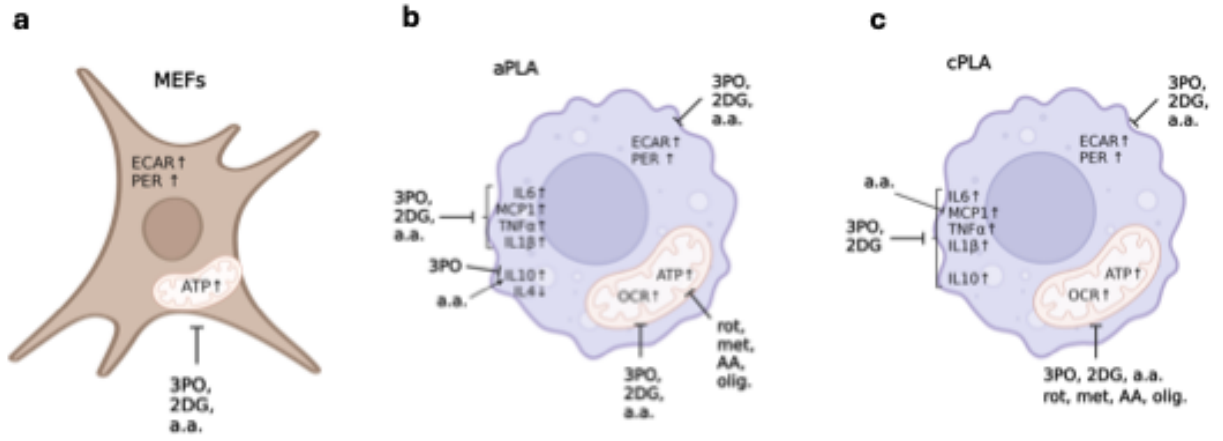

Figure 4.26 Graphic showing effects of amorphous polylactide (aPLA) and semi-crystalline polylactide (cPLA) extracts and metabolic inhibitors on fibroblasts (MEFs; a), effects of aPLA and metabolic inhibitors on macrophages (BMDMs; b), and effects of cPLA and metabolic inhibitors on BMDMs (c). Extracellular acidification rate (ECAR), proton efflux rate (PER), , oxygen consumption rate (OCR), 3-(3-pyridinyl)−1-(4-pyridinyl)−2-propen-1-one (3PO), 2-deoxyglucose (2DG), aminooxyacetic acid (a.a.), rotenone (rot), metformin (met), antimycin A (AA), oligomycin (olig.), arginase-1 (Arg1), interleukin (IL), monocyte chemoattractant protein (MCP1), tumor necrosis factor (TNF). Created with *BioRender.com*.

In aPLA and cPLA s.c. implants, metformin modulated macrophage and dendritic cell numbers and activation, as outlined in Figure 4.27. In composite biomaterials comprising aPLA and HA, 2DG and/or a.a. decreased CD45 nucleated hematopoietic cell infiltrate, decreased proinflammatory neutrophil infiltration, and modulated macrophage and dendritic cell infiltrate and activation, as outlined in Figure 4.27.

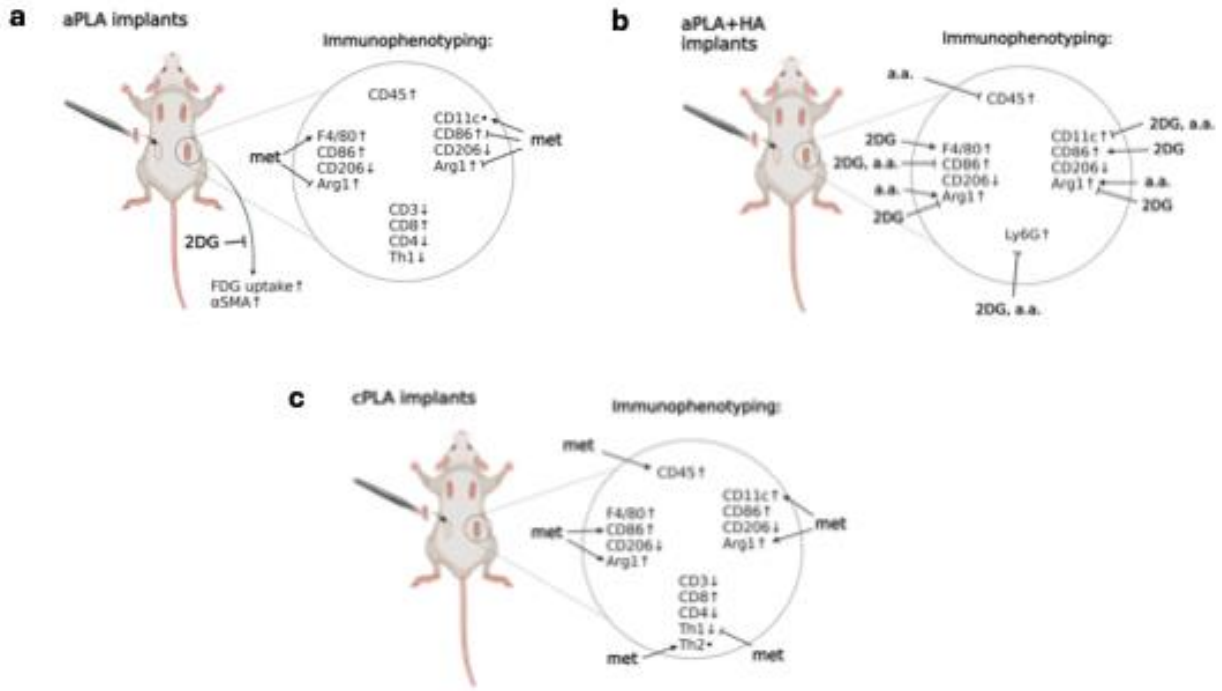

Figure 4.27 Graphic showing in vivo effects of amorphous polylactide (aPLA) implants (a), aPLA and hydroxyapatite (aPLA+HA) composite biomaterial implants (b), and semi-crystalline polylactide (cPLA) implants (c). F-18 fluorodeoxyglucose (FDG), 2-deoxyglucose (2DG), aminooxyacetic acid (a.a.), metformin (met), arginase-1 (Arg1), interleukin (IL), monocyte chemoattractant protein (MCP1), tumor necrosis factor (TNF). Created with *BioRender.com*.

Thus, the immunometabolic activation induced by PLA implants has been shown to be therapeutically targeted by glycolysis and ox-phos inhibitors in a preclinical model.

Clinical implications

Despite its role as a neutralizer of acidity, we found that hydroxyapatite (HA) increases proinflammatory infiltrate into the implant microenvironment. We found increased numbers of nucleated hematopoietic cells and F4/80^{+} macrophages. We also found increased numbers of CD11c dendritic cells. Both macrophages and dendritic cells had increased proinflammatory CD86 expression as compared with anti-inflammatory CD206, suggesting a predominantly M1-like and D1-like cells present

in the implant microenvironment; however, the plasticity in polarization of these immune cells is demonstrated by additionally increased anti-inflammatory Arg1 expression, which shows an intermediate or overlapping polarization phenotype in the immune infiltrate populations surrounding the PLA explant.

In conclusion, we uncover new ways by which different biomaterials affect the immune microenvironment, such as altering the ratio of proinflammatory to anti-inflammatory cell populations. We demonstrate that controlling metabolic states by modifying glycolytic flux around implanted composite biomaterials is capable of: a) decreasing neutrophil recruitment; b) decreasing proinflammatory macrophage populations; c) decreasing dendritic cell numbers; d) and increasing Arg1 expression among dendritic cells. Aminoxyacetic acid (a.a.), one of the metabolic inhibitors, has already been used safely in clinical trials for the treatment of other disease conditions[364], making it a translatable small molecule for incorporation into composite biomaterials for future clinical use. Prior to translation, additional studies are needed to characterize the release profiles of metabolic inhibitors from composite biomaterials as well as the effects of implanting composite biomaterials containing embedded metabolic inhibitors in musculoskeletal tissues, such as bone defects, for regenerative medicine applications. It may thus be beneficial to reevaluate our clinical approach to mitigating PLA extract-induced chronic inflammation.

CHAPTER 5:

DISCUSSION, PROPOSED FUTURE STUDIES, AND THERAPEUTIC POTENTIAL

DISCUSSION

Conceptual origins of extracellular vesicle mediated immunocarcinogenesis

Under homeostatic conditions, colon cells proliferate rapidly in a highly regulated context. Cancerous colon cells (CRCs) exhibit genetic and epigenetic alterations leading to uncontrolled proliferation and invasion of colon cancer cells into the underlying stroma. Ulcerative colitis is known to induce field cancerization, commonly resulting in chromosomal instability[34], founder mutations in TP53 and KRAS genes [23], and epigenetic changes such as methylation-induced gene silencing[36]. Signals secreted by aberrantly active immune and stromal cells in chronic inflammation such as colitis remarkably resemble that of the tumor microenvironment (TME)[407]. However, current treatments to target prediscovered mediators have not eradicated the progression of cancer in patients with colitis, suggesting potential for a different signaling mediator of immunocarcinogenesis.

We discovered EVs from LPS-activated macrophages, modeling macrophages in ulcerative colitis, can contribute to colonic inflammation and complex tumorigenesis, and revealed some contradictory, "push and pull", results from adding EVs to various transformed cells in culture and to tissues in vivo models of cancer. A review of the literature in 2016[37] revealed that EVs from various cell types, cancer-associated immune cells or cancer cells, can affect each of the Hallmarks of Cancer as originally described by Hanahan and Weinberg in 2000 and then revised in 2011[408, 409]. The effects of EVs were dependent on cell type of origin of the EVs being studied, and the state of that cell type, and their effects on cancer or stromal cells in the tumor. The involvement of EVs, as a cellular communication mechanism, has been well established in cancer and cancer progression, but the role each type of EV from each type of cell in the tumor microenvironment, and the yin-yang of pro-tumor or anti-tumor effects are complex and are part of the balance/imbalance of cancer growth and immune control.

A main hallmark of cancer is invasion and the ability of cells to be mobile and metastasize. As part of this hallmark, there was early evidence of a cellular signal(s) from primary tumors that could create premetastatic niches in distant organs[410], indicating that there was information transfer from cells in the primary tumor to distant sites that would precede the colonization of those sites with cancer cells. The concept that a tumor could condition a tissue for colonization over significant distances in the body, was suggestive of a communication mechanism that was more complex than secreted soluble signaling factors. Extracellular vesicles were implicated in this process and then more recently, their role has been further validated[411, 412] and has been shown to be regulated through immunometabolic reprogramming[413] much like the results described here in chapter 4, and in our published reports, on

immune responses to biomaterials. Preconditioning of a metastatic niche has been demonstrated in models of colorectal cancer[414] and many other cancers[415]. These observations and the early studies of the premetastatic niche were foundational to the ideation that EVs mediate immunocarcinogenesis.

Our foundational immunocarcinogenesis hypothesis can be stated as, signals from chronically activated immune cells could create a premalignant niche, much like the premetastatic niche, in which epithelial cells aberrantly receive signals from EVs from activated immune cells that precondition the epithelium to become malignant. These aberrant immune signals act to predispose the dysregulated epithelial cells to subsequent cellular changes that transform them and lead to primary cancers. Although easily stated, proving this hypothesis in the complex environment of intact organs and tissues of immunocompetent animals where localizing the initial premalignant events is a daunting "needle in a haystack" problem is difficult. It is daunting because the act of "unstacking the hay" to find the needle would disassemble the mechanism being studied, i.e., cells in tissues with active immune surveillance. This is, in effect, a cancer analogy of Schrodinger's cat where epithelial cells are in a box with relatively opaque walls, the body, and the cells exist in a state of superposition in which they are simultaneously both normal and premalignant. The concept of immunocarcinogenesis proposes that the immune system, when chronically over stimulated, is a "poison" for the cells within the box, the body, and the organs in which they are contained. With these studies, we have only just scratched the surface of this problem. Revealing the signals and processes of immunocarcinogenesis is a challenge, and here we describe some initial models that have revealed potential signals and have led to provocative observations. These models have supported our fundamental hypothesis, but leaves many questions for cancer biologists and immunologists to address in the future.

Clinical implications of our experimental findings

The discovered effects of EVs from LPS-activated macrophages (EV_{LPS}) on colon cells in culture and the tumor microenvironment (TME), and protein contents detected to be differentially expressed relative to EVs from non-activated macrophages (EV_{non}), are outlined in Figure 5.1.

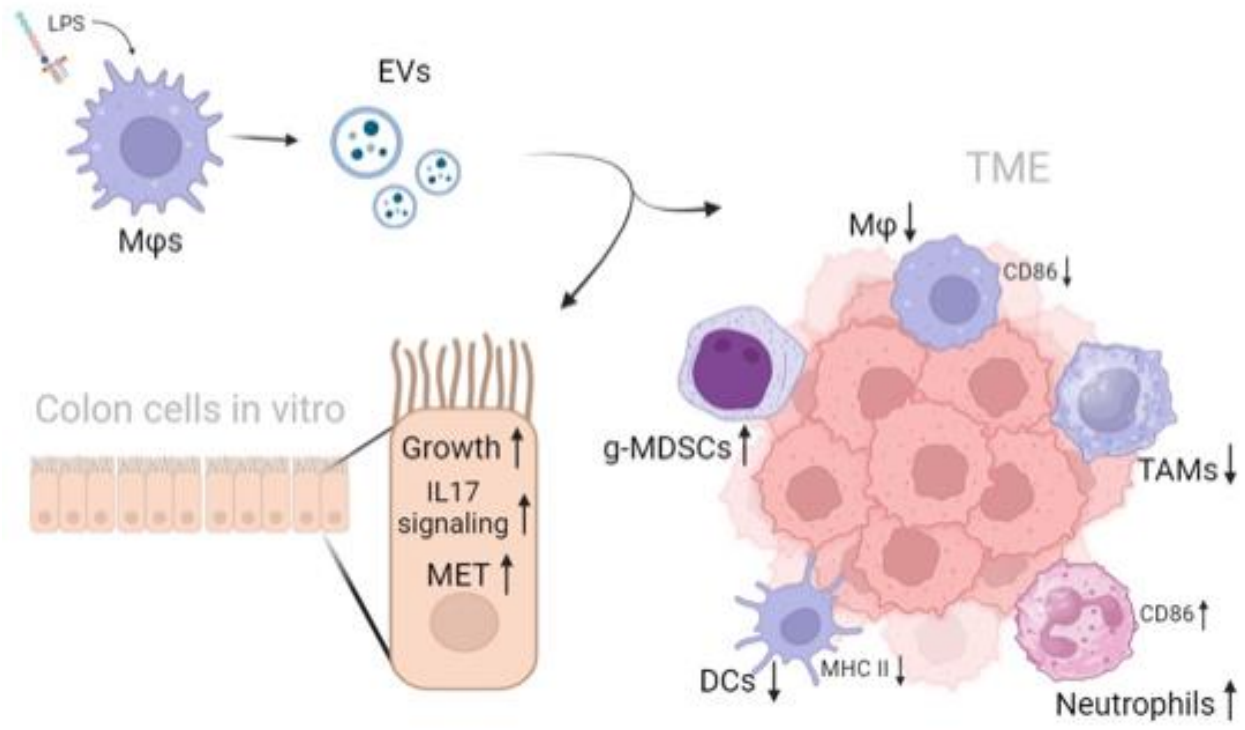

Figure 5.1 Summary of the effects from extracellular vesicles (EVs) from macrophages (Mφs) activated with lipopolysaccharide (LPS) on colon cells in vitro culture and on immune infiltrate in the tumor microenvironment (TME). Mesenchymal to epithelial transition (MET), tumor-associated macrophages (TAMs), dendritic cells (DCs), major histocompatibility complex II (MHC II), granulocytic myeloid-derived suppressor cells (g-MDSCs). Created with *BioRender.com.*

I found that EVs from Raw264.7 macrophages activated with IFNγ plus LPS decreased the growth rate of recipient CT26 colon cancer cells. However, EVs from Raw264.7 macrophages activated with LPS alone increased anchorage-independent growth rate of CT26 cells and increased growth rate of 4T1 breast cancer cells. Because LPS-activation of macrophages eventually induces IFNγ secretion, these cells are still being exposed to lower levels of IFNγ. This suggests that directly activating macrophages with LPS and higher concentrations of IFNγ at the same time affects macrophage-secreted EV signaling toward a more cytotoxic profile; this coincides with evidence in the literature showing these "M1-EVs" to be anti-tumorigenic, as is described in the introduction for Chapter 2. Parsing out the pro- and anti-cancer effects of activated macrophage-derived EVs required a molecular dissection of the processes involved, which revealed some of the complexities of the immune-epithelial cell interactions involved in immunocarcinogenesis.

The immune response of certain patients in response to colitis is context-dependent, and consequent tumorigenicity may be affected by many factors including composition of the microbiome.

We have shown that response of macrophages to LPS, a gram-negative bacterial component present in the context of chronic inflammation, may be concentration dependent. Other investigators have observed that the concentration of LPS used to stimulate macrophages can differentially affect cellular responses; for example, at high concentrations of LPS stimulation (100 – 1000 ng/ml), CD14 is not necessary for macrophages to produce TNF-α [416]. I found that stimulating primary bone marrow-derived macrophages with 10 ng/ml LPS led to increased nitric oxide (NO) secretion over time than BMDMs activated with 100 ng/ml LPS. However, EVs from BMDMs activated with 100 ng/ml LPS induced increased cell growth rate in recipient colon cancer cells compared to EVs from BMDMs treated with 10 ng/ml LPS. Relative to acute inflammation, chronic inflammation is characterized by long-term, low-level activation of immune infiltrate. When stimulated with 100 ng/ml LPS, BMDMs secreted lower NO which classically indicates a lower M1 activation status; "lower-level" activated BMDM-secreted EVs induced increased proliferation in recipient colon cells, implying that chronic inflammation may have different effects on tumorigenesis than acute inflammation that is followed by repair. The caveat to this finding is that stimulating BMDMs with higher LPS concentrations may decrease cell viability, so there may have been decreased number of BMDMs secreting NO which led to decreased detection relative to 10 ng/ml. It should also be noted that I administered the same number of EV_{LPS} and EV_{non} to recipient colon cells and tumors. However, inflammation and colitis has been shown to increase number of macrophages present in tissue[415]; experimentally identifying the relative concentration of EVs secreted by macrophages in homeostatic conditions as compared to colitis and applying this to my in vitro in vivo model may produce more relevant results. However, even if I am administering a higher number of EV_{non} than is physiologically relevant, my results still show a difference with EV_{LPS} administration and sufficiently proves functional effect changes. However, this weakens the potential finding of increased levels of GSN in non-activated macrophages, since there would theoretically be fewer EV_{non} present in homeostatic conditions.

Of note, EVs from non-activated iBMDMs (EV_{non}), a model of macrophages in the homeostatic colon, decreased anchorage independent growth of MC38 colon cells relative to untreated colon cells, a hallmark of transformation. This may be due to increased levels of GSN protein inducing tumor suppressive effects, which we found to be downregulated in EVs from LPS-activated macrophages (EV_{LPS}). Indeed, macrophages have been shown to be involved in mediating homeostasis in the colonic epithelium[40], which requires involved regulation of the rapid proliferation and turnover rate required of epithelial and stromal cells. This suggests that EV_{non} is involved in regulating uncontrolled proliferation of colon cells, which may suggest a tumor suppressive function of EV_{non} that is lost in EV_{LPS}. Investigating

the therapeutic potential of administering EVs containing tumor suppressive proteins such as GSN may offer a promising approach to reduce cancer risk in colitis patients.

Though EVs are very prevalent and promising as biomarkers and potential therapeutic targets to prevent disease progression, EV studies are limited because different models may lack EV traceability, throughput, clinical translatability, or feasibility[417]. The main purpose of my using macrophage cell line-secreted EVs is feasibility, as it would have required an excessive number of mice to isolate enough EVs for my experiments. I showed similar effects on colon cell growth treated with EVs from primary bone marrow-derived macrophages (BMDMs) compared to immortalized BMDMs (iBMDMs), which implies iBMDM EVs are a physiologically relevant model in this sense. However, cell lines seem to behave differently, in our studies, possibly due to endotoxin desensitization in culture and the fact that cell lines are, by definition, immortalized and hence malignant or at least premalignant with some of the cellular controls dysregulated. For example, THP1 macrophages secreted more TNF-α upon LPS treatment, and also produced EVs that increased epithelial cell growth rate more than did THP1 monocyte-derived EVs. In contrast, EVs from primary BMDMs that secreted less NO (treated with higher concentration of LPS) increased colon cell growth rate to a greater extent than EVs from BMDMs that secreted higher NO (treated with lower concentration of LPS).

Importantly, we discovered that EV_{LPS} can mediate immune infiltrate within the TME even when introduced to tissue preceding tumor emergence. Specifically, administration of EVs from LPS-activated macrophages into tissue before tumor emergence resulted in subsequently induced tumors to express: decreased number of TAMs, increased CD86 expression in non-TAM macrophages, and increased CD86 expression in neutrophils relative to all other conditions. This crucial observation suggests that EVs from activated macrophages can mediate tissues in premalignant states to affect subsequent tumorigenesis. However, whether these effects are overall pro-tumorigenic or anti-tumorigenic is yet to be fully defined.

LPS- vs Lactic acid-induced activation of macrophages

We showed that the PLA degradation product L-lactic acid directly signals to macrophages to increase metabolism and activation. Specifically, PLA extracts tend to increase ECAR and OCR in primary murine BMDMs. One group elucidated the immunometabolic effects of LPS and lactate in primary murine BMDMs[418]. In comparison, LPS treatment of BMDMs increased ECAR but decreased OCR[418]. This suggests that LPS increases glycolysis but decreases mitochondrial respiration in BMDMs, whereas lactate increases both. Metabolic reprogramming is a hallmark of cancer, but each cancer tissue has its own metabolic features[419]. In oral squamous cell carcinoma cell lines, for instance, ECAR and OCR were

found to be increased relative to non-cancer cells[420]. One study showed inhibiting glycolysis (ECAR) and mitochondrial respiration (OCR) in colon cancer cells resulted in increased apoptosis[421].

Interestingly, LPS-activated BMDMs secreted higher levels of lactate relative to non-activated BMDMs[418]. Thus, these two signaling molecules may affect immunometabolism and chronic inflammation in conjunction. Also, 2DG and olig. were found to decrease macrophage secretion of IL-6 and/or IL-10 induced by LPS activation[418]. Moreover, macrophage EVs have also been shown to mediate bone regeneration[91]. This suggests that in sterile chronic inflammation in the absence of bacterial components such as LPS, L-lactic acid could signal to activate macrophages, affecting EV secretion and mediating bone regeneration.

Gender disparities in colitis-associated cancer

Many epidemiology studies in eastern and western countries have shown no marked sex disparities in incidence of ulcerative colitis between genders[422]. Blumenstein et al. reported men to have an increased risk of IBD-associated CRC, though this may be due to alcohol and diet [423]. A population-based study in Western countries reported men had a higher incidence of colitis than women only after age 45 [424]. However, other studies show higher familial expression of IBD in females, especially in Crohn's disease[425]. Relative to males, IL-10 deficient female mice were found to be more susceptible to developing inflammation linked with an increase in fecal miR-21 levels[426], which can induce CAC through many signaling networks[427]. Women with IBD experience increased stress, sexual and psychological issues relevant to the disease. Importantly, stress has been shown to contribute to colon cancer incidence in mouse models of CAC; daily restraint-induced stress in mice increased tumor numbers upon AOM/DSS treatment [280]. Moreover, female hormones play a notable role in IBD, and active IBD is correlated with decreased fertility in females[422]. In our study, female mice were used because females typically exhibit stronger immune responses. Further studies will be necessary to compare sex call for future research in male mice as well.

PROPOSED FUTURE STUDIES

It should be recognized that using transformed cells to represent a premalignant context is inherently a flawed model; use of EVs from non-transformed HOXB3-differentiated macrophages may mitigate this concern. This sheds light on the need for more in vivo studies, which contain components of the immune system that we simply do not have the capacity to replicate the entirety of the complex environment of chronic inflammation or cancer in vitro. Future experiments using orthotopic models (e.g., AOM/DSS mouse or rat model of colitis-associated cancer) is ideal, to include tissue-resident cells such as goblet cells and tissue-resident macrophages, as well as involvement of the microbiome. This

could also elucidate the role of tissue-resident macrophages, as some of embryonic origin are found in colon but this population may slowly get replaced by bone marrow macrophages over time, and their role is unclear[171]. Depletion of certain cell types may elucidate their role in response to EVs from LPS-activated macrophages (EV_{LPS}) through tumorigenesis.

We are currently completing single-cell RNA sequencing of $CD45^+$ cells, as well as bulk RNA sequencing of live cells and $CD11b^+$ myeloid cells isolated from mouse tumors treated with conditions outlined in Figure 3.15 and Table 3.1. Further characterization of other cell subtypes affected by EV_{LPS} in vivo may further elucidate signaling effects. For example, because ASS1 expression has been found to be associated with increased number of cancer-associated fibroblasts[428], it would be interesting to characterize fibroblast and stromal cell infiltrate in our in vivo experimental model. I also proposed to characterize expression of markers that are highly expressed in human CRC including CD163 (M2 marker), iNOS (M1), and Arg1 (M2)[429].

I also propose to perform studies on different colon cancer cell types with different mutational statuses. For example, CT26 tumors are Kras mutant and p53 WT, opposite to MC38 tumors. Furthermore, using human tumor models induced with or without certain immune cell subtypes in immunodeficient mice may elucidate the role of individual immune cells in response to EVs from LPS-activated macrophages as the sole source of inflammatory signals representing colitis. Developing these models would require balancing physiological relevance with dissecting signals for easier comprehension of functional effects.

However, the clinical translatability of preclinical cancer models is low[430, 431]. Along with Dr. Aitor Aguirre, we are proposing a model showing clinical translatability using human induced pluripotent stem cells (iPSC)-derived macrophages to stimulate and isolate EVs, for administration onto iPSC-derived human colonic organoids (HCOs). This model dissects EV signaling for ease of characterization of functional effects while also remaining physiologically relevant in a non-cancer, premalignant context in 3D.

THERAPEUTIC POTENTIAL

My findings reveal macrophage EVs in colitis as a potential mediator of immunocarcinogenesis. Identifying more EV-associated proteins and RNAs that mediate colitis-associated cancer may elucidate therapeutic targets with the potential to prevent or irradicate cancer in patients with inflammatory bowel disease and other chronic inflammatory conditions. Targeting potential mediators in macrophage-derived EVs—either by inhibiting protumorigenic cargo like ASS1 or by enhancing tumor-suppressive elements like GSN—may offer new therapeutic strategies for preventing cancer in colitis

patients. Further characterization of how these interventions affect CRC cell transformation and cancer progression could validate these EV components as viable clinical targets. Therapies could include engineered EVs to target macrophage EVs driving colitis-associated cancer, e.g., polyethylene glycol (PEG) surface modification may enhance targeting efficiency[432].

The concept of immunocarcinogenesis is applicable to many other GI organs, including cells of the esophagus, liver, stomach, and pancreas, as well as other organs that are at risk of malignancy subsequent to inflammation including breast, prostate, lung and bladder. For example, many cancer types, including melanoma, hepatocellular carcinoma, and prostate cancer, silence argininosuccinate synthase 1 (ASS1) expression, making tumor cells dependent on external arginine delivery for metabolic activity, i.e., arginine auxotrophic[433]. In theory, delivery of EVs from LPS-activated macrophages containing ASS1 to these tumor cells has the potential of providing a survival advantage for these ASS1-silenced tumor cells. This reveals ASS1 as a potential target for these cancer types. Future studies confirming this could elucidate an improved combination therapy for ASS1-silenced cancers.

REFERENCES

1. Grivennikov, S. I., Greten, F. R. and Karin, M. Immunity, inflammation, and cancer. *Cell* **140**, 883-99, doi:10.1016/j.cell.2010.01.025 (2010).

2. Dahlhamer, J. M., Zammitti, E. P., Ward, B. W., Wheaton, A. G. and Croft, J. B. Prevalence of Inflammatory Bowel Disease Among Adults Aged ≥18 Years - United States, 2015. *Mmwr-Morbid Mortal W* **65**, 1166-1169, doi:DOI 10.15585/mmwr.mm6542a3 (2016).

3. Frolkis, A., Dieleman, L. A., Barkema, H. W., Panaccione, R., Ghosh, S., Fedorak, R. N., Madsen, K., Kaplan, G. G. and Alberta, I. B. D. C. Environment and the inflammatory bowel diseases. *Can J Gastroenterol* **27**, e18-24, doi:10.1155/2013/102859 (2013).

4. Azer, S. A. Overview of molecular pathways in inflammatory bowel disease associated with colorectal cancer development. *Eur J Gastroenterol Hepatol* **25**, 271-81, doi:10.1097/MEG.0b013e32835b5803 (2013).

5. Feuerstein, J. D. and Cheifetz, A. S. Ulcerative colitis: epidemiology, diagnosis, and management. *Mayo Clin Proc* **89**, 1553-63, doi:10.1016/j.mayocp.2014.07.002 (2014).

6. Van Der Kraak, L., Gros, P. and Beauchemin, N. Colitis-associated colon cancer: Is it in your genes? *World J Gastroenterol* **21**, 11688-99, doi:10.3748/wjg.v21.i41.11688 (2015).

7. Serafino, A., Moroni, N., Zonfrillo, M., Andreola, F., Mercuri, L., Nicotera, G., Nunziata, J., Ricci, R., Antinori, A., Rasi, G. and Pierimarchi, P. WNT-pathway components as predictive markers useful for diagnosis, prevention and therapy in inflammatory bowel disease and sporadic colorectal cancer. *Oncotarget* **5**, 978-92, doi:10.18632/oncotarget.1571 (2014).

8. Mattar, M. C., Lough, D., Pishvaian, M. J. and Charabaty, A. Current management of inflammatory bowel disease and colorectal cancer. *Gastrointest Cancer Res* **4**, 53-61, (2011).

9. Fernandes, J. V., Cobucci, R. N., Jatoba, C. A., Fernandes, T. A., de Azevedo, J. W. and de Araujo, J. M. The role of the mediators of inflammation in cancer development. *Pathol Oncol Res* **21**, 527-34, doi:10.1007/s12253-015-9913-z (2015).

10. Aggarwal, B. B., Shishodia, S., Sandur, S. K., Pandey, M. K. and Sethi, G. Inflammation and cancer: how hot is the link? *Biochem Pharmacol* **72**, 1605-21, doi:10.1016/j.bcp.2006.06.029 (2006).

11. Coussens, L. M. and Werb, Z. Inflammation and cancer. *Nature* **420**, 860-7, doi:10.1038/nature01322 (2002).

12. Drew, D. A., Cao, Y. and Chan, A. T. Aspirin and colorectal cancer: the promise of precision chemoprevention. *Nat Rev Cancer* **16**, 173-86, doi:10.1038/nrc.2016.4 (2016).

13. Zhao, L. N., Li, J. Y., Yu, T., Chen, G. C., Yuan, Y. H. and Chen, Q. K. 5-Aminosalicylates reduce the risk of colorectal neoplasia in patients with ulcerative colitis: an updated meta-analysis. *PLoS One* **9**, e94208, doi:10.1371/journal.pone.0094208 (2014).

14. Wang, D. and Dubois, R. N. The role of COX-2 in intestinal inflammation and colorectal cancer. *Oncogene* **29**, 781-8, doi:10.1038/onc.2009.421 (2010).

15. Stolfi, C., Pallone, F. and Monteleone, G. Colorectal cancer chemoprevention by mesalazine and its derivatives. *J Biomed Biotechnol* **2012**, 980458, doi:10.1155/2012/980458 (2012).

16. Bernstein, C. N., Nugent, Z. and Blanchard, J. F. 5-aminosalicylate is not chemoprophylactic for colorectal cancer in IBD: a population based study. *Am J Gastroenterol* **106**, 731-6, doi:10.1038/ajg.2011.50 (2011).

17. Irrazabal, T., Thakur, B. K., Croitoru, K. and Martin, A. Preventing Colitis-Associated Colon Cancer With Antioxidants: A Systematic Review. *Cell Mol Gastroenterol Hepatol* **11**, 1177-1197, doi:10.1016/j.jcmgh.2020.12.013 (2021).

18. Burr, N. E., Hull, M. A. and Subramanian, V. Does aspirin or non-aspirin non-steroidal anti-inflammatory drug use prevent colorectal cancer in inflammatory bowel disease? *World J Gastroenterol* **22**, 3679-86, doi:10.3748/wjg.v22.i13.3679 (2016).

19. Munkholm, P. Review article: the incidence and prevalence of colorectal cancer in inflammatory bowel disease. *Aliment Pharmacol Ther* **18 Suppl 2**, 1-5, doi:10.1046/j.1365-2036.18.s2.2.x (2003).

20. Curtius, K., Wright, N. A. and Graham, T. A. An evolutionary perspective on field cancerization. *Nat Rev Cancer* **18**, 19-32, doi:10.1038/nrc.2017.102 (2018).

21. Bauer, G. M., Stypula-Cyrus, Y., Subramanian, H., Cherkezyan, L., Viswanathan, P., Zhang, D., Iyengar, R., Bagalkar, S., Derbas, J., Graff, T., Gladstein, S., Almassalha, L. M., Chandler, J. E., Roy, H. K. and Backman, V. The transformation of the nuclear nanoarchitecture in human field carcinogenesis. *Future Sci OA* **3**, doi:10.4155/fsoa-2017-0027 (2017).

22. Weinberg, R. A. The Biology of Cancer. **2**, doi:10.1201/9780429258794 (2013).

23. Leedham, S. J., Graham, T. A., Oukrif, D., McDonald, S. A., Rodriguez-Justo, M., Harrison, R. F., Shepherd, N. A., Novelli, M. R., Jankowski, J. A. and Wright, N. A. Clonality, founder mutations, and field cancerization in human ulcerative colitis-associated neoplasia. *Gastroenterology* **136**, 542-50 e6, doi:10.1053/j.gastro.2008.10.086 (2009).

24. Dame, M. K., Huang, S., Attili, D., Spence, J. R. and Colacino, J. A. Identification and Isolation of Human LGR5+ Cells Using an Antibody-Based Strategy. *Methods Mol Biol* **2171**, 3-23, doi:10.1007/978-1-0716-0747-3_1 (2020).

25. Bauer, G. M., Stypula-Cyrus, Y., Subramanian, H., Cherkezyan, L., Viswanathan, P., Zhang, D., Iyengar, R., Bagalkar, S., Derbas, J., Graff, T., Gladstein, S., Almassalha, L. M., Chandler, J. E., Roy, H. K. and Backman, V. The transformation of the nuclear nanoarchitecture in human field carcinogenesis. *Futur Sci Oa* **3**, doi:10.4155/fsoa-2017-0027 (2017).

26. Subramanian, H., Roy, H. K., Pradhan, P., Goldberg, M. J., Muldoon, J., Brand, R. E., Sturgis, C., Hensing, T., Ray, D., Bogojevic, A., Mohammed, J., Chang, J. S. and Backman, V. Nanoscale Cellular Changes in Field Carcinogenesis Detected by Partial Wave Spectroscopy. *Cancer Res* **69**, 5357-5363, doi:10.1158/0008-5472.Can-08-3895 (2009).

27. Stypula-Cyrus, Y., Damania, D., Kunte, D. P., Cruz, M. D., Subramanian, H., Roy, H. K. and Backman, V. HDAC up-regulation in early colon field carcinogenesis is involved in cell tumorigenicity through regulation of chromatin structure. *PLoS One* **8**, e64600, doi:10.1371/journal.pone.0064600 (2013).

28. Luo, Y., Yu, M. and Grady, W. M. Field cancerization in the colon: a role for aberrant DNA methylation? *Gastroenterol Rep (Oxf)* **2**, 16-20, doi:10.1093/gastro/got039 (2014).

29. Damania, D., Subramanian, H., Tiwari, A. K., Stypula, Y., Kunte, D., Pradhan, P., Roy, H. K. and Backman, V. Role of cytoskeleton in controlling the disorder strength of cellular nanoscale architecture. *Biophys J* **99**, 989-96, doi:10.1016/j.bpj.2010.05.023 (2010).

30. Polley, A. C., Mulholland, F., Pin, C., Williams, E. A., Bradburn, D. M., Mills, S. J., Mathers, J. C. and Johnson, I. T. Proteomic analysis reveals field-wide changes in protein expression in the morphologically normal mucosa of patients with colorectal neoplasia. *Cancer Res* **66**, 6553-62, doi:10.1158/0008-5472.CAN-06-0534 (2006).

31. Yakoub, D., Keun, H. C., Goldin, R. and Hanna, G. B. Metabolic profiling detects field effects in nondysplastic tissue from esophageal cancer patients. *Cancer Res* **70**, 9129-36, doi:10.1158/0008-5472.CAN-10-1566 (2010).

32. Kunte, D. P., DelaCruz, M., Wali, R. K., Menon, A., Du, H., Stypula, Y., Patel, A., Backman, V. and Roy, H. K. Dysregulation of microRNAs in colonic field carcinogenesis: implications for screening. *PLoS One* **7**, e45591, doi:10.1371/journal.pone.0045591 (2012).

33. Keku, T. O., Amin, A., Galanko, J., Martin, C., Schliebe, B. and Sandler, R. S. Apoptosis in normal rectal mucosa, baseline adenoma characteristics, and risk of future adenomas. *Cancer Epidemiol Biomarkers Prev* **17**, 306-10, doi:10.1158/1055-9965.EPI-07-0066 (2008).

34. Rabinovitch, P. S., Dziadon, S., Brentnall, T. A., Emond, M. J., Crispin, D. A., Haggitt, R. C. and Bronner, M. P. Pancolonic chromosomal instability precedes dysplasia and cancer in ulcerative colitis. *Cancer Res* **59**, 5148-53, (1999).

35. Baker, K. T., Salk, J. J., Brentnall, T. A. and Risques, R. A. Precancer in ulcerative colitis: the role of the field effect and its clinical implications. *Carcinogenesis* **39**, 11-20, doi:10.1093/carcin/bgx117 (2018).

36. Hahn, M. A., Li, A. X., Wu, X., Yang, R., Drew, D. A., Rosenberg, D. W. and Pfeifer, G. P. Loss of the polycomb mark from bivalent promoters leads to activation of cancer-promoting genes in colorectal tumors. *Cancer Res* **74**, 3617-3629, doi:10.1158/0008-5472.CAN-13-3147 (2014).

37. Kanada, M., Bachmann, M. H. and Contag, C. H. Signaling by Extracellular Vesicles Advances Cancer Hallmarks. *Trends Cancer* **2**, 84-94, doi:10.1016/j.trecan.2015.12.005 (2016).

38. Hyenne, V., Ghoroghi, S., Collot, M., Bons, J., Follain, G., Harlepp, S., Mary, B., Bauer, J., Mercier, L., Busnelli, I., Lefebvre, O., Fekonja, N., Garcia-Leon, M. J., Machado, P., Delalande, F., Lopez, A. A., Silva, S. G., Verweij, F. J., van Niel, G., Djouad, F., Peinado, H., Carapito, C., Klymchenko, A. S. and Goetz, J. G. Studying the Fate of Tumor Extracellular Vesicles at High Spatiotemporal Resolution Using the Zebrafish Embryo. *Dev Cell* **48**, 554-572 e7, doi:10.1016/j.devcel.2019.01.014 (2019).

39. Barros, F. M., Carneiro, F., Machado, J. C. and Melo, S. A. Exosomes and Immune Response in Cancer: Friends or Foes? *Front Immunol* **9**, 730, doi:10.3389/fimmu.2018.00730 (2018).

40. Chang, X., Wang, S. L., Zhao, S. B., Shi, Y. H., Pan, P., Gu, L., Yao, J., Li, Z. S. and Bai, Y. Extracellular Vesicles with Possible Roles in Gut Intestinal Tract Homeostasis and IBD. *Mediators Inflamm* **2020**, 1945832, doi:10.1155/2020/1945832 (2020).

41. Valter, M., Verstockt, S., Finalet Ferreiro, J. A. and Cleynen, I. Extracellular Vesicles in Inflammatory Bowel Disease: Small Particles, Big Players. *J Crohns Colitis* **15**, 499-510, doi:10.1093/ecco-jcc/jjaa179 (2021).

42. Kotelevets, L. and Chastre, E. Extracellular Vesicles in Colorectal Cancer: From Tumor Growth and Metastasis to Biomarkers and Nanomedications. *Cancers (Basel)* **15**, doi:10.3390/cancers15041107 (2023).

43. Buzas, E. I. The roles of extracellular vesicles in the immune system. *Nat Rev Immunol* **23**, 236-250, doi:10.1038/s41577-022-00763-8 (2023).

44. Wang, Y., Tian, J., Tang, X., Rui, K., Tian, X., Ma, J., Ma, B., Xu, H., Lu, L. and Wang, S. Exosomes released by granulocytic myeloid-derived suppressor cells attenuate DSS-induced colitis in mice. *Oncotarget* **7**, 15356-68, doi:10.18632/oncotarget.7324 (2016).

45. Raposo, G., Nijman, H. W., Stoorvogel, W., Liejendekker, R., Harding, C. V., Melief, C. J. and Geuze, H. J. B lymphocytes secrete antigen-presenting vesicles. *J Exp Med* **183**, 1161-72, doi:10.1084/jem.183.3.1161 (1996).

46. Sung, B. H., Parent, C. A. and Weaver, A. M. Extracellular vesicles: Critical players during cell migration. *Dev Cell* **56**, 1861-1874, doi:10.1016/j.devcel.2021.03.020 (2021).

47. Yin, Y., Shelke, G. V., Lasser, C., Brismar, H. and Lotvall, J. Extracellular vesicles from mast cells induce mesenchymal transition in airway epithelial cells. *Respir Res* **21**, 101, doi:10.1186/s12931-020-01346-8 (2020).

48. Wiklander, O. P., Nordin, J. Z., O'Loughlin, A., Gustafsson, Y., Corso, G., Mager, I., Vader, P., Lee, Y., Sork, H., Seow, Y., Heldring, N., Alvarez-Erviti, L., Smith, C. I., Le Blanc, K., Macchiarini, P., Jungebluth, P., Wood, M. J. and Andaloussi, S. E. Extracellular vesicle in vivo biodistribution is determined by cell source, route of administration and targeting. *J Extracell Vesicles* **4**, 26316, doi:10.3402/jev.v4.26316 (2015).

49. Shen, M. and Ren, X. New insights into the biological impacts of immune cell-derived exosomes within the tumor environment. *Cancer Lett* **431**, 115-122, doi:10.1016/j.canlet.2018.05.040 (2018).

50. Mahida, Y. R. The key role of macrophages in the immunopathogenesis of inflammatory bowel disease. *Inflamm Bowel Dis* **6**, 21-33, doi:10.1097/00054725-200002000-00004 (2000).

51. Edin, S., Wikberg, M. L., Dahlin, A. M., Rutegard, J., Oberg, A., Oldenborg, P. A. and Palmqvist, R. The distribution of macrophages with a M1 or M2 phenotype in relation to prognosis and the molecular characteristics of colorectal cancer. *PLoS One* **7**, e47045, doi:10.1371/journal.pone.0047045 (2012).

52. Mannavola, F., Salerno, T., Passarelli, A., Tucci, M., Interno, V. and Silvestris, F. Revisiting the Role of Exosomes in Colorectal Cancer: Where Are We Now? *Front Oncol* **9**, 521, doi:10.3389/fonc.2019.00521 (2019).

53. Nedaeinia, R., Manian, M., Jazayeri, M. H., Ranjbar, M., Salehi, R., Sharifi, M., Mohaghegh, F., Goli, M., Jahednia, S. H., Avan, A. and Ghayour-Mobarhan, M. Circulating exosomes and exosomal microRNAs as biomarkers in gastrointestinal cancer. *Cancer Gene Ther* **24**, 48-56, doi:10.1038/cgt.2016.77 (2017).

54. Erreni, M., Mantovani, A. and Allavena, P. Tumor-associated Macrophages (TAM) and Inflammation in Colorectal Cancer. *Cancer Microenviron* **4**, 141-54, doi:10.1007/s12307-010-0052-5 (2011).

55. Lan, J., Sun, L., Xu, F., Liu, L., Hu, F., Song, D., Hou, Z., Wu, W., Luo, X., Wang, J., Yuan, X., Hu, J. and Wang, G. M2 Macrophage-Derived Exosomes Promote Cell Migration and Invasion in Colon Cancer. *Cancer Res* **79**, 146-158, doi:10.1158/0008-5472.CAN-18-0014 (2019).

56. Cao, L., Xu, H., Wang, G., Liu, M., Tian, D. and Yuan, Z. Extracellular vesicles derived from bone marrow mesenchymal stem cells attenuate dextran sodium sulfate-induced ulcerative colitis by promoting M2 macrophage polarization. *Int Immunopharmacol* **72**, 264-274, doi:10.1016/j.intimp.2019.04.020 (2019).

57. Delfini, M., Stakenborg, N., Viola, M. F. and Boeckxstaens, G. Macrophages in the gut: Masters in multitasking. *Immunity* **55**, 1530-1548, doi:10.1016/j.immuni.2022.08.005 (2022).

58. Zhang, M., Li, X., Zhang, Q., Yang, J. and Liu, G. Roles of macrophages on ulcerative colitis and colitis-associated colorectal cancer. *Front Immunol* **14**, 1103617, doi:10.3389/fimmu.2023.1103617 (2023).

59. Shapouri-Moghaddam, A., Mohammadian, S., Vazini, H., Taghadosi, M., Esmaeili, S. A., Mardani, F., Seifi, B., Mohammadi, A., Afshari, J. T. and Sahebkar, A. Macrophage plasticity, polarization, and function in health and disease. *J Cell Physiol* **233**, 6425-6440, doi:10.1002/jcp.26429 (2018).

60. Francescone, R., Hou, V. and Grivennikov, S. I. Cytokines, IBD, and colitis-associated cancer. *Inflamm Bowel Dis* **21**, 409-18, doi:10.1097/MIB.0000000000000236 (2015).

61. Wei, M., Gao, X., Liu, L., Li, Z., Wan, Z., Dong, Y., Chen, X., Niu, Y., Zhang, J. and Yang, G. Visceral Adipose Tissue Derived Exosomes Exacerbate Colitis Severity via Pro-inflammatory MiRNAs in High Fat Diet Fed Mice. *ACS Nano* **14**, 5099-5110, doi:10.1021/acsnano.0c01860 (2020).

62. An, J. H., Li, Q., Ryu, M. O., Nam, A. R., Bhang, D. H., Jung, Y. C., Song, W. J. and Youn, H. Y. TSG-6 in extracellular vesicles from canine mesenchymal stem/stromal is a major factor in relieving DSS-induced colitis. *PLoS One* **15**, e0220756, doi:10.1371/journal.pone.0220756 (2020).

63. Tu, F., Wang, X., Zhang, X., Ha, T., Wang, Y., Fan, M., Yang, K., Gill, P. S., Ozment, T. R., Dai, Y., Liu, L., Williams, D. L. and Li, C. Novel Role of Endothelial Derived Exosomal HSPA12B in Regulating Macrophage Inflammatory Responses in Polymicrobial Sepsis. *Front Immunol* **11**, 825, doi:10.3389/fimmu.2020.00825 (2020).

64. Shinohara, H., Kuranaga, Y., Kumazaki, M., Sugito, N., Yoshikawa, Y., Takai, T., Taniguchi, K., Ito, Y. and Akao, Y. Regulated Polarization of Tumor-Associated Macrophages by miR-145 via Colorectal Cancer-Derived Extracellular Vesicles. *J Immunol* **199**, 1505-1515, doi:10.4049/jimmunol.1700167 (2017).

65. Yin, Y., Liu, B., Cao, Y., Yao, S., Liu, Y., Jin, G., Qin, Y., Chen, Y., Cui, K., Zhou, L., Bian, Z., Fei, B., Huang, S. and Huang, Z. Colorectal Cancer-Derived Small Extracellular Vesicles Promote Tumor Immune Evasion by Upregulating PD-L1 Expression in Tumor-Associated Macrophages. *Adv Sci (Weinh)* **9**, 2102620, doi:10.1002/advs.202102620 (2022).

66. Kim, S. Y., Park, S., Kim, S. and Ko, J. CD133-containing microvesicles promote cancer progression by inducing M2-like tumor-associated macrophage polarization in the tumor microenvironment of colorectal cancer. *Carcinogenesis* **45**, 300-310, doi:10.1093/carcin/bgad093 (2024).

67. Bhatta, B., Luz, I., Krueger, C., Teo, F. X., Lane, D. P., Sabapathy, K. and Cooks, T. Cancer Cells Shuttle Extracellular Vesicles Containing Oncogenic Mutant p53 Proteins to the Tumor Microenvironment. *Cancers (Basel)* **13**, doi:10.3390/cancers13122985 (2021).

68. Popena, I., Abols, A., Saulite, L., Pleiko, K., Zandberga, E., Jekabsons, K., Endzelins, E., Llorente, A., Line, A. and Riekstina, U. Effect of colorectal cancer-derived extracellular vesicles on the immunophenotype and cytokine secretion profile of monocytes and macrophages. *Cell Commun Signal* **16**, 17, doi:10.1186/s12964-018-0229-y (2018).

69. Cianciaruso, C., Beltraminelli, T., Duval, F., Nassiri, S., Hamelin, R., Mozes, A., Gallart-Ayala, H., Ceada Torres, G., Torchia, B., Ries, C. H., Ivanisevic, J. and De Palma, M. Molecular Profiling and Functional Analysis of Macrophage-Derived Tumor Extracellular Vesicles. *Cell Rep* **27**, 3062-3080 e11, doi:10.1016/j.celrep.2019.05.008 (2019).

70. Zhou, J., Li, X., Wu, X., Zhang, T., Zhu, Q., Wang, X., Wang, H., Wang, K., Lin, Y. and Wang, X. Exosomes Released from Tumor-Associated Macrophages Transfer miRNAs That Induce a Treg/Th17 Cell Imbalance in Epithelial Ovarian Cancer. *Cancer Immunol Res* **6**, 1578-1592, doi:10.1158/2326-6066.CIR-17-0479 (2018).

71. Yin, Z., Ma, T., Huang, B., Lin, L., Zhou, Y., Yan, J., Zou, Y. and Chen, S. Macrophage-derived exosomal microRNA-501-3p promotes progression of pancreatic ductal adenocarcinoma through the TGFBR3-mediated TGF-beta signaling pathway. *J Exp Clin Cancer Res* **38**, 310, doi:10.1186/s13046-019-1313-x (2019).

72. Zhu, X., Shen, H., Yin, X., Yang, M., Wei, H., Chen, Q., Feng, F., Liu, Y., Xu, W. and Li, Y. Macrophages derived exosomes deliver miR-223 to epithelial ovarian cancer cells to elicit a chemoresistant phenotype. *J Exp Clin Cancer Res* **38**, 81, doi:10.1186/s13046-019-1095-1 (2019).

73. Wang, Y. X., Lin, C., Cui, L. J., Deng, T. Z., Li, Q. M., Chen, F. Y. and Miao, X. P. Mechanism of M2 macrophage-derived extracellular vesicles carrying lncRNA MEG3 in inflammatory responses in ulcerative colitis. *Bioengineered* **12**, 12722-12739, doi:10.1080/21655979.2021.2010368 (2021).

74. Li, C. J., Liu, Y., Chen, Y., Yu, D., Williams, K. J. and Liu, M. L. Novel proteolytic microvesicles released from human macrophages after exposure to tobacco smoke. *Am J Pathol* **182**, 1552-62, doi:10.1016/j.ajpath.2013.01.035 (2013).

75. Guo, J., Wang, X., Guo, Q., Zhu, S., Li, P., Zhang, S. and Min, L. M2 Macrophage Derived Extracellular Vesicle-Mediated Transfer of MiR-186-5p Promotes Colon Cancer Progression by Targeting DLC1. *Int J Biol Sci* **18**, 1663-1676, doi:10.7150/ijbs.69405 (2022).

76. Reales-Calderon, J. A., Vaz, C., Monteoliva, L., Molero, G. and Gil, C. Candida albicans Modifies the Protein Composition and Size Distribution of THP-1 Macrophage-Derived Extracellular Vesicles. *J Proteome Res* **16**, 87-105, doi:10.1021/acs.jproteome.6b00605 (2017).

77. Esser, J., Gehrmann, U., D'Alexandri, F. L., Hidalgo-Estevez, A. M., Wheelock, C. E., Scheynius, A., Gabrielsson, S. and Radmark, O. Exosomes from human macrophages and dendritic cells contain enzymes for leukotriene biosynthesis and promote granulocyte migration. *J Allergy Clin Immunol* **126**, 1032-40, 1040 e1-4, doi:10.1016/j.jaci.2010.06.039 (2010).

78. Sjölander, A. Leukotrienes. *Encyclopedia of Cancer* 1672–1674, (2009).

79. de Carvalho, T. G., Lara, P., Jorquera-Cordero, C., Aragao, C. F. S., de Santana Oliveira, A., Garcia, V. B., de Paiva Souza, S. V., Schomann, T., Soares, L. A. L., da Matta Guedes, P. M. and de Araujo Junior, R. F. Inhibition of murine colorectal cancer metastasis by targeting M2-TAM through STAT3/NF-kB/AKT signaling using macrophage 1-derived extracellular vesicles loaded with oxaliplatin, retinoic acid, and Libidibia ferrea. *Biomed Pharmacother* **168**, 115663, doi:10.1016/j.biopha.2023.115663 (2023).

80. Li, Q., Yuan, M., Jiao, X., Huang, Y., Li, J., Li, D., Ji, M. and Wang, G. M1 Macrophage-Derived Nanovesicles Repolarize M2 Macrophages for Inhibiting the Development of Endometriosis. *Front Immunol* **12**, 707784, doi:10.3389/fimmu.2021.707784 (2021).

81. Vakili, S., Ahooyi, T. M., Yarandi, S. S., Donadoni, M., Rappaport, J. and Sariyer, I. K. Molecular and Cellular Impact of Inflammatory Extracellular Vesicles (EVs) Derived from M1 and M2 Macrophages on Neural Action Potentials. *Brain Sci* **10**, doi:10.3390/brainsci10070424 (2020).

82. Saleh, N. A., Rode, M. P., Cisilotto, J., Silva, A. H., Prigol, A. N., da Luz Efe, F., Winter, E., Filippin-Monteiro, F. B. and Creczynski-Pasa, T. B. MicroRNA-Mediated Antiproliferative Effects of M1 Macrophage-Derived Extracellular Vesicles on Melanoma Cells. *Immunol Invest* **53**, 70-89, doi:10.1080/08820139.2023.2278774 (2024).

83. Ding, J., Zhang, Y., Cai, X., Zhang, Y., Yan, S., Wang, J., Zhang, S., Yin, T., Yang, C. and Yang, J. Extracellular vesicles derived from M1 macrophages deliver miR-146a-5p and miR-146b-5p to suppress trophoblast migration and invasion by targeting TRAF6 in recurrent spontaneous abortion. *Theranostics* **11**, 5813-5830, doi:10.7150/thno.58731 (2021).

84. Peng, S., Yan, Y., Li, R., Dai, H. and Xu, J. Extracellular vesicles from M1-polarized macrophages promote inflammation in the temporomandibular joint via miR-1246 activation of the Wnt/beta-catenin pathway. *Ann N Y Acad Sci* **1503**, 48-59, doi:10.1111/nyas.14590 (2021).

85. Chen, G., Wang, Z., Wang, D., Qiu, C., Liu, M., Chen, X., Zhang, Q., Yan, G. and Cui, Q. LncRNADisease: a database for long-non-coding RNA-associated diseases. *Nucleic Acids Res* **41**, D983-6, doi:10.1093/nar/gks1099 (2013).

86. Chen, B., Luo, L., Wei, X., Gong, D., Li, Z., Li, S., Tang, W. and Jin, L. M1 Bone Marrow-Derived Macrophage-Derived Extracellular Vesicles Inhibit Angiogenesis and Myocardial Regeneration Following Myocardial Infarction via the MALAT1/MicroRNA-25-3p/CDC42 Axis. *Oxid Med Cell Longev* **2021**, 9959746, doi:10.1155/2021/9959746 (2021).

87. Zhang, X., Hamblin, M. H. and Yin, K. J. The long noncoding RNA Malat1: Its physiological and pathophysiological functions. *RNA Biol* **14**, 1705-1714, doi:10.1080/15476286.2017.1358347 (2017).

88. Ji, Q., Liu, X., Fu, X., Zhang, L., Sui, H., Zhou, L., Sun, J., Cai, J., Qin, J., Ren, J. and Li, Q. Resveratrol inhibits invasion and metastasis of colorectal cancer cells via MALAT1 mediated Wnt/beta-catenin signal pathway. *PLoS One* **8**, e78700, doi:10.1371/journal.pone.0078700 (2013).

89. Zheng, H. T., Shi, D. B., Wang, Y. W., Li, X. X., Xu, Y., Tripathi, P., Gu, W. L., Cai, G. X. and Cai, S. J. High expression of lncRNA MALAT1 suggests a biomarker of poor prognosis in colorectal cancer. *Int J Clin Exp Pathol* **7**, 3174-81, (2014).

90. Pantazi, P., Clements, T., Veno, M., Abrahams, V. M. and Holder, B. Distinct non-coding RNA cargo of extracellular vesicles from M1 and M2 human primary macrophages. *J Extracell Vesicles* **11**, e12293, doi:10.1002/jev2.12293 (2022).

91. Kang, M., Huang, C. C., Lu, Y., Shirazi, S., Gajendrareddy, P., Ravindran, S. and Cooper, L. F. Bone regeneration is mediated by macrophage extracellular vesicles. *Bone* **141**, 115627, doi:10.1016/j.bone.2020.115627 (2020).

92. Liu, S., Chen, J., Shi, J., Zhou, W., Wang, L., Fang, W., Zhong, Y., Chen, X., Chen, Y., Sabri, A. and Liu, S. M1-like macrophage-derived exosomes suppress angiogenesis and exacerbate cardiac

dysfunction in a myocardial infarction microenvironment. *Basic Res Cardiol* **115**, 22, doi:10.1007/s00395-020-0781-7 (2020).

93. Cao, H., Huang, S., Liu, A. and Chen, Z. Up-regulated expression of miR-155 in human colonic cancer. *J Cancer Res Ther* **14**, 604-607, doi:10.4103/0973-1482.175432 (2018).

94. Wang, Z., Zhu, H., Shi, H., Zhao, H., Gao, R., Weng, X., Liu, R., Li, X., Zou, Y., Hu, K., Sun, A. and Ge, J. Exosomes derived from M1 macrophages aggravate neointimal hyperplasia following carotid artery injuries in mice through miR-222/CDKN1B/CDKN1C pathway. *Cell Death Dis* **10**, 422, doi:10.1038/s41419-019-1667-1 (2019).

95. Luo, F., Zhou, J., Wang, S., Sun, Z., Han, Q. and Bai, C. microRNA-222 promotes colorectal cancer cell migration and invasion by targeting MST3. *FEBS Open Bio* **9**, 901-913, doi:10.1002/2211-5463.12623 (2019).

96. Fukata, M., Hernandez, Y., Conduah, D., Cohen, J., Chen, A., Breglio, K., Goo, T., Hsu, D., Xu, R. and Abreu, M. T. Innate immune signaling by Toll-like receptor-4 (TLR4) shapes the inflammatory microenvironment in colitis-associated tumors. *Inflamm Bowel Dis* **15**, 997-1006, doi:10.1002/ibd.20880 (2009).

97. Pastille, E., Fassnacht, T., Adamczyk, A., Ngo Thi Phuong, N., Buer, J. and Westendorf, A. M. Inhibition of TLR4 Signaling Impedes Tumor Growth in Colitis-Associated Colon Cancer. *Front Immunol* **12**, 669747, doi:10.3389/fimmu.2021.669747 (2021).

98. Tong, L., Hao, H., Zhang, Z., Lv, Y., Liang, X., Liu, Q., Liu, T., Gong, P., Zhang, L., Cao, F., Pastorin, G., Lee, C. N., Chen, X., Wang, J. W. and Yi, H. Milk-derived extracellular vesicles alleviate ulcerative colitis by regulating the gut immunity and reshaping the gut microbiota. *Theranostics* **11**, 8570-8586, doi:10.7150/thno.62046 (2021).

99. Caradonna, L., Amati, L., Magrone, T., Pellegrino, N. M., Jirillo, E. and Caccavo, D. Enteric bacteria, lipopolysaccharides and related cytokines in inflammatory bowel disease: biological and clinical significance. *J Endotoxin Res* **6**, 205-14, (2000).

100. Waldner, M. J. and Neurath, M. F. Mechanisms of Immune Signaling in Colitis-Associated Cancer. *Cell Mol Gastroenterol Hepatol* **1**, 6-16, doi:10.1016/j.jcmgh.2014.11.006 (2015).

101. Dixson, A. C., Dawson, T. R., Di Vizio, D. and Weaver, A. M. Context-specific regulation of extracellular vesicle biogenesis and cargo selection. *Nat Rev Mol Cell Biol* **24**, 454-476, doi:10.1038/s41580-023-00576-0 (2023).

102. Yang, H., Mirsepasi-Lauridsen, H. C., Struve, C., Allaire, J. M., Sivignon, A., Vogl, W., Bosman, E. S., Ma, C., Fotovati, A., Reid, G. S., Li, X., Petersen, A. M., Gouin, S. G., Barnich, N., Jacobson, K., Yu, H. B., Krogfelt, K. A. and Vallance, B. A. Ulcerative Colitis-associated E. coli pathobionts potentiate colitis in susceptible hosts. *Gut Microbes* **12**, 1847976, doi:10.1080/19490976.2020.1847976 (2020).

103. Lorenz, E., Patel, D. D., Hartung, T. and Schwartz, D. A. Toll-like receptor 4 (TLR4)-deficient murine macrophage cell line as an in vitro assay system to show TLR4-independent signaling of Bacteroides fragilis lipopolysaccharide. *Infect Immun* **70**, 4892-6, doi:10.1128/IAI.70.9.4892-4896.2002 (2002).

104. Maduka, C. V., Alhaj, M., Ural, E., Habeeb, O. M., Kuhnert, M. M., Smith, K., Makela, A. V., Pope, H., Chen, S., Hix, J. M., Mallett, C. L., Chung, S. J., Hakun, M., Tundo, A., Zinn, K. R., Hankenson, K. D., Goodman, S. B., Narayan, R. and Contag, C. H. Polylactide Degradation Activates Immune Cells

by Metabolic Reprogramming. *Advanced Science* **10**, e2304632, doi:10.1002/advs.202304632 (2023).

105. Zhang, X., Goncalves, R. and Mosser, D. M. The isolation and characterization of murine macrophages. *Curr Protoc Immunol* **Chapter 14**, 14 1 1-14 1 14, doi:10.1002/0471142735.im1401s83 (2008).

106. De Nardo, D., Kalvakolanu, D. V. and Latz, E. Immortalization of Murine Bone Marrow-Derived Macrophages. *Methods Mol Biol* **1784**, 35-49, doi:10.1007/978-1-4939-7837-3_4 (2018).

107. Liu, J., Xiang, J., Jin, C., Ye, L., Wang, L., Gao, Y., Lv, N., Zhang, J., You, F., Qiao, H. and Shi, L. Medicinal plant-derived mtDNA via nanovesicles induces the cGAS-STING pathway to remold tumor-associated macrophages for tumor regression. *J Nanobiotechnology* **21**, 78, doi:10.1186/s12951-023-01835-0 (2023).

108. Suh, N., Honda, T., Finlay, H. J., Barchowsky, A., Williams, C., Benoit, N. E., Xie, Q. W., Nathan, C., Gribble, G. W. and Sporn, M. B. Novel triterpenoids suppress inducible nitric oxide synthase (iNOS) and inducible cyclooxygenase (COX-2) in mouse macrophages. *Cancer Res* **58**, 717-23, (1998).

109. Thery, C., Amigorena, S., Raposo, G. and Clayton, A. Isolation and characterization of exosomes from cell culture supernatants and biological fluids. *Curr Protoc Cell Biol* **Chapter 3**, Unit 3 22, doi:10.1002/0471143030.cb0322s30 (2006).

110. Shang, J. and Gao, X. Nanoparticle counting: towards accurate determination of the molar concentration. *Chem Soc Rev* **43**, 7267-78, doi:10.1039/c4cs00128a (2014).

111. Kanada, M., Kim, B. D., Hardy, J. W., Ronald, J. A., Bachmann, M. H., Bernard, M. P., Perez, G. I., Zarea, A. A., Ge, T. J., Withrow, A., Ibrahim, S. A., Toomajian, V., Gambhir, S. S., Paulmurugan, R. and Contag, C. H. Microvesicle-Mediated Delivery of Minicircle DNA Results in Effective Gene-Directed Enzyme Prodrug Cancer Therapy. *Mol Cancer Ther* **18**, 2331-2342, doi:10.1158/1535-7163.MCT-19-0299 (2019).

112. Humphrey, S. J., Karayel, O., James, D. E. and Mann, M. High-throughput and high-sensitivity phosphoproteomics with the EasyPhos platform. *Nat Protoc* **13**, 1897-1916, doi:10.1038/s41596-018-0014-9 (2018).

113. Masuda, T., Tomita, M. and Ishihama, Y. Phase transfer surfactant-aided trypsin digestion for membrane proteome analysis. *J Proteome Res* **7**, 731-40, doi:10.1021/pr700658q (2008).

114. Rappsilber, J., Mann, M. and Ishihama, Y. Protocol for micro-purification, enrichment, pre-fractionation and storage of peptides for proteomics using StageTips. *Nat Protoc* **2**, 1896-906, doi:10.1038/nprot.2007.261 (2007).

115. Wisniewski, J. R., Zougman, A., Nagaraj, N. and Mann, M. Universal sample preparation method for proteome analysis. *Nat Methods* **6**, 359-62, doi:10.1038/nmeth.1322 (2009).

116. Cox, J. and Mann, M. MaxQuant enables high peptide identification rates, individualized p.p.b.-range mass accuracies and proteome-wide protein quantification. *Nat Biotechnol* **26**, 1367-72, doi:10.1038/nbt.1511 (2008).

117. Humphrey, S. J., Azimifar, S. B. and Mann, M. High-throughput phosphoproteomics reveals in vivo insulin signaling dynamics. *Nat Biotechnol* **33**, 990-5, doi:10.1038/nbt.3327 (2015).

118. Cox, J., Neuhauser, N., Michalski, A., Scheltema, R. A., Olsen, J. V. and Mann, M. Andromeda: a peptide search engine integrated into the MaxQuant environment. *J Proteome Res* **10**, 1794-805, doi:10.1021/pr101065j (2011).

119. Rashidian, A., Muhammadnejad, A., Dehpour, A. R., Mehr, S. E., Akhavan, M. M., Shirkoohi, R., Chamanara, M., Mousavi, S. E. and Rezayat, S. M. Atorvastatin attenuates TNBS-induced rat colitis: the involvement of the TLR4/NF-kB signaling pathway. *Inflammopharmacology* **24**, 109-18, doi:10.1007/s10787-016-0263-6 (2016).

120. Ruckdeschel, K. and Richter, K. Lipopolysaccharide desensitization of macrophages provides protection against Yersinia enterocolitica-induced apoptosis. *Infect Immun* **70**, 5259-64, doi:10.1128/IAI.70.9.5259-5264.2002 (2002).

121. Cohly, H., Stephens, J., Markhov, A., Angel, M., Campbell, W., Ndebele, K. and Jenkins, J. Cell culture conditions affect LPS inducibility of the inflammatory mediators in J774A.1 murine macrophages. *Immunol Invest* **30**, 1-15, doi:10.1081/imm-100103686 (2001).

122. Thery, C., Witwer, K. W., Aikawa, E., Alcaraz, M. J., Anderson, J. D., Andriantsitohaina, R., Antoniou, A., Arab, T., Archer, F., Atkin-Smith, G. K., Ayre, D. C., Bach, J. M., Bachurski, D., Baharvand, H., Balaj, L., Baldacchino, S., Bauer, N. N., Baxter, A. A., Bebawy, M., Beckham, C., Bedina Zavec, A., Benmoussa, A., Berardi, A. C., Bergese, P., Bielska, E., Blenkiron, C., Bobis-Wozowicz, S., Boilard, E., Boireau, W., Bongiovanni, A., Borras, F. E., Bosch, S., Boulanger, C. M., Breakefield, X., Breglio, A. M., Brennan, M. A., Brigstock, D. R., Brisson, A., Broekman, M. L., Bromberg, J. F., Bryl-Gorecka, P., Buch, S., Buck, A. H., Burger, D., Busatto, S., Buschmann, D., Bussolati, B., Buzas, E. I., Byrd, J. B., Camussi, G., Carter, D. R., Caruso, S., Chamley, L. W., Chang, Y. T., Chen, C., Chen, S., Cheng, L., Chin, A. R., Clayton, A., Clerici, S. P., Cocks, A., Cocucci, E., Coffey, R. J., Cordeiro-da-Silva, A., Couch, Y., Coumans, F. A., Coyle, B., Crescitelli, R., Criado, M. F., D'Souza-Schorey, C., Das, S., Datta Chaudhuri, A., de Candia, P., De Santana, E. F., De Wever, O., Del Portillo, H. A., Demaret, T., Deville, S., Devitt, A., Dhondt, B., Di Vizio, D., Dieterich, L. C., Dolo, V., Dominguez Rubio, A. P., Dominici, M., Dourado, M. R., Driedonks, T. A., Duarte, F. V., Duncan, H. M., Eichenberger, R. M., Ekstrom, K., El Andaloussi, S., Elie-Caille, C., Erdbrugger, U., Falcon-Perez, J. M., Fatima, F., Fish, J. E., Flores-Bellver, M., Forsonits, A., Frelet-Barrand, A., Fricke, F., Fuhrmann, G., Gabrielsson, S., Gamez-Valero, A., Gardiner, C., Gartner, K., Gaudin, R., Gho, Y. S., Giebel, B., Gilbert, C., Gimona, M., Giusti, I., Goberdhan, D. C., Gorgens, A., Gorski, S. M., Greening, D. W., Gross, J. C., Gualerzi, A., Gupta, G. N., Gustafson, D., Handberg, A., Haraszti, R. A., Harrison, P., Hegyesi, H., Hendrix, A., Hill, A. F., Hochberg, F. H., Hoffmann, K. F., Holder, B., Holthofer, H., Hosseinkhani, B., Hu, G., Huang, Y., Huber, V., Hunt, S., Ibrahim, A. G., Ikezu, T., Inal, J. M., Isin, M., Ivanova, A., Jackson, H. K., Jacobsen, S., Jay, S. M., Jayachandran, M., Jenster, G., Jiang, L., Johnson, S. M., Jones, J. C., Jong, A., Jovanovic-Talisman, T., Jung, S., Kalluri, R., Kano, S. I., Kaur, S., Kawamura, Y., Keller, E. T., Khamari, D., Khomyakova, E., Khvorova, A., Kierulf, P., Kim, K. P., Kislinger, T., Klingeborn, M., Klinke, D. J., 2nd, Kornek, M., Kosanovic, M. M., Kovacs, A. F., Kramer-Albers, E. M., Krasemann, S., Krause, M., Kurochkin, I. V., Kusuma, G. D., Kuypers, S., Laitinen, S., Langevin, S. M., Languino, L. R., Lannigan, J., Lasser, C., Laurent, L. C., Lavieu, G., Lazaro-Ibanez, E., Le Lay, S., Lee, M. S., Lee, Y. X. F., Lemos, D. S., Lenassi, M., Leszczynska, A., Li, I. T., Liao, K., Libregts, S. F., Ligeti, E., Lim, R., Lim, S. K., Line, A., Linnemannstons, K., Llorente, A., Lombard, C. A., Lorenowicz, M. J., Lorincz, A. M., Lotvall, J., Lovett, J., Lowry, M. C., Loyer, X., Lu, Q., Lukomska, B., Lunavat, T. R., Maas, S. L., Malhi, H., Marcilla, A., Mariani, J., Mariscal, J., Martens-Uzunova, E. S., Martin-Jaular, L., Martinez, M. C., Martins, V. R., Mathieu, M., Mathivanan, S., Maugeri, M., McGinnis, L. K., McVey, M. J., Meckes, D. G., Jr., Meehan, K. L., Mertens, I., Minciacchi, V. R., Moller, A., Moller Jorgensen, M., Morales-

Kastresana, A., Morhayim, J., Mullier, F., Muraca, M., Musante, L., Mussack, V., Muth, D. C., Myburgh, K. H., Najrana, T., Nawaz, M., Nazarenko, I., Nejsum, P., Neri, C., Neri, T., Nieuwland, R., Nimrichter, L., Nolan, J. P., Nolte-'t Hoen, E. N., Noren Hooten, N., O'Driscoll, L., O'Grady, T., O'Loghlen, A., Ochiya, T., Olivier, M., Ortiz, A., Ortiz, L. A., Osteikoetxea, X., Ostergaard, O., Ostrowski, M., Park, J., Pegtel, D. M., Peinado, H., Perut, F., Pfaffl, M. W., Phinney, D. G., Pieters, B. C., Pink, R. C., Pisetsky, D. S., Pogge von Strandmann, E., Polakovicova, I., Poon, I. K., Powell, B. H., Prada, I., Pulliam, L., Quesenberry, P., Radeghieri, A., Raffai, R. L., Raimondo, S., Rak, J., Ramirez, M. I., Raposo, G., Rayyan, M. S., Regev-Rudzki, N., Ricklefs, F. L., Robbins, P. D., Roberts, D. D., Rodrigues, S. C., Rohde, E., Rome, S., Rouschop, K. M., Rughetti, A., Russell, A. E., Saa, P., Sahoo, S., Salas-Huenuleo, E., Sanchez, C., Saugstad, J. A., Saul, M. J., Schiffelers, R. M., Schneider, R., Schoyen, T. H., Scott, A., Shahaj, E., Sharma, S., Shatnyeva, O., Shekari, F., Shelke, G. V., Shetty, A. K., Shiba, K., Siljander, P. R., Silva, A. M., Skowronek, A., Snyder, O. L., 2nd, Soares, R. P., Sodar, B. W., Soekmadji, C., Sotillo, J., Stahl, P. D., Stoorvogel, W., Stott, S. L., Strasser, E. F., Swift, S., Tahara, H., Tewari, M., Timms, K., Tiwari, S., Tixeira, R., Tkach, M., Toh, W. S., Tomasini, R., Torrecilhas, A. C., Tosar, J. P., Toxavidis, V., Urbanelli, L., Vader, P., van Balkom, B. W., van der Grein, S. G., Van Deun, J., van Herwijnen, M. J., Van Keuren-Jensen, K., van Niel, G., van Royen, M. E., van Wijnen, A. J., Vasconcelos, M. H., Vechetti, I. J., Jr., Veit, T. D., Vella, L. J., Velot, E., Verweij, F. J., Vestad, B., Vinas, J. L., Visnovitz, T., Vukman, K. V., Wahlgren, J., Watson, D. C., Wauben, M. H., Weaver, A., Webber, J. P., Weber, V., Wehman, A. M., Weiss, D. J., Welsh, J. A., Wendt, S., Wheelock, A. M., Wiener, Z., Witte, L., Wolfram, J., Xagorari, A., Xander, P., Xu, J., Yan, X., Yanez-Mo, M., Yin, H., Yuana, Y., Zappulli, V., Zarubova, J., Zekas, V., Zhang, J. Y., Zhao, Z., Zheng, L., Zheutlin, A. R., Zickler, A. M., Zimmermann, P., Zivkovic, A. M., Zocco, D. and Zuba-Surma, E. K. Minimal information for studies of extracellular vesicles 2018 (MISEV2018): a position statement of the International Society for Extracellular Vesicles and update of the MISEV2014 guidelines. *J Extracell Vesicles* **7**, 1535750, doi:10.1080/20013078.2018.1535750 (2018).

123. Midekessa, G., Godakumara, K., Ord, J., Viil, J., Lattekivi, F., Dissanayake, K., Kopanchuk, S., Rinken, A., Andronowska, A., Bhattacharjee, S., Rinken, T. and Fazeli, A. Zeta Potential of Extracellular Vesicles: Toward Understanding the Attributes that Determine Colloidal Stability. *ACS Omega* **5**, 16701-16710, doi:10.1021/acsomega.0c01582 (2020).

124. Bachurski, D., Schuldner, M., Nguyen, P. H., Malz, A., Reiners, K. S., Grenzi, P. C., Babatz, F., Schauss, A. C., Hansen, H. P., Hallek, M. and Pogge von Strandmann, E. Extracellular vesicle measurements with nanoparticle tracking analysis - An accuracy and repeatability comparison between NanoSight NS300 and ZetaView. *J Extracell Vesicles* **8**, 1596016, doi:10.1080/20013078.2019.1596016 (2019).

125. Vaughan-Jackson, A., Stodolak, S., Ebrahimi, K. H., Johnson, E., Reardon, P. K., Dupont, M., Zhang, S., McCullagh, J. S. O. and James, W. S. Density dependent regulation of inflammatory responses in macrophages. *Front Immunol* **13**, 895488, doi:10.3389/fimmu.2022.895488 (2022).

126. Daigneault, M., Preston, J. A., Marriott, H. M., Whyte, M. K. and Dockrell, D. H. The identification of markers of macrophage differentiation in PMA-stimulated THP-1 cells and monocyte-derived macrophages. *PLoS One* **5**, e8668, doi:10.1371/journal.pone.0008668 (2010).

127. Genin, M., Clement, F., Fattaccioli, A., Raes, M. and Michiels, C. M1 and M2 macrophages derived from THP-1 cells differentially modulate the response of cancer cells to etoposide. *BMC Cancer* **15**, 577, doi:10.1186/s12885-015-1546-9 (2015).

128. Spera, I., Sanchez-Rodriguez, R., Favia, M., Menga, A., Venegas, F. C., Angioni, R., Munari, F., Lanza, M., Campanella, A., Pierri, C. L., Canton, M. and Castegna, A. The J2-Immortalized Murine Macrophage Cell Line Displays Phenotypical and Metabolic Features of Primary BMDMs in Their M1 and M2 Polarization State. *Cancers (Basel)* **13**, doi:10.3390/cancers13215478 (2021).

129. Xie, D. K., Yao, J., Li, P. H., Zhu, Y. W., Chen, J. N., Cao, X. L., Cheng, S. L., Chen, Y. M., Huang, Y. F., Wang, L., Wang, Z. H., Qiao, R., Ge, J. M., Yue, H., Wei, L., Liu, Z. Y., Han, H., Qin, H. Y. and Zhao, J. L. Phenotypic comparison and the potential antitumor function of immortalized bone marrow-derived macrophages (iBMDMs). *Front Immunol* **15**, 1379853, doi:10.3389/fimmu.2024.1379853 (2024).

130. Kowal, J., Arras, G., Colombo, M., Jouve, M., Morath, J. P., Primdal-Bengtson, B., Dingli, F., Loew, D., Tkach, M. and Thery, C. Proteomic comparison defines novel markers to characterize heterogeneous populations of extracellular vesicle subtypes. *Proc Natl Acad Sci U S A* **113**, E968-77, doi:10.1073/pnas.1521230113 (2016).

131. Siri, S., Maier, F., Chen, L., Santos, S., Pierce, D. M. and Feng, B. Differential biomechanical properties of mouse distal colon and rectum innervated by the splanchnic and pelvic afferents. *Am J Physiol Gastrointest Liver Physiol* **316**, G473-G481, doi:10.1152/ajpgi.00324.2018 (2019).

132. Hamam, D., Abdouh, M., Gao, Z. H., Arena, V., Arena, M. and Arena, G. O. Transfer of malignant trait to BRCA1 deficient human fibroblasts following exposure to serum of cancer patients. *J Exp Clin Cancer Res* **35**, 80, doi:10.1186/s13046-016-0360-9 (2016).

133. Abdouh, M., Floris, M., Gao, Z. H., Arena, V., Arena, M. and Arena, G. O. Colorectal cancer-derived extracellular vesicles induce transformation of fibroblasts into colon carcinoma cells. *J Exp Clin Cancer Res* **38**, 257, doi:10.1186/s13046-019-1248-2 (2019).

134. Harmsen, S., Rogalla, S., Huang, R., Spaliviero, M., Neuschmelting, V., Hayakawa, Y., Lee, Y., Tailor, Y., Toledo-Crow, R., Kang, J. W., Samii, J. M., Karabeber, H., Davis, R. M., White, J. R., van de Rijn, M., Gambhir, S. S., Contag, C. H., Wang, T. C. and Kircher, M. F. Detection of Premalignant Gastrointestinal Lesions Using Surface-Enhanced Resonance Raman Scattering-Nanoparticle Endoscopy. *ACS Nano* **13**, 1354-1364, doi:10.1021/acsnano.8b06808 (2019).

135. Murphy, E. A., Davis, J. M., McClellan, J. L., Gordon, B. T. and Carmichael, M. D. Curcumin's effect on intestinal inflammation and tumorigenesis in the ApcMin/+ mouse. *J Interferon Cytokine Res* **31**, 219-26, doi:10.1089/jir.2010.0051 (2011).

136. Kuhl, A. A., Erben, U., Kredel, L. I. and Siegmund, B. Diversity of Intestinal Macrophages in Inflammatory Bowel Diseases. *Front Immunol* **6**, 613, doi:10.3389/fimmu.2015.00613 (2015).

137. El-Zayat, S. R., Sibaii, H. and Mannaa, F. A. Toll-like receptors activation, signaling, and targeting: an overview. *Bulletin of the National Research Centre* **43, 187**, doi:10.1186/s42269-019-0227-2 (2019).

138. Zhang, L., Wei, X., Zhang, R., Si, D., Petitte, J. N., Ahmad, B. and Zhang, M. A Novel Peptide Ameliorates LPS-Induced Intestinal Inflammation and Mucosal Barrier Damage via Its Antioxidant and Antiendotoxin Effects. *Int J Mol Sci* **20**, doi:10.3390/ijms20163974 (2019).

139. Li, Q., von Ehrlich-Treuenstatt, V., Schardey, J., Wirth, U., Zimmermann, P., Andrassy, J., Bazhin, A. V., Werner, J. and Kuhn, F. Gut Barrier Dysfunction and Bacterial Lipopolysaccharides in Colorectal Cancer. *J Gastrointest Surg* **27**, 1466-1472, doi:10.1007/s11605-023-05654-4 (2023).

140. Fukata, M., Chen, A., Vamadevan, A. S., Cohen, J., Breglio, K., Krishnareddy, S., Hsu, D., Xu, R., Harpaz, N., Dannenberg, A. J., Subbaramaiah, K., Cooper, H. S., Itzkowitz, S. H. and Abreu, M. T. Toll-like receptor-4 promotes the development of colitis-associated colorectal tumors. *Gastroenterology* **133**, 1869-81, doi:10.1053/j.gastro.2007.09.008 (2007).

141. Rafa, H., Benkhelifa, S., AitYounes, S., Saoula, H., Belhadef, S., Belkhelfa, M., Boukercha, A., Toumi, R., Soufli, I., Morales, O., de Launoit, Y., Mahfouf, H., Nakmouche, M., Delhem, N. and Touil-Boukoffa, C. All-Trans Retinoic Acid Modulates TLR4/NF-kappaB Signaling Pathway Targeting TNF-alpha and Nitric Oxide Synthase 2 Expression in Colonic Mucosa during Ulcerative Colitis and Colitis Associated Cancer. *Mediators Inflamm* **2017**, 7353252, doi:10.1155/2017/7353252 (2017).

142. Murray, P. J. and Smale, S. T. Restraint of inflammatory signaling by interdependent strata of negative regulatory pathways. *Nat Immunol* **13**, 916-24, doi:10.1038/ni.2391 (2012).

143. Fukata, M., Chen, A., Klepper, A., Krishnareddy, S., Vamadevan, A. S., Thomas, L. S., Xu, R., Inoue, H., Arditi, M., Dannenberg, A. J. and Abreu, M. T. Cox-2 is regulated by Toll-like receptor-4 (TLR4) signaling: Role in proliferation and apoptosis in the intestine. *Gastroenterology* **131**, 862-77, doi:10.1053/j.gastro.2006.06.017 (2006).

144. De Benedetti, F., Prencipe, G., Bracaglia, C., Marasco, E. and Grom, A. A. Targeting interferon-gamma in hyperinflammation: opportunities and challenges. *Nat Rev Rheumatol* **17**, 678-691, doi:10.1038/s41584-021-00694-z (2021).

145. Ito, R., Shin-Ya, M., Kishida, T., Urano, A., Takada, R., Sakagami, J., Imanishi, J., Kita, M., Ueda, Y., Iwakura, Y., Kataoka, K., Okanoue, T. and Mazda, O. Interferon-gamma is causatively involved in experimental inflammatory bowel disease in mice. *Clin Exp Immunol* **146**, 330-8, doi:10.1111/j.1365-2249.2006.03214.x (2006).

146. Lee, J. Y. and Sullivan, K. E. Gamma interferon and lipopolysaccharide interact at the level of transcription to induce tumor necrosis factor alpha expression. *Infect Immun* **69**, 2847-52, doi:10.1128/IAI.69.5.2847-2852.2001 (2001).

147. Held, T. K., Weihua, X., Yuan, L., Kalvakolanu, D. V. and Cross, A. S. Gamma interferon augments macrophage activation by lipopolysaccharide by two distinct mechanisms, at the signal transduction level and via an autocrine mechanism involving tumor necrosis factor alpha and interleukin-1. *Infect Immun* **67**, 206-12, doi:10.1128/IAI.67.1.206-212.1999 (1999).

148. Kang, K., Bachu, M., Park, S. H., Kang, K., Bae, S., Park-Min, K. H. and Ivashkiv, L. B. IFN-gamma selectively suppresses a subset of TLR4-activated genes and enhancers to potentiate macrophage activation. *Nat Commun* **10**, 3320, doi:10.1038/s41467-019-11147-3 (2019).

149. Sun, N. and Zhao, X. Argininosuccinate synthase 1, arginine deprivation therapy and cancer management. *Front Pharmacol* **13**, 935553, doi:10.3389/fphar.2022.935553 (2022).

150. van der Meer, J. H. M., de Boer, R. J., Meijer, B. J., Smit, W. L., Vermeulen, J. L. M., Meisner, S., van Roest, M., Koelink, P. J., Dekker, E., Hakvoort, T. B. M., Koster, J., Hawinkels, L., Heijmans, J., Struijs, E. A., Boermeester, M. A., van den Brink, G. R. and Muncan, V. Epithelial argininosuccinate synthetase is dispensable for intestinal regeneration and tumorigenesis. *Cell Death Dis* **12**, 897, doi:10.1038/s41419-021-04173-x (2021).

151. Bateman, L. A., Ku, W. M., Heslin, M. J., Contreras, C. M., Skibola, C. F. and Nomura, D. K. Argininosuccinate Synthase 1 is a Metabolic Regulator of Colorectal Cancer Pathogenicity. *ACS Chem Biol* **12**, 905-911, doi:10.1021/acschembio.6b01158 (2017).

152. Marti, I. L. A. A. and Reith, W. Arginine-dependent immune responses. *Cell Mol Life Sci* **78**, 5303-5324, doi:10.1007/s00018-021-03828-4 (2021).

153. Wang, H., Wang, L., Xie, Z., Zhou, S., Li, Y., Zhou, Y. and Sun, M. Nitric Oxide (NO) and NO Synthases (NOS)-Based Targeted Therapy for Colon Cancer. *Cancers (Basel)* **12**, doi:10.3390/cancers12071881 (2020).

154. Kolios, G., Valatas, V. and Ward, S. G. Nitric oxide in inflammatory bowel disease: a universal messenger in an unsolved puzzle. *Immunology* **113**, 427-37, doi:10.1111/j.1365-2567.2004.01984.x (2004).

155. Cianchi, F., Cortesini, C., Fantappie, O., Messerini, L., Schiavone, N., Vannacci, A., Nistri, S., Sardi, I., Baroni, G., Marzocca, C., Perna, F., Mazzanti, R., Bechi, P. and Masini, E. Inducible nitric oxide synthase expression in human colorectal cancer: correlation with tumor angiogenesis. *Am J Pathol* **162**, 793-801, doi:10.1016/S0002-9440(10)63876-X (2003).

156. Stettner, N., Rosen, C., Bernshtein, B., Gur-Cohen, S., Frug, J., Silberman, A., Sarver, A., Carmel-Neiderman, N. N., Eilam, R., Biton, I., Pevsner-Fischer, M., Zmora, N., Brandis, A., Bahar Halpern, K., Mazkereth, R., di Bernardo, D., Brunetti-Pierri, N., Premkumar, M. H., Dank, G., Nagamani, S. C. S., Jung, S., Harmelin, A. and Erez, A. Induction of Nitric-Oxide Metabolism in Enterocytes Alleviates Colitis and Inflammation-Associated Colon Cancer. *Cell Rep* **23**, 1962-1976, doi:10.1016/j.celrep.2018.04.053 (2018).

157. Smillie, C. S., Biton, M., Ordovas-Montanes, J., Sullivan, K. M., Burgin, G., Graham, D. B., Herbst, R. H., Rogel, N., Slyper, M., Waldman, J., Sud, M., Andrews, E., Velonias, G., Haber, A. L., Jagadeesh, K., Vickovic, S., Yao, J., Stevens, C., Dionne, D., Nguyen, L. T., Villani, A. C., Hofree, M., Creasey, E. A., Huang, H., Rozenblatt-Rosen, O., Garber, J. J., Khalili, H., Desch, A. N., Daly, M. J., Ananthakrishnan, A. N., Shalek, A. K., Xavier, R. J. and Regev, A. Intra- and Inter-cellular Rewiring of the Human Colon during Ulcerative Colitis. *Cell* **178**, 714-730 e22, doi:10.1016/j.cell.2019.06.029 (2019).

158. Rho, J. H., Qin, S., Wang, J. Y. and Roehrl, M. H. Proteomic expression analysis of surgical human colorectal cancer tissues: up-regulation of PSB7, PRDX1, and SRP9 and hypoxic adaptation in cancer. *J Proteome Res* **7**, 2959-72, doi:10.1021/pr8000892 (2008).

159. Phillips, M. M., Sheaff, M. T. and Szlosarek, P. W. Targeting arginine-dependent cancers with arginine-degrading enzymes: opportunities and challenges. *Cancer Res Treat* **45**, 251-62, doi:10.4143/crt.2013.45.4.251 (2013).

160. Alexandrou, C., Al-Aqbi, S. S., Higgins, J. A., Boyle, W., Karmokar, A., Andreadi, C., Luo, J. L., Moore, D. A., Viskaduraki, M., Blades, M., Murray, G. I., Howells, L. M., Thomas, A., Brown, K., Cheng, P. N. and Rufini, A. Sensitivity of Colorectal Cancer to Arginine Deprivation Therapy is Shaped by Differential Expression of Urea Cycle Enzymes. *Sci Rep* **8**, 12096, doi:10.1038/s41598-018-30591-7 (2018).

161. Delage, B., Fennell, D. A., Nicholson, L., McNeish, I., Lemoine, N. R., Crook, T. and Szlosarek, P. W. Arginine deprivation and argininosuccinate synthetase expression in the treatment of cancer. *Int J Cancer* **126**, 2762-72, doi:10.1002/ijc.25202 (2010).

162. Wang, X., Xiang, H., Toyoshima, Y., Shen, W., Shichi, S., Nakamoto, H., Kimura, S., Sugiyama, K., Homma, S., Miyagi, Y., Taketomi, A. and Kitamura, H. Arginase-1 inhibition reduces migration ability and metastatic colonization of colon cancer cells. *Cancer Metab* **11**, 1, doi:10.1186/s40170-022-00301-z (2023).

163. Phillips, M. and Szlosarek, P. W. Arginine Metabolism and Tumour-Associated Macrophages. *Tumour-Associated Macrophages* 77-90, doi:10.1007/978-1-4614-0662-4_6 (2011).

164. Chen, Z., Li, K., Yin, X., Li, H., Li, Y., Zhang, Q., Wang, H. and Qiu, Y. Lower Expression of Gelsolin in Colon Cancer and Its Diagnostic Value in Colon Cancer Patients. *J Cancer* **10**, 1288-1296, doi:10.7150/jca.28529 (2019).

165. Vitali, R., Palone, F., Armuzzi, A., Fulci, V., Negroni, A., Carissimi, C., Cucchiara, S. and Stronati, L. Proteomic Analysis Identifies Three Reliable Biomarkers of Intestinal Inflammation in the Stools of Patients With Inflammatory Bowel Disease. *J Crohns Colitis* **17**, 92-102, doi:10.1093/ecco-jcc/jjac110 (2023).

166. Gremm, D. and Wegner, A. Gelsolin as a calcium-regulated actin filament-capping protein. *Eur J Biochem* **267**, 4339-45, doi:10.1046/j.1432-1327.2000.01463.x (2000).

167. Li, W. X., Yang, M. X., Hong, X. Q., Dong, T. G., Yi, T., Lin, S. L., Qin, X. Y. and Niu, W. X. Overexpression of gelsolin reduces the proliferation and invasion of colon carcinoma cells. *Mol Med Rep* **14**, 3059-65, doi:10.3892/mmr.2016.5652 (2016).

168. Grivennikov, S., Karin, E., Terzic, J., Mucida, D., Yu, G. Y., Vallabhapurapu, S., Scheller, J., Rose-John, S., Cheroutre, H., Eckmann, L. and Karin, M. IL-6 and Stat3 are required for survival of intestinal epithelial cells and development of colitis-associated cancer. *Cancer Cell* **15**, 103-13, doi:10.1016/j.ccr.2009.01.001 (2009).

169. Han, J. and Theiss, A. L. Stat3: friend or foe in colitis and colitis-associated cancer? *Inflamm Bowel Dis* **20**, 2405-11, doi:10.1097/MIB.0000000000000180 (2014).

170. Wang, H. C., Chen, C. W., Yang, C. L., Tsai, I. M., Hou, Y. C., Chen, C. J. and Shan, Y. S. Tumor-Associated Macrophages Promote Epigenetic Silencing of Gelsolin through DNA Methyltransferase 1 in Gastric Cancer Cells. *Cancer Immunol Res* **5**, 885-897, doi:10.1158/2326-6066.CIR-16-0295 (2017).

171. Hegarty, L. M., Jones, G. R. and Bain, C. C. Macrophages in intestinal homeostasis and inflammatory bowel disease. *Nat Rev Gastroenterol Hepatol* **20**, 538-553, doi:10.1038/s41575-023-00769-0 (2023).

172. Saha, S., Aranda, E., Hayakawa, Y., Bhanja, P., Atay, S., Brodin, N. P., Li, J., Asfaha, S., Liu, L., Tailor, Y., Zhang, J., Godwin, A. K., Tome, W. A., Wang, T. C., Guha, C. and Pollard, J. W. Macrophage-derived extracellular vesicle-packaged WNTs rescue intestinal stem cells and enhance survival after radiation injury. *Nat Commun* **7**, 13096, doi:10.1038/ncomms13096 (2016).

173. Matozaki, T., Kotani, T., Murata, Y. and Saito, Y. Roles of Src family kinase, Ras, and mTOR signaling in intestinal epithelial homeostasis and tumorigenesis. *Cancer Sci* **112**, 16-21, doi:10.1111/cas.14702 (2021).

174. Curran, T., Sun, Z., Gerry, B., Findlay, V. J., Wallace, K., Li, Z., Paulos, C., Ford, M., Rubinstein, M. P., Chung, D. and Camp, E. R. Differential immune signatures in the tumor microenvironment are associated with colon cancer racial disparities. *Cancer Med* **10**, 1805-1814, doi:10.1002/cam4.3753 (2021).

175. Zou, X., Qiao, H., Jiang, X., Dong, X., Jiang, H. and Sun, X. Downregulation of developmentally regulated endothelial cell locus-1 inhibits the growth of colon cancer. *J Biomed Sci* **16**, 33, doi:10.1186/1423-0127-16-33 (2009).

176. Watanabe, T., Kobunai, T., Yamamoto, Y., Ikeuchi, H., Matsuda, K., Ishihara, S., Nozawa, K., Iinuma, H., Kanazawa, T., Tanaka, T., Yokoyama, T., Konishi, T., Eshima, K., Ajioka, Y., Hibi, T., Watanabe, M., Muto, T. and Nagawa, H. Predicting ulcerative colitis-associated colorectal cancer using reverse-transcription polymerase chain reaction analysis. *Clin Colorectal Cancer* **10**, 134-41, doi:10.1016/j.clcc.2011.03.011 (2011).

177. Dosh, R. H., Jordan-Mahy, N., Sammon, C. and Le Maitre, C. Interleukin 1 is a key driver of inflammatory bowel disease-demonstration in a murine IL-1Ra knockout model. *Oncotarget* **10**, 3559-3575, doi:10.18632/oncotarget.26894 (2019).

178. Wang, Y., Wang, K., Han, G. C., Wang, R. X., Xiao, H., Hou, C. M., Guo, R. F., Dou, Y., Shen, B. F., Li, Y. and Chen, G. J. Neutrophil infiltration favors colitis-associated tumorigenesis by activating the interleukin-1 (IL-1)/IL-6 axis. *Mucosal Immunol* **7**, 1106-15, doi:10.1038/mi.2013.126 (2014).

179. Chen, Y., Yang, Z., Deng, B., Wu, D., Quan, Y. and Min, Z. Interleukin 1beta/1RA axis in colorectal cancer regulates tumor invasion, proliferation and apoptosis via autophagy. *Oncol Rep* **43**, 908-918, doi:10.3892/or.2020.7475 (2020).

180. Ito, H. and Miki, C. Profile of circulating levels of interleukin-1 receptor antagonist and interleukin-6 in colorectal cancer patients. *Scand J Gastroenterol* **34**, 1139-43, doi:10.1080/003655299750024959 (1999).

181. Zhu, L., Wang, J. and Hu, J. High expression of IL4I1 is correlated with poor prognosis and immune infiltration in thyroid cancer. *BMC Endocr Disord* **23**, 148, doi:10.1186/s12902-023-01407-1 (2023).

182. Groden, J., Joslyn, G., Samowitz, W., Jones, D., Bhattacharyya, N., Spirio, L., Thliveris, A., Robertson, M., Egan, S., Meuth, M. and et al. Response of colon cancer cell lines to the introduction of APC, a colon-specific tumor suppressor gene. *Cancer Res* **55**, 1531-9, (1995).

183. Belshaw, N. J., Elliott, G. O., Foxall, R. J., Dainty, J. R., Pal, N., Coupe, A., Garg, D., Bradburn, D. M., Mathers, J. C. and Johnson, I. T. Profiling CpG island field methylation in both morphologically normal and neoplastic human colonic mucosa. *Br J Cancer* **99**, 136-42, doi:10.1038/sj.bjc.6604432 (2008).

184. Moser, A. R., Mattes, E. M., Dove, W. F., Lindstrom, M. J., Haag, J. D. and Gould, M. N. ApcMin, a mutation in the murine Apc gene, predisposes to mammary carcinomas and focal alveolar hyperplasias. *Proc Natl Acad Sci U S A* **90**, 8977-81, doi:10.1073/pnas.90.19.8977 (1993).

185. Chen, L. C., Hao, C. Y., Chiu, Y. S., Wong, P., Melnick, J. S., Brotman, M., Moretto, J., Mendes, F., Smith, A. P., Bennington, J. L., Moore, D. and Lee, N. M. Alteration of gene expression in normal-appearing colon mucosa of APC(min) mice and human cancer patients. *Cancer Res* **64**, 3694-700, doi:10.1158/0008-5472.CAN-03-3264 (2004).

186. Boman, B. M. and Fields, J. Z. An APC:WNT Counter-Current-Like Mechanism Regulates Cell Division Along the Human Colonic Crypt Axis: A Mechanism That Explains How APC Mutations Induce Proliferative Abnormalities That Drive Colon Cancer Development. *Front Oncol* **3**, 244, doi:10.3389/fonc.2013.00244 (2013).

187. Choi, C. R., Bakir, I. A., Hart, A. L. and Graham, T. A. Clonal evolution of colorectal cancer in IBD. *Nat Rev Gastroenterol Hepatol* **14**, 218-229, doi:10.1038/nrgastro.2017.1 (2017).

188. Zhou, R. W., Harpaz, N., Itzkowitz, S. H. and Parsons, R. E. Molecular mechanisms in colitis-associated colorectal cancer. *Oncogenesis* **12**, 48, doi:10.1038/s41389-023-00492-0 (2023).

189. Cooper, H. S., Everley, L., Chang, W. C., Pfeiffer, G., Lee, B., Murthy, S. and Clapper, M. L. The role of mutant Apc in the development of dysplasia and cancer in the mouse model of dextran sulfate sodium-induced colitis. *Gastroenterology* **121**, 1407-16, doi:10.1053/gast.2001.29609 (2001).

190. De Santis, S., Verna, G., Serino, G., Armentano, R., Cavalcanti, E., Liso, M., Dicarlo, M., Coletta, S., Mastronardi, M., Lippolis, A., Tafaro, A., Santino, A., Pinto, A., Campiglia, P., Huang, A. Y., Cominelli, F., Pizarro, T. T. and Chieppa, M. Winnie-APC(Min/+) Mice: A Spontaneous Model of Colitis-Associated Colorectal Cancer Combining Genetics and Inflammation. *Int J Mol Sci* **21**, doi:10.3390/ijms21082972 (2020).

191. Yen, T., Stanich, P. P., Axell, L. and Patel, S. G. APC-Associated Polyposis Conditions. *GeneReviews((R))* (1993).

192. Labayle, D., Fischer, D., Vielh, P., Drouhin, F., Pariente, A., Bories, C., Duhamel, O., Trousset, M. and Attali, P. Sulindac causes regression of rectal polyps in familial adenomatous polyposis. *Gastroenterology* **101**, 635-9, doi:10.1016/0016-5085(91)90519-q (1991).

193. Nugent, K. P., Farmer, K. C., Spigelman, A. D., Williams, C. B. and Phillips, R. K. Randomized controlled trial of the effect of sulindac on duodenal and rectal polyposis and cell proliferation in patients with familial adenomatous polyposis. *Br J Surg* **80**, 1618-9, doi:10.1002/bjs.1800801244 (1993).

194. Giardiello, F. M., Hamilton, S. R., Krush, A. J., Piantadosi, S., Hylind, L. M., Celano, P., Booker, S. V., Robinson, C. R. and Offerhaus, G. J. Treatment of colonic and rectal adenomas with sulindac in familial adenomatous polyposis. *N Engl J Med* **328**, 1313-6, doi:10.1056/NEJM199305063281805 (1993).

195. Steinbach, G., Lynch, P. M., Phillips, R. K., Wallace, M. H., Hawk, E., Gordon, G. B., Wakabayashi, N., Saunders, B., Shen, Y., Fujimura, T., Su, L. K., Levin, B., Godio, L., Patterson, S., Rodriguez-Bigas, M. A., Jester, S. L., King, K. L., Schumacher, M., Abbruzzese, J., DuBois, R. N., Hittelman, W. N., Zimmerman, S., Sherman, J. W. and Kelloff, G. The effect of celecoxib, a cyclooxygenase-2 inhibitor, in familial adenomatous polyposis. *N Engl J Med* **342**, 1946-52, doi:10.1056/NEJM200006293422603 (2000).

196. Chen, C. COX-2's new role in inflammation. *Nat Chem Biol* **6**, 401-2, doi:10.1038/nchembio.375 (2010).

197. Slater, T. W., Finkielsztein, A., Mascarenhas, L. A., Mehl, L. C., Butin-Israeli, V. and Sumagin, R. Neutrophil Microparticles Deliver Active Myeloperoxidase to Injured Mucosa To Inhibit Epithelial Wound Healing. *J Immunol* **198**, 2886-2897, doi:10.4049/jimmunol.1601810 (2017).

198. Butin-Israeli, V., Bui, T. M., Wiesolek, H. L., Mascarenhas, L., Lee, J. J., Mehl, L. C., Knutson, K. R., Adam, S. A., Goldman, R. D., Beyder, A., Wiesmuller, L., Hanauer, S. B. and Sumagin, R. Neutrophil-induced genomic instability impedes resolution of inflammation and wound healing. *J Clin Invest* **129**, 712-726, doi:10.1172/JCI122085 (2019).

199. Ozawa, N., Yokobori, T., Osone, K., Katayama, C., Suga, K., Komine, C., Shibasaki, Y., Shiraishi, T., Okada, T., Kato, R., Ogawa, H., Sano, A., Sakai, M., Sohda, M., Ojima, H., Miyazaki, T., Motegi, Y.,

Ide, M., Yao, T., Kuwano, H., Shirabe, K. and Saeki, H. PD-L1 upregulation is associated with activation of the DNA double-strand break repair pathway in patients with colitic cancer. *Sci Rep* **11**, 13077, doi:10.1038/s41598-021-92530-3 (2021).

200. Deville, S., Garcia Romeu, H., Oeyen, E., Mertens, I., Nelissen, I. and Salvati, A. Macrophages Release Extracellular Vesicles of Different Properties and Composition Following Exposure to Nanoparticles. *Int J Mol Sci* **24**, doi:10.3390/ijms24010260 (2022).

201. Dechantsreiter, S., Ambrose, A. R., Worboys, J. D., Lim, J. M. E., Liu, S., Shah, R., Montero, M. A., Quinn, A. M., Hussell, T., Tannahill, G. M. and Davis, D. M. Heterogeneity in extracellular vesicle secretion by single human macrophages revealed by super-resolution microscopy. *J Extracell Vesicles* **11**, e12215, doi:10.1002/jev2.12215 (2022).

202. Dvorak, H. F. Tumors: wounds that do not heal. Similarities between tumor stroma generation and wound healing. *N Engl J Med* **315**, 1650-9, doi:10.1056/NEJM198612253152606 (1986).

203. Dvorak, H. F. Tumors: wounds that do not heal-redux. *Cancer Immunol Res* **3**, 1-11, doi:10.1158/2326-6066.CIR-14-0209 (2015).

204. Dekaney, C. M., Gulati, A. S., Garrison, A. P., Helmrath, M. A. and Henning, S. J. Regeneration of intestinal stem/progenitor cells following doxorubicin treatment of mice. *Am J Physiol Gastrointest Liver Physiol* **297**, G461-70, doi:10.1152/ajpgi.90446.2008 (2009).

205. van Es, J. H., Sato, T., van de Wetering, M., Lyubimova, A., Yee Nee, A. N., Gregorieff, A., Sasaki, N., Zeinstra, L., van den Born, M., Korving, J., Martens, A. C. M., Barker, N., van Oudenaarden, A. and Clevers, H. Dll1+ secretory progenitor cells revert to stem cells upon crypt damage. *Nat Cell Biol* **14**, 1099-1104, doi:10.1038/ncb2581 (2012).

206. Wang, X., Ding, H., Li, Z., Peng, Y., Tan, H., Wang, C., Huang, G., Li, W., Ma, G. and Wei, W. Exploration and functionalization of M1-macrophage extracellular vesicles for effective accumulation in glioblastoma and strong synergistic therapeutic effects. *Signal Transduct Target Ther* **7**, 74, doi:10.1038/s41392-022-00894-3 (2022).

207. Shi, Y., Luo, P., Wang, W., Horst, K., Blasius, F., Relja, B., Xu, D., Hildebrand, F. and Greven, J. M1 But Not M0 Extracellular Vesicles Induce Polarization of RAW264.7 Macrophages Via the TLR4-NFkappaB Pathway In Vitro. *Inflammation* **43**, 1611-1619, doi:10.1007/s10753-020-01236-7 (2020).

208. Tacconi, S., Vari, F., Sbarigia, C., Vardanyan, D., Longo, S., Mura, F., Angile, F., Jalabert, A., Blangero, F., Eljaafari, A., Canaple, L., Vergara, D., Fanizzi, F. P., Rossi, M., Da Silva, C. C., Errazuriz-Cerda, E., Cassin, C., Nieuwland, R., Giudetti, A. M., Rome, S. and Dini, L. M1-derived extracellular vesicles polarize recipient macrophages into M2-like macrophages and alter skeletal muscle homeostasis in a hyper-glucose environment. *Cell Commun Signal* **22**, 193, doi:10.1186/s12964-024-01560-7 (2024).

209. Kuchimaru, T., Iwano, S., Kiyama, M., Mitsumata, S., Kadonosono, T., Niwa, H., Maki, S. and Kizaka-Kondoh, S. A luciferin analogue generating near-infrared bioluminescence achieves highly sensitive deep-tissue imaging. *Nat Commun* **7**, 11856, doi:10.1038/ncomms11856 (2016).

210. Feoktistova, M., Geserick, P. and Leverkus, M. Crystal Violet Assay for Determining Viability of Cultured Cells. *Cold Spring Harb Protoc* **2016**, pdb prot087379, doi:10.1101/pdb.prot087379 (2016).

211. Cai, L., Qin, X., Xu, Z., Song, Y., Jiang, H., Wu, Y., Ruan, H. and Chen, J. Comparison of Cytotoxicity Evaluation of Anticancer Drugs between Real-Time Cell Analysis and CCK-8 Method. *ACS Omega* **4**, 12036-12042, doi:10.1021/acsomega.9b01142 (2019).

212. Ip, W. K. E., Hoshi, N., Shouval, D. S., Snapper, S. and Medzhitov, R. Anti-inflammatory effect of IL-10 mediated by metabolic reprogramming of macrophages. *Science* **356**, 513-519, doi:10.1126/science.aal3535 (2017).

213. Mills, E. L., Kelly, B., Logan, A., Costa, A. S. H., Varma, M., Bryant, C. E., Tourlomousis, P., Dabritz, J. H. M., Gottlieb, E., Latorre, I., Corr, S. C., McManus, G., Ryan, D., Jacobs, H. T., Szibor, M., Xavier, R. J., Braun, T., Frezza, C., Murphy, M. P. and O'Neill, L. A. Succinate Dehydrogenase Supports Metabolic Repurposing of Mitochondria to Drive Inflammatory Macrophages. *Cell* **167**, 457-470 e13, doi:10.1016/j.cell.2016.08.064 (2016).

214. Tannahill, G. M., Curtis, A. M., Adamik, J., Palsson-McDermott, E. M., McGettrick, A. F., Goel, G., Frezza, C., Bernard, N. J., Kelly, B., Foley, N. H., Zheng, L., Gardet, A., Tong, Z., Jany, S. S., Corr, S. C., Haneklaus, M., Caffrey, B. E., Pierce, K., Walmsley, S., Beasley, F. C., Cummins, E., Nizet, V., Whyte, M., Taylor, C. T., Lin, H., Masters, S. L., Gottlieb, E., Kelly, V. P., Clish, C., Auron, P. E., Xavier, R. J. and O'Neill, L. A. Succinate is an inflammatory signal that induces IL-1beta through HIF-1alpha. *Nature* **496**, 238-42, doi:10.1038/nature11986 (2013).

215. MacLean, B., Tomazela, D. M., Shulman, N., Chambers, M., Finney, G. L., Frewen, B., Kern, R., Tabb, D. L., Liebler, D. C. and MacCoss, M. J. Skyline: an open source document editor for creating and analyzing targeted proteomics experiments. *Bioinformatics* **26**, 966-8, doi:10.1093/bioinformatics/btq054 (2010).

216. Demichev, V., Messner, C. B., Vernardis, S. I., Lilley, K. S. and Ralser, M. DIA-NN: neural networks and interference correction enable deep proteome coverage in high throughput. *Nat Methods* **17**, 41-44, doi:10.1038/s41592-019-0638-x (2020).

217. Multhaup, M., Karlen, A. D., Swanson, D. L., Wilber, A., Somia, N. V., Cowan, M. J. and McIvor, R. S. Cytotoxicity associated with artemis overexpression after lentiviral vector-mediated gene transfer. *Hum Gene Ther* **21**, 865-75, doi:10.1089/hum.2009.162 (2010).

218. Serezani, C. H., Chung, J., Ballinger, M. N., Moore, B. B., Aronoff, D. M. and Peters-Golden, M. Prostaglandin E2 suppresses bacterial killing in alveolar macrophages by inhibiting NADPH oxidase. *Am J Respir Cell Mol Biol* **37**, 562-70, doi:10.1165/rcmb.2007-0153OC (2007).

219. Jin, K., Qian, C., Lin, J. and Liu, B. Cyclooxygenase-2-Prostaglandin E2 pathway: A key player in tumor-associated immune cells. *Front Oncol* **13**, 1099811, doi:10.3389/fonc.2023.1099811 (2023).

220. Zheng, J. Energy metabolism of cancer: Glycolysis versus oxidative phosphorylation (Review). *Oncol Lett* **4**, 1151-1157, doi:10.3892/ol.2012.928 (2012).

221. Hyun, Y. S., Han, D. S., Lee, A. R., Eun, C. S., Youn, J. and Kim, H. Y. Role of IL-17A in the development of colitis-associated cancer. *Carcinogenesis* **33**, 931-6, doi:10.1093/carcin/bgs106 (2012).

222. Hu, X., Li, J., Fu, M., Zhao, X. and Wang, W. The JAK/STAT signaling pathway: from bench to clinic. *Signal Transduct Target Ther* **6**, 402, doi:10.1038/s41392-021-00791-1 (2021).

223. Schwartz, M. A. Integrins, oncogenes, and anchorage independence. *J Cell Biol* **139**, 575-8, doi:10.1083/jcb.139.3.575 (1997).

224. Borowicz, S., Van Scoyk, M., Avasarala, S., Karuppusamy Rathinam, M. K., Tauler, J., Bikkavilli, R. K. and Winn, R. A. The soft agar colony formation assay. *J Vis Exp* e51998, doi:10.3791/51998 (2014).

225. Deng, Z., Wang, H., Liu, J., Deng, Y. and Zhang, N. Comprehensive understanding of anchorage-independent survival and its implication in cancer metastasis. *Cell Death Dis* **12**, 629, doi:10.1038/s41419-021-03890-7 (2021).

226. Bakir, B., Chiarella, A. M., Pitarresi, J. R. and Rustgi, A. K. EMT, MET, Plasticity, and Tumor Metastasis. *Trends Cell Biol* **30**, 764-776, doi:10.1016/j.tcb.2020.07.003 (2020).

227. Lu, J., Kornmann, M. and Traub, B. Role of Epithelial to Mesenchymal Transition in Colorectal Cancer. *Int J Mol Sci* **24**, doi:10.3390/ijms241914815 (2023).

228. Iwano, S., Sugiyama, M., Hama, H., Watakabe, A., Hasegawa, N., Kuchimaru, T., Tanaka, K. Z., Takahashi, M., Ishida, Y., Hata, J., Shimozono, S., Namiki, K., Fukano, T., Kiyama, M., Okano, H., Kizaka-Kondoh, S., McHugh, T. J., Yamamori, T., Hioki, H., Maki, S. and Miyawaki, A. Single-cell bioluminescence imaging of deep tissue in freely moving animals. *Science* **359**, 935-939, doi:10.1126/science.aaq1067 (2018).

229. Yao, Z., Brennan, C. K., Scipioni, L., Chen, H., Ng, K. K., Tedeschi, G., Parag-Sharma, K., Amelio, A. L., Gratton, E., Digman, M. A. and Prescher, J. A. Multiplexed bioluminescence microscopy via phasor analysis. *Nat Methods* **19**, 893-898, doi:10.1038/s41592-022-01529-9 (2022).

230. Baklaushev, V. P., Kilpeläinen, A., Petkov, S., Abakumov, M. A., Grinenko, N. F., Yusubalieva, G. M., Latanova, A. A., Gubskiy, I. L., Zabozlaev, F. G., Starodubova, E. S., Abakumova, T. O., Isaguliants, M. G. and Chekhonin, V. P. Luciferase Expression Allows Bioluminescence Imaging But Imposes Limitations on the Orthotopic Mouse (4T1) Model of Breast Cancer. *Sci Rep-Uk* **7**, doi:10.1038/s41598-017-07851-z (2017).

231. Rodgers, L. T., Pauly, J. A. S., Maloney, B. J., Hartz, A. M. S. and Bauer, B. Optimization, Characterization, and Comparison of Two Luciferase-Expressing Mouse Glioblastoma Models. *Cancers* **16**, doi:10.3390/cancers16111997 (2024).

232. Veglia, F., Perego, M. and Gabrilovich, D. Myeloid-derived suppressor cells coming of age. *Nat Immunol* **19**, 108-119, doi:10.1038/s41590-017-0022-x (2018).

233. Veglia, F., Sanseviero, E. and Gabrilovich, D. I. Myeloid-derived suppressor cells in the era of increasing myeloid cell diversity. *Nat Rev Immunol* **21**, 485-498, doi:10.1038/s41577-020-00490-y (2021).

234. Wynn, T. A. Myeloid-cell differentiation redefined in cancer. *Nat Immunol* **14**, 197-9, doi:10.1038/ni.2539 (2013).

235. Lasser, S. A., Ozbay Kurt, F. G., Arkhypov, I., Utikal, J. and Umansky, V. Myeloid-derived suppressor cells in cancer and cancer therapy. *Nat Rev Clin Oncol* **21**, 147-164, doi:10.1038/s41571-023-00846-y (2024).

236. Mantovani, A., Marchesi, F., Jaillon, S., Garlanda, C. and Allavena, P. Tumor-associated myeloid cells: diversity and therapeutic targeting. *Cell Mol Immunol* **18**, 566-578, doi:10.1038/s41423-020-00613-4 (2021).

237. Zhao, F., Gong, W., Song, J., Shen, Z. and Cui, D. The paradoxical role of MDSCs in inflammatory bowel diseases: From bench to bedside. *Front Immunol* **13**, 1021634, doi:10.3389/fimmu.2022.1021634 (2022).

238. Gabrilovich, D. I. Myeloid-Derived Suppressor Cells. *Cancer Immunol Res* **5**, 3-8, doi:10.1158/2326-6066.CIR-16-0297 (2017).

239. James, K. R., Gomes, T., Elmentaite, R., Kumar, N., Gulliver, E. L., King, H. W., Stares, M. D., Bareham, B. R., Ferdinand, J. R., Petrova, V. N., Polanski, K., Forster, S. C., Jarvis, L. B., Suchanek, O., Howlett, S., James, L. K., Jones, J. L., Meyer, K. B., Clatworthy, M. R., Saeb-Parsy, K., Lawley, T. D. and Teichmann, S. A. Distinct microbial and immune niches of the human colon. *Nat Immunol* **21**, 343-353, doi:10.1038/s41590-020-0602-z (2020).

240. Liu, Q., Peng, Z., Zhou, L., Peng, R., Li, X., Zuo, W., Gou, J., Zhou, F., Yu, S., Huang, M. and Liu, H. Short-Chain Fatty Acid Decreases the Expression of CEBPB to Inhibit miR-145-Mediated DUSP6 and Thus Further Suppresses Intestinal Inflammation. *Inflammation* **45**, 372-386, doi:10.1007/s10753-021-01552-6 (2022).

241. Im, E., Riegler, F. M., Pothoulakis, C. and Rhee, S. H. Elevated lipopolysaccharide in the colon evokes intestinal inflammation, aggravated in immune modulator-impaired mice. *Am J Physiol Gastrointest Liver Physiol* **303**, G490-7, doi:10.1152/ajpgi.00120.2012 (2012).

242. Guo, K., Gong, W., Wang, Q., Gu, G., Zheng, T., Li, Y., Li, W., Fang, M., Xie, H., Yue, C., Yang, J. and Zhu, Z. LINC01106 drives colorectal cancer growth and stemness through a positive feedback loop to regulate the Gli family factors. *Cell Death Dis* **11**, 869, doi:10.1038/s41419-020-03026-3 (2020).

243. Brabletz, T., Hlubek, F., Spaderna, S., Schmalhofer, O., Hiendlmeyer, E., Jung, A. and Kirchner, T. Invasion and metastasis in colorectal cancer: epithelial-mesenchymal transition, mesenchymal-epithelial transition, stem cells and beta-catenin. *Cells Tissues Organs* **179**, 56-65, doi:10.1159/000084509 (2005).

244. Okumura, R. and Takeda, K. Roles of intestinal epithelial cells in the maintenance of gut homeostasis. *Exp Mol Med* **49**, e338, doi:10.1038/emm.2017.20 (2017).

245. Soderholm, A. T. and Pedicord, V. A. Intestinal epithelial cells: at the interface of the microbiota and mucosal immunity. *Immunology* **158**, 267-280, doi:10.1111/imm.13117 (2019).

246. Li, X., Bechara, R., Zhao, J., McGeachy, M. J. and Gaffen, S. L. IL-17 receptor-based signaling and implications for disease. *Nat Immunol* **20**, 1594-1602, doi:10.1038/s41590-019-0514-y (2019).

247. Li, Q., Liu, L., Zhang, Q., Liu, S., Ge, D. and You, Z. Interleukin-17 Indirectly Promotes M2 Macrophage Differentiation through Stimulation of COX-2/PGE2 Pathway in the Cancer Cells. *Cancer Res Treat* **46**, 297-306, doi:10.4143/crt.2014.46.3.297 (2014).

248. Song, D., Lian, Y. and Zhang, L. The potential of activator protein 1 (AP-1) in cancer targeted therapy. *Front Immunol* **14**, 1224892, doi:10.3389/fimmu.2023.1224892 (2023).

249. Liu, H., Ren, G., Wang, T., Chen, Y., Gong, C., Bai, Y., Wang, B., Qi, H., Shen, J., Zhu, L., Qian, C., Lai, M. and Shao, J. Aberrantly expressed Fra-1 by IL-6/STAT3 transactivation promotes colorectal cancer aggressiveness through epithelial-mesenchymal transition. *Carcinogenesis* **36**, 459-68, doi:10.1093/carcin/bgv017 (2015).

250. Hong, S., Skaist, A. M., Wheelan, S. J. and Friedman, A. D. AP-1 protein induction during monopoiesis favors C/EBP: AP-1 heterodimers over C/EBP homodimerization and stimulates FosB transcription. *J Leukoc Biol* **90**, 643-51, doi:10.1189/jlb.0111043 (2011).

251. Wang, Z., Pang, J., Wang, L., Dong, Q. and Jin, D. CEBPB regulates the bile acid receptor FXR to accelerate colon cancer progression by modulating aerobic glycolysis. *J Clin Lab Anal* **36**, e24703, doi:10.1002/jcla.24703 (2022).

252. Wu, D., Wu, P., Huang, Q., Liu, Y., Ye, J. and Huang, J. Interleukin-17: a promoter in colorectal cancer progression. *Clin Dev Immunol* **2013**, 436307, doi:10.1155/2013/436307 (2013).

253. Fujino, S., Andoh, A., Bamba, S., Ogawa, A., Hata, K., Araki, Y., Bamba, T. and Fujiyama, Y. Increased expression of interleukin 17 in inflammatory bowel disease. *Gut* **52**, 65-70, doi:10.1136/gut.52.1.65 (2003).

254. Menesy, A., Hammad, M., Aref, S. and Abozeid, F. A. M. Level of interleukin 17 in inflammatory bowel disease and its relation with disease activity. *BMC Gastroenterol* **24**, 135, doi:10.1186/s12876-024-03218-7 (2024).

255. Liu, J., Duan, Y., Cheng, X., Chen, X., Xie, W., Long, H., Lin, Z. and Zhu, B. IL-17 is associated with poor prognosis and promotes angiogenesis via stimulating VEGF production of cancer cells in colorectal carcinoma. *Biochem Biophys Res Commun* **407**, 348-54, doi:10.1016/j.bbrc.2011.03.021 (2011).

256. De Robertis, M., Massi, E., Poeta, M. L., Carotti, S., Morini, S., Cecchetelli, L., Signori, E. and Fazio, V. M. The AOM/DSS murine model for the study of colon carcinogenesis: From pathways to diagnosis and therapy studies. *J Carcinog* **10**, 9, doi:10.4103/1477-3163.78279 (2011).

257. Han, D. IL-17 is required for development of colitis associated cancer. P-071. *Inflammatory Bowel Diseases* **17**, doi:10.1093/ibd/17.supplement1.S33 (2011).

258. Ito, R., Kita, M., Shin-Ya, M., Kishida, T., Urano, A., Takada, R., Sakagami, J., Imanishi, J., Iwakura, Y., Okanoue, T., Yoshikawa, T., Kataoka, K. and Mazda, O. Involvement of IL-17A in the pathogenesis of DSS-induced colitis in mice. *Biochem Biophys Res Commun* **377**, 12-6, doi:10.1016/j.bbrc.2008.09.019 (2008).

259. Zhang, Z., Zheng, M., Bindas, J., Schwarzenberger, P. and Kolls, J. K. Critical role of IL-17 receptor signaling in acute TNBS-induced colitis. *Inflamm Bowel Dis* **12**, 382-8, doi:10.1097/01.MIB.0000218764.06959.91 (2006).

260. Chae, W. J., Gibson, T. F., Zelterman, D., Hao, L., Henegariu, O. and Bothwell, A. L. Ablation of IL-17A abrogates progression of spontaneous intestinal tumorigenesis. *Proc Natl Acad Sci U S A* **107**, 5540-4, doi:10.1073/pnas.0912675107 (2010).

261. Zhang, M., Wang, G., Tao, Y. and Zhang, H. The proinflammatory effect and molecular mechanism of IL- 17 in the intestinal epithelial cell line HT-29. *J BUON* **20**, 120-7, (2015).

262. Agoff, S. N., Brentnall, T. A., Crispin, D. A., Taylor, S. L., Raaka, S., Haggitt, R. C., Reed, M. W., Afonina, I. A., Rabinovitch, P. S., Stevens, A. C., Feng, Z. and Bronner, M. P. The role of cyclooxygenase 2 in ulcerative colitis-associated neoplasia. *Am J Pathol* **157**, 737-45, doi:10.1016/S0002-9440(10)64587-7 (2000).

263. Gupta, R. A. and Dubois, R. N. Colorectal cancer prevention and treatment by inhibition of cyclooxygenase-2. *Nat Rev Cancer* **1**, 11-21, doi:10.1038/35094017 (2001).

264. Tsujii, M., Kawano, S. and DuBois, R. N. Cyclooxygenase-2 expression in human colon cancer cells increases metastatic potential. *Proc Natl Acad Sci U S A* **94**, 3336-40, doi:10.1073/pnas.94.7.3336 (1997).

265. Tsujii, M., Kawano, S., Tsuji, S., Sawaoka, H., Hori, M. and DuBois, R. N. Cyclooxygenase regulates angiogenesis induced by colon cancer cells. *Cell* **93**, 705-16, doi:10.1016/s0092-8674(00)81433-6 (1998).

266. Sheng, H., Shao, J., Washington, M. K. and DuBois, R. N. Prostaglandin E2 increases growth and motility of colorectal carcinoma cells. *J Biol Chem* **276**, 18075-81, doi:10.1074/jbc.M009689200 (2001).

267. Sheng, H., Shao, J., Morrow, J. D., Beauchamp, R. D. and DuBois, R. N. Modulation of apoptosis and Bcl-2 expression by prostaglandin E2 in human colon cancer cells. *Cancer Res* **58**, 362-6, (1998).

268. Chinery, R., Coffey, R. J., Graves-Deal, R., Kirkland, S. C., Sanchez, S. C., Zackert, W. E., Oates, J. A. and Morrow, J. D. Prostaglandin J2 and 15-deoxy-delta12,14-prostaglandin J2 induce proliferation of cyclooxygenase-depleted colorectal cancer cells. *Cancer Res* **59**, 2739-46, (1999).

269. Hsiao, S. W., Yen, H. H. and Chen, Y. Y. Chemoprevention of Colitis-Associated Dysplasia or Cancer in Inflammatory Bowel Disease. *Gut Liver* **16**, 840-848, doi:10.5009/gnl210479 (2022).

270. Sheng, H., Shao, J., Kirkland, S. C., Isakson, P., Coffey, R. J., Morrow, J., Beauchamp, R. D. and DuBois, R. N. Inhibition of human colon cancer cell growth by selective inhibition of cyclooxygenase-2. *J Clin Invest* **99**, 2254-9, doi:10.1172/JCI119400 (1997).

271. Oshima, M., Dinchuk, J. E., Kargman, S. L., Oshima, H., Hancock, B., Kwong, E., Trzaskos, J. M., Evans, J. F. and Taketo, M. M. Suppression of intestinal polyposis in Apc delta716 knockout mice by inhibition of cyclooxygenase 2 (COX-2). *Cell* **87**, 803-9, doi:10.1016/s0092-8674(00)81988-1 (1996).

272. Boolbol, S. K., Dannenberg, A. J., Chadburn, A., Martucci, C., Guo, X. J., Ramonetti, J. T., Abreu-Goris, M., Newmark, H. L., Lipkin, M. L., DeCosse, J. J. and Bertagnolli, M. M. Cyclooxygenase-2 overexpression and tumor formation are blocked by sulindac in a murine model of familial adenomatous polyposis. *Cancer Res* **56**, 2556-60, (1996).

273. Marcum, Z. A. and Hanlon, J. T. Recognizing the Risks of Chronic Nonsteroidal Anti-Inflammatory Drug Use in Older Adults. *Ann Longterm Care* **18**, 24-27, (2010).

274. Ramji, D. P. and Foka, P. CCAAT/enhancer-binding proteins: structure, function and regulation. *Biochem J* **365**, 561-75, doi:10.1042/BJ20020508 (2002).

275. Ge, C. Y., Wei, L. Y., Tian, Y. and Wang, H. H. A Seven-NF-kappaB-Related Gene Signature May Distinguish Patients with Ulcerative Colitis-Associated Colorectal Carcinoma. *Pharmgenomics Pers Med* **13**, 707-718, doi:10.2147/PGPM.S274258 (2020).

276. Nowak, J. K., Adams, A. T., Kalla, R., Lindstrom, J. C., Vatn, S., Bergemalm, D., Keita, A. V., Gomollon, F., Jahnsen, J., Vatn, M. H., Ricanek, P., Ostrowski, J., Walkowiak, J., Halfvarson, J., Satsangi, J. and Consortium, I. B. D. C. Characterisation of the Circulating Transcriptomic Landscape in Inflammatory Bowel Disease Provides Evidence for Dysregulation of Multiple Transcription Factors Including NFE2, SPI1, CEBPB, and IRF2. *J Crohns Colitis* **16**, 1255-1268, doi:10.1093/ecco-jcc/jjac033 (2022).

277. Abate, E., Mehdi, M., Addisu, S., Degef, M., Tebeje, S. and Kelemu, T. Emerging roles of cytosolic phosphoenolpyruvate kinase 1 (PCK1) in cancer. *Biochem Biophys Rep* **35**, 101528, doi:10.1016/j.bbrep.2023.101528 (2023).

278. Chu, L. Y., Huang, B. L., Huang, X. C., Peng, Y. H., Xie, J. J. and Xu, Y. W. EFNA1 in gastrointestinal cancer: Expression, regulation and clinical significance. *World J Gastrointest Oncol* **14**, 973-988, doi:10.4251/wjgo.v14.i5.973 (2022).

279. Ma, Y., Chen, Y., Zhan, L., Dong, Q., Wang, Y., Li, X., He, L. and Zhang, J. CEBPB-mediated upregulation of SERPINA1 promotes colorectal cancer progression by enhancing STAT3 signaling. *Cell Death Discov* **10**, 219, doi:10.1038/s41420-024-01990-9 (2024).

280. Zhou, Z., Shu, Y., Bao, H., Han, S., Liu, Z., Zhao, N., Yuan, W., Jian, C. and Shu, X. Stress-induced epinephrine promotes epithelial-to-mesenchymal transition and stemness of CRC through the CEBPB/TRIM2/P53 axis. *J Transl Med* **20**, 262, doi:10.1186/s12967-022-03467-8 (2022).

281. Hasselblatt, P., Gresh, L., Kudo, H., Guinea-Viniegra, J. and Wagner, E. F. The role of the transcription factor AP-1 in colitis-associated and beta-catenin-dependent intestinal tumorigenesis in mice. *Oncogene* **27**, 6102-9, doi:10.1038/onc.2008.211 (2008).

282. Wang, X., Guo, R., Lv, Y. and Fu, R. The regulatory role of Fos related antigen-1 in inflammatory bowel disease. *Mol Med Rep* **17**, 1979-1985, doi:10.3892/mmr.2017.8071 (2018).

283. Wang, H. L., Wang, J., Xiao, S. Y., Haydon, R., Stoiber, D., He, T. C., Bissonnette, M. and Hart, J. Elevated protein expression of cyclin D1 and Fra-1 but decreased expression of c-Myc in human colorectal adenocarcinomas overexpressing beta-catenin. *Int J Cancer* **101**, 301-10, doi:10.1002/ijc.10630 (2002).

284. Takada, Y., Ray, N., Ikeda, E., Kawaguchi, T., Kuwahara, M., Wagner, E. F. and Matsuo, K. Fos proteins suppress dextran sulfate sodium-induced colitis through inhibition of NF-kappaB. *J Immunol* **184**, 1014-21, doi:10.4049/jimmunol.0901196 (2010).

285. Delgado-Ramirez, Y., Baltazar-Perez, I., Martinez, Y., Callejas, B. E., Medina-Andrade, I., Olguin, J. E., Delgado-Buenrostro, N. L., Chirino, Y. I., Terrazas, L. I. and Leon-Cabrera, S. STAT1 Is Required for Decreasing Accumulation of Granulocytic Cells via IL-17 during Initial Steps of Colitis-Associated Cancer. *Int J Mol Sci* **22**, doi:10.3390/ijms22147695 (2021).

286. Leon-Cabrera, S., Vazquez-Sandoval, A., Molina-Guzman, E., Delgado-Ramirez, Y., Delgado-Buenrostro, N. L., Callejas, B. E., Chirino, Y. I., Perez-Plasencia, C., Rodriguez-Sosa, M., Olguin, J. E., Salinas, C., Satoskar, A. R. and Terrazas, L. I. Deficiency in STAT1 Signaling Predisposes Gut Inflammation and Prompts Colorectal Cancer Development. *Cancers (Basel)* **10**, doi:10.3390/cancers10090341 (2018).

287. Rogler, G., Brand, K., Vogl, D., Page, S., Hofmeister, R., Andus, T., Knuechel, R., Baeuerle, P. A., Scholmerich, J. and Gross, V. Nuclear factor kappaB is activated in macrophages and epithelial cells of inflamed intestinal mucosa. *Gastroenterology* **115**, 357-69, doi:10.1016/s0016-5085(98)70202-1 (1998).

288. Greten, F. R., Eckmann, L., Greten, T. F., Park, J. M., Li, Z. W., Egan, L. J., Kagnoff, M. F. and Karin, M. IKKbeta links inflammation and tumorigenesis in a mouse model of colitis-associated cancer. *Cell* **118**, 285-96, doi:10.1016/j.cell.2004.07.013 (2004).

289. Ghosh, S., May, M. J. and Kopp, E. B. NF-kappa B and Rel proteins: evolutionarily conserved mediators of immune responses. *Annu Rev Immunol* **16**, 225-60, doi:10.1146/annurev.immunol.16.1.225 (1998).

290. Liu, T., Zhang, L., Joo, D. and Sun, S. C. NF-kappaB signaling in inflammation. *Signal Transduct Target Ther* **2**, 17023-, doi:10.1038/sigtrans.2017.23 (2017).

291. Stopfer, P., Obermeier, F., Dunger, N., Falk, W., Farkas, S., Janotta, M., Moller, A., Mannel, D. N. and Hehlgans, T. Blocking lymphotoxin-beta receptor activation diminishes inflammation via reduced mucosal addressin cell adhesion molecule-1 (MAdCAM-1) expression and leucocyte margination in chronic DSS-induced colitis. *Clin Exp Immunol* **136**, 21-9, doi:10.1111/j.1365-2249.2004.02402.x (2004).

292. Herold, Z., Herold, M., Herczeg, G., Fodor, A., Szasz, A. M., Dank, M. and Somogyi, A. High plasma CD40 ligand level is associated with more advanced stages and worse prognosis in colorectal cancer. *World J Clin Cases* **10**, 4084-4096, doi:10.12998/wjcc.v10.i13.4084 (2022).

293. Zhang, Y., Tao, M., Chen, C., Zhao, X., Feng, Q., Chen, G. and Fu, Y. BAFF Blockade Attenuates DSS-Induced Chronic Colitis via Inhibiting NLRP3 Inflammasome and NF-kappaB Activation. *Front Immunol* **13**, 783254, doi:10.3389/fimmu.2022.783254 (2022).

294. Liang, Q., Wang, Y., Lu, Y., Zhu, Q., Xie, W., Tang, N., Huang, L., An, T., Zhang, D., Yan, A., Liu, S., Ye, L. and Zhu, C. RANK promotes colorectal cancer migration and invasion by activating the Ca(2+)-calcineurin/NFATC1-ACP5 axis. *Cell Death Dis* **12**, 336, doi:10.1038/s41419-021-03642-7 (2021).

295. Ghosh, S. and Karin, M. Missing pieces in the NF-kappaB puzzle. *Cell* **109 Suppl**, S81-96, doi:10.1016/s0092-8674(02)00703-1 (2002).

296. Viennois, E., Chen, F. and Merlin, D. NF-kappaB pathway in colitis-associated cancers. *Transl Gastrointest Cancer* **2**, 21-29, doi:10.3978/j.issn.2224-4778.2012.11.01 (2013).

297. Temby, M., Boye, T. L., Hoang, J., Nielsen, O. H. and Gubatan, J. Kinase Signaling in Colitis-Associated Colon Cancer and Inflammatory Bowel Disease. *Biomolecules* **13**, doi:10.3390/biom13111620 (2023).

298. Zhang, P., Kawakami, H., Liu, W., Zeng, X., Strebhardt, K., Tao, K., Huang, S. and Sinicrope, F. A. Targeting CDK1 and MEK/ERK Overcomes Apoptotic Resistance in BRAF-Mutant Human Colorectal Cancer. *Mol Cancer Res* **16**, 378-389, doi:10.1158/1541-7786.MCR-17-0404 (2018).

299. Mahid, S. S., Minor, K. S., Brangers, B. C., Cobbs, G. A. and Galandiuk, S. SMAD2 and the relationship of colorectal cancer to inflammatory bowel disease. *Int J Biol Markers* **23**, 169-75, doi:10.5301/jbm.2008.785 (2008).

300. Kim, K. W., Kim, N., Choi, Y., Kim, W. S., Yoon, H., Shin, C. M., Park, Y. S., Lee, D. H., Park, Y. S., Ahn, S. H., Park, D. J., Kim, H. H., Lee, H. S., Kim, J. W., Kim, J. W., Lee, K. W., Chang, W., Park, J. H., Lee, Y. J., Lee, K. H. and Kim, Y. H. Different effects of p53 protein overexpression on the survival of gastric cancer patients according to Lauren histologic classification: a retrospective study. *Gastric Cancer* **24**, 844-857, doi:10.1007/s10120-021-01163-y (2021).

301. Yaeger, R., Shah, M. A., Miller, V. A., Kelsen, J. R., Wang, K., Heins, Z. J., Ross, J. S., He, Y., Sanford, E., Yantiss, R. K., Balasubramanian, S., Stephens, P. J., Schultz, N., Oren, M., Tang, L. and Kelsen, D. Genomic Alterations Observed in Colitis-Associated Cancers Are Distinct From Those Found in Sporadic Colorectal Cancers and Vary by Type of Inflammatory Bowel Disease. *Gastroenterology* **151**, 278-287 e6, doi:10.1053/j.gastro.2016.04.001 (2016).

302. Liebl, M. C. and Hofmann, T. G. The Role of p53 Signaling in Colorectal Cancer. *Cancers (Basel)* **13**, doi:10.3390/cancers13092125 (2021).

303. Gupta, J., del Barco Barrantes, I., Igea, A., Sakellariou, S., Pateras, I. S., Gorgoulis, V. G. and Nebreda, A. R. Dual function of p38alpha MAPK in colon cancer: suppression of colitis-associated tumor initiation but requirement for cancer cell survival. *Cancer Cell* **25**, 484-500, doi:10.1016/j.ccr.2014.02.019 (2014).

304. Wang, L., Zhou, J., Zhang, C., Chen, R., Sun, Q., Yang, P., Peng, C., Tan, Y., Jin, C., Wang, T., Ji, J. and Sun, Y. A novel tumour suppressor protein encoded by circMAPK14 inhibits progression and metastasis of colorectal cancer by competitively binding to MKK6. *Clin Transl Med* **11**, e613, doi:10.1002/ctm2.613 (2021).

305. Abu-Freha, N., Cohen, B., Gordon, M., Weissmann, S., Kestenbaum, E. H., Vosko, S., Abu-Tailakh, M., Ben-Shoshan, L., Cohen, D. L. and Shirin, H. Colorectal cancer among inflammatory bowel disease patients: risk factors and prevalence compared to the general population. *Front Med (Lausanne)* **10**, 1225616, doi:10.3389/fmed.2023.1225616 (2023).

306. Hashemi, M., Abbaszadeh, S., Rashidi, M., Amini, N., Talebi Anaraki, K., Motahhary, M., Khalilipouya, E., Harif Nashtifani, A., Shafiei, S., Ramezani Farani, M., Nabavi, N., Salimimoghadam, S., Aref, A. R., Raesi, R., Taheriazam, A., Entezari, M. and Zha, W. STAT3 as a newly emerging target in colorectal cancer therapy: Tumorigenesis, therapy response, and pharmacological/nanoplatform strategies. *Environ Res* **233**, 116458, doi:10.1016/j.envres.2023.116458 (2023).

307. Irey, E. A., Lassiter, C. M., Brady, N. J., Chuntova, P., Wang, Y., Knutson, T. P., Henzler, C., Chaffee, T. S., Vogel, R. I., Nelson, A. C., Farrar, M. A. and Schwertfeger, K. L. JAK/STAT inhibition in macrophages promotes therapeutic resistance by inducing expression of protumorigenic factors. *Proc Natl Acad Sci U S A* **116**, 12442-12451, doi:10.1073/pnas.1816410116 (2019).

308. Pathria, P., Gotthardt, D., Prchal-Murphy, M., Putz, E. M., Holcmann, M., Schlederer, M., Grabner, B., Crncec, I., Svinka, J., Musteanu, M., Hoffmann, T., Filipits, M., Berger, W., Poli, V., Kenner, L., Bilban, M., Casanova, E., Muller, M., Strobl, B., Bayer, E., Mohr, T., Sexl, V. and Eferl, R. Myeloid STAT3 promotes formation of colitis-associated colorectal cancer in mice. *Oncoimmunology* **4**, e998529, doi:10.1080/2162402X.2014.998529 (2015).

309. Vogelstein, B., Fearon, E. R., Kern, S. E., Hamilton, S. R., Preisinger, A. C., Nakamura, Y. and White, R. Allelotype of colorectal carcinomas. *Science* **244**, 207-11, doi:10.1126/science.2565047 (1989).

310. Lee, J., Kim, J. C., Lee, S. E., Quinley, C., Kim, H., Herdman, S., Corr, M. and Raz, E. Signal transducer and activator of transcription 3 (STAT3) protein suppresses adenoma-to-carcinoma transition in Apcmin/+ mice via regulation of Snail-1 (SNAI) protein stability. *J Biol Chem* **287**, 18182-9, doi:10.1074/jbc.M111.328831 (2012).

311. Yamagiwa, K. and Ichikawa, K. Experimental study of the pathogenesis of carcinoma. *CA Cancer J Clin* **27**, 174-81, doi:10.3322/canjclin.27.3.174 (1977).

312. Kwak, T., Wang, F., Deng, H., Condamine, T., Kumar, V., Perego, M., Kossenkov, A., Montaner, L. J., Xu, X., Xu, W., Zheng, C., Schuchter, L. M., Amaravadi, R. K., Mitchell, T. C., Karakousis, G. C., Mulligan, C., Nam, B., Masters, G., Hockstein, N., Bennett, J., Nefedova, Y. and Gabrilovich, D. I. Distinct Populations of Immune-Suppressive Macrophages Differentiate from Monocytic Myeloid-Derived Suppressor Cells in Cancer. *Cell Rep* **33**, 108571, doi:10.1016/j.celrep.2020.108571 (2020).

313. Wang, H., Tian, T. and Zhang, J. Tumor-Associated Macrophages (TAMs) in Colorectal Cancer (CRC): From Mechanism to Therapy and Prognosis. *Int J Mol Sci* **22**, doi:10.3390/ijms22168470 (2021).

314. Talmadge, J. E. and Gabrilovich, D. I. History of myeloid-derived suppressor cells. *Nat Rev Cancer* **13**, 739-52, doi:10.1038/nrc3581 (2013).

315. Wang, K., Wang, Y. and Yin, K. Role played by MDSC in colitis-associated colorectal cancer and potential therapeutic strategies. *J Cancer Res Clin Oncol* **150**, 243, doi:10.1007/s00432-024-05755-w (2024).

316. Toor, S. M., Syed Khaja, A. S., El Salhat, H., Bekdache, O., Kanbar, J., Jaloudi, M. and Elkord, E. Increased Levels of Circulating and Tumor-Infiltrating Granulocytic Myeloid Cells in Colorectal Cancer Patients. *Front Immunol* **7**, 560, doi:10.3389/fimmu.2016.00560 (2016).

317. Gabrilovich, D. I. and Nagaraj, S. Myeloid-derived suppressor cells as regulators of the immune system. *Nat Rev Immunol* **9**, 162-74, doi:10.1038/nri2506 (2009).

318. Wang, Y., Ding, Y., Deng, Y., Zheng, Y. and Wang, S. Role of myeloid-derived suppressor cells in the promotion and immunotherapy of colitis-associated cancer. *J Immunother Cancer* **8**, doi:10.1136/jitc-2020-000609 (2020).

319. de Barrios, O., Sanchez-Moral, L., Cortes, M., Ninfali, C., Profitos-Peleja, N., Martinez-Campanario, M. C., Siles, L., Del Campo, R., Fernandez-Acenero, M. J., Darling, D. S., Castells, A., Maurel, J., Salas, A., Dean, D. C. and Postigo, A. ZEB1 promotes inflammation and progression towards inflammation-driven carcinoma through repression of the DNA repair glycosylase MPG in epithelial cells. *Gut* **68**, 2129-2141, doi:10.1136/gutjnl-2018-317294 (2019).

320. Ichikawa, M., Williams, R., Wang, L., Vogl, T. and Srikrishna, G. S100A8/A9 activate key genes and pathways in colon tumor progression. *Mol Cancer Res* **9**, 133-48, doi:10.1158/1541-7786.MCR-10-0394 (2011).

321. Wang, Y., Yin, K., Tian, J., Xia, X., Ma, J., Tang, X., Xu, H. and Wang, S. Granulocytic Myeloid-Derived Suppressor Cells Promote the Stemness of Colorectal Cancer Cells through Exosomal S100A9. *Adv Sci (Weinh)* **6**, 1901278, doi:10.1002/advs.201901278 (2019).

322. Al-Mterin, M. A. and Elkord, E. Myeloid-derived suppressor cells in colorectal cancer: prognostic biomarkers and therapeutic targets. *Explor Target Antitumor Ther* **3**, 497-510, doi:10.37349/etat.2022.00097 (2022).

323. Shields, N. J., Peyroux, E. M., Ferguson, A. L., Steain, M., Neumann, S. and Young, S. L. Late-stage MC38 tumours recapitulate features of human colorectal cancer - implications for appropriate timepoint selection in preclinical studies. *Front Immunol* **14**, 1152035, doi:10.3389/fimmu.2023.1152035 (2023).

324. Sieminska, I. and Baran, J. Myeloid-Derived Suppressor Cells in Colorectal Cancer. *Front Immunol* **11**, 1526, doi:10.3389/fimmu.2020.01526 (2020).

325. Nathan, C. Neutrophils and immunity: challenges and opportunities. *Nat Rev Immunol* **6**, 173-82, doi:10.1038/nri1785 (2006).

326. Mizuno, R., Kawada, K., Itatani, Y., Ogawa, R., Kiyasu, Y. and Sakai, Y. The Role of Tumor-Associated Neutrophils in Colorectal Cancer. *Int J Mol Sci* **20**, doi:10.3390/ijms20030529 (2019).

327. Triner, D., Xue, X., Schwartz, A. J., Jung, I., Colacino, J. A. and Shah, Y. M. Epithelial Hypoxia-Inducible Factor 2alpha Facilitates the Progression of Colon Tumors through Recruiting Neutrophils. *Mol Cell Biol* **37**, doi:10.1128/MCB.00481-16 (2017).

328. Lin, Y., Cheng, L., Liu, Y., Wang, Y., Wang, Q., Wang, H. L., Shi, G., Li, J. S., Wang, Q. N., Yang, Q. M., Chen, S., Su, X. L., Yang, Y., Jiang, M., Hu, X., Fan, P., Fang, C., Zhou, Z. G., Dai, L. and Deng, H. X. Intestinal epithelium-derived BATF3 promotes colitis-associated colon cancer through facilitating CXCL5-mediated neutrophils recruitment. *Mucosal Immunol* **14**, 187-198, doi:10.1038/s41385-020-0297-3 (2021).

329. Shang, K., Bai, Y. P., Wang, C., Wang, Z., Gu, H. Y., Du, X., Zhou, X. Y., Zheng, C. L., Chi, Y. Y., Mukaida, N. and Li, Y. Y. Crucial involvement of tumor-associated neutrophils in the regulation of chronic colitis-associated carcinogenesis in mice. *PLoS One* **7**, e51848, doi:10.1371/journal.pone.0051848 (2012).

330. Mudatsir, Labeda, I., Uwuratuw, J. A., Hendarto, J., Warsinggih, Lusikooy, R. E., Mappincara, Sampetoding, S., Kusuma, M. I., Syarifuddin, E., Arsyad, A. and Faruk, M. Relationship between metalloproteinase-9 (MMP-9) expression and clinicopathology in colorectal cancer: a cross-sectional study. *Ann Med Surg (Lond)* **85**, 4277-4282, doi:10.1097/MS9.0000000000000892 (2023).

331. Jia, W., Mao, Y., Luo, Q., Wu, J. and Guan, Q. Targeting neutrophil elastase is a promising direction for future cancer treatment. *Discov Oncol* **15**, 167, doi:10.1007/s12672-024-01010-3 (2024).

332. Triner, D., Devenport, S. N., Ramakrishnan, S. K., Ma, X., Frieler, R. A., Greenson, J. K., Inohara, N., Nunez, G., Colacino, J. A., Mortensen, R. M. and Shah, Y. M. Neutrophils Restrict Tumor-Associated Microbiota to Reduce Growth and Invasion of Colon Tumors in Mice. *Gastroenterology* **156**, 1467-1482, doi:10.1053/j.gastro.2018.12.003 (2019).

333. Arora, M., Poe, S. L., Oriss, T. B., Krishnamoorthy, N., Yarlagadda, M., Wenzel, S. E., Billiar, T. R., Ray, A. and Ray, P. TLR4/MyD88-induced CD11b+Gr-1 int F4/80+ non-migratory myeloid cells suppress Th2 effector function in the lung. *Mucosal Immunol* **3**, 578-93, doi:10.1038/mi.2010.41 (2010).

334. Butin-Israeli, V., Houser, M. C., Feng, M., Thorp, E. B., Nusrat, A., Parkos, C. A. and Sumagin, R. Deposition of microparticles by neutrophils onto inflamed epithelium: a new mechanism to disrupt epithelial intercellular adhesions and promote transepithelial migration. *FASEB J* **30**, 4007-4020, doi:10.1096/fj.201600734R (2016).

335. Bui, T. M. and Sumagin, R. Progressing from Recurring Tissue Injury to Genomic Instability: A New Mechanism of Neutrophil Pathogenesis. *DNA Cell Biol* **38**, 747-753, doi:10.1089/dna.2019.4842 (2019).

336. Legitimo, A., Consolini, R., Failli, A., Orsini, G. and Spisni, R. Dendritic cell defects in the colorectal cancer. *Hum Vaccin Immunother* **10**, 3224-35, doi:10.4161/hv.29857 (2014).

337. Gulubova, M. V., Ananiev, J. R., Vlaykova, T. I., Yovchev, Y., Tsoneva, V. and Manolova, I. M. Role of dendritic cells in progression and clinical outcome of colon cancer. *Int J Colorectal Dis* **27**, 159-69, doi:10.1007/s00384-011-1334-1 (2012).

338. Garrett, W. S., Punit, S., Gallini, C. A., Michaud, M., Zhang, D., Sigrist, K. S., Lord, G. M., Glickman, J. N. and Glimcher, L. H. Colitis-associated colorectal cancer driven by T-bet deficiency in dendritic cells. *Cancer Cell* **16**, 208-19, doi:10.1016/j.ccr.2009.07.015 (2009).

339. Hsu, Y. L., Chen, Y. J., Chang, W. A., Jian, S. F., Fan, H. L., Wang, J. Y. and Kuo, P. L. Interaction between Tumor-Associated Dendritic Cells and Colon Cancer Cells Contributes to Tumor Progression via CXCL1. *Int J Mol Sci* **19**, doi:10.3390/ijms19082427 (2018).

340. Farah, S., Anderson, D. G. and Langer, R. Physical and mechanical properties of PLA, and their functions in widespread applications - A comprehensive review. *Adv Drug Deliv Rev* **107**, 367-392, doi:10.1016/j.addr.2016.06.012 (2016).

341. Chalidis, B., Kitridis, D., Savvidis, P., Papalois, A. and Givissis, P. Does the Inion OTPS(TM) absorbable plating system induce higher foreign-body reaction than titanium implants? An experimental randomized comparative study in rabbits. *Biomed Mater* **15**, 065011, doi:10.1088/1748-605X/aba326 (2020).

342. Maduka, C. V., Makela, A. V., Tundo, A., Ural, E. E., Stivers, K. B., Kuhnert, M. M., Alhaj, M., Hoque Apu, E., Ashammakhi, N., Hankenson, K. D., Narayan, R., Elisseeff, J. H. and Contag, C. H. Regulating the proinflammatory response to composite biomaterials by targeting immunometabolism. *Bioactive Materials* 64-73, doi:10.1016/j.bioactmat.2024.05.046 (2024).

343. Maduka, C. V., Makela, A. V., Tundo, A., Ural, E. E., Stivers, K. B., Alhaj, M., Narayan, R., Goodman, S. B., Ashammakhi, N., Elisseeff, J. H., Hankenson, K. D. and Contag, C. H. Role of mitochondrial complex I in the proinflammatory response to polylactide implants. *ACS Applied Engineering Materials* **2**, doi:10.1021/acsaenm.4c00393 (2024).

344. Givissis, P. K., Stavridis, S. I., Papagelopoulos, P. J., Antonarakos, P. D. and Christodoulou, A. G. Delayed foreign-body reaction to absorbable implants in metacarpal fracture treatment. *Clin Orthop Relat Res* **468**, 3377-83, doi:10.1007/s11999-010-1388-3 (2010).

345. Laine, P., Kontio, R., Lindqvist, C. and Suuronen, R. Are there any complications with bioabsorbable fixation devices? A 10 year review in orthognathic surgery. *Int J Oral Maxillofac Surg* **33**, 240-4, doi:10.1006/ijom.2003.0510 (2004).

346. Poh, P. S. P., Chhaya, M. P., Wunner, F. M., De-Juan-Pardo, E. M., Schilling, A. F., Schantz, J. T., van Griensven, M. and Hutmacher, D. W. Polylactides in additive biomanufacturing. *Adv Drug Deliv Rev* **107**, 228-246, doi:10.1016/j.addr.2016.07.006 (2016).

347. Ramot, Y., Haim-Zada, M., Domb, A. J. and Nyska, A. Biocompatibility and safety of PLA and its copolymers. *Adv Drug Deliv Rev* **107**, 153-162, doi:10.1016/j.addr.2016.03.012 (2016).

348. Mosier-Laclair, S., Pike, H. and Pomeroy, G. Intraosseous bioabsorbable poly-L-lactic acid screw presenting as a late foreign-body reaction: a case report. *Foot Ankle Int* **22**, 247-51, doi:10.1177/107110070102200313 (2001).

349. Athanasiou, K. A., Agrawal, C. M., Barber, F. A. and Burkhart, S. S. Orthopaedic applications for PLA-PGA biodegradable polymers. *Arthroscopy* **14**, 726-37, doi:10.1016/s0749-8063(98)70099-4 (1998).

350. Waris, E., Ashammakhi, N., Lehtimaki, M., Tulamo, R. M., Tormala, P., Kellomaki, M. and Konttinen, Y. T. Long-term bone tissue reaction to polyethylene oxide/polybutylene terephthalate copolymer (Polyactive) in metacarpophalangeal joint reconstruction. *Biomaterials* **29**, 2509-15, doi:10.1016/j.biomaterials.2008.02.013 (2008).

351. Agrawal, C. M. and Athanasiou, K. A. Technique to control pH in vicinity of biodegrading PLA-PGA implants. *J Biomed Mater Res* **38**, 105-14, doi:10.1002/(sici)1097-4636(199722)38:2<105::aid-jbm4>3.0.co;2-u (1997).

352. Taylor, M. S., Daniels, A. U., Andriano, K. P. and Heller, J. Six bioabsorbable polymers: in vitro acute toxicity of accumulated degradation products. *J Appl Biomater* **5**, 151-7, doi:10.1002/jab.770050208 (1994).

353. Deng, M., Nair, L. S., Nukavarapu, S. P., Jiang, T., Kanner, W. A., Li, X., Kumbar, S. G., Weikel, A. L., Krogman, N. R., Allcock, H. R. and Laurencin, C. T. Dipeptide-based polyphosphazene and polyester blends for bone tissue engineering. *Biomaterials* **31**, 4898-908, doi:10.1016/j.biomaterials.2010.02.058 (2010).

354. Pajares-Chamorro, N., Wagley, Y., Maduka, C. V., Youngstrom, D. W., Yeger, A., Badylak, S. F., Hammer, N. D., Hankenson, K. and Chatzistavrou, X. Silver-doped bioactive glass particles for in vivo bone tissue regeneration and enhanced methicillin-resistant Staphylococcus aureus (MRSA) inhibition. *Mater Sci Eng C Mater Biol Appl* **120**, 111693, doi:10.1016/j.msec.2020.111693 (2021).

355. Lih, E., Park, W., Park, K. W., Chun, S. Y., Kim, H., Joung, Y. K., Kwon, T. G., Hubbell, J. A. and Han, D. K. A Bioinspired Scaffold with Anti-Inflammatory Magnesium Hydroxide and Decellularized Extracellular Matrix for Renal Tissue Regeneration. *ACS Cent Sci* **5**, 458-467, doi:10.1021/acscentsci.8b00812 (2019).

356. Xu, T. O., Kim, H. S., Stahl, T. and Nukavarapu, S. P. Self-neutralizing PLGA/magnesium composites as novel biomaterials for tissue engineering. *Biomed Mater* **13**, 035013, doi:10.1088/1748-605X/aaaa29 (2018).

357. Kamata, M., Sakamoto, Y. and Kishi, K. Foreign-Body Reaction to Bioabsorbable Plate and Screw in Craniofacial Surgery. *J Craniofac Surg* **30**, e34-e36, doi:10.1097/SCS.0000000000004945 (2019).

358. Narayanan, G., Vernekar, V. N., Kuyinu, E. L. and Laurencin, C. T. Poly (lactic acid)-based biomaterials for orthopaedic regenerative engineering. *Adv Drug Deliv Rev* **107**, 247-276, doi:10.1016/j.addr.2016.04.015 (2016).

359. Gonzalez-Lomas, G., Cassilly, R. T., Remotti, F. and Levine, W. N. Is the etiology of pretibial cyst formation after absorbable interference screw use related to a foreign body reaction? *Clin Orthop Relat Res* **469**, 1082-8, doi:10.1007/s11999-010-1580-5 (2011).

360. Xie, N., Tan, Z., Banerjee, S., Cui, H., Ge, J., Liu, R. M., Bernard, K., Thannickal, V. J. and Liu, G. Glycolytic Reprogramming in Myofibroblast Differentiation and Lung Fibrosis. *Am J Respir Crit Care Med* **192**, 1462-74, doi:10.1164/rccm.201504-0780OC (2015).

361. O'Neill, L. A. and Pearce, E. J. Immunometabolism governs dendritic cell and macrophage function. *J Exp Med* **213**, 15-23, doi:10.1084/jem.20151570 (2016).

362. Clem, B., Telang, S., Clem, A., Yalcin, A., Meier, J., Simmons, A., Rasku, M. A., Arumugam, S., Dean, W. L., Eaton, J., Lane, A., Trent, J. O. and Chesney, J. Small-molecule inhibition of 6-phosphofructo-2-kinase activity suppresses glycolytic flux and tumor growth. *Mol Cancer Ther* **7**, 110-20, doi:10.1158/1535-7163.MCT-07-0482 (2008).

363. Kauppinen, R. A., Sihra, T. S. and Nicholls, D. G. Aminooxyacetic acid inhibits the malate-aspartate shuttle in isolated nerve terminals and prevents the mitochondria from utilizing glycolytic substrates. *Biochim Biophys Acta* **930**, 173-8, doi:10.1016/0167-4889(87)90029-2 (1987).

364. Korangath, P., Teo, W. W., Sadik, H., Han, L., Mori, N., Huijts, C. M., Wildes, F., Bharti, S., Zhang, Z., Santa-Maria, C. A., Tsai, H., Dang, C. V., Stearns, V., Bhujwalla, Z. M. and Sukumar, S. Targeting

Glutamine Metabolism in Breast Cancer with Aminooxyacetate. *Clin Cancer Res* **21**, 3263-73, doi:10.1158/1078-0432.CCR-14-1200 (2015).

365. Maduka, C. V., Kuhnert, M. M., Habeeb, O. M., Tundo, A., Makela, A. V., Goodman, S. B. and Contag, C. H. Elevated oxidative phosphorylation is critical for immune cell activation by polyethylene wear particles. *Journal of Immunology and Regenerative Medicine* (2023).

366. Kelly, B., Tannahill, G. M., Murphy, M. P. and O'Neill, L. A. Metformin Inhibits the Production of Reactive Oxygen Species from NADH:Ubiquinone Oxidoreductase to Limit Induction of Interleukin-1beta (IL-1beta) and Boosts Interleukin-10 (IL-10) in Lipopolysaccharide (LPS)-activated Macrophages. *J Biol Chem* **290**, 20348-59, doi:10.1074/jbc.M115.662114 (2015).

367. Mosser, D. M. and Gonçalves, R. Activation of Murine Macrophages. *Current Protocols in Immunology* **111**, 14.2.1-14.2.10, doi:10.1002/0471142735.im1402s111 (2015).

368. Kanada, M., Bachmann, M. H., Hardy, J. W., Frimannson, D. O., Bronsart, L., Wang, A., Sylvester, M. D., Schmidt, T. L., Kaspar, R. L., Butte, M. J., Matin, A. C. and Contag, C. H. Differential fates of biomolecules delivered to target cells via extracellular vesicles. *Proc Natl Acad Sci U S A* **112**, E1433-42, doi:10.1073/pnas.1418401112 (2015).

369. Negrin, R. S. and Contag, C. H. In vivo imaging using bioluminescence: a tool for probing graft-versus-host disease. *Nat Rev Immunol* **6**, 484-90, doi:10.1038/nri1879 (2006).

370. Sprague, L., Muccioli, M., Pate, M., Singh, M., Xiong, C., Ostermann, A., Niese, B., Li, Y., Li, Y., Courreges, M. C. and Benencia, F. Dendritic cells: In vitro culture in two- and three-dimensional collagen systems and expression of collagen receptors in tumors and atherosclerotic microenvironments. *Exp Cell Res* **323**, 7-27, doi:10.1016/j.yexcr.2014.01.031 (2014).

371. Poon, C. Measuring the density and viscosity of culture media for optimized computational fluid dynamics analysis of in vitro devices. *J Mech Behav Biomed Mater* **126**, 105024, doi:10.1016/j.jmbbm.2021.105024 (2022).

372. Pérez, E. Mechanical performance of in vitro degraded polylactic acid/hydroxyapatite composites. *Journal of Materials Science* **56**, 19915–19935, doi:10.1007/s10853-021-06508-7 (2021).

373. Bravo-Hernandez, M., Tadokoro, T., Navarro, M. R., Platoshyn, O., Kobayashi, Y., Marsala, S., Miyanohara, A., Juhas, S., Juhasova, J., Skalnikova, H., Tomori, Z., Vanicky, I., Studenovska, H., Proks, V., Chen, P., Govea-Perez, N., Ditsworth, D., Ciacci, J. D., Gao, S., Zhu, W., Ahrens, E. T., Driscoll, S. P., Glenn, T. D., McAlonis-Downes, M., Da Cruz, S., Pfaff, S. L., Kaspar, B. K., Cleveland, D. W. and Marsala, M. Spinal subpial delivery of AAV9 enables widespread gene silencing and blocks motoneuron degeneration in ALS. *Nat Med* **26**, 118-130, doi:10.1038/s41591-019-0674-1 (2020).

374. Tan, Z., Xie, N., Banerjee, S., Cui, H., Fu, M., Thannickal, V. J. and Liu, G. The monocarboxylate transporter 4 is required for glycolytic reprogramming and inflammatory response in macrophages. *J Biol Chem* **290**, 46-55, doi:10.1074/jbc.M114.603589 (2015).

375. Mosser, D. M. and Zhang, X. Activation of murine macrophages. *Curr Protoc Immunol* **Chapter 14**, 14 2 1-14 2 8, doi:10.1002/0471142735.im1402s83 (2008).

376. Infantino, V., Iacobazzi, V., Palmieri, F. and Menga, A. ATP-citrate lyase is essential for macrophage inflammatory response. *Biochem Biophys Res Commun* **440**, 105-11, doi:10.1016/j.bbrc.2013.09.037 (2013).

377. Jijon, H. B., Churchill, T., Malfair, D., Wessler, A., Jewell, L. D., Parsons, H. G. and Madsen, K. L. Inhibition of poly(ADP-ribose) polymerase attenuates inflammation in a model of chronic colitis. *Am J Physiol Gastrointest Liver Physiol* **279**, G641-51, doi:10.1152/ajpgi.2000.279.3.G641 (2000).

378. Bonora, M., Patergnani, S., Rimessi, A., De Marchi, E., Suski, J. M., Bononi, A., Giorgi, C., Marchi, S., Missiroli, S., Poletti, F., Wieckowski, M. R. and Pinton, P. ATP synthesis and storage. *Purinergic Signal* **8**, 343-57, doi:10.1007/s11302-012-9305-8 (2012).

379. Philpott, G. W., Schwarz, S. W., Anderson, C. J., Dehdashti, F., Connett, J. M., Zinn, K. R., Meares, C. F., Cutler, P. D., Welch, M. J. and Siegel, B. A. RadioimmunoPET: detection of colorectal carcinoma with positron-emitting copper-64-labeled monoclonal antibody. *J Nucl Med* **36**, 1818-24, (1995).

380. Tang, C. Y. and Mauro, C. Similarities in the Metabolic Reprogramming of Immune System and Endothelium. *Front Immunol* **8**, 837, doi:10.3389/fimmu.2017.00837 (2017).

381. Chong, G. O., Lee, Y. H., Hong, D. G., Cho, Y. L. and Lee, Y. S. Unabsorbed polylactide adhesion barrier mimicking recurrence of gynecologic malignant diseases with increased (1)(8)F-FDG uptake on PET/CT. *Arch Gynecol Obstet* **292**, 191-5, doi:10.1007/s00404-014-3587-8 (2015).

382. Hsieh, T. C. and Hsu, C. W. Foreign body reaction mimicking local recurrence from polyactide adhesion barrier film after laparoscopic colorectal cancer surgery: A retrospective cohort study. *Medicine (Baltimore)* **101**, e28692, doi:10.1097/MD.0000000000028692 (2022).

383. Bostman, O. M. and Pihlajamaki, H. K. Adverse tissue reactions to bioabsorbable fixation devices. *Clin Orthop Relat Res* 216-27, (2000).

384. Veiseh, O., Doloff, J. C., Ma, M., Vegas, A. J., Tam, H. H., Bader, A. R., Li, J., Langan, E., Wyckoff, J., Loo, W. S., Jhunjhunwala, S., Chiu, A., Siebert, S., Tang, K., Hollister-Lock, J., Aresta-Dasilva, S., Bochenek, M., Mendoza-Elias, J., Wang, Y., Qi, M., Lavin, D. M., Chen, M., Dholakia, N., Thakrar, R., Lacik, I., Weir, G. C., Oberholzer, J., Greiner, D. L., Langer, R. and Anderson, D. G. Size- and shape-dependent foreign body immune response to materials implanted in rodents and non-human primates. *Nat Mater* **14**, 643-51, doi:10.1038/nmat4290 (2015).

385. Bernardo, M. P., da Silva, B. C. R., Hamouda, A. E. I., de Toledo, M. A. S., Schalla, C., Rutten, S., Goetzke, R., Mattoso, L. H. C., Zenke, M. and Sechi, A. PLA/Hydroxyapatite scaffolds exhibit in vitro immunological inertness and promote robust osteogenic differentiation of human mesenchymal stem cells without osteogenic stimuli. *Sci Rep* **12**, 2333, doi:10.1038/s41598-022-05207-w (2022).

386. Maduka, C. V., Schmitter-Sánchez, A. D., Makela, A. V., Ural, E. E., Stivers, K. B., Pope, H., Kuhnert, M. M., Habeeb, O. M., Tundo, A., Alhaj, M., Kiselev, A., Chen, S., Olive, A. J., Hankenson, K. D., Narayan, R., Park, S., Elisseeff, J. H. and Contag, C. H. Immunometabolic cues recompose and reprogram the microenvironment around implanted biomaterials. *Nature Biomedical Engineering* **8**, 1308-1321, doi:10.1038/s41551-024-01260-0 (2024).

387. Jaynes, J. M., Sable, R., Ronzetti, M., Bautista, W., Knotts, Z., Abisoye-Ogunniyan, A., Li, D., Calvo, R., Dashnyam, M., Singh, A., Guerin, T., White, J., Ravichandran, S., Kumar, P., Talsania, K., Chen, V., Ghebremedhin, A., Karanam, B., Bin Salam, A., Amin, R., Odzorig, T., Aiken, T., Nguyen, V., Bian, Y., Zarif, J. C., de Groot, A. E., Mehta, M., Fan, L., Hu, X., Simeonov, A., Pate, N., Abu-Asab, M., Ferrer, M., Southall, N., Ock, C. Y., Zhao, Y., Lopez, H., Kozlov, S., de Val, N., Yates, C. C., Baljinnyam, B., Marugan, J. and Rudloff, U. Mannose receptor (CD206) activation in tumor-

associated macrophages enhances adaptive and innate antitumor immune responses. *Sci Transl Med* **12**, doi:10.1126/scitranslmed.aax6337 (2020).

388. Sadtler, K., Estrellas, K., Allen, B. W., Wolf, M. T., Fan, H., Tam, A. J., Patel, C. H., Luber, B. S., Wang, H., Wagner, K. R., Powell, J. D., Housseau, F., Pardoll, D. M. and Elisseeff, J. H. Developing a pro-regenerative biomaterial scaffold microenvironment requires T helper 2 cells. *Science* **352**, 366-70, doi:10.1126/science.aad9272 (2016).

389. Wang, Y., Smith, W., Hao, D., He, B. and Kong, L. M1 and M2 macrophage polarization and potentially therapeutic naturally occurring compounds. *Int Immunopharmacol* **70**, 459-466, doi:10.1016/j.intimp.2019.02.050 (2019).

390. Maduka, C. V., Alhaj, M., Ural, E., Kuhnert, M. M., Habeeb, O. M., Schilmiller, A. L., Hankenson, K. D., Goodman, S. B., Narayan, R. and Contag, C. H. Stereochemistry Determines Immune Cellular Responses to Polylactide Implants. *ACS Biomater Sci Eng* **9**, 932-943, doi:10.1021/acsbiomaterials.2c01279 (2023).

391. Lange, T., Schilling, A. F., Peters, F., Haag, F., Morlock, M. M., Rueger, J. M. and Amling, M. Proinflammatory and osteoclastogenic effects of beta-tricalciumphosphate and hydroxyapatite particles on human mononuclear cells in vitro. *Biomaterials* **30**, 5312-8, doi:10.1016/j.biomaterials.2009.06.023 (2009).

392. Mahon, O. R., Kelly, D. J., McCarthy, G. M. and Dunne, A. Osteoarthritis-associated basic calcium phosphate crystals alter immune cell metabolism and promote M1 macrophage polarization. *Osteoarthritis Cartilage* **28**, 603-612, doi:10.1016/j.joca.2019.10.010 (2020).

393. Edwards, F. C., Taheri, A., Dann, S. C. and Dye, J. F. Characterization of cytolytic neutrophil activation in vitro by amorphous hydrated calcium phosphate as a model of biomaterial inflammation. *J Biomed Mater Res A* **96**, 552-65, doi:10.1002/jbm.a.32937 (2011).

394. Sadtler, K., Wolf, M. T., Ganguly, S., Moad, C. A., Chung, L., Majumdar, S., Housseau, F., Pardoll, D. M. and Elisseeff, J. H. Divergent immune responses to synthetic and biological scaffolds. *Biomaterials* **192**, 405-415, doi:10.1016/j.biomaterials.2018.11.002 (2019).

395. Huang, L. R., Wohlleber, D., Reisinger, F., Jenne, C. N., Cheng, R. L., Abdullah, Z., Schildberg, F. A., Odenthal, M., Dienes, H. P., van Rooijen, N., Schmitt, E., Garbi, N., Croft, M., Kurts, C., Kubes, P., Protzer, U., Heikenwalder, M. and Knolle, P. A. Intrahepatic myeloid-cell aggregates enable local proliferation of CD8(+) T cells and successful immunotherapy against chronic viral liver infection. *Nat Immunol* **14**, 574-83, doi:10.1038/ni.2573 (2013).

396. Li, X., Cho, B., Martin, R., Seu, M., Zhang, C., Zhou, Z., Choi, J. S., Jiang, X., Chen, L., Walia, G., Yan, J., Callanan, M., Liu, H., Colbert, K., Morrissette-McAlmon, J., Grayson, W., Reddy, S., Sacks, J. M. and Mao, H. Q. Nanofiber-hydrogel composite-mediated angiogenesis for soft tissue reconstruction. *Sci Transl Med* **11**, doi:10.1126/scitranslmed.aau6210 (2019).

397. Yang, L., Xiao, L., Gao, W., Huang, X., Wei, F., Zhang, Q. and Xiao, Y. Macrophages at Low-Inflammatory Status Improved Osteogenesis via Autophagy Regulation. *Tissue Eng Part A* doi:10.1089/ten.TEA.2021.0015 (2021).

398. Velard, F., Laurent-Maquin, D., Braux, J., Guillaume, C., Bouthors, S., Jallot, E., Nedelec, J. M., Belaaouaj, A. and Laquerriere, P. The effect of zinc on hydroxyapatite-mediated activation of human polymorphonuclear neutrophils and bone implant-associated acute inflammation. *Biomaterials* **31**, 2001-9, doi:10.1016/j.biomaterials.2009.11.066 (2010).

399. Mahon, O. R., O'Hanlon, S., Cunningham, C. C., McCarthy, G. M., Hobbs, C., Nicolosi, V., Kelly, D. J. and Dunne, A. Orthopaedic implant materials drive M1 macrophage polarization in a spleen tyrosine kinase- and mitogen-activated protein kinase-dependent manner. *Acta Biomater* **65**, 426-435, doi:10.1016/j.actbio.2017.10.041 (2018).

400. Xue, H., Zhang, Z., Lin, Z., Su, J., Panayi, A. C., Xiong, Y., Hu, L., Hu, Y., Chen, L., Yan, C., Xie, X., Shi, Y., Zhou, W., Mi, B. and Liu, G. Enhanced tissue regeneration through immunomodulation of angiogenesis and osteogenesis with a multifaceted nanohybrid modified bioactive scaffold. *Bioact Mater* **18**, 552-568, doi:10.1016/j.bioactmat.2022.05.023 (2022).

401. Guo, M., Dong, Y., Xiao, J., Gu, R., Ding, M., Huang, T., Li, J., Zhao, N. and Liao, H. In vivo immuno-reactivity analysis of the porous three-dimensional chitosan/SiO(2) and chitosan/SiO(2) /hydroxyapatite hybrids. *J Biomed Mater Res A* **106**, 1223-1235, doi:10.1002/jbm.a.36320 (2018).

402. Jha, A. K., Huang, S. C., Sergushichev, A., Lampropoulou, V., Ivanova, Y., Loginicheva, E., Chmielewski, K., Stewart, K. M., Ashall, J., Everts, B., Pearce, E. J., Driggers, E. M. and Artyomov, M. N. Network integration of parallel metabolic and transcriptional data reveals metabolic modules that regulate macrophage polarization. *Immunity* **42**, 419-30, doi:10.1016/j.immuni.2015.02.005 (2015).

403. Manoharan, I., Prasad, P. D., Thangaraju, M. and Manicassamy, S. Lactate-Dependent Regulation of Immune Responses by Dendritic Cells and Macrophages. *Front Immunol* **12**, 691134, doi:10.3389/fimmu.2021.691134 (2021).

404. Zhang, A., Xu, Y., Xu, H., Ren, J., Meng, T., Ni, Y., Zhu, Q., Zhang, W. B., Pan, Y. B., Jin, J., Bi, Y., Wu, Z. B., Lin, S. and Lou, M. Lactate-induced M2 polarization of tumor-associated macrophages promotes the invasion of pituitary adenoma by secreting CCL17. *Theranostics* **11**, 3839-3852, doi:10.7150/thno.53749 (2021).

405. Samuvel, D. J., Sundararaj, K. P., Nareika, A., Lopes-Virella, M. F. and Huang, Y. Lactate boosts TLR4 signaling and NF-kappaB pathway-mediated gene transcription in macrophages via monocarboxylate transporters and MD-2 up-regulation. *J Immunol* **182**, 2476-84, doi:10.4049/jimmunol.0802059 (2009).

406. Yang, K., Xu, J., Fan, M., Tu, F., Wang, X., Ha, T., Williams, D. L. and Li, C. Lactate Suppresses Macrophage Pro-Inflammatory Response to LPS Stimulation by Inhibition of YAP and NF-kappaB Activation via GPR81-Mediated Signaling. *Front Immunol* **11**, 587913, doi:10.3389/fimmu.2020.587913 (2020).

407. Multhoff, G., Molls, M. and Radons, J. Chronic inflammation in cancer development. *Front Immunol* **2**, 98, doi:10.3389/fimmu.2011.00098 (2011).

408. Hanahan, D. and Weinberg, R. A. The hallmarks of cancer. *Cell* **100**, 57-70, doi:10.1016/s0092-8674(00)81683-9 (2000).

409. Hanahan, D. and Weinberg, R. A. Hallmarks of cancer: the next generation. *Cell* **144**, 646-74, doi:10.1016/j.cell.2011.02.013 (2011).

410. Sleeman, J. P. The metastatic niche and stromal progression. *Cancer Metastasis Rev* **31**, 429-40, doi:10.1007/s10555-012-9373-9 (2012).

411. Wortzel, I., Dror, S., Kenific, C. M. and Lyden, D. Exosome-Mediated Metastasis: Communication from a Distance. *Dev Cell* **49**, 347-360, doi:10.1016/j.devcel.2019.04.011 (2019).

412. Yuan, X., Qian, N., Ling, S., Li, Y., Sun, W., Li, J., Du, R., Zhong, G., Liu, C., Yu, G., Cao, D., Liu, Z., Wang, Y., Qi, Z., Yao, Y., Wang, F., Liu, J., Hao, S., Jin, X., Zhao, Y., Xue, J., Zhao, D., Gao, X., Liang, S., Li, Y., Song, J., Yu, S. and Li, Y. Breast cancer exosomes contribute to pre-metastatic niche formation and promote bone metastasis of tumor cells. *Theranostics* **11**, 1429-1445, doi:10.7150/thno.45351 (2021).

413. Morrissey, S. M., Zhang, F., Ding, C., Montoya-Durango, D. E., Hu, X., Yang, C., Wang, Z., Yuan, F., Fox, M., Zhang, H. G., Guo, H., Tieri, D., Kong, M., Watson, C. T., Mitchell, R. A., Zhang, X., McMasters, K. M., Huang, J. and Yan, J. Tumor-derived exosomes drive immunosuppressive macrophages in a pre-metastatic niche through glycolytic dominant metabolic reprogramming. *Cell Metab* **33**, 2040-2058 e10, doi:10.1016/j.cmet.2021.09.002 (2021).

414. Zhao, S., Mi, Y., Guan, B., Zheng, B., Wei, P., Gu, Y., Zhang, Z., Cai, S., Xu, Y., Li, X., He, X., Zhong, X., Li, G., Chen, Z. and Li, D. Tumor-derived exosomal miR-934 induces macrophage M2 polarization to promote liver metastasis of colorectal cancer. *J Hematol Oncol* **13**, 156, doi:10.1186/s13045-020-00991-2 (2020).

415. Dong, Q., Liu, X., Cheng, K., Sheng, J., Kong, J. and Liu, T. Pre-metastatic Niche Formation in Different Organs Induced by Tumor Extracellular Vesicles. *Front Cell Dev Biol* **9**, 733627, doi:10.3389/fcell.2021.733627 (2021).

416. Borzecka, K., Plociennikowska, A., Bjorkelund, H., Sobota, A. and Kwiatkowska, K. CD14 mediates binding of high doses of LPS but is dispensable for TNF-alpha production. *Mediators Inflamm* **2013**, 824919, doi:10.1155/2013/824919 (2013).

417. Ural, E. E., Toomajian, V., Hoque Apu, E., Veletic, M., Balasingham, I., Ashammakhi, N., Kanada, M. and Contag, C. H. Visualizing Extracellular Vesicles and Their Function in 3D Tumor Microenvironment Models. *Int J Mol Sci* **22**, doi:10.3390/ijms22094784 (2021).

418. Vijayan, V., Pradhan, P., Braud, L., Fuchs, H. R., Gueler, F., Motterlini, R., Foresti, R. and Immenschuh, S. Human and murine macrophages exhibit differential metabolic responses to lipopolysaccharide - A divergent role for glycolysis. *Redox Biol* **22**, 101147, doi:10.1016/j.redox.2019.101147 (2019).

419. Plitzko, B. and Loesgen, S. Measurement of Oxygen Consumption Rate (OCR) and Extracellular Acidification Rate (ECAR) in Culture Cells for Assessment of the Energy Metabolism. *Bio Protoc* **8**, e2850, doi:10.21769/BioProtoc.2850 (2018).

420. Marumo, T., Maduka, C. V., Ural, E., Apu, E. H., Chung, S. J., Tanabe, K., van den Berg, N. S., Zhou, Q., Martin, B. A., Miura, T., Rosenthal, E. L., Shibahara, T. and Contag, C. H. Flavinated SDHA underlies the change in intrinsic optical properties of oral cancers. *Commun Biol* **6**, 1134, doi:10.1038/s42003-023-05510-w (2023).

421. Bessa, C., Loureiro, J. B., Barros, M., Isca, V. M. S., Sardao, V. A., Oliveira, P. J., Bernardino, R. L., Herman-de-Sousa, C., Costa, M. A., Correia-de-Sa, P., Alves, M. G., Rijo, P. and Saraiva, L. Counteracting Colon Cancer by Inhibiting Mitochondrial Respiration and Glycolysis with a Selective PKCdelta Activator. *Int J Mol Sci* **24**, doi:10.3390/ijms24065710 (2023).

422. Lungaro, L., Costanzini, A., Manza, F., Barbalinardo, M., Gentili, D., Guarino, M., Caputo, F., Zoli, G., De Giorgio, R. and Caio, G. Impact of Female Gender in Inflammatory Bowel Diseases: A Narrative Review. *J Pers Med* **13**, doi:10.3390/jpm13020165 (2023).

423. Blumenstein, I. and Sonnenberg, E. Sex- and gender-related differences in inflammatory bowel diseases. *Frontiers in Gastroenterology* **2**, (2023).

424. Shah, S. C., Khalili, H., Gower-Rousseau, C., Olen, O., Benchimol, E. I., Lynge, E., Nielsen, K. R., Brassard, P., Vutcovici, M., Bitton, A., Bernstein, C. N., Leddin, D., Tamim, H., Stefansson, T., Loftus, E. V., Jr., Moum, B., Tang, W., Ng, S. C., Gearry, R., Sincic, B., Bell, S., Sands, B. E., Lakatos, P. L., Vegh, Z., Ott, C., Kaplan, G. G., Burisch, J. and Colombel, J. F. Sex-Based Differences in Incidence of Inflammatory Bowel Diseases-Pooled Analysis of Population-Based Studies From Western Countries. *Gastroenterology* **155**, 1079-1089 e3, doi:10.1053/j.gastro.2018.06.043 (2018).

425. Zelinkova, Z., Stokkers, P. C., van der Linde, K., Kuipers, E. J., Peppelenbosch, M. P. and van der Woude, C. P. Maternal imprinting and female predominance in familial Crohn's disease. *J Crohns Colitis* **6**, 771-6, doi:10.1016/j.crohns.2012.01.002 (2012).

426. Maite, C. B., Roy, M. and Emilie, V. The Effect of Sex-Specific Differences on IL-10(-/-) Mouse Colitis Phenotype and Microbiota. *Int J Mol Sci* **24**, doi:10.3390/ijms241210364 (2023).

427. Lai, C. Y., Yeh, K. Y., Liu, B. F., Chang, T. M., Chang, C. H., Liao, Y. F., Liu, Y. W. and Her, G. M. MicroRNA-21 Plays Multiple Oncometabolic Roles in Colitis-Associated Carcinoma and Colorectal Cancer via the PI3K/AKT, STAT3, and PDCD4/TNF-alpha Signaling Pathways in Zebrafish. *Cancers (Basel)* **13**, doi:10.3390/cancers13215565 (2021).

428. Ding, Q., Li, R., Wang, Q., Yu, L. and Zi, F. A pan-cancer analysis of the role of argininosuccinate synthase 1 in human tumors. *Front Oncol* **13**, 1049147, doi:10.3389/fonc.2023.1049147 (2023).

429. Wu, K., Lin, K., Li, X., Yuan, X., Xu, P., Ni, P. and Xu, D. Redefining Tumor-Associated Macrophage Subpopulations and Functions in the Tumor Microenvironment. *Front Immunol* **11**, 1731, doi:10.3389/fimmu.2020.01731 (2020).

430. Mahajan, R. and Gupta, K. Food and drug administration's critical path initiative and innovations in drug development paradigm: Challenges, progress, and controversies. *J Pharm Bioallied Sci* **2**, 307-13, doi:10.4103/0975-7406.72130 (2010).

431. Mak, I. W., Evaniew, N. and Ghert, M. Lost in translation: animal models and clinical trials in cancer treatment. *Am J Transl Res* **6**, 114-8, (2014).

432. Baek, S., Jeon, M., Jung, H. N., Lee, W., Hwang, J. E., Lee, J. S., Choi, Y. and Im, H. J. M1 Macrophage-Derived Exosome-Mimetic Nanovesicles with an Enhanced Cancer Targeting Ability. *ACS Appl Bio Mater* **5**, 2862-2869, doi:10.1021/acsabm.2c00246 (2022).

433. Riess, C., Shokraie, F., Classen, C. F., Kreikemeyer, B., Fiedler, T., Junghanss, C. and Maletzki, C. Arginine-Depleting Enzymes - An Increasingly Recognized Treatment Strategy for Therapy-Refractory Malignancies. *Cell Physiol Biochem* **51**, 854-870, doi:10.1159/000495382 (2018).

APPENDIX A: MATERIALS

Table A.1 Antibodies used for immunoblotting and flow cytometry.

Use	Antibody Name	Primary/ Secondary	Dilution	Catalog No	Vendor
WB	Cebpb	1°	1200	ab32358	Abcam
WB	COX2	1°	500	A3560	ABClonal
WB	Fra1	1°	500	sc-28310	Santa Cruz Bio
WB	CD81	1°		10037	Cell Signaling Technology
WB	Alix	1°		12422-1-AP	Protein Tech
WB	Flot-1	1°		BDB610820	Fisher Scientific
WB	GAPDH	1°	2000	10494-1-AP	Protein Tech
WB	Anti-rabbit IgG, HRP-linked	2°	2000	7074	Cell Signaling Technology
WB	Anti-mouse IgG, HRP-linked	2°	2000	7076	Cell Signaling Technology
Flow	CD45 BV605	1°-conjugated	300	103140	Biolegend
Flow	CD11b AF700	1°-conjugated	400	101222	Biolegend
Flow	F4/80 BV785	1°-conjugated	300	123141	Biolegend
Flow	MHC II PerCP	1°-conjugated	200	107624	BioLegend
Flow	CD86 BV421	1°-conjugated	200	105032	BioLegend
Flow	CD206 APC	1°-conjugated	200	141708	BioLegend
Flow	IL-4 BV650	1°-conjugated	1200	BDB564004	Biolegend
Flow	Arg1 PE-Cy7	1°-conjugated	400	25-3697-80	ThermoFish
Flow	iNOS BUV 615	1°-conjugated	500	366-5920-82	ThermoFish
Flow	CD3 SparkBlue 550	1°-conjugated	100	100260	BioLegend
Flow	CD4 APC-Fire 810	1°-conjugated	100	100480	BioLegend
Flow	CD8a BB700	1°-conjugated	100	566409	BD
Flow	IL-17a AF647	1°-conjugated	200	506911	BioLegend
Flow	IFNγ APC-Fire 750	1°-conjugated	500	505859	BioLegend
Flow	FoxP3 PE	1°-conjugated	40	320007	Biolegend
Flow	Ly6C BV510	1°-conjugated	200	128033	Biolegend
Flow	Ly6G PacBlue	1°-conjugated	250	127612	BioLegend
Flow	CD11c PE/Dazzle 594	1°-conjugated	500	117348	BioLegend
Flow	CD31 BUV 737	1°-conjugated	200	612802	BD

Table A.2 Cell lines used throughout this dissertation.

Cell Line	Host Species	Cell Type	Source
Raw264.7	Balb/c mouse	Macrophage (leukemia)	ATCC
J774			Stanford Contag Lab stock
THP1	Human	Promonocyte (leukemia)	ATCC
U937	Human	Promonocyte (leukemia)	Stanford Contag Lab stocks
4T1	Balb/c mouse	Triple negative breast cancer*	Dr. Michael Bachmann
Immortalized bone marrow-derived macrophages (iBMDMs)	C57Bl/6 mouse	Macrophages (J2 virus introduced v-myc and v-raf/mil oncogenes)	Dr. Andrew Olive
Caco2	Human	Colorectal carcinoma*	Dr. Michael Bachmann
CT26	Balb/c mouse	Colorectal carcinoma (fibroblast)	Stanford Contag Lab stocks
MC38	C57Bl/6 mouse	Colorectal carcinoma	Kerafast
NIH 3T3	mouse	Mouse embryonic fibroblast (MEF)*	Dr. Michael Bachmann

*Stably transfected with LuBiG plasmid containing genes encoding blastocidin resistance, green fluorescence protein and luciferase under the CMV promoter

Table A.3 Primers used for RT-qPCR.

	Transcript Name	Target Species	Forward primer	Reverse primer	Vendor
1	E-cadherin	Mouse	atcctcgccctgctgatt	accaccgttctcctccgta	IDT
2	Vimentin	Mouse	ATGCTTCTCTGGCACGTCTT	AGCCACGCTTTCATACTGCT	IDT
3	N-cadherin	Mouse	gccatcatcgctatccttct	ccgtttcatccataccacaaa	IDT
4	Snai1	Mouse	gtccccaactacgggaaact	gggatcctgccaactcct	IDT
5	Twist1	Mouse	agctacgccttctccgtct	tccttctctggaaacaatgaca	IDT
6	Slug	Mouse	cattgccttgtgtctgcaag	agaaaggcttttccccagtg	IDT
7	ZEB1	Mouse	aggtgatccagccaaacg	ggtggcgtggagtcagag	IDT
8	B-catenin	Mouse	ATGGAGCCGGACAGAAAAGC	TGGGAGGTGTCAACATCTTCTT	IDT
9	mGAPDH	Mouse	AACTTTGGCATTGTGGAAGG	ACACATTGGGGGTAGGAACA	IDT

APPENDIX B: PERMISSIONS

Chapter 4 contains modified text, with some direct excerpts, from the previously published papers that are listed below (all excerpted text and figures are marked as such in the dissertation text). These papers and manuscript relate to the chronic inflammatory responses to biomaterials as a comparator to chronic inflammation associated with LPS exposure and colitis. My contributions to this work focuses on the immune response as both a means to learn new approaches, study unique mechanisms of immune activation, and assess chronicity of immune stimulation.

1. Maduka, C. V., Alhaj, M., **Ural, E. E.**, Habeeb, O. M., Kuhnert, M. M., Smith, K., Makela, A. V., Pope, H., Chen, S., Hix, J. M., Mallett, C. L., Chung, S. J., Hakun, M., Tundo, A., Zinn, K. R., Hankenson, K. D., Goodman, S. B., Narayan, R. and Contag, C. H. Polylactide Degradation Activates Immune Cells by Metabolic Reprogramming. *Advanced Science* **10**, e2304632, doi:10.1002/advs.202304632 (2023).
2. Maduka, C. V., Makela, A. V., Tundo, A., **Ural, E. E.**, Stivers, K. B., Kuhnert, M. M., Alhaj, M., Hoque Apu, E., Ashammakhi, N., Hankenson, K. D., Narayan, R., Elisseeff, J. H. and Contag, C. H. Regulating the proinflammatory response to composite biomaterials by targeting immunometabolism. *Bioactive Materials* 64-73, doi:10.1016/j.bioactmat.2024.05.046 (2024).
3. Maduka, C. V., Makela, A. V., Tundo, A., **Ural, E. E.**, Stivers, K. B., Alhaj, M., Narayan, R., Goodman, S. B., Ashammakhi, N., Elisseeff, J. H., Hankenson, K. D. and Contag, C. H. Role of mitochondrial complex I in the proinflammatory response to polylactide implants. *ACS Applied Engineering Materials* **2**, doi:10.1021/acsaenm.4c00393 (2024).

APPENDIX C: PUBLICATIONS, CONFERENCE PRESENTATIONS, AND AWARDS

Publications, preprints and submitted manuscripts at time of writing

1. Maduka, C. V., Makela, A. V., Tundo, A., **Ural, E. E.**, Stivers, K. B., Kuhnert, M. M., Alhaj, M., Hoque Apu, E., Ashammakhi, N., Hankenson, K. D., Narayan, R., Elisseeff, J. H. and Contag, C. H. Regulating the proinflammatory response to composite biomaterials by targeting immunometabolism. *Bioactive Materials* 64-73, doi:10.1016/j.bioactmat.2024.05.046 (2024).
2. Toomajian, V. A., Tundo, A., **Ural, E. E.**, Greeson, E. M., Contag, C. H., & Makela, A. V. Magnetic particle imaging reveals that iron-labeled extracellular vesicles accumulate in brains of mice with metastases. *ACS Applied Materials & Interfaces* **16**, doi:10.1021/acsami.4c04920 (2024).
3. Maduka, C. V., Alhaj, M., **Ural, E. E.**, Habeeb, O. M., Kuhnert, M. M., Smith, K., Makela, A. V., Pope, H., Chen, S., Hix, J. M., Mallett, C. L., Chung, S. J., Hakun, M., Tundo, A., Zinn, K. R., Hankenson, K. D., Goodman, S. B., Narayan, R. and Contag, C. H. Polylactide Degradation Activates Immune Cells by Metabolic Reprogramming. *Advanced Science* **10**, e2304632, doi:10.1002/advs.202304632 (2023).
4. Maduka, C. V., Alhaj, M., **Ural, E. E.**, Kuhnert, M. M., Habeeb, O. M., Schilmiller, A. L., Hankenson, K. D., Goodman, S. B., Narayan, R. and Contag, C. H. Stereochemistry Determines Immune Cellular Responses to Polylactide Implants. *ACS Biomater Sci Eng* **9**, 932-943, doi:10.1021/acsbiomaterials.2c01279 (2023).
5. Marumo, T., Maduka, C. V., **Ural, E. E.**, Apu, E. H., Chung, S. J., Tanabe, K., van den Berg, N. S., Zhou, Q., Martin, B. A., Miura, T., Rosenthal, E. L., Shibahara, T. and Contag, C. H. Flavinated SDHA underlies the change in intrinsic optical properties of oral cancers. *Commun Biol* **6**, 1134, doi:10.1038/s42003-023-05510-w (2023).
6. Maduka, C. V., Schmitter-Sánchez, A. D., Makela, A. V., **Ural, E. E.**, Stivers, K. B., Pope, H., Kuhnert, M. M., Habeeb, O. M., Tundo, A., Alhaj, M., Kiselev, A., Chen, S., Olive, A. J., Hankenson, K. D., Narayan, R., Park, S., Elisseeff, J. H. and Contag, C. H. Immunometabolic cues recompose and reprogram the microenvironment around implanted biomaterials. *Nature Biomedical Engineering* **8**, 1308-1321, doi:10.1038/s41551-024-01260-0 (2024).
7. **Ural, E. E.**, Toomajian, V., Hoque Apu, E., Veletic, M., Balasingham, I., Ashammakhi, N., Kanada, M. and Contag, C. H. Visualizing Extracellular Vesicles and Their Function in 3D Tumor Microenvironment Models. *Int J Mol Sci* **22**, doi:10.3390/ijms22094784 (2021).
8. Wu, B., Durisin, E. K., Decker, J. T., **Ural, E. E.**, Shea, L. D., & Coleman, R. M. Phosphate regulates chondrogenesis in a biphasic and maturation-dependent manner. *Differentiation*, 95, 54-62, doi:10.1016/j.diff.2017.04.002 (2017).

Conference presentations

1. **Ural, E. E.**, Neeb, E., Maduka, C. V., Greeson, E. M., Makela, A. V., Liby, K., & Contag, C. H. Investigating the pro-tumorigenic effects of lipopolysaccharide-activated macrophage-derived extracellular vesicles on colonic epithelial cells. Presented at Institute for Quantitative Health Sciences and Engineering Research Day (2023).
2. Rudsari, H. K., O'Hern, C., **Ural, E. E.**, Damrath, M., Neeb, E., Zoofaghari, M., & Contag, C. H. Human Heart Organoid-derived Extracellular Vesicles for Cardiac Intercellular Communication. Proceedings of the 10th ACM International Conference on Nanoscale Computing and Communication (2023).

3. Greeson, E. M., Madsen, C. S., **Ural, E. E.**, Makela, A. V., Toomajian, V. A., & Contag, C. H. Engineered Bacillus subtilis capable of epithelial cell invasion. Presented at SEED Conference (2023).
4. Toomajian, V. A., **Ural, E. E.**, Greeson, E. M., Contag, C. H., & Makela A. V. In Vivo Tracking of Iron Labeled Extracellular Vesicles in Breast Cancer and Associated Metastases Using Magnetic Particle Imaging. Presented at Michigan State University Engineering Symposium (2022).
5. **Ural, E. E.** & Contag, C. H. The role of exosomes in driving field carcinogenesis in the inflammatory niche of the gut. Presented at Cancer Research Network (2021).
6. Toomajian, V. A., **Ural, E. E.**, Contag, C. H., & Makela, A.V. In Vivo Tracking of Labeled Extracellular Vesicles in Breast Cancer and Associated Metastases Using Magnetic Particle Imaging. Presented at World Molecular Imaging Conference (2021).
7. **Ural, E. E.** & Contag, C. H. The role of exosomes in driving field carcinogenesis in the inflammatory niche of the gut. Presented at Michigan State University Gastrointestinal Grant Group Meeting (2020).
8. **Ural, E. E.** & Contag C. H. Exosomes as Primary Drivers of Immunocarcinogenesis; Inflammatory Bowel Disease-Associated Colorectal Cancer. Presented at Institute for Quantitative Health Sciences and Engineering Division Meeting (2019).
9. **Ural, E. E.** & Contag, C. H. Exosomes as the Primary Drivers of Immunocarcinogenesis. Presented at Institute for Quantitative Health Sciences and Engineering Research Day (2019).
10. **Ural, E. E.**, Sempere, L. F. & Moore, A. MicroRNA-10b Therapy in Breast and Pancreatic Cancer. Chalk talk presented at Institute for Quantitative Health Sciences and Engineering Retreat (2018).

Awards

1. Michigan State University College of Engineering Summer Fellowship
2. Michigan State University Biomedical Engineering, College of Engineering Fellowship
3. Michigan State University Engineering Graduate Dissertation Completion Fellowship
4. Michigan State University Microbiology and Molecular Genetics, College of Natural Sciences Fellowship
5. Michigan State University Summer Research Fellowship

Services & Leadership Positions

1. Michigan State University Biomedical Engineering Graduate Student Association (BME GSA) Social and Events Committee Chair
2. Contag Laboratory Immune Control Subgroup Leader
3. Michigan State University Committee on Faculty Tenure (UCFT) Council of Graduate Students Representative
4. Michigan State University Council of Graduate Students (COGS) Biomedical Engineering Representative
5. Co-Founder and Vice President of Michigan State University Science Communications (MSU SciComm) Organization
6. Cyber-Ambassador Certification in Communication, Teamwork, Ethics and Leadership Training for Multidisciplinary Research Teams

7. Michigan State University Council of Graduate Students (COGS) Finance Committee Representative
8. Scientific Writing Consultant Specialist at Michigan State University Writing Center
9. Social and Professional Development Co-Chair of MSU Graduate Women in Science Program